Graphene based materials and their potential applications

Dawid Pakulski

ADAM MICKIEWICZ UNIVERSITY IN POZNAŃ

FACULTY OF CHEMISTRY

UNIVERSITÉ DE STRASBOURG

ÉCOLE DOCTORALE DES SCIENCES CHIMIQUES

UMR7006 - Institut de Science et d'Ingénierie Supramoléculaires

THESIS

presented by:

Dawid Pakulski

„**Graphene based materials and their potential applications**”

„Matériaux à base de graphène et leurs potentielles applications”

„Materiały grafenowe i ich potencjalne zastosowania”

to obtain the rank: **Doctor of Adam Mickiewicz University in Poznań and Université de Strasbourg**

Specialty: **Chemistry/Physical Chemistry**

THESIS supervisors:

Prof. Violetta Patroniak (AMU)

Dr. Artur Ciesielski (HDR) (Unistra)

THESIS co-supervisor:

Prof. Paolo Samorì (Unistra)

Reviewers:

Prof. Ewa Mijowska, West Pomeranian University of Technology Szczecin

Prof. Mihail Barboiu, Institut Européen des Membranes - UMR5635, Montpellier

Other jury members:

Prof. Marcin Hoffmann, Adam Mickiewicz University in Poznań

Assoc. Prof. Piotr Pawluć, Adam Mickiewicz University in Poznań

Prof. Maciej Kubicki, Adam Mickiewicz University in Poznań

Poznań 6th December 2019

I dedicate this work to my wonderful wife Ilona.

Thank you for your patience, support in difficult times and faith in me.

Acknowledgment

It is my great pleasure to express my sincere gratitude to my research supervisors: Prof. Violetta Patroniak, Faculty of Chemistry of Adam Mickiewicz University in Poznań and Dr. Artur Ciesielski, Institut de Science et d'Ingénierie Supramoléculaires UMR7006, (Université de Strasbourg) for their guidance, fruitful scientific discussions, and for their help during this period of my research. Without their constant support and encouragement, it would not have been possible to complete my research work and finally this thesis.

I would like to express my profound gratitude to my co-supervisor Prof. Paolo Samorì, who provided me an opportunity to join his team in Strasbourg as an intern and later as a team member.

I sincerely thank all the faculty members, former and present, post-docs, PhD and M.Sc. students, secretaries and technical staff at both laboratories (Nanochemistry laboratory in Strasbourg and Department of Bioinorganic Chemistry in Poznań) especially: Dr. Adam Gorczyński, Dr. Marta Fik and M.Sc. Włodzimierz Czepa for the discussions, encouragement, kindness and unforgettable atmosphere during the course of my work. Thanks to Dr. Marc-Antoine Stoeckel for the support regarding the French part of my thesis.

I would like to thank my friends especially Karol Głowienka for countless conversations and Michał Markiewicz for travels and joint widening of horizons.

Last but not the least I want to specially thank my family for their motivation and support.

This work was partially supported by grants of National Science Centre in Poland (UMO-2017/27/N/ST5/00173), Foundation for Polish Science (FNP) and the French Embassy in Poland within the frame of cotutelle program.

Streszczenie w języku polskim

Nanotechnologia jest uważana za jedną z najbardziej przyszłościowych dziedzin nauki, która otwiera nowe możliwości wśród naukowców na całym świecie oraz bezpośrednio wpływa na poprawę jakości ludzkiego życia. Ten błyskawicznie rozwijający się obszar nauki polega na wytwarzaniu funkcjonalnych układów w skali nanometrycznej na poziomie molekularnym o specyficznych właściwościach i zastosowaniach. Ciągły rozwój sektorów technologicznych i przemysłowych przynosi oprócz wielu korzyści pewne poważne konsekwencje. Jedną z nich jest zanieczyszczanie środowiska. Uwolnienie ogromnej ilości zanieczyszczeń do wód, gleb oraz powietrza spowodowało potrzebę opracowania nowoczesnych technologii do usuwania tych niepożądanych i szkodliwych substancji. Wśród wielu dotychczas stosowanych metod poprawy jakości oraz czystości wody procesy adsorpcyjne oparte na wychwytywaniu zanieczyszczeń przez adsorbent cieszą się dużym powodzeniem.

Pomyślne wyizolowanie grafenu w 2004 przez A. Geima i K. Novoselova miało ogromny wpływ na rozwój wielu dziedzin nauki, zwłaszcza nanotechnologii, a w 2010 zostali oni uhonorowani nagrodą Nobla z fizyki za przełomowe badania naukowe dotyczące materiału dwuwymiarowego. Grafen definiowany jest jako pojedyncza warstwa atomów węgla o hybrydyzacji sp^2 i strukturze sześcioczłonowych pierścieni wyglądem przypominającej plaster miodu (Rysunek 1). Grafen dzięki swoim specyficznym właściwościom tj. ogromna powierzchnia właściwa, doskonała wytrzymałość mechaniczna oraz bardzo wysoka przewodność elektryczna znajduje praktyczne zastosowanie w wielu gałęziach przemysłu m.in. w energetyce (elastyczne układy elektroniczne, baterie słoneczne, ekrany dotykowe, fotodetektory), optoelektronice, magazynowaniu gazów i energii, a także w procesach oczyszczania wody metodami membranowymi.

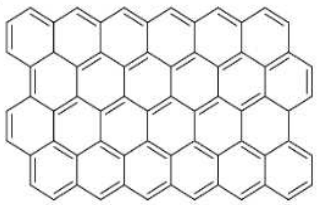

Rysunek 1. Struktura grafenu.

Zarówno struktura jak i właściwości grafenu zależą w główniej mierze od metody ich otrzymywania. Istnieje wiele technologii stosowanych do produkcji grafenu, które można podzielić na dwie główne grupy: "*top-down*" *oraz* "*bottom-up*". Metoda "*top-down*" (odgórna) opiera się na miniaturyzacji istniejących układów w procesach

rozwarstwiania materiału bazowego przy udziale m.in. ultradźwięków, rozdrabniania mechanicznego czy też elektrochemii. Z kolei metoda "*bottom-up*" (oddolna) polega na otrzymywaniu nanostruktur w wyniku samoorganizacji pojedynczych cząsteczek lub atomów w procesie m.in chemicznego osadzania z fazy gazowej (CVD) na metalicznym substracie lub epitaksjalny wzrost na powierzchni węgliku krzemu (SiC), pozwala ona na lepszą kontrolę procesu oraz uzyskanie materiału dwuwymiarowego o bardziej jednolitej morfologii i stosunkowo niewielkiej ilości defektów, dlatego też jest częściej stosowana.

Grafen można poddawać rozmaitym modyfikacjom bazujących zarówno na wiązaniach kowalencyjnych jak i oddziaływaniach niekowalencyjnych. Jednym z najpopularniejszych materiałów otrzymywanych w wyniku modyfikacji kowalencyjnej jest tlenek grafenu, który posiada w swojej budowie liczne grupy funkcyjne zawierające tlen, takie jak grupy karbonylowe na krawędziach arkuszy oraz grupy epoksydowe i hydroksylowe umiejscowione na jego powierzchni (Rysunek 2). Obecność grup funkcyjnych bogatych w elektrony znacząco wpływa na hydrofilowość oraz wysoką gęstość ładunku ujemnego tlenku grafenu. Dzięki tym cechom tlenek grafenu z łatwością może oddziaływać ze związkami organicznymi oraz jonami metali m.in. poprzez oddziaływania elektrostatyczne, co przekłada się na jego szerokie zastosowanie w procesach adsorpcyjnych. Oprócz tego, duża różnorodność grup tlenowych znajdujących się na jego powierzchni powoduje, że materiał ten jest idealnym kandydatem do dalszych funkcjonalizacji kowalencyjnych wykorzystując proste reakcje organiczne.

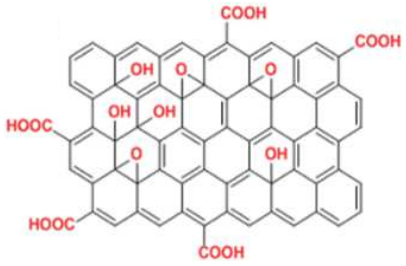

Rysunek 2. Struktura tlenku grafenu.

Celem przedstawionej pracy naukowej jest synteza sfunkcjonalizowanych materiałów dwuwymiarowych (grafen i tlenek grafenu) i ich wieloaspektowa charakterystyka struktury i właściwości ze szczególnym uwzględnieniem procesów adsorpcyjnych oraz magazynowania energii elektrycznej. Badania naukowe przeprowadzone w ramach prezentowanej rozprawy doktorskiej można podzielić na trzy główne części eksperymentalne. Dwie z nich dotyczą produkcji nowoczesnych adsorbentów bazujących na tlenku grafenu stosując prostą i zarazem bardzo wydajną

reakcję kondensacji zachodzącą na powierzchni tlenku grafenu. Ostatnia z części eksperymentalnych prezentowanych w tej rozprawie doktorskiej obejmuje syntezę hybrydy organiczno-nieorganicznej wykorzystując grafen uzyskany metodą elektrochemicznego rozwarstwienia (EEG) oraz jej potencjalne zastosowanie w elektronice.

Główne części eksperymentalne zostały schematycznie przedstawione poniżej na Rysunku 3 i obejmują:

1. Opracowanie nowych wysokowydajnych adsorbentów jonów metali ciężkich (Pb^{2+}, Cd^{2+}, Cu^{2+}) w procesie kowalencyjnej modyfikacji tlenku grafenu sfunkcjonalizowanym polimerem zawierającym ugrupowania aminowe (BPEI-polietylenoimina).
2. Syntezę efektywnego adsorbenta kationowych barwników organicznych (MB - błękit metylenowy, MV- fiolet metylenowa, RHB - rodamina B) wykorzystując tlenek grafenu zmodyfikowany mezoporowatą aminokrzemionką (SiO_2NH_2-GO).
3. Badania strukturalne i elektryczne hybrydy organiczno-nieorganicznej (Mo_{132}-DTAB-EEG) opartej na grafenie otrzymanym metodą elektrochemicznego rozwarstwienia oraz jej potencjalne wykorzystanie przy produkcji superkondensatorów.

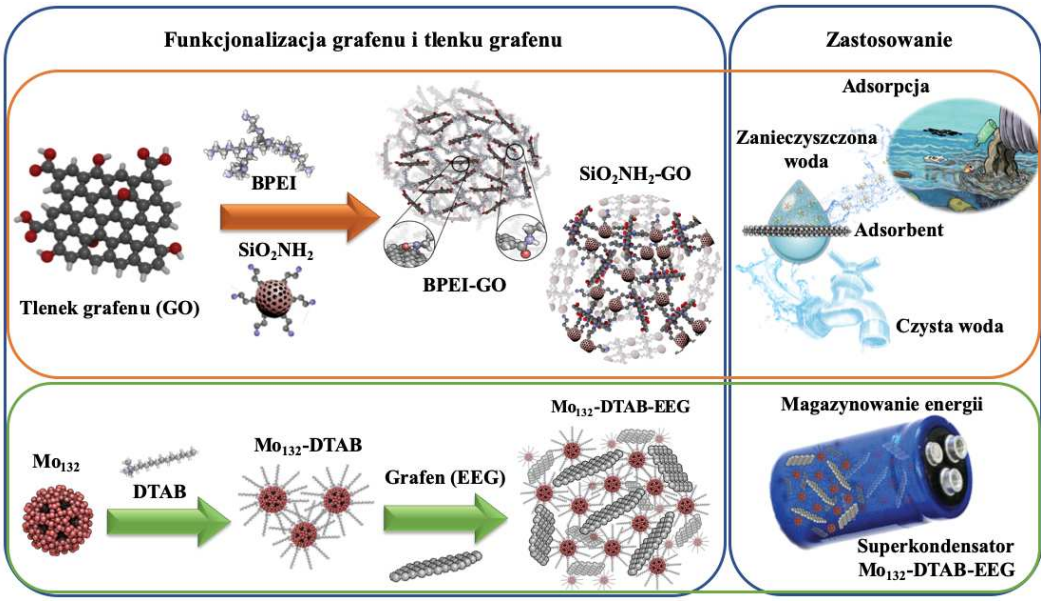

Rysunek 3. Schematyczne przedstawienie głównych założeń syntetycznych rozprawy doktorskiej.

Pierwsza część eksperymentalna, dotyczy procesu adsorpcji zanieczyszczeń nieorganicznych (jonów metali ciężkich) z roztworów wodnych wykorzystując nowe wysokowydajne adsorbenty oparte na sfunkcjonalizowanym tlenku grafenu organicznym polimerem - polietylenoiminą (BPEI). Układ ten charakteryzuje się wysoką stabilnością, bardzo dużą powierzchnią właściwą oraz wysokim powinowactwem do jonów metali ciężkich. Funkcjonalizacja kowalencyjna tlenku grafenu poprzez wprowadzenie podstawionych grup aminowych jest jedną z najczęściej stosowanych metod, która została zaimplementowana w powyższej pracy. W wyniku prostej reakcji nukleofilowego otwarcia pierścieni epoksydowych otrzymano materiał o wysokim stopniu funkcjonalizacji. Metodyka syntetyczna została sprzężona wraz z wieloaspektową charakterystyką fizyko-chemiczną otrzymanych adsorbentów wykorzystując m.in. spektroskopię Ramana, skaningową mikroskopię elektronową (SEM), spektroskopię fotoelektronów w zakresie promieniowania rentgenowskiego (XPS) oraz płomieniową absorpcyjną spektrometrię atomową (FAAS). Po przeprowadzeniu szczegółowej analizy spektralno-strukturalnej aminowe pochodne tlenku grafenu zostały bezpośrednio zastosowane w procesie adsorpcji jonów metali ciężkich (Pb^{2+}, Cd^{2+}, Cu^{2+}) z roztworów wodnych. Maksymalna pojemność adsorpcyjna (q_{max}) definiowana jako ilość zanieczyszczeń (w tym przypadku jonów metali ciężkich) wychwycona przez 1g adsorbenta została określona przy pomocy dwóch powszechnie używanych modeli izoterm: Langmuira i Freundlicha. Dokładne analizy właściwości adsorpcyjnych potwierdziły, iż wzbogacenie tlenku grafenu o dodatkowe kieszenie koordynacyjne poskutkowało otrzymaniem adsorbentu o niespotykanych do tej pory (w odniesieniu do materiałów węglowych) wartościach q_{max} dla jonów miedzi (Cu^{2+} - 1096 mg g^{-1}), kadmu (Cd^{2+} - 2051 mg g^{-1}) oraz ołowiu (Pb^{2+} - 3390 mg g^{-1}). W prezentowanej pracy wyznaczono również parametry kinetyczne oraz termodynamiczne potwierdzające spontaniczną oraz egzotermiczną naturę procesu adsorpcji. Wykazano również, że istnieje możliwość skutecznej regeneracji adsorbentu BPEI-GO używając odpowiednich roztworów kwasów (0.1M EDTA oraz 0.1M HNO_3), co jest niezbędne w praktycznym zastosowaniu materiału sorpcyjnego na skalę przemysłową.

Ostatnie badania wykazały, że zarówno tlenek grafenu jak i sfunkcjonalizowany tlenek grafenu posiadają ogromny potencjał jako aktywny materiał w procesie usuwania barwników kationowych z roztworów wody. W następstwie tego, druga część

eksperymentalna poświęcona jest syntezie adsorbentów opartych na zmodyfikowanym tlenku grafenu przez mezoporowatą aminokrzemionkę (SiO_2NH_2) oraz zbadanie ich właściwości adsorpcyjnych w odniesieniu do wybranych barwników kationowych (MB - błękit metylenowy, MV - fiolet metylenowa, RhB - rodamina B). Metodologia otrzymania adsorbenta jest analogiczna do materiału otrzymanego w pierwszej części eksperymentalnej i dotyczy reakcji kondensacji grup epoksydowych znajdujących się na tlenku grafenu z podjednostkami aminokrzemionki. Otrzymany kompozyt (SiO_2NH_2-GO) charakteryzuje się wysokimi wartościami q_{max} dla kationowych barwników organicznych (MB - 300 mg g^{-1}, MV - 178 mg g^{-1}, RhB - 358 mg g^{-1}) oraz wysoką wartością szybkości reakcji procesu adsorpcji, dzięki czemu materiał zastosowano w procesie kolumnowej ekstrakcji w fazie stałej. Wykazano również, że istnieje możliwość skutecznej regeneracji adsorbentu w obecności 0,1 M HCl.

W ostatniej części eksperymentalnej przedstawiono syntezę hybrydy organiczno-nieorganicznej bazującej na sfunkcjonalizowanym heteropolianionie skondensowanym typu Keplera (Mo_{132}) surfaktantem (DTAB – bromek dodecylotrimetyloamoniowy) oraz grafenie otrzymanym metodą elektrochemicznego rozwarstwiania (EEG). W ostatnim czasie, elektrochemiczne złuszczanie grafitu w fazie ciekłej stało się bardzo popularną metodą otrzymywania grafenu na dużą skalę ze względu na szybkość i wydajność tego procesu. Z kolei, heteropolianiony skondensowane należą do interesujących grupy związków nieorganicznych o rozmiarach nanometrycznych składających się z dwóch głównych podjednostek: jonów metali przejściowych na najwyższym możliwym stopniu utlenienia (Mo^{+6}, V^{+5}, W^{+6}, Nb^{+5}) oraz terminalnych atomów tlenu, które pełnią funkcję mostka dla innych jonów oraz ligandów. Ze względu na dużą masę cząsteczkową, wysoki ładunek ujemny oraz bardzo dobrą rozpuszczalność w roztworach polarnych POM-y wykazują interesujące właściwości katalityczne, fotochemiczne i elektryczne. Oprócz tego, heteropolianiony skondensowane posiadają zdolności adsorpcyjne jonów metali alkalicznych (m.in. Na^+, Li^+), co czyni je obiecującymi platformami do budowy zaawansowanych materiałów elektrycznych. Zatem, głównym założeniem tej sekcji było wykorzystanie właściwości elektrycznych nowo otrzymanego materiału hybrydowego (Mo_{132}-DTAB-EEG) w odniesieniu do ich potencjalnego wykorzystania jako elektrody przy produkcji superkondensatorów. Dokładna charakterystyka przy użyciu m.in. mikroskopii elektronowej o wysokiej

rozdzielczości HR-TEM, dyfrakcji promieniowania rentgenowskiego XRD oraz spektroskopii XPS potwierdziła, że otrzymano stabilny materiał hybrydowy Mo_{132}-DTAB-EEG. Ponadto, porowate, trójwymiarowe układy Mo_{132}-DTAB-EEG synergicznie łączą ze sobą właściwości redoks POM-ów oraz wysoką przewodność elektryczną grafenu. Otrzymane wyniki pokazują, że tego typu układy posiadają interesujące właściwości elektryczne oraz mogą znaleźć potencjalne zastosowanie w produkcji superkondensatorów.

Pomijając aspekt nowości wygenerowanych zmodyfikowanych materiałów dwuwymiarowych, wykonane w ramach pracy doktorskiej badania dowiodły, że:

- Modyfikacja kowalencyjna tlenku grafenu polimerem organicznym (BPEI) bardzo korzystnie wpływa na wydajność procesu adsorpcji. Wartości maksymalnej pojemności adsorpcyjnej (q_{max}) dla jonów metali ciężkich znacznie wyróżniają ten materiał w odniesieniu do większości znanych adsorbentów węglowych.

- Modyfikacja tlenku grafenu mezoporowatą aminokrzemionką (SiO_2NH_2-GO) prowadzi do uzyskania efektywnego adsorbenta barwników kationowych (MB, RHB, MV). Materiał ten został z powodzeniem zastosowany jako wypełnienie kolumny w procesie ekstrakcji w fazie stałej, umożliwiając tym samym bardzo wydajne oczyszczanie wody z barwników w przepływie ciągłym.

- Heteropolianiony skondensowane typu Keplera z powodzeniem zaaplikowano w tworzeniu hybryd molekularnych z kationowymi surfaktantami wykorzystując słabe oddziaływania elektrostatyczne. Funkcjonalizacja elektrochemicznie rozwarstwionego grafenu podjednostkami POM-surfaktant dowiodła, że tego typu hybrydy organiczno-nieorganiczne oprócz wysokiej stabilności posiadają interesujące właściwości elektryczne o potencjalnym zastosowaniu przy produkcji superkondensatorów.

Podsumowując, prezentowana rozprawa doktorska w głównej mierze eksploruje tematykę związaną z adsorpcją zanieczyszczeń wykorzystując sfunkcjonalizowany tlenek grafenu oraz zgłębia wiedzę na temat hybryd molekularnych opartych na grafenie otrzymanym metodą elektrochemicznego rozwarstwienia. Aby w pełni odkryć potencjał nowych sfunkcjonalizowanych materiałów dwuwymiarowych otrzymywanych metodą „*bottom-up*" i umożliwić ich przyszłe wykorzystanie kluczowe jest zrozumienie zależności pomiędzy strukturą i właściwościami.

Summary in English

The nanotechnology is considered to be one of the most prospective fields of science and technology; its continuous development is expected to open up new opportunities to worldwide researchers and improve the quality of people's lives. Nanotechnology creates functional systems on a nanometric scale at the molecular level. Advancements in technological and industrial sectors bring in addition to many benefits some serious problems. One of them is environmental pollution. The wide spectrum of contaminants released into water, soil and air necessitated the development of techniques for the removal of these undesirable and harmful factors. Adsorption is one of the most important process to improve the quality and in particular the cleanliness of the groundwater and wastewater, which has a tremendous impact on environmental protection. Nowadays, various nanomaterials are continuously produced and then tested for their properties and industrial suitability in regarding to the high effectiveness of the removal of pollutants, at a low cost of obtaining and the possibility of regeneration. However, their impact on the environment and all living organisms including humans' health are still poorly understood. The complete understanding of the nature of nanomaterials requires an interdisciplinary approach and knowledge not only in the field of material engineering, but also in physics, chemistry, biology and medicine.

Recently, graphene and its derivative graphene oxide (GO) are becoming one of the most developed low-dimensional materials and are receiving widespread attention in academic and industrial research labs. This two-dimensional materials (2DMs) with unique physicochemical properties (*e.g.* exceptional electrical and thermal conductivity) have shown great potential as components in sensors, supercapacitors and platforms for adsorption of various pollutants in aqueous environment.

The successful isolation of single-layer graphene in 2004 by A. Geim and K. Novoselov followed by Nobel Prize in physics in 2010 had triggered a great interest for development of wide variety of potential technological applications. Graphene, a monolayer of graphite, contains sp^2-hybridized carbon atoms arranged into a two-dimensional honeycomb crystal lattice (Figure 1). Due to these features, graphene can find wide range of practical applications, including power engineering (flexible electronic

circuits, solar batteries, touch screens, photodetectors), optoelectronics, energy storage, and even in water purification using membrane-based methods. The unique structure of this single-atom-thick sheet of carbon results in specific physicochemical properties, including large surface to volume area, excellent mechanical strength and high electrical conductivity. The so-called "graphene rush" has triggered new trends in material chemistry, and not surprisingly other 2DMs became a new exciting subject of research by many scientists around the world.

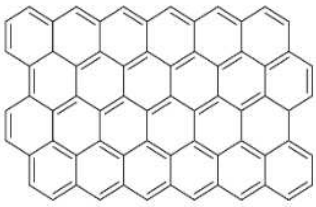

Figure 1. Schematic representation of graphene.

However, to take full advantage of the potential of graphene-related materials, the knowledge improvement of the production of graphene on an industrial scale with very high quality is needed. Noteworthy, both the structure and the properties of graphene such as the number of layers, quality and lateral size are mainly dependent on the production route. There are many technologies used for graphene production, which can be divided into two main approaches: *top-down* and *bottom-up*. The former relies on the miniaturization of existing systems in the processes of delamination of the base material using external factors *e.g.* ultrasounds, mechanical grinding or electrochemistry. So far, the most commonly used method to produce high-quality pristine graphene sheets concerns "scotch-tape" method, which was exploited to isolate this 2DM for the first time. Unfortunately, this method is hardly exploited in large scale production, thus limit any technological application. The latter approach consists of the production of nanostructures as a result of self-assembly of individual molecules or atoms in the process of *e.g.* chemical vapor deposition (CVD) on metal substrates or epitaxial growth on silicon carbide (SiC). This approach is often used because it allows for better process control and synthesis of a two-dimensional material with a more uniform morphology and a relatively small number of defects. Nevertheless, the further improvements of *bottom-up* approach are necessary to tackle the requirement of industrial manufacture, *e.g.* low cost, reproducibility and high quality.

Graphene can be subjected to various modifications based on both covalent bonds' formation and non-covalent interactions. One of the most popular materials obtained as a result of covalent modification is graphene oxide (GO), which displays numerous oxygen-rich functional groups identified as mostly in the form of hydroxy and epoxy groups on the basal plane and carbonyl groups at the sheet edges (Figure 2). The presence of electron-rich functional groups on GO significantly influences the hydrophilicity and high density of the negative charge. Due to these unique properties, GO can easily interact with organic compounds and metal ions *via* dipolar or strong electrostatic interactions, which has found widespread use in adsorption processes. In addition, the large diversity of oxygen groups on the GO surface makes this material an ideal candidate for further covalent functionalization involving simple organic reactions.

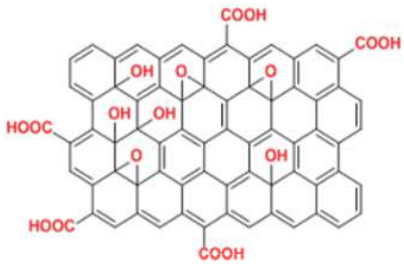

Figure 2. Schematic representation of graphene oxide (GO).

Scientific purpose of this doctoral dissertation concerns synthesis of functionalized two-dimensional materials (graphene and GO) by using approaches that may enable mass production and their comprehensive physico-chemical characterization, with particular emphasis on adsorption and energy storage properties. We endeavour to overcome some difficulties that are crucial for the practical application of 2D-based adsorbents including the difficulties in scaling-up the synthesis methodology and their limited reproducibility in adsorption process. One of the main purposes is related to the deepen knowledge of the structure-properties relationship in presented materials being an obligatory stage for their future applications. The scientific research carried out as part of the doctoral dissertation can be divided into three main experimental parts presented below, with the former two focused on the production of novel graphene oxide based-adsorbents using simple and efficient condensation reaction between oxygen functional groups on the GO surface and amine anchoring group. Accurate physico-chemical analysis proved the high efficiency towards heavy metal ions, when we use as functionalization agent branched polymer (BPEI- branched polyethyleneimine). In turn, graphene oxide modified by aminosilica nanoparticles (SiO_2NH_2-GO) exhibit high value of kinetic rate, which was directly used in adsorption of cationic dyes in solid phase extraction (SPE) process. The latter experimental part

focused on the possible uses of functionalized 2DMs in electronics. As the first, we combined graphene obtained *via* electrochemically exfoliation method (EEG) with Keplerate type polyoxometalate decorated linear surfactants composite (Mo_{132}-DTAB-EEG). The synthetic approach combined with electrical measurements revealed interesting properties in terms of potential supercapacitor applications.

The main experimental parts schematically presented in Figure 3 involve:

1. Synthesis of graphene oxide-branched polyethyleneimine hybrid material (BPEI-GO) for removal heavy metal ions (Pb^{2+}, Cd^{2+}, Cu^{2+}) from aqueous solution.
2. Preparation of graphene oxide-aminosilica mesoporous composite (SiO_2NH_2-GO) for fast and efficient sequester organic cationic dyes (MB-methylene blue, MV-methylene violet, RhB- Rhodamine B).
3. Structural and electrical properties of electrochemically exfoliated graphene modified with surfactant encapsulated cluster (Mo_{132}-DTAB-EEG) as advanced electrode for supercapacitors application.

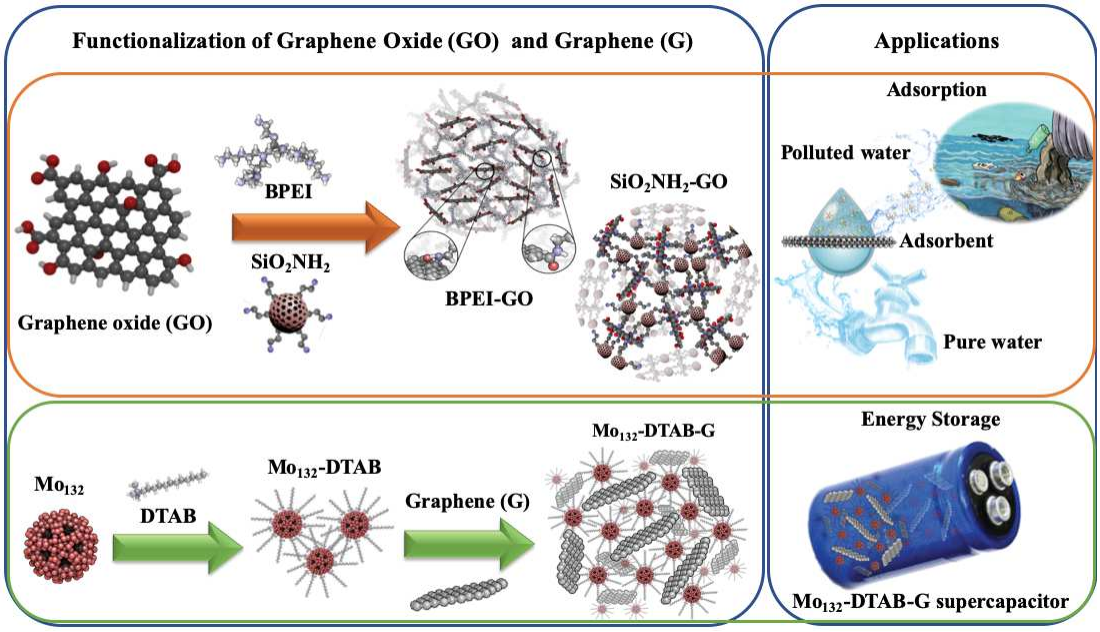

Figure 3. Schematic representation of the projects concern in doctoral dissertation.

Exploration on the structure and properties of the new functionalized 2DMs produced *via bottom-up* approach and achieving precise control over their properties are key aspects to reveal their potential and to allow their integration in novel daily life equipment. In the first experimental section, the most important strategies involve

development of novel high-performance adsorbent (BPEI-GO) prepared *via* covalent modification of graphene oxide with polymer containing amine moieties (BPEI - branched polyethyleneimine), which was characterized by high stability, high specific surface area and high affinity towards various chemical substances. Introduction of system with substituted amino groups is one of the most commonly used methods of GO covalent modification, which was used in the above work. The growth of 2D covalently functionalized architectures with a high degree of functionalization will be attained by exploring the functionalization of GO through the ring-opening reaction of epoxy groups. The synthetic approach was combined with a multiscale physico-chemical characterization of the produced materials by means of techniques such as Raman spectroscopy, scanning electron microscopies (SEM), X-ray photoelectron spectroscopy (XPS) and flame atomic absorption spectrometry (FAAS) used to adsorption measurements. After detailed spectro-structural characterizations, amine derivatives of GO were directly used in adsorption processes in aqueous solutions of heavy metal salts (Pb^{2+}, Cd^{2+}, Cu^{2+}). The maximum adsorption capacity (q_{max}) defined as the amount of pollutant (ions) captured by the 1 gram of adsorbent, was determined using two commonly isothermal models: Langmuir and Freundlich. Precise analyzes of adsorption properties confirmed that the enrichment of GO with additional coordinating pockets in the BPEI-GO system resulted in an adsorption of unprecedently high values (with respect to carbonaceous materials) of q_{max} for heavy metal ions (Cu^{2+} - 1096 mg g^{-1}, Cd^{2+} - 2051 mg g^{-1}, Pb^{2+} - 3390 mg g^{-1}). This work also determined kinetic and thermodynamic parameters that confirmed the spontaneous and exothermic nature of the adsorption process. It was shown that there is a possibility of effective regeneration of adsorbents in the presence of acid solutions (0.1 M EDTA and/or 0.1 M HNO_3), which is necessary for the practical use of sorption material on a larger scale.

Environment protection by removal of diverse contaminant from aqueous solution is a topical field of science as it will provide a key contribution to the improvement of people's quality of life by offering concrete solutions towards food safety, environmental and biohealth monitoring (as early diagnostics and continuous monitoring of diseases). Recent studies have revealed that GO and functionalized graphene oxide (fGO) holds a great potential as an active material for removal cationic dyes from water. Thanks to its unique chemical and physical properties, fGO can interact with the pollutant adsorbed on

its surface. The second experimental part is dedicated to the investigation of newly obtained compounds based on modified GO by aminosilica (SiO_2NH_2) and their adsorption properties with respect to selected cationic dyes. Similarly, to previously presented methodology, the growth of 2D covalently functionalized architectures with a high degree of functionalization was attained by exploring the functionalization of GO through the condensation reaction on epoxy groups. The SiO_2NH_2-GO composite is characterized by high q_{max} values for organic dyes (RhB - 358 mg g^{-1}, MB - 300 mg g^{-1}, MV - 178 mg g^{-1}) and a high parameter of the adsorption reaction rate, which found direct application in the SPE process. This part also determined kinetic and thermodynamic parameters that confirmed the spontaneous and exothermic nature of the adsorption process. It was shown that there is a possibility of effective regeneration of adsorbents in the presence of 0.1 M HCl, which is necessary in the practical use of sorption material on a larger scale. Both experimental parts present a novel approach combining supramolecular and dynamic covalent chemistry methods aimed at forming porous and functional adsorbents exhibiting high affinity towards various types of contaminants.

Finally, in the last experimental section of this thesis, we have exploited electrochemically exfoliation method for the production of graphene (EEG) in liquid media. This method is a recently developed approach for the large scale and fast production graphene. We involved the use of molecular systems, *e.g.* surfactant encapsulated cluster (SEC) in combination with 2DMs (EEG). The main goal of this work concerns exploiting the electrical properties of modified graphene with Keplerate-type polyoxometalate surfactant encapsulated cluster (Mo_{132}-DTAB) by non-covalent interactions in the context of potential application as supercapacitors. Polyoxometalates belong to an interesting family of inorganic compounds with nanometric dimensions consisting of two main subunits: transition metal ions on the highest oxidation state (Mo^{+6}, V^{+5}, W^{+6}, Nb^{+5}) and terminal oxygen atoms that act as a bridge for other ions and ligands. Due to the high molecular weight, high negative charge and very good solubility in polar solutions, POMs have interesting catalytic, photochemical and electrical properties. In addition, the POMs possess ability to adsorb alkali metal ions (including Na^+, Li^+), which makes them promising platforms for building advanced electrical materials. Therefore, initially the project was targeted on the investigation of our material towards alkali metal sorption. However, after careful analyses including

e.g. adsorption properties, the project has been altered because of weak adsorption capacity in comparison to the starting materials. Nevertheless, accurate physicochemical analysis (HR-TEM - high-resolution transmission electron microscopy, XRD - X-ray diffraction, XPS) confirmed that formation of stable Mo_{132}-DTAB-EEG material was realized. Porous, three-dimensional systems of Mo_{132}-DTAB-EEG synergistically combine with each other a POM redox properties and high electrical conductivity of graphene. The obtained results show that such systems have interesting electrical properties and may find potential application in the production of supercapacitors.

In conclusion, this doctoral dissertation mostly focuses on the issues related to the adsorption of pollutants by functionalized GO and explores the knowledge about molecular hybrids based on EEG. Apart from the novelty aspects regarding the production of modified two-dimensional materials, we could demonstrate the following structure/property rationale:

- Covalent modification of GO with an organic polymer (BPEI) very favourably affects the efficiency of the adsorption process. The maximum adsorption capacity (q_{max}) values for heavy metal ions significantly highlight this material in comparison to the majority of known carbon adsorbents.

- Functionalization of GO with mesoporous aminosilica leads to obtaining an efficient and rapid adsorbent (SiO_2NH_2-GO) of organic cationic dyes (MB, RhB, MV). The material has been successfully used as a column filler in the SPE process, thus enabling very fast purification of water in continuous flow.

- The family of Keplerate-type polyoxometalates are a very interesting group of inorganic compounds that can form stable molecular hybrids with cationic surfactants based on electrostatic interactions. Functionalization of electrochemically exfoliated graphene (EEG) using the POM-surfactant subunits (Mo_{132}-DTAB) proved that this type of organic-inorganic hybrids material is very stable and have interesting electrical properties with potential application in the production of supercapacitors.

Résumé en Français

Les nanotechnologies sont considérées comme l'un des domaines les plus prometteurs de la science et de la technologie; son développement continu devrait permettre d'ouvrir de nouvelles opportunités pour les chercheurs du monde entier et d'améliorer la qualité de vie de la population. Les nanotechnologies créent des systèmes fonctionnels à l'échelle nanométrique au niveau moléculaire. Les progrès réalisés dans les secteurs technologiques et industriels apportent, outre de nombreux avantages, des problèmes sévères. L'un d'eux est la pollution de l'environnement. La large gamme de contaminants rejetée dans l'eau, le sol et l'air nécessite la mise au point de techniques permettant d'éliminer ces facteurs indésirables et nocifs. L'adsorption est l'un des processus les plus importants pour améliorer la qualité, et plus particulièrement, la propreté des eaux souterraines et des eaux usées, ce qui a un impact considérable sur la protection de l'environnement. Les processus d'adsorption sont connus depuis longtemps. De nos jours, divers nanomatériaux sont produits en continu et ensuite testées pour leurs propriétés et leur aptitude industrielle pour ce qui est de leur grande efficacité d'élimination des polluants, à un faible coût et avec la possibilité d'être régénéré. Cependant, leur impact sur l'environnement et sur tous les organismes vivants, y compris la santé humaine, reste mal compris. La compréhension complète de la nature des nanomatériaux nécessite une approche interdisciplinaire et des connaissances non seulement dans le domaine de l'ingénierie des matériaux, mais également dans les domaines de la physique, de la chimie, de la biologie et de la médecine.

Récemment, le graphène et son dérivé l'oxyde de graphène (GO), sont en train de devenir un des matériaux de faible dimension les plus développés qui soient et font l'objet d'une attention toute particulière dans les laboratoires de recherche académiques et industriels. Ces matériaux bidimensionnels (2DM) dotés de propriétés physicochimiques uniques (par exemple, une conductivité électrique et thermique exceptionnelle) ont montré un grand potentiel en tant que composants de capteurs, de supercondensateurs et de plates-formes d'adsorption de divers polluants en milieu aqueux.

L'isolement du graphène sous forme de monocouche en 2004 par A. Geim et K. Novoselov, suivi du prix Nobel de physique en 2010, a suscité un intérêt croissant pour le développement d'une grande variété d'applications technologiques à base de graphène. Le graphène, une monocouche de graphite, contient des atomes de carbone hybrides sp^2 disposés en un réseau cristallin à deux dimensions sous forme de nid d'abeille (Figure 1). Grâce à ces caractéristiques, le graphène peut être utilisé dans une large gamme d'applications pratiques, y compris l'ingénierie énergétique (circuits électroniques flexibles, batteries solaires, écrans tactiles, photodétecteurs), l'optoélectronique, le stockage d'énergie et même la purification de l'eau à l'aide de méthodes basées sur des membranes. La structure unique de cette couche de carbone épaisse d'un atome donne des propriétés physico-chimiques spécifiques, notamment une grand ratio surface sur volume, une excellente résistance mécanique et une conductivité électrique élevée. La « ruée vers le graphène » a déclenché de nouvelles tendances en chimie des matériaux et, sans surprise, d'autres 2DM sont devenus un nouveau sujet de recherche passionnant pour de nombreux scientifiques du monde entier.

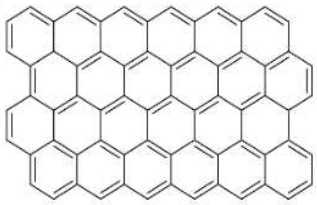

Figure 1. Graphène.

Cependant, pour tirer pleinement parti du potentiel des matériaux liés au graphène, l'amélioration des connaissances sur la production de graphène à l'échelle industrielle avec une très haute qualité est nécessaire. Il convient de noter qu'à la fois la structure et les propriétés du graphène tels que comme le nombre de couches, la qualité et la taille des bords dépendent principalement du processus de production. Il existe de nombreuses technologies utilisées pour la production de graphène, qui peuvent être divisées en deux approches principales: l'approche *top-down* et *bottom-up*. La première repose sur la miniaturisation des systèmes existants dans les processus de délamination du matériau de base en utilisant des facteurs externes tels que les ultrasons, le broyage mécanique ou par électrochimie. Jusqu'à présent, la méthode la plus couramment utilisée pour produire des feuillets de graphène de haute qualité est la méthode du «scotch-tape», qui a été exploitée pour isoler ce 2DM pour la première fois. Malheureusement, cette méthode est difficilement exploitable dans la production à grande échelle, limitant ainsi toute application technologique à grande échelle. La dernière approche consiste à produire des via l'autoassemblage de molécules ou d'atomes individuels dans lors de processus tels

que le dépôt chimique en phase vapeur (CVD) sur des substrats métalliques ou par croissance épitaxiale sur du carbure de silicium (SiC). Cette approche est souvent utilisée car elle permet de mieux contrôler les processus impliqués, et de synthétiser un matériau à deux dimensions présentant une morphologie plus uniforme avec nombre relativement limité de défauts. Néanmoins, les améliorations ultérieures de l'approche *bottom-up* sont nécessaires pour répondre à l'exigence de fabrication industrielle, à savoir un faible coût de production, une reproductibilité et une qualité élevées.

Le graphène peut être soumis à diverses modifications basées à la fois sur la formation de liaisons covalentes et sur des interactions non covalentes. L'un des matériaux les plus populaires obtenus à la suite d'une modification covalente est l'oxyde de graphène (GO), qui présente de nombreux groupes fonctionnels riches en oxygène, identifiés principalement sous la forme de groupes hydroxy et époxy sur le plan de base et de groupes carbonyle aux bords de la feuille. (Figure 2). La présence de groupes fonctionnels riches en électrons sur GO influence de manière significative l'hydrophilie et la densité élevée de la charge négative. Grâce à ces propriétés uniques, GO peut facilement interagir avec des composés organiques et des ions métalliques par le biais d'interactions dipolaires ou électrostatiques fortes, ce qui a été largement utilisé dans les processus d'adsorption. De plus, la grande diversité de groupes oxygène sur la surface GO fait de ce matériau un candidat idéal pour une fonctionnalisation covalente ultérieure impliquant des réactions organiques simples.

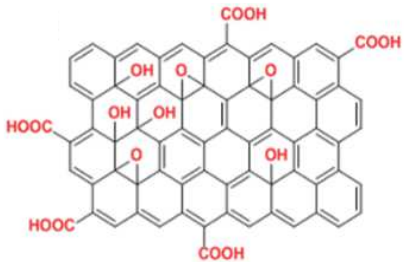

Figure 2. L'oxyde de graphene.

L'objectif scientifique de cette thèse concerne la synthèse de matériaux bidimensionnels fonctionnalisés (graphène et GO) en utilisant des approches permettant une production en série tout en procédant à caractérisation physico-chimique complète, avec un accent particulier sur les propriétés d'adsorption et de stockage d'énergie. Nous nous sommes efforçés de surmonter certaines difficultés pour l'application pratique des adsorbants à base 2D tels que les difficultés rencontrées dans l'augmentation de l'échelle de production, de la méthodologie de synthèse et de la reproductibilité limitée qui en découle, lors le processus d'adsorption. L'un des objectifs principaux est lié à l'approfondissement des connaissances de la relation structure-

propriétés dans les matériaux présentés, qui est une étape obligatoire pour leurs applications futures. La recherche scientifique menée dans le cadre de la thèse de doctorat peut être divisée en trois parties expérimentales principales présentées ci-dessous, les deux premières étant axées sur la production de nouveaux adsorbants à base d'oxyde de graphène utilisant une réaction de condensation simple et efficace entre des groupes fonctionnels de type oxygène à la surface de GO et un groupe d'ancrage de type amine. Une analyse physico-chimique précise a prouvé une haute efficacité d'adsorption vis-à-vis des ions de métaux lourds, lorsque nous utilisons comme agent de fonctionnalisation un polymère ramifié (polyéthylèneimine ramifié BPEI). À leur tour, l'oxyde de graphène modifié par des nanoparticules d'aminosilicates (SiO_2NH_2-GO) présente une valeur élevée de la vitesse cinétique, qui a été directement utilisée dans l'adsorption des colorants cationiques lors d'un processus d'extraction en phase solide (SPE). La dernière partie expérimentale s'est concentrée sur les utilisations possibles des 2DM fonctionnalisés en électronique. Premièrement, nous avons combiné le graphène obtenu par la méthode d'exfoliation électrochimique (EEG) avec un composite de surfactant linéaire décoré par des polyoxométallate de type Keplerate (Mo_{132}-DTAB-EEG). L'approche synthétique combinée à des mesures électriques a révélé des propriétés intéressantes en termes d'applications de supercondensateurs.

Les principales parties expérimentales présentées schématiquement Figure 3 concernent :

1. La synthèse d'un matériau hybride polyéthylèneimine ramifié (oxyde de graphène) (BPEI-GO) pour l'élimination des ions de métaux lourds (Pb^{2+}, Cd^{2+}, Cu^{2+}) de l'eau.

2. La préparation du composite mésoporeux oxyde de graphène-aminosilique (SiO_2NH_2-GO) pour capter rapidement et efficacement des colorants organiques cationiques (MB-méthylène bleu, MV-méthylène violet, RhB-Rhodamine B).

3. L'étude des propriétés structurelles et électriques du graphène électrochimiquement exfolié, modifié encapsulé dans un tensioactif (Mo_{132}-DTAB-EEG) servant d'électrode avancée pour des applications de supercondensateur.

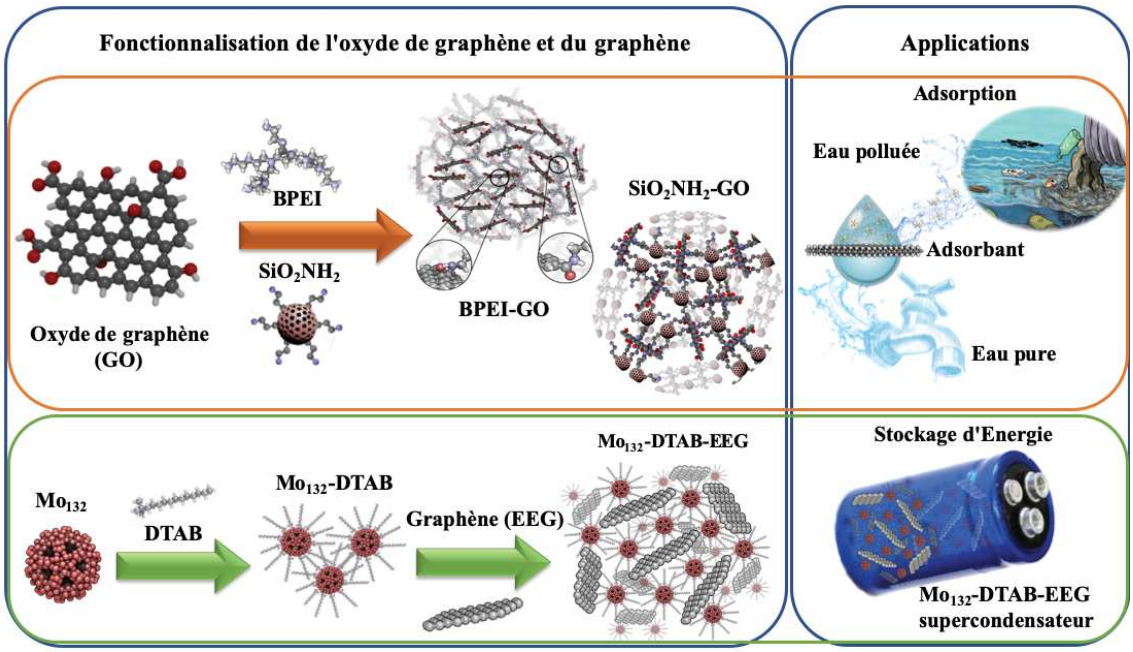

Figure 3. Représentation schématique des principales hypothèses de synthèse de la thèse.

L'exploration de la structure et des propriétés de nouveaux 2DM fonctionnalisés produits *via* une approche *bottom-up* et la réalisation d'un contrôle précis de leurs propriétés sont des aspects clés pour révéler leur potentiel et permettre leur intégration dans de nouveaux équipements de la vie quotidienne. Dans la première partie expérimentale, les stratégies les plus importantes impliquent le développement d'un nouvel adsorbant à haute performance (BPEI-GO) préparé par modification covalente de l'oxyde de graphène avec un polymère contenant des fractions amine (BPEI - polyéthylèneimine ramifiée), caractérisé par une stabilité élevée, une surface spécifique et forte affinité pour diverses substances chimiques. L'introduction d'un système avec des groupes amino substitués est l'une des méthodes de modification covalente de GO les plus couramment utilisées, et à donc été employé dans le travail susmentionné. La croissance d'architectures 2D fonctionnalisées de manière covalente avec un degré élevé est obtenue en explorant la fonctionnalisation de GO par la réaction d'ouverture de cycle des groupes époxy. L'approche synthétique a été associée à une caractérisation physico-chimique multi-échelles des matériaux produits à l'aide de techniques telles que la spectroscopie Raman, la microscopie électronique à balayage (SEM), la spectroscopie photoélectronique à rayons X (XPS) et la spectrométrie d'absorption atomique à flamme (FAAS) utilisées pour les mesures d'adsorption. Après

des caractérisations spectro-structurelles détaillées, les dérivés aminés de GO ont été directement utilisés dans des processus d'adsorption dans des solutions aqueuses de sels de métaux lourds (Pb^{2+}, Cd^{2+}, Cu^{2+}). La capacité maximale d'adsorption (q_{max}) définie comme la quantité de polluant (ions) capturée par 1 gramme d'adsorbant a été déterminée à l'aide de deux modèles isothermes : Langmuir et Freundlich. Des analyses précises des propriétés d'adsorption ont confirmé que l'enrichissement de GO en sites de coordination supplémentaires dans le système BPEI-GO engendrait des valeurs d'absorption sans précédents (pour ce qui est des matériaux carbonés) de q_{max} pour les ions de métaux lourds (Cu^{2+} - 1096 mg g^{-1}, Cd^{2+} - 2051 mg g^{-1}, Pb^{2+} - 3390 mg g^{-1}). Ce travail a également permis de déterminer les paramètres cinétiques et thermodynamiques confirmant le caractère spontané et exothermique du processus d'adsorption. Il a été démontré qu'il était possible de régénérer efficacement les adsorbants en présence de solutions acides (0,1 M EDTA et / ou 0,1 M HNO_3), ce qui est nécessaire pour une utilisation pratique du matériau de sorption à plus grande échelle.

La protection de l'environnement par l'élimination de divers contaminants des solutions aqueuses est un domaine d'actualité scientifique car elle apportera une contribution essentielle à l'amélioration de la qualité de vie de la population, en proposant des solutions concrètes pour la surveillance de la sécurité sanitaire des aliments, de l'environnement et de la biosanté (diagnostic précoce et surveillance continue des maladies). Des études récentes ont révélé que le GO et l'oxyde de graphène fonctionnalisé (fGO) présentaient un grand potentiel en tant que matériaux actifs pour l'élimination des colorants cationiques de l'eau. Grâce à ses propriétés chimiques et physiques uniques, le fGO peut interagir avec le polluant adsorbé à sa surface. La deuxième partie expérimentale est consacrée à l'étude des composés nouvellement obtenus à base de GO modifié par l'aminosilicate (SiO_2NH_2) et leurs propriétés d'adsorption vis-à-vis de colorants cationiques sélectionnés. De même, comme dans la méthodologie présentée précédemment, la croissance d'architectures 2D fonctionnalisées de manière covalente avec un degré élevé de fonctionnalisation a été obtenue en employant la fonctionnalisation de GO par la réaction de condensation sur des groupes époxy. Le composite SiO_2NH_2-GO est caractérisé par des valeurs de q_{max} élevées pour les colorants organiques (RhB - 358 mg g^{-1}, MB - 300 mg g^{-1}, MV - 178 mg g^{-1}) ainsi qu'un paramètre élevé de la vitesse de réaction d'adsorption, ce qui lui trouve une application directe dans

le processus SPE. Ce travail a également permis de déterminer les paramètres cinétiques et thermodynamiques qui ont confirmé la nature spontanée et exothermique du processus d'adsorption. Il a été démontré qu'il existe une possibilité de régénération efficace d'adsorbants en présence de HCl 0,1 M, ce qui est nécessaire dans l'utilisation pratique du matériau de sorption à plus grande échelle. Les deux parties expérimentales présentent une nouvelle approche combinant des méthodes de chimie covalente supramoléculaire et dynamique visant à la formation d'adsorbants poreux et fonctionnels présentant une forte affinité pour divers types de contaminants.

Enfin, dans la dernière partie expérimentale de cette thèse, nous avons exploité la méthode d'exfoliation électrochimique pour la production de graphène (EEG) en milieu liquide. Cette méthode est une approche récemment développée pour la production de graphène à grande échelle de manière rapide. Nous avons utilisé de systèmes moléculaires tels que des clusters de surfactant (SEC) en combinaison avec le 2DM (EEG). L'objectif principal de ce travail consiste en l'exploitation des propriétés électriques du graphène modifié avec un cluster encapsulé dans un tensioactif polyoxométalate de type Keplerate (Mo_{132}-DTAB) par des interactions non covalentes dans le contexte d'applications potentielle tels que des supercondensateurs. Les polyoxométallates appartiennent à une famille intéressante de composés inorganiques de dimensions nanométriques constitués de deux sous-unités principales : les ions de métaux de transition sur l'état d'oxydation le plus élevé (Mo^{+6}, $V^{+5,}$ W^{+6}, Nb^{+5}) et les atomes d'oxygène terminaux agissant comme un pont pour d'autres ions et ligands. En raison de leur poids moléculaire élevé, de la charge négative élevée et de la très bonne solubilité dans les solutions polaires, les POM ont des propriétés catalytiques, électriques et photochimiques intéressantes. En outre, les POM possèdent la capacité d'adsorber les ions de métaux alcalins (y compris Na^+, Li^+), ce qui en fait des plateformes prometteuses pour la construction de matériaux électriques avancés. Par conséquent, le projet visait initialement à étudier notre matériau en vue de la sorption des métaux alcalins. Cependant, après des analyses minutieuses comprenant par exemple les propriétés d'adsorption, le projet a été modifié en raison de la faible capacité d'adsorption par rapport aux matériaux de départ. Néanmoins, une analyse physico-chimique précise (HR-TEM - microscopie électronique à transmission à haute résolution, DRX - diffraction des rayons X, XPS) a confirmé la formation d'un matériau stable Mo_{132}-DTAB-EEG. Les systèmes tridimensionnels poreux de Mo_{132}-DTAB-EEG

combinent de manière synergique les propriétés redox POM et la haute conductivité électrique du graphène. Les résultats obtenus montrent que ces systèmes ont des propriétés électriques intéressantes et peuvent trouver une application potentielle dans la production de supercondensateurs.

En conclusion, cette thèse de doctorat porte principalement sur les problèmes liés à l'adsorption de polluants par le GO fonctionnalisé et explore les connaissances sur les hybrides moléculaires basés sur l'EEG. Outre les aspects liés à la nouveauté concernant la production de matériaux bidimensionnels modifiés, nous pourrions démontrer la logique des relations structure/propriété suivante:

- La modification covalente de GO avec un polymère organique (BPEI) affecte très favorablement l'efficacité du processus d'adsorption. Les valeurs de capacité maximale d'adsorption (q_{max}) pour les ions de métaux lourds soulignent de manière significative ce matériau par rapport à la majorité des adsorbants à base de carbone connus.

- La fonctionnalisation de GO avec l'aminosilicate mésoporeuse (SiO_2NH_2) conduit à l'obtention d'un adsorbant efficace et rapide des colorants organiques cationiques (MB, RhB, MV). Le matériau a été utilisé avec succès comme charge de colonne dans le procédé SPE, permettant ainsi une purification très rapide de l'eau en flux continu.

- La famille des polyoxométallates de type Keplerate constitue un groupe très intéressant de composés inorganiques pouvant former des hybrides moléculaires stables avec des tensioactifs cationiques à basé sur des interactions électrostatiques. La fonctionnalisation du graphène électrochimiquement exfolié (EEG) avec les sous-unités de surfactant POM (Mo_{132}-DTAB) a prouvé que ce type de matériau hybride organique-inorganique est très stable et présente des propriétés électriques intéressantes pouvant être utilisées dans la production de supercondensateurs.

Table of contents

Chapter 1.

Introduction

In the last decade the research on two-dimensional materials (2DMs) has attracted great attention due to their remarkable properties, which render them appealing platforms for many classical fields of research such as chemistry and condensed matter physics, and it is particularly blooming in the interdisciplinary realms of nanoscience and materials science, including energy generation and storage,[1,2] optical devices[3] and chemical sensors.[4-6] Among their different unique properties, 2DMs feature extremely high surface area-to-volume ratio and ultra-high surface sensitivity to the environment, being key characteristics for applications in chemical sensing. Moreover, 2DMs' superior electrical and optical properties, combined with excellent mechanical characteristics such as flexibility and robustness, make these materials ideal components for the fabrication of a new generation of high-performance chemical sensors. Depending on the specific device, 2DMs can be tailored to interact with various chemical species at the noncovalent level making them powerful platforms for fabricating devices expressing a high sensitivity towards detection of various analytes including gas, ions and small biomolecules.

The history of graphene, which is one of the most important 2DM began more than 170 years ago, when the German scientist Schafhaeutl in 1840 described the first exfoliation of graphite using nitric and sulfuric acids.[7] In turn, Sir Benjamin Collins Brodie (2nd Baronet) in 1859 fabricated and described the highly lamellar structure of graphite oxide.[8] A good understanding over their structures was obtained only in early 1930s with the introduction of X-ray diffraction techniques. Nearly 30 years later, Boehm and co-workers observed by electron microscope ultrathin carbon film obtained *via* reduction of graphite oxide.[9] Unfortunately, there were experimental limitations regarding the isolation due to the thermodynamical instability of the material. However, after more than two decades Boehm, Setton and Stumpp proposed the term "graphene" for the determination of a single graphite layer. While occasional attempts to study graphene can be traced back (Figure 1.1), the ground-breaking experiments by Geim and

Novoselov on the fabrication, isolation and study of the outstanding physical properties of graphene using mechanical exfoliation method were conducted in 2004,[10] for what they were awarded the Nobel Prize in Physics in 2010.

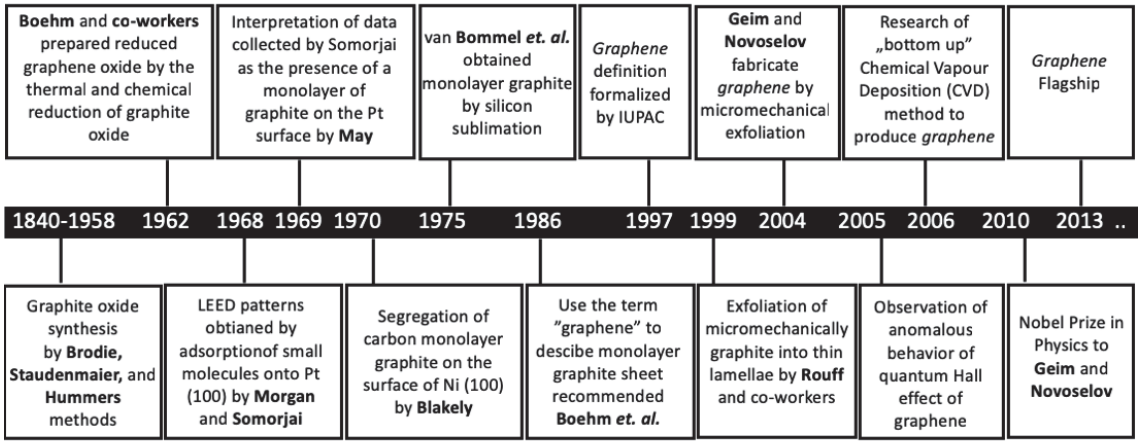

Figure 1.1. Roadmap of graphene. Reproduced with permission. [11]

Graphene is defined as a single layer of sp^2 hybridized carbon atoms, arranged in a honeycomb crystal lattice. The sp^2 hybridization in graphene sheets is responsible for the generation of a flat rhombohedral structure, in which carbon atoms are connected by strong σ bonds which affect their mechanical strength. In single- and multi-layered structure of graphene three valence electrons are sp^2 hybridized, whereas the last valence electron creates π bond responsible for electron transport behavior and interaction between graphene layers.[12, 13] One-atom thick graphene is arguably the most glorified material of the last decade; it's fascinating physico-chemical properties have spread beyond the academic community and drawn the attention of world-leading chemical and materials oriented companies as well as public institutions, especially since graphene-based products are going on sale.[14] This so called 'graphene rush' has triggered the pursuit of atomically thin sheets of other layered materials, such as semiconducting transition metal dichalcogenides (TMDCs),[15] hexagonal boron nitride and, more recently, MXenes which include transition metal carbides, nitrides and carbonitrides,[16] and phosphorene.[17-19] Graphene can be seen as a single layer of graphite, and while the latter behaves metallically, graphene is a semi-metal featuring a unique zero band gap.[20] In addition, graphene possesses many extraordinary properties including excellent thermal (above 3000 W/mK)[21] and electrical (~6000 S/m) conductivity.[22] Single two-dimensional

graphene layer exhibits the mobility of electrons of ~10,000 cm^2 V^{-1} s^{-1},[10] while theoretical calculations on a single layer without defects show that it can reach up to 200,000 cm^2 V^{-1} s^{-1},[23] which is even better than copper – one of the superior conductive materials. Additional features that distinguish this 2DM are: extremely high specific surface area (up to 2630 m^2/g), a Young's modulus of 1 TPa, essential tensile strength of 130 GPa,[24] and possibility to further chemical functionalization, which allows to control and design its specific properties. Graphene is particularly promising for sensing by virtue of its extremely high conductivity, and its large surface area. Despite being only one atom thick graphene is impermeable in its pristine form, effectively blocking the passage of even the smallest molecules.[25] The impermeable nature of graphene has triggered extensive studies on its application as a barrier for liquid and gas permeation,[26, 27] as well as on its use as shielding material protecting metallic surfaces against corrosion.[28] Such unique property of graphene has triggered extensive efforts towards the use graphene and other 2DMs for the design of ultrathin water-separation membranes and as platforms to absorb (heavy) metal ions. The chemical and structural diversity of these 2DMs, whose properties are indeed dictated by their dimensionality,[29] offer immense opportunities for fundamental and applied research. Different optical and electronic properties may be obtained ranging from the exceptional semi-metallic conductivity of graphene[30, 31] to the semiconducting characteristics of some transition metal dichalcogenides (TMDs) that possess sizeable and tuneable bandgaps, which change from indirect (bulk material) to direct (single layer form).[32] Graphene is also extremely appealing in the field of energy storage applications as an electrochemical double-layer supercapacitors,[2,33] cathodes/anodes in batteries[34] as well as sensors, ranging from gas, metal (alkali and heavy metal), to biologically relevant molecules (*e.g.* glucose and DNA). Noteworthy, unlike classical digital sensors, 2DMs-based sensors do not possess physical gates for selectively reacting to the targeted species (gas molecules,[35,36] metal ions or biomolecules[37, 38]).

To take full advantage of the potential of graphene materials, knowledge improvement on the production of graphene on an industrial scale with very high quality is needed. Noteworthy, both the structure and properties of graphene including the number of layers, quality and lateral size are mainly dependent on the undertaken production route. Additionally, 2DMs obtained by different synthetic approaches can be

very different from the pristine form due to the presence of defects which leads to different behaviors and consequently different performance in the final sensing device. There are many technologies used for 2DMs production, which can be divided into two main panels: *top-down* and *bottom-up* as illustrated on Figure 1.2. The *top-down* approach is based on the miniaturization of existing systems in the processes of delamination of the base material using external factors *e.g.* ultrasounds, mechanical grinding or electrochemistry. The graphene layers are most commonly exfoliated from the bulk graphite *via* the "scotch tape" method.[39] Unfortunately, the flakes produced with such a method have high quality, yet very limited lateral size. On the other hand, the *bottom-up* method consists of the production of nanostructures as a result of self-assembly of individual molecules or atoms in the process of *e.g.* chemical vapor deposition (CVD) on metal substrates or epitaxial growth on silicon carbide (SiC). This approach is often used because it allows for better process control and synthesis of a two-dimensional material with a more uniform morphology and a relatively small number of defects. CVD graphene is usually obtained through a catalytical decomposition of hydrocarbons (usually methane) on a hot (~1000 °C) metal surface (Cu, Ni and Co) under vacuum.[40] Since the graphene grows directly onto the metal surface, different techniques have been developed to transfer it onto dielectric substrates.[41] Epitaxial growth is another method to obtain large and uniform high-quality graphene films.[42] Typically, SiC is heated under high vacuum at high temperature (> 1200 °C); this allows the surface silicon atoms to evaporate, yielding the rearrangement of the carbon atoms to form a graphene layer. Mechanical exfoliation makes it possible to obtain high quality graphene monolayers, but the very low throughput and yield of the so-obtained graphene flakes hinder any industrial application, while CVD and epitaxial grow allow to obtain large-area graphene monolayers, although the production costs remain high. The production of GO followed by its reduction is a high throughput, easily scalable and cheap method to obtain large amount of graphene.[43] It is however fair to note that reduced graphene oxide (rGO) is less conductive and have numerous structural defects and residual functional groups compared to pristine graphene, yet their presence could offer a clear route for improvement of the sensing capabilities as already discussed.[44] Similarly GO has a higher number of oxygen functional groups, but it is an electrical insulator.[43] A compromise in terms of quality of the flakes and yield is offered by the liquid-phase exfoliation (LPE) of

graphite: graphene flakes dispersed in water/surfactants or organic solvents can be obtained with the aid of ultrasonication,[45,46] shear mixing[47] or electrochemical approach.[48]

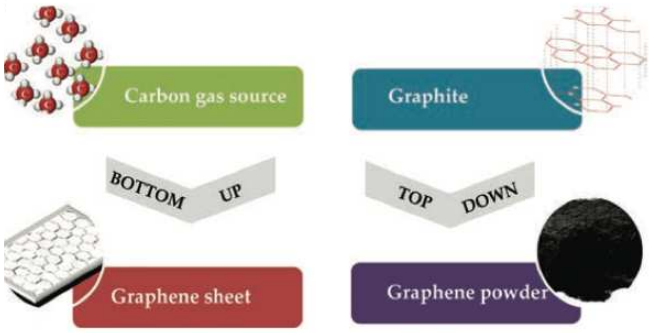

Figure 1.2. *Bottom-up* and *top-down* approaches Reproduced with permission.[49]

The interaction between 2DMs sheets and molecules/ions is accompanied by the adjustment of the properties of both initial components. Such interaction can occur *via*: a) the physisorption of molecular building blocks onto basal plane of 2DMs sheets through non-covalent interactions or b) the chemisorption of reactive species undergoing chemical reactions with 2DMs to form covalent bonds onto their basal planes. In the field of sensing since non-covalent interactions may be preferred when a quick response and a fast recovery rate is required (*i.e.* real-time monitoring), while the weakness of the bond can be disadvantageous when biomolecules (*i.e.* enzyme) need to be immobilized on the surface and to be stable during the assay (*i.e.* in buffered saline solution), thus a covalent bond can be more suitable. The most commonly used modifying agent of graphene include organic polymers, inorganic hybrid materials, surfactants, small aromatic molecules and even biomolecules.[50, 51] In addition, the large diversity of oxygen groups on the GO surface makes this material an ideal candidate for further covalent functionalization involving simple organic reactions. One of the most commonly used methods of chemical functionalization of GO is epoxy-ring opening reaction induced *via* free electron pairs of organic molecules.[52-54] The organic moieties used in functionalization are mostly based on amino-containing groups including polypyrrole,[55] hyperbranched polyamine ,[56] poly(allylamine) hydrochloride,[57] polyamidoamine dendrimers,[58] poly(acrylamide),[59] poly(N-vinyl- carbazole),[60] benzidine,[61] glycine,[62] aminosilica[63] *etc*. Additionally, many research groups have investigated numerous hybrid

materials that include combinations of GO with iron oxide,[64-66] chitosan,[9, 35, 37,] ethylenediaminetetraacetic acid,[67, 68] *etc*.

The physisorption of molecules onto surface depends on the nature of both analyte and surface; for example, graphene is an extended honeycomb network of sp^2 hybridized carbon atoms characterized by a long-range π-conjugation. Consequently, noncovalent intermolecular interactions involving π-systems are pivotal in the recognition events since subtle changes in the electronic characteristics of the π systems can lead to modifications of the structure and properties,[69, 70] as well as they may enhance the stability of the physisorbed compounds as observed for proteins, enzyme−drug and DNA−protein complexes.[71, 72] The understanding of the nature of π-complexes has indeed high importance for graphene based sensors since the gas−π interaction,[73] H−π interaction,[74-77] π−π interaction,[78-83] cation−π interaction,[84-91] and anion−π interaction[78, 92-102] possess different strength which is determined by a combination of attractive and repulsive forces. Compared to graphene, the family of TMDs, which includes molybdenum disulfide (MoS_2), tungsten disulfide (WS_2), molybdenum diselenide ($MoSe_2$) and tungsten diselenide (WSe_2) as the most studied, has not been investigated extensively from this point of view. More generally, 2DMs produced by means of different methods can be very different due to the presence of structural defects which leads to different behaviours, and consequently different performance in the final sensing device. In the last years the term "defects"[103-107] has become a keyword in the field of 2DMs as the presence of defects play a major role in modifying the properties of 2DMs. Although it might have a negative implication when one targets applications in fast opto-electronics, well-designed defects might lead to new and tuneable properties opening a wide range of interesting applications that pristine materials cannot afford such as enhanced electron transfer rate and electrochemical activity as observed for graphene based electrochemical sensors.[108] Lattice vacancies affect the electronic properties of the TMDs sheets, by lowering their charge carrier mobility and density[109, 110] as well as triggering photoluminescence[111, 112] and modifying chemical reactivity.[113] In graphene the defects within the honeycomb network of C=C, whose number depends mainly on the protocol employed for its fabrication, typically consists in point defects, *i.e.* the absence some sp^2 carbon atoms, and/or the presence of carbon atoms with sp^3 hybridization. The carbon atoms surrounding these defects are electronically perturbed thus they exhibit different

electronic structures; therefore, they are chemically activated for further chemical reactions. In other words, the presence of points defects enhances the chemical reactivity of graphene.[114] Carbon atoms with sp^2 hybridization located on graphene can react with highly reactive free radicals, such as those produced by diazonium salts[115-117] or benzoyl peroxide;[118] as well as dienophiles which react with C=C of graphene through a 1,3 dipolar cycloaddition.[119] However, a massive introduction of defects can be achieved by exposing graphite to strong oxidizing agents[120] resulting in the formation of graphite oxide. The latter when immersed in water tends to spontaneously exfoliate, into single layers of graphene oxide, due to the negative charged oxygen functionalities decorating both basal plane and edges.[121] Such material is probably the most investigated 2DM in the field of sensing[122-126] because of its ease functionalization. The negative charges on its surface can interact non-covalently with a wide range of positively charged molecules; for example, outstanding sorption properties for heavy metal cations have been reported.[127, 128] Moreover, the oxygen functionalities, which consist mostly of hydroxyl and epoxy groups exposed on the basal plane and carboxy and carbonyl functionalities located at the sheet edges,[129, 130] are extremely reactive thus allowing further modification of GO.[131, 132] Importantly, the electrical conductivity can be to a great extent restored and tuned during the reduction step of the functionalized graphene oxide (fGO)[133] making it an extremely versatile material for sensing with electrical read out. The use of defects to introduce functionalities has been also successfully extended to the family of TMDs where the presence of chalcogen deficiency can be used to decorate the surface of the 2DM with different functionalities. For example reactive sulphur vacancies in MoS_2 may simply arise during the exfoliation process[109,134] or be introduced on purpose electrochemically[135] or by ion-beam irradiation.[136] These reactive sites can readily react with sulphur-containing moieties such as alkanethiol molecules resulting into a covalent bond formation.[136-138] Alternatively, defects can be further expanded into (sub)-nanometre sized pores transforming the 2DMs into permselective membranes[139] or ultrasensitive sensors even able to sequence DNA.[140, 141] Such property can be further tuned and harnessed to achieve enhanced permselectivity by controlled chemical functionalization of both pore edges and surface in a post-process chemical treatment.[139] As already anticipated the 2D nature of such materials offers several advantages in the field of sensing since the atomic thickness provides a direct interaction of all the atoms

with the analyte while the large lateral size not only guarantees a large active surface for the sensing event, but it also facilitates the assembly of the device, as demonstrated for field-effect transistor (FETs), *i.e.* by enabling a better contact with metal electrodes and better control over the channel structures.[142] Obviously, the architecture of the sensing device depends on which properties of the 2DMs the analytes is affecting mostly as well as on the nature of both the 2DM and the analyte. Electrochemical sensors based on graphene have been probably the most investigated so far since they provide a direct electrical response[143]. Graphene offers indeed a large electrochemical window (up to 2.5 V),[122] thus enabling the detection of molecules with high reduction or oxidation potential (*e.g.* nucleic acids), and good electrocatalytic activities for many redox reactions.[144] Furthermore, due its ambipolar character, the functionalization with both electron withdrawing or donating groups can lead to chemical gating resulting in a change of conductivity of the material.[145] The combination of the atomic thickness of the 2DMs with the chemical gating that results when the surface potential is changed due to the binding of molecules has led to the generation of new FETs sensors based on 2DMs, as recently reviewed by Mao *et al.*[142] Interestingly in such a kind of sensors, 2D semiconducting materials outperform their conducting counterparts since the presence of a finite band gap decreases the initial conductance inside the channel thus improving the signal-to-noise ratio. Consequently, the performance of the device is mainly dictated by the band gap which can be tuned by defects engineering, doping, as well as by playing with the thickness of the material opening a wide range of opportunities as recently demonstrated by Cui *et al.*[146] in a phosphorene-based FET gas sensor. While a direct electrical response is generally preferred for practical applications, the interactions of the 2DMs with analytes give rise to interesting optical phenomena such as the modulation of the photoluminescent properties opening up a wide range of opportunities. Graphene and GO are known to be highly efficient fluorescence quenchers if compared to organic compounds, thus Förster resonance energy transfer (FRET) sensors have attracted increasing interest in the last years especially for biomedical applications since they can be used to measure precisely nanometre-scale distance and changes both *in vivo* and *in vitro*[147] resulting into nanobiosensors with excellent sensitivity, selectivity, and biostability.[148] Even single-layer MoS_2 nanosheet possesses high fluorescence quenching efficiency and by taking advantage of such a characteristic it has been exploited as sensing

platforms for the detection of DNA and small molecules.[149] However, the use of 2DMs in FRET is not limited to energy acceptor since a proper functionalization may result in photoluminescent flakes which can act as energy donor and be quenched by more electron deficient molecules such as nitro compounds which are common constituent to prepare powerful explosives.[150] The use of 2DMs as substrate for enhancing the Raman signals of adsorbed molecules represented a major breakthrough in the field of sensing.[151, 152] Different Raman vibrational modes can be enhanced depending on which layered material the molecule is adsorbed onto. Surface enhanced Raman spectroscopy (SERS) is mainly employed to explore the detection of chemical and biological species[153-156] due its high sensitivity (even down to single molecules)[157, 158] and the bar-code like reading that comes from the narrow vibrational bands in the Raman spectrum. Different Raman enhancement mechanisms have been proposed for different 2DMs, however, like in the previous examples, surface modification[159] as well as the thickness[160] play a fundamental role in terms of selectivity and Raman signal enhancement.

The intensive research on 2DMs for sensing application has been further motivated by their intrinsic mechanical properties such as robustness, flexibility, lightweight which makes possible the realization of portable and wearable sensors with tremendous impact on our society enabling the monitoring of the wearers' health, fitness, and their surroundings.[161] The development of wearable chemical sensors faces multiple challenges on various fronts such as power, analytical procedure, communication, data acquisition, processing and security. Nevertheless, several examples of flexible graphene-based wearable gas and chemical sensors has been recently reviewed[162] and also a wearable patch for sweat-based diabetes monitoring and feedback therapy has been reported,[163] which combines a heater, temperature, humidity, glucose and pH detection.

1.1. 2DMs based sensing of metal ions

The rapid escalation of agricultural and industrial activities as a result of the population growth is yielding a dramatic proliferation of the amount of pollutants released daily worldwide into the environment.[164-166] Metal ions and dyes in the aqueous environment have determined various diseases and seriously threaten ecosystem and public health with the rapid development of the industry in recent years.[167, 168] A great effort has been made to fabricate portable sensors for monitoring heavy metals in the environment. Within this framework also 2DMs-based materials have been integrated in different types of sensors capable of detecting heavy and alkali metal ions *via* electrical [142, 169-184] and optical outputs.[185-196] The interaction between 2DMs and metal ions have been extensively explored in the past years and as a result outstanding adsorption capabilities have been achieved, opening new avenues in the field of wastewater purification and sensing.[139] Among various approaches, those based on physisorption or chemisorption, relying on the capturing of the pollutant (*i.e.* analyte) by an adsorbent (*i.e.* receptor), are chemically programmable as they exploit supramolecular recognition events. The intensive research on 2D materials for sensing application has been further motivated by their intrinsic mechanical properties such as robustness, flexibility, lightweight which makes possible the realization of wearable sensors with tremendous impact on our society enabling the monitoring of the wearers' health, fitness, and their surroundings.[161] The development of wearable chemical sensors faces multiple challenges on various fronts such as power, analytical procedure, communication, data acquisition, processing and security; however several examples of flexible graphene-based wearable gas and chemical sensors has been recently reviewed[162] and also a wearable patch for sweat-based diabetes monitoring and feedback therapy has been reported,[163] which combines a heater, temperature, humidity, glucose and pH sensors, as well as polymeric microneedles that can be thermally activated to deliver drugs transcutaneously. The development of *ad hoc* receptors of metal ions and cationic dyes makes it possible to exploit the reversible process of adsorption and desorption as an extremely versatile strategy in a variety of environments. Moreover, by relying on the reversible nature of non-covalent interactions, the sensor can exhibit a quick response, a fast recovery rate (*i.e.* real-time monitoring) and a facile regeneration to enable its use

multiple times. 2DMs are atomically thick and possess two planar surfaces available for metal ion adsorption, thus featuring extremely high surface-to-volume ratios. In particular, GO is very interesting for the removal of metal ions due to its unique hydrophilic nature and the presence of functional groups containing oxygen atoms, which can efficiently bind the metal ions to form strong surface complexes.[128, 197] On the other hand, TMDs intrinsically possess numerous chalcogen atoms, which can act as a potential coordination sites for certain heavy metal ions. The adsorption capabilities of 2DMs will be evaluated through the maximum adsorption capacity (q_{max}) defined as the ratio between the maximum loaded mass of analyte expressed in milligrams and the mass of the absorbent expressed in grams. Among numerous factors affecting the adsorption capacity, initial concentration of the solution, phase contact time, temperature and pH are found to play a crucial role in the process of adsorption of metal ions on GO.

Alongside the capacity of pristine 2DMs to detect various analytes, extensive efforts have been devoted towards the development of 2DMs-based sensors through the non-covalent functionalization of the 2DMs with both inorganic and organic moieties which act as spacers/pillars imposing a certain distance between adjacent sheets. This results in an enhanced porosity of 2DM-based composite which determines a greater sensitivity for the analyte of choice. Such an approach enables the tailoring of the properties of 2DM-based sensors, which could preserve many of the unique characteristics of the individual 2DM sheets and benefit from the presence of (in)organic moieties. Such moieties, besides acting as separators, can by design incorporate the receptor of the analyte of choice, endowing highest selectivity in the recognition and sensing process. In this context, the fabrication of 2DM-based sensors through non-covalent interactions between individual 2DM sheets is extremely appealing, as it could result in the structures exhibiting a remarkable enhancement of sensitivity towards specific analytes.

Graphene-based materials are being considered as the most promising absorbents for capturing various heavy metal ions.[198-200] Remarkably, graphene can be easily produced in the form of GO, which displays numerous oxygen-rich functional groups such as carbonyls, epoxides, and hydroxides that act both as reactive sites for further covalent functionalization, and can interact *via* dipole-dipole or strong electrostatic interactions with the metal ions, enhancing the occurrence of adsorption event.

Conventional methods for the quantification of heavy metal ions include plasma mass spectrometry (ICP-AES), atomic absorption/emission spectroscopy (*e.g.* FAAS, UV-VIS), and polarography. To define the concentration of the remaining heavy metal ions after adsorption we should calculate the difference between the initial (C_0; mg L^{-1}) and the equilibrium (C_e; mg L^{-1}) concentration. The equilibrium sorption capacity and time-dependent capacity were determined using Equation 1:

$$q_e = \frac{(C_0 - C_e) \times V}{m_{adsorbent}} \qquad \text{(Equation 1)}$$

where: q_e - equilibrium amount of heavy metal ions adsorbed per unit mass (m) of adsorbent (mg/g), V - volume of the metal ion solution.

Among various adsorption isotherm models Freundlich and Langmuir are most commonly used for estimate the maximum adsorption capacity (q_{max}) of metal ions on both 2D and 3D carbon-based adsorbents.[58, 197, 199, 201] GO and chemically modified graphene oxide (CMGO) are considered as a promising adsorbents for the removal of heavy metal ions such as Pb^{2+}, [56, 58-60, 64-68, 128, 197, 201-222] Cu^{2+}, [58, 67, 128, 204, 205, 213, 215, 217, 222-232] Cr^{6+}, [165, 204, 221, 233-244] Cd^{2+}, [58, 128, 206, 215, 221] Hg^{2+}, [67, 215, 221, 245, 246] Ni^{2+}, [221, 247] Co^{2+}, [248] Mn^{2+}, [58] Pd^{2+}, [249] Sr^{2+}, [250] Au^{3+}, [249] As^{5+} [251] and U^{6+}. [252-254] Moreover, in order to increase the adsorption capacity and simplify the separation of the GO from water, numerous hybrid materials have been investigated and include combination of GO/CMGO with poly(acrylamide) (PAM),[59, 202] poly(*N*-vinylcarbazole) (PVK)[60], hyperbranched polyamine (HPA),[56] iron oxide (Fe_3O_4),[64-66] polyamidoamine dendrimers (PAMAMs)[58], ethylenediamine tetraacetic acid (EDTA),[67, 68] chitosan (CS),[204, 205, 216, 240, 249] *etc*. Hybrids of GO with other polymers have also been used to remove organic contaminants from water.[255] Among numerous factors affecting the adsorption capacity, initial concentration of the solution, phase contact time, temperature and pH are found to play a crucial role in the process of adsorption of metal ions on GO. The adsorption properties of neat GO towards divalent metal ions (copper, zinc, cadmium and lead) were investigated by Sitko *et al.*[128] In this seminal work, it was shown that GO prepared *via* the oxidation of synthetic graphite flakes using potassium dichromate possesses an impressive maximum adsorption capacity (q_{max}) for Cu^{2+} (223 mg g^{-1}), Zn^{2+} (345 mg g^{-1}), Cd^{2+} (530 mg g^{-1}), and Pb^{2+} ions (1120 mg g^{-1}). The single and competitive adsorption of Cu^{2+}, Zn^{2+}, Cd^{2+} and Pb^{2+} shows that the affinities of GO for these metal

ions follow the order of Pb^{2+} > Cu^{2+} >> Cd^{2+} > Zn^{2+}. Since then, many groups have investigated the impact of GO functionalization (with chemical groups and inorganic compounds) on its maximum adsorption capacity. The most relevant results reported so far have been listed in Table 1.1.

Table 1.1. Maximum adsorption capacities of CMGO composites used in Pb^{2+} removal process.

Adsorbent	q_{max} (mg g^{-1})	Conditions	Ref.
Few layers GO	1850[a]	pH = 6, T = 333 K	197
	758[a]	pH = 5.5, T = 333	203
GO	1119[a]	pH = 5, T = 298 K	128
rGO/PAM	1000[a]	pH = 6, T = 298 K	59
PVK-GO	888[a]	pH = 7, T = 298 K	60
HPA-GO	820[a]	pH = 5.9, T = 318 K	56
PAM-G	820[a]	pH = 6, T = 288 K	202
$MnFe_2O_4$/GO	673[a]	pH = 5, T = 298 K	64
GO/Fe_3O_4	588[a]	pH = 5, T = 303 K	65
GO/PAMAMs	568[b]	pH = 6, T = 283 K	58
EDTA/CMGO	508[a]	pH = 4.2, T = 298 K	67
EDTA/GO	479[a]	pH = 6.8, T = 298 K	68
CS/GO	461[c]	pH = 6, T = 318 K	204
	99[a]	pH = 6, T = 298 K	218
Fe_3O_4/Cysteine	459[a]	pH = 6, T = 298 K	66
CS/GO-SH	447[b]	pH = 5, T = 293 K	205
Polydopamine/GO	365[a]	pH NA, T = 298 K	206
NH_2-SiO_2/GO	345[a]	pH = 5, T = 313 K	207
Mesoporous silica/GO	333[a]	pH = 7.1, T = 298 K	208
Ag/GO	313[a]	pH = 5.3, T = 298 K	209
Hydroxyapatite/GO	278[a]	pH = 4.5, T = 308 K	210
Polysiolxane/GO	256[a]	pH = 5, T = 313 K	211
Phenylenediamine/ rGO	228[a]	pH = 7, T = 298 K	212
Tryptophan/GO	222[a]	pH = 4, T = 293 K	213
GO/Polyaniline	217[a]	pH = 5, T = 303 K	214
CS/FeOOH/GO	111[a]	pH = 5.5, T = 313 K	216
GO-SH	108[a]	pH = 4-10, T = 298 K	217
GO-NH_2	96[a]	pH = 6, T = 298 K	201

MHCGO	79[a]	pH = 5.5, T = 298 K	[219]
CMGO	77[a]	pH = 5, T = 298 K	[220]
Fe_3O_4-G	28[b]	pH = 6, T = 293 K	[221]
NH_2-SiO_2/GO	14[a]	pH = 5.5, T = 298 K	[222]

List of abbreviations. rGO : reduced graphene oxide, PAM : poly(acrylamide), PVK : Poly(*N*-vinylcarbazole), HPA : hyperbranched polyamine, $MnFe_2O_4$: manganese iron oxide, Fe_3O_4 : iron oxide, PAMAM : polyamidoamine, EDTA : Ethylenediaminetetraacetic acid, CMGO : chemically modified graphene oxide, CS : chitosan, GO-SH : Sulfydryl-functionalized graphene oxide, NH_2-SiO_2 : amino siloxane, FeOOH : iron (III) oxide-hydroxide, GO-NH_2: aminosilanized graphene oxide, MHCGO : magnetic carboxymethyl chitosan. Q_{max} values were calculated using (a) Langmuir, (b) Freundlich or (c) Redlich Peterson isotherms.

Zhao *et al.* demonstrated that q_{max} of two- or three-layer thick GO nanosheets synthesized from flake-graphite through modified Hummers method can be tuned with temperature.[197] Interestingly, it has been shown that the adsorption of Pb^{2+} ions on few-layer thick GO nanosheets was independent of the ionic strength, *i.e.* not affected by concentrations of background electrolyte ($NaClO_4$) at the pH ranging from 1 to 13. In particular, q_{max} of Pb^{2+} ions calculated from the Langmuir model amount to 842, 1150, and 1850 mg g^{-1} at 293, 313, and 333 K, respectively. Yang *et al*. proposed a different approach which relies on the functionalization of rGO with water-soluble poly(acrylamide) (PAM).[59] The GO prepared following the Staudenmaier method was thermally reduced yielding rGO. PAM is a polymer with a large number of acetylamine groups in its macromolecular chains, which can interact with metal ions *via* coordination. In particular, the carboxyl groups at the periphery of rGO sheets were converted to amine groups by reaction with N-hydroxysuccinimide and 1,3-diaminopropane, and a free-radical polymerization initiator was anchored to the rGO sheets. The highest adsorption capacities of rGO/PAM for Pb^{2+} amounted to 1000 mg g^{-1} (298 K), which is comparable to the neat rGO.

Aqueous solutions containing copper ions have been exploited for technological applications in the fields of mechanical manufacturing, electroplating, light industry and architecture. Yet, these solutions may cause serious diseases in the human central nervous system.[227] According to EPA regulations, copper concentration in drinking water should not exceed 1300 ng mL^{-1}.[217] Tan *et al*. prepared a hybrid composite including L-tryptophan (L-Trp) and GO by nucleophilic substitution reaction in order to increase the

hydrophobicity of GO and to promote the sorption.[213] It was found that such chemical modification of GO increases its sorption capacity from 223 to 588 mg g^{-1}. It has been shown that that high removal efficiencies can be obtained reaching values exceeding 95% at pH 5 and 4 for Cu^{2+} and Pb^{2+}, respectively. Several examples of chemically modified GO (CMGO)-based adsorbents rely on the use of chitosan as molecule possessing a high affinity for heavy metal ions.[204, 205, 216, 240, 249] Chitosan reacts with GO carboxyl groups of GO and forms amide bonds.[220, 244] In particular, chitosan modified GO has been prepared *via* covalent modification and electrostatic self-assembly by Li *et al.* [205] The introduction of GO-SH sheets as an interlayer can offer extra space into the chitosan structure and further increase the specific surface area. The results indicated that a new type of sorbent material, with functional groups such as -OH, -COOH, -SH and $-NH_2$ has a high adsorption capacity of copper ions (425 mg g^{-1}, see Table 1.2). Furthermore, the recyclability of the sorbent has been studied by treating it with HNO_3 and EDTA solutions. The chitosan (CS)/GO-SH revealed a decrease of the adsorption capacity over three cycles by 23% for Cu^{2+}, 25% for Pb^{2+} and 26% for Cd^{2+} ions. Chitosan/GO hybrid in the form of nanofibrous composite has been studied by Najafabadi *et al.*[204] The nanofibrous morphology of the hybrid material has been achieved through the use of electrospinning process. The maximum Cu^{2+} adsorption capacity was estimated as 423.8 mg g^{-1}. It was shown that the q_{max} decreased slowly with the increasing cycle number; such behaviour was attributed to the decrease in availability of active sites of adsorbent for metal ions. CS/GO-SH nanofibers could be used up to the fifth cycle of regeneration using HNO_3 solution by retaining 91.5% of the initial adsorption capacity Cu^{2+} ions sorption.

Table 1.2. Maximum adsorption capacities of CMGO composites used in Cu^{2+} removal process.

Adsorbent	q_{max} (mg g^{-1})	Conditions	Ref.
Trp/GO	588[a]	pH = 5, T = 293 K	213
CS/GO	425[a]	pH = 5, T = 293 K	205
	424[c]	pH = 6, T = 318 K	204
	203[b]	pH = 5, T = 293 K	224
	162[a]	pH = 5.5, T = 303 K	225
	54[a]	pH = 5, T = 293 K	232
Polyallylamine/GO	349[a]	pH = 6, T = 293 K	223
EDTA/CMGO	301[a]	pH = 5, T = 298 K	67
GO	294[a]	pH = 5, T = 298 K	128
	117[b]	pH = 5.3, T = 293 K	227
GO/CdS	137[a]	pH = 6, T = 298 K	226
GO-EDTA	109[a]	pH = 5, T = 293 K	228
GO-NH_2	103[a]	pH = 6, T = 298 K	229
GO-SH	100[a]	pH = 6, T = 298 K	229
	42[a]	pH = 5-10, T = 293 K	217
GO/PAMAMs	69[a]	pH = 4.5, T = 298 K	58
SMGO	63[a]	pH = 4.7, T = 323 K	230
Alginate/GO	60[a]	pH = NA, T = 293 K	231
NH_2-SiO_2/GO	6 [a]	pH = 5.5, T = 293 K	222

List of abbreviations. Trp : tryptophan, CS : chitosan, EDTA : Ethylenediaminetetraacetic acid, CMGO : chemically modified graphene oxide, CdS : cadmium sulfide, GO-NH_2 : aminosilanized graphene oxide, GO-SH : Sulfydryl-functionalized graphene oxide PAMAM : polyamidoamine, SMGO : sulfonated magnetic graphene oxide ,NH_2-SiO_2 : amino siloxane. Q_{max} values were calculated using (a) Langmuir, (b) Freundlich or (c) Redlich Peterson isotherms.

Numerous organic and inorganic compounds have been used to functionalize GO and form composites in order to detect and capture other heavy metal ions like Cd^{2+},[58, 128, 206, 215, 221] Hg^{2+},[67, 215, 245, 246] Ni^{2+},[221, 247] Co^{2+},[248] Mn^{2+},[58] Pd^{2+},[249] Sr^{2+},[250] Au^{3+},[249] As^{2+} [251] and U^{3+} [252-254] efficiently from aqueous solutions. Zhang *et al.* have demonstrated that efficient CMGO-based sorbent can be achieved by decorating GO with polyamidoamine dendrimers (GO/PAMAMs).[58] The adsorption behaviour of GO/PAMAMs for heavy metal ions in water solution was studied by changing the concentration of heavy metal

ions, pH values, and temperature. The maximum adsorption capacities of GO/PAMAMs were found to be 568.18, 253.81, 68.68, and 18.29 mg g^{-1} for Pb^{2+}, Cd^{2+}, Cu^{2+}, and Mn^{2+}, respectively. Noteworthy, it was also found that adsorption capacities of the GO/PAMAMs for the heavy metal ions were highly pH dependent. In particular, at pH < 3, the hydronium ions of higher concentration compete with M^{2+} to grasp the adsorption sites. With an increase of pH, the protonation degree of the amino groups was weakened, and the coordination and chelating ability of PAMAM's amino groups toward Pb^{2+}, Cd^{2+}, Cu^{2+} and Mn^{2+} reinforced. Conducting polymers interfaced with carbon and carbon-based derivatives have displayed enhanced removal of mercury and other toxic materials from water (Table 1.3). A facile chemical route was reported by Chandra *et al.* [245] In particular, they showed that polypyrrole (PPy)-rGO composites possess a highly selective Hg^{2+} removal capacity. rGO sheets cross-linked with polypyrrole exhibited an increased surface area of 166 m^2 g^{-1}. The uptake of Hg^{2+} by PPy/rGO has been estimated being as high as 980 mg g^{-1}. Furthermore, PPy/rGO possess an extremely high desorption capacity of up to 92.3%. Chitosan/GO (CSGO) composites with three different loadings of GO, *i.e.* 5, 10 and 15 wt% were prepared for the adsorption of Au^{3+} and Pd^{2+} by Liu *et al.*[249] The adsorption capacity of Au^{3+} and Pd^{2+} onto CSGO composites revealed high values at pH 3.0–5.0 for Au^{3+} and pH 3.0–4.0 for Pd^{2+}. It was found, that the composite with 5 wt% of GO had the largest adsorption capacity for Au^{3+} and Pd^{2+} compared with the other prepared adsorbents, where the maximum adsorption capacity amounted to 1076.6 mg g^{-1} and 216.9 mg g^{-1} for Au^{3+} and Pd^{2+}, respectively. Noteworthy, GO-based composites can also be used in adsorption process of radioactive ions.[252-254] Chen *et al.* reported on the amino functionalized magnetic graphene oxide composite (AMGO) synthesized by a facile, one-step solvothermal method, tailor made for the U^{6+} removal from aqueous solutions.[254] It was shown, that the sorption of U^{6+} on AMGO occurs *via* the formation of coordination complexes with the nitrogen- and oxygen-containing functional groups. It was concluded that the chemical affinity of the U^{6+} for the nitrogen containing functional groups is stronger than that for the oxygen containing functional groups. Interestingly, the AMGO composite could be recovered from the solution with the magnetic separation within one minute. The same group has demonstrated that the adsorption capacity of CMGO towards uranium can be improved by functionalizing GO with activated carbon felt (ACF) through electrophoretic deposition and subsequent

thermal annealing.[252] The q_{max} of GO-ACF for U^{6+} amounted to 298 mg g^{-1} at pH 5.5, being much higher than the one of ACF (173 mg g^{-1}), thus suggesting that the carboxyl functional groups of GO-ACF play an salient role in the sorption process, yielding a high efficiency for the removal of U^{6+}.

Table 1.3. Maximum adsorption capacities of CMGO composites used in various metal ions removal process.

Adsorbent	Contaminant	q_{max} (mg g^{-1})	Conditions	Ref.
GO	Cd(II)	530[a]	pH = 5, T = 298 K	128
GO/PAMAMs		253[b]	pH = 5, T = 298 K	58
PDA/GO		210[a]	pH = NA, T = 298 K	206
Fe_3O_4/G		28[b]	pH = 6-7, T = 293 K	221
PPy-rGO	Hg(II)	980[a]	pH = 3, T = 293 K	245
Ferrite/CS/G		361[a]	pH = 7, T = 323 K	246
EDTA-GO		268[b]	pH = 4.1, T = 298 K	67
Fe_3O_4-G		23[b]	pH = 6-7, T = 293 K	221
GO-G	Ni(II)	37[a]	pH = 6, T = 293 K	247
Fe_3O_4-G		22[b]	pH = 6-7, T = 293K	221
GO-NH_2	Co(II)	116[a]	pH = 6, T = 298 K	248
GO/PAMAMs	Mn(II)	18[a]	pH = 4, T = 298 K	58
CS/GO	Pd(II)	216[a]	pH = 3, T = 323 K	249
PAM/GO	Sr(II)	185[a]	pH = 8.5, T = 303 K	250
CS/GO	Au(III)	1076[a]	pH = 4, T = 303 K	249
GO-FeOOH	As(V)	73[a]	pH = 7, T = 298 K	251
GO/AC	U(VI)	298[a]	pH = 5, T = 298 K	252
GO-sepiolite		161[a]	pH = 5, T = 298 K	253
GO-NH_2		141[a]	pH = 6, T = 298 K	254

List of abbreviations. PAMAM: polyamidoamine, PDA: polydopamine, Fe_3O_4: iron oxide, PPy : polypyrrole, CS: chitosan, EDTA: Ethylenediaminetetraacetic acid, GO-NH_2 : aminosilanized graphene oxide, PAM : poly(acrylamide), FeOOH : iron (III) oxide-hydroxide, AC : activated carbon. Q_{max} values were calculated using (a) Langmuir or (b) Freundlich isotherms

1.1.1. Fluorescence-based metal sensors

Colorimetric sensors for metal ions feature two key elements, *i.e.* a metal chelating or binding (coordination) pocket and at least one fluorophore capable of absorbing and/or emitting light. Fluorescence sensing is based on analyte-induced changes in the physicochemical properties of fluorophores including fluorescence intensity, lifetime, and anisotropy, which are related to charge transfer or energy transfer processes. To function as a sensor, the electronic structure of the sensor must be altered upon metal binding. Changes in the electronic structure of the sensor can lead to the changes in the intensity or wavelength of light absorption or emission, while changes in the molecular structure can modify the distance or alignment between a pair of fluorophores that serve as a donor−acceptor pair. Graphene oxide has superb fluorescence quenching capability.[257,258] For example, a fluorescent quantum dots (QD)−aptamer−GO sensor based on the nanometal surface energy transfer (NSET) mechanism was designed by Qian et al in order to detect Pb^{2+} ions. In particular, photoinduced electron transfer between graphene quantum dots and GO was employed to achieve the controllable fluorescence turn-on process. The capability of QD-aptamer-GO nanosensor to detect Pb^{2+} and other ions with high sensitivity and good reproducibility was demonstrated on Figure 1.3.

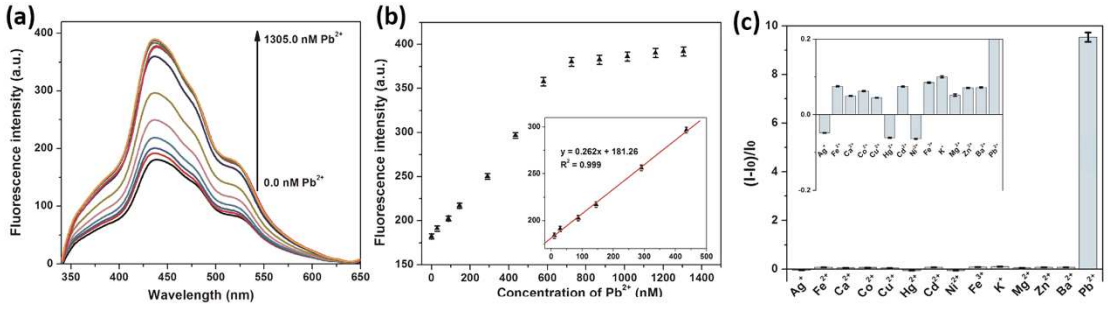

Figure 1.3. (a) The fluorescence recovery of aptamer–rGQDs/GO system after incubation with various concentrations of Pb^{2+} (0.0, 29.0, 87.0, 145.0, 290.0, 435.0, 580.0, 725.0, 870.0, 1015.0, 1160.0, 1305.0 nM). (b) The linear relationship between the fluorescence intensity and concentration of Pb^{2+}. (c) Fluorescence intensity changes (I-I_0/I_0) of the sensor in the presence of various metal ions. Reproduced with permission. [185]

Li *et al.* demonstrated that the single-stranded DNA (ssDNA) aptamer attached on GO can specifically bind to the mercury ions, leading to the formation of a hairpin-shaped double-stranded DNA (dsDNA) structure.[186] The water-dispersible GO sheets, which are functionalized with ssDNA aptamer, exhibit strong fluorescence emission at 600 nm under the excitation of 488 nm in the absence of Hg^{2+} ions. When Hg^{2+} ions appear in the aqueous solution, they are being sandwiched between the hairpin-shaped dsDNA due to the formation of the thymine–Hg^{2+}–thymine complex, which grasps the Hg^{2+} ions in proximity to the surface of GO. As a result, the fluorescence emission of GO is quenched. Such sensor shows a limit of detection as low as 0.92 nM and excellent selectivity towards Hg^{2+} over a wide range of metal ions including K^{+}, Ag^{+}, Ca^{2+}, Cd^{2+}, Cu^{2+}, Pb^{2+}, Ni^{2+}, Co^{2+} and Fe^{3+}. Recently, Wen *et al.* reported a FRET sensor based on a cytosine rich DNA probe and GO.[187] In the presence of Ag^{+}, a DNA–Ag^{+} complex was formed, and the conformation of the probe changed to straight stiff, resulting in desorption of DNA from the surface of GO and fluorescence recovery (Figure 1.4a). Fluorescence spectra of cytosine-rich oligonucleotide (SSO) probe upon incubation with a series of concentrations of Ag^{+} and then mixed with GO is portrayed in Figure 1.4b. This assay is based on the interaction between the target-induced conformational change of the SSO fluorogenic probe and graphene oxide quenching effects. The use of a simple mix-and-detect analysis revealed a high selectivity toward Ag^{+} as determined in the presence of a ten times higher concentration of 12 different interference metal ions (Figure 1.4c).

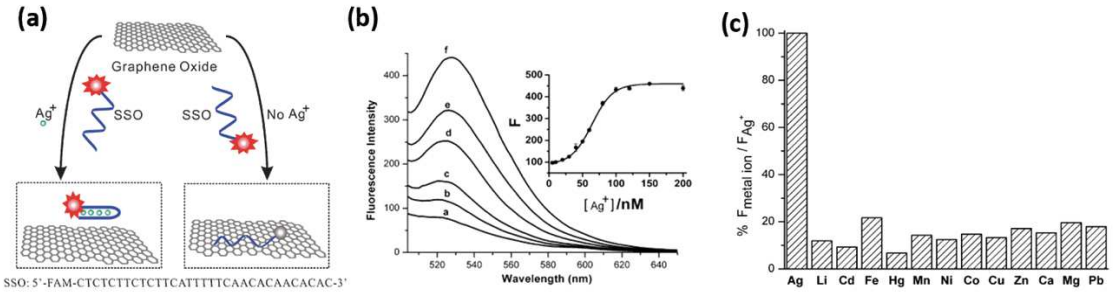

Figure 1.4. Schematic illustration of the fluorescence sensor for Ag^+ ions based on the target-induced conformational change of a silver specific cytosine-rich oligonucleotide (SSO) and the interactions between the fluorogenic SSO probe and graphene oxide. SSO: (a) FAM-labelled silver-specific oligonucleotide probe. (b) Fluorescence spectra of SSO probe upon incubation with a series of concentrations of Ag^+ and then mixed with GO: a 0 M, b 20 nM, c 40 nM, d 60 nM, e 80 nM and f 150 nM. All experiments were carried out in MOPS buffer (10 mM, pH 7.0) containing 50 mM of $NaNO_3$ and 10 nM of SSO. Ag^+ of different concentrations were incubated in this solution for 5 min at 23°C and then the fluorescence spectra were recorded 2 min after GO (10 mg) were added to this mixture. λ_{ex} = 494 nm. (c) Selectivity of the analysis of Ag^+ ions in the presence of different metal ions. The concentration of Ag^+ was 100 nM whereas all other interference metal ions were 1 μM. Reproduced with permission. [187]

1.1.2. Field-effect transistor based metal sensor

2DMs nanosheets integrated in FET have recently revealed their enormous potential for detection of heavy metals. The working principle of 2DM-based FET sensor is based on the changes of the critical parameters of a FET containing 2DMs nanosheets upon adsorption of targeted heavy metal ions. This includes primarily the field-effect mobility, threshold voltage and I_{on}/I_{off} ratio. 2D semiconducting sheets are of particular interest because their high carrier mobility and very high surface-to-volume ratio, leading to high sensitivity. Chemical sensors based on FETs can overcome the obstacles of previous detection methods. For example, aforementioned optical methods have some limitations such as multiple sensing steps, the need for using chemical agents, a higher cost, and a longer detection time. In contrast, the use of 2DM-based FET sensors enables the rapid label-free detection of metal ions in real-time by monitoring the resistance or the Dirac point shift caused by the adsorption of target analytes. Such devices can be characterized also by low power consumption and can be miniaturized for the development of portable sensors, eventually supported on flexible foils. In a typical graphene field-effect transistor (GFET) based sensor, graphene is used as conducting material in the channel between drain and source electrodes. Gate potential is applied through back-gate (typical thin SiO_2 layer)[259] or top-gate (electric double layer in electrolyte).[20] The absorption of analyte molecules or change of local environment leads to the change of graphene electrical conductance. Zhang *et al.* reported the functionalization of mechanically exfoliated graphene with a self-assembled monolayer of 1-octadecanethiol and its application in Hg^{2+} sensing.[169] Substituted alkane derivatives were found to self-assemble into large-scale highly-ordered physisorbed monolayers on single-layer graphene supported by the SiO_2 dielectric substrate. According to AFM imaging, the height of graphene increased to 1.6 nm when exposed to Hg^{2+}, indicating the successful uptake of mercury ions by the thiol groups exposed on the graphene surface. Such graphene-FET sensor revealed a detection limit for Hg^{2+} as low as 10 ppm.

Alternative approaches based on solution processable rGO, [170, 171] and graphene functionalization[142, 172-174] are being pursued with the ultimate goal of developing low-cost, scalable fabrication of graphene-FET sensors. Recently, Sudibya *et al*. presented a FET sensor using micropatterned, metallothionein type II protein (MT II)-functionalized

rGO films which bind with both physiological (*e.g.* Cu^{2+}, Zn^{2+}) and xenobiotic (*e.g.* Hg^{2+}, Cd^{2+}) metals ions with high affinity (see schematic illustration in Figure 1.5a).[170] A typical plot of drain-to-source current (I_{ds}) versus solution-gate voltage (V_g) of rGO-FET sensor is displayed in Figure 1.5b. Such a nanoelectronic sensor is capable of detecting various metal ions in real-time with high sensitivity. The addition of mercury (Hg^{2+}), at a concentration as low as 1 nM, caused the obvious current increase in the rGO-FET which was biased at V_{ds}= 400 mV and V_g=-0.6 V (Figure 1.5c). The magnitude of the device response scales with the Hg^{2+} concentration, and its polarity depends on the gate voltage (V_g). The detection limit for Hg^{2+} was estimated being as low as ~1 nM with a signal-to-noise ratio of 25-30 (Figure 1.5d). The very same device exhibited also Cd^{2+} detection at 1 nM with a slightly smaller change of current signal-to-noise ratio of 15-20 (Figure 1.5e).

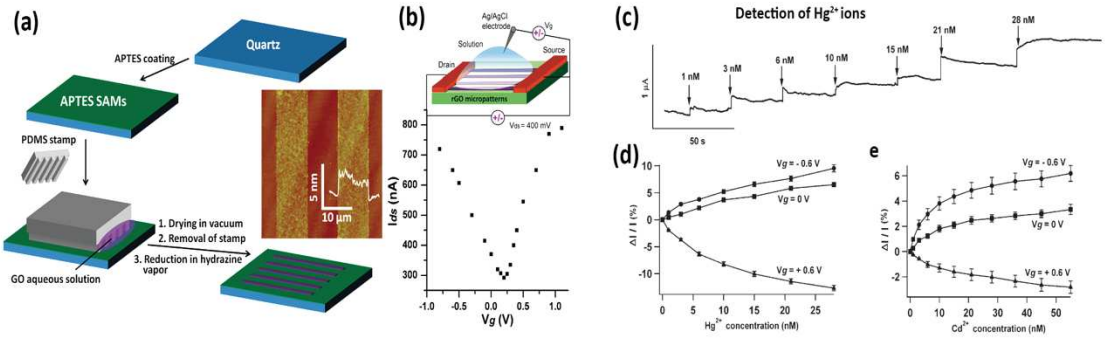

Figure 1.5. (a) Schematic illustration for fabrication of patterned rGO thin films on APTES-coated quartz. Inset: AFM image of the obtained rGO micropatterns on APTES-coated quartz. (b) Ambipolar characteristics of rGO-FET measured in 0.1 M of phosphate buffer saline (PBS) solution. Inset: Schematic of solution-gated configuration of rGO-FET. (c) Typical real-time recording of I_{ds} with the addition of Hg^{2+} ions. (d,e) Change of I_{ds} in rGO-FETs (tested sample number n= 6) with the addition of (d) Hg^{2+} and (e) Cd^{2+} ions at V_{ds}= 0.4 V and V_g= -0.6 (circle), 0 (square), and +0.6 V(triangle). Reproduced with permission.[170]

For heavy metal ion GFET sensors, biomolecules are frequently used as sensing nanoprobes due to their high binding affinity to inorganic contaminants.[142] An *et. al.*, reported high-performance flexible graphene aptasensor for Hg^{2+} detection.[172] 1,5-diaminonaphthalene (DAN) and glutaraldehyde (GA) were employed as cross-linking

agents, while the aptamer (3'-amine-TTC TTT CTT CCC CTT GTT TGT-C10 carboxylic acid-5') was non-covalently linked onto the graphene surface as a probe for Hg^{2+}. The field-induced responses from the graphene aptasensor had excellent sensing performance: Hg^{2+} ions with very low concentration of 10 pM could be detected (Figure 1.6a) being 2-3 orders of magnitude higher than previously reported mercury sensors using electrochemical devices.[259, 260] GFET-sensor was characterized with the experimental setup presented schematically in Figure 1.6b. The sensor response time was rapid, with values below 1 s. Noteworthy, the pristine graphene devices showed no significant current changes upon the exposure to Hg^{2+}. It was concluded, that the origin of current changes in the sensor relies on the *p*-doping effect resulting from the thymine–Hg–thymine complex formed between Hg^{2+} ions and thymine base pairs in the aptamer (Figure 1.6c). Additionally, the aptasensor is selective towards Hg^{2+} metal ions (Figure 1.6d).

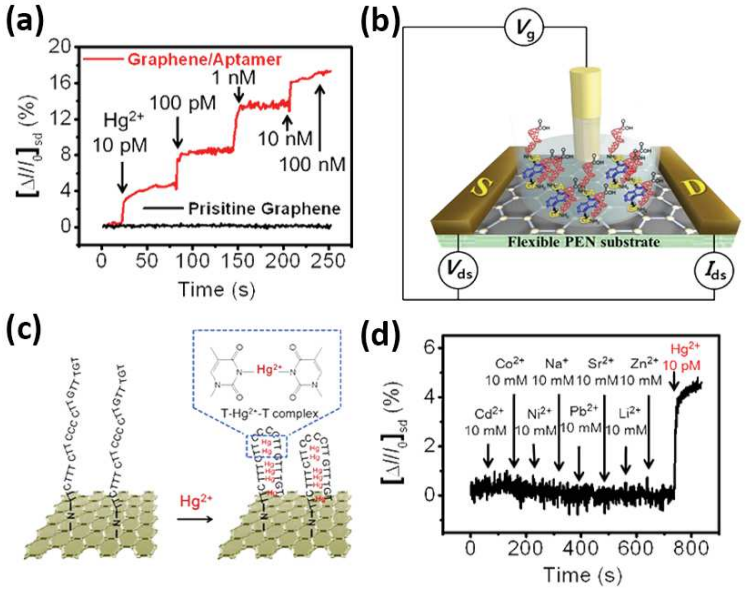

Figure 1.6. (a) Real-time responses curve of the aptasensor with various Hg^{2+} concentrations (10 pM to 100 nM). Graphene substrate without aptamer was introduced as a control sample. (b) Schematic diagram of a liquid-ion gated FET using graphene conjugated with aptamer. (V_g, S and D indicate gating voltage and source/drain electrodes). (c) Interaction of Hg^{2+} ions with thymine base pairs in the aptamer immobilized on the surface of the modified graphene layer (d) Selective responses of the aptasensor toward target metal ion (Hg^{2+}, 10 pM) and nontarget metal ions (Cd^{2+}, Co^{2+}, Ni^{2+}, Na^{+}, Pb^{2+}, Sr^{2+} and Zn^{2+}, 10 mM). Reproduced with permission. [172]

Noteworthy, graphene-based FET sensors can be exploited not only for the detection heavy metal ions (*e.g.* Hg^{2+} and Pb^{2+}) but also alkali metal ions in water including K^{+} and Na^{+}.[173,17]

1.1.3. Electrochemical based metal sensors

Electrochemical sensing of heavy metal ions relies on the use of sensing electrodes that are employed for passing the current to the aqueous solution and generate electrical signal which corresponds to the electrochemical reaction within the solution due to presence of metal ions. Common experimental setups for electrochemical detection of heavy metal ions consist of an electrolytic cell containing an electrolyte, *i.e.* solution of heavy metal ions, in contact with an electrode. The cell potential is measured at the interface of the electrode with the electrolyte solution. Noteworthy, because heavy metal ions have defined redox potential, the selectivity toward specific heavy metal ions can be achieved by using bare electrodes without the need of a molecular recognition probe. Numerous techniques are employed in electrochemical sensing, including potentiometry, voltammetry, impedimetry, amperometry and conductometry. In particular, the anodic stripping voltammetry (ASV) method is widely explored for detection of heavy metals. ASV analysis typically involves two steps, *i.e.* deposition of heavy metals onto the electrode surface, and stripping or dissolution of the deposited analyte from the electrode surface. Recent advancements in the field have revealed the potential of 2DMs in electroanalysis. Several electrochemical sensors based on 2DMs for bioanalysis and environmental analyses have been developed. In particular, Zhao *et al.* presented for the first time that Hg^{2+} can be selectively identified using a PPy–rGO nanocomposite-modified glassy carbon electrode (GCE).[178] Such selectivity was achieved by using square wave anodic stripping voltammetry (SWASV), which determines a reduction of adsorbed Hg^{2+} to Hg^{0} at a certain potential. The anodic stripping current was obtained in a potential range for the identification of Hg^{2+}. In addition, excellent sensitivity (0.124 $\mu A\ nM^{-1}$) and limit of detection (LOD) (15 nM) results were achieved. The measured stripping current toward Hg^{2+} at the PPy modified electrode was found to be 3–9 times higher than that towards other ions, indicating that rGO in the nanocomposite plays an important role in the highly selective detection.

Sahhoo *et al.* reported a facile *in situ* approach for the fabrication rGO/bismuth(Bi) nanocomposite by employing modified Hummers method without the use of any surfactants. Bi nanoparticles were uniformly anchored onto the surfaces of individual graphene nanosheets, which prevent restacking of rGO, resulting in good dispersion in

solvents. rGO/Bi nanocomposite was used as an electrode material for the stripping voltammetric determination of heavy metal ions in water. The detection limits of the proposed electrochemical sensor for Cd^{2+}, Pb^{2+}, Zn^{2+} and Cu^{2+} were found amounting to 2.8, 0.55, 17 and 26 ppb, respectively.[179] Wei *et al.* developed a SnO_2/rGO-based electrochemical sensor, which could simultaneously and selectively analyse four heavy metal ions such as Cd^{2+}, Pb^{2+}, Cu^{2+} and Hg^{2+}.[180] SWASV has been employed for the detection of heavy metal ions (Figure 1.7a). The SnO_2/rGO nanocomposite modified glass carbon electrode synthesized by a simple wet chemical method showed enhanced sensing performance compared with single SnO_2 and single rGO (Figure 1.7b).

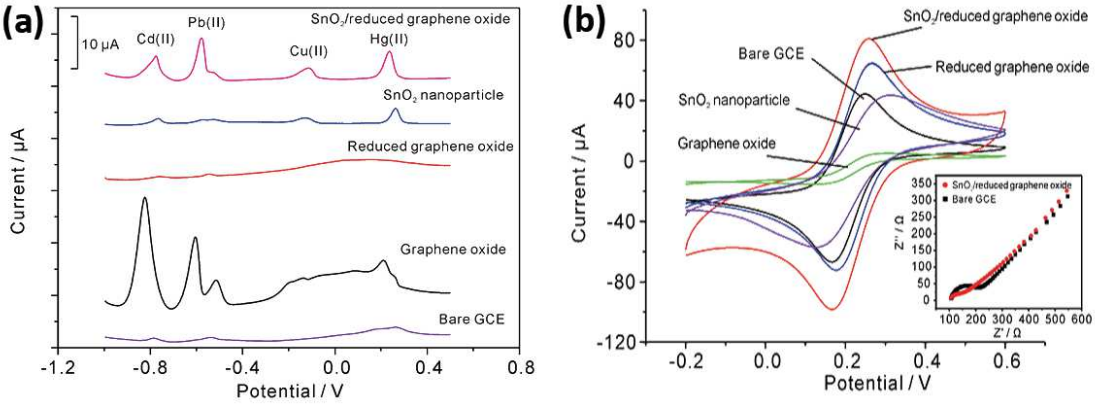

Figure 1.7. (a) Square Wave Anodic Stripping Voltammetry (SWASV) curves for 0.5 μM each of Cd(II), Pb(II), Cu(II), and Hg(II) on bare (violet line), graphene oxide (black line), reduced graphene oxide (red line), SnO_2 nanoparticle (blue line), and SnO_2/reduced graphene oxide nanocomposite (pink line) modified GCE in 0.1 M acetate buffer (pH 5.0). Deposition potential = -1.0 V; deposition time = 120 s; amplitude = 25 mV; increment potential = 4 mV; frequency = 15 Hz; *vs*. Ag/AgCl. (b) Cyclic voltammograms measured with bare, GO, rGO, SnO_2 nanoparticle, and SnO_2/reduced graphene oxide nanocomposite modified GCE in the solution of 5 mM $Fe(CN)_6^{3-/4-}$ containing 0.1 M KCl. Inset: Nyquist diagram of electrochemical impedance spectra for bare and SnO_2/reduced graphene oxide nanocomposite modified GCE in the solution of 5 mM $Fe(CN)_6^{3-/4-}$ containing 0.1 M KCl. Reproduced with permission.[180]

Li *et.al.* used Nafion and rGO for anodic stripping voltammetric analysis of cadmium with detection limit 0.005 ppb. [181] Willemse *et al.* reported on the determination of Cd^{2+}, Pb^{2+}, Zn^{2+} and Cu^{2+} by making use of the platform based on the Nafion-graphene nanocomposite film.[261] LODs of 0.07–0.08 ppb have been achieved for the individual

ions, which are comparable to those determined with ICP-MS, and ascribed to a combination of enhanced electron conduction of rGO and the cation exchange capacity of Nafion. Similarly, Chaiyo *et al.* constructed a Nafion/ionic liquid/graphene electrochemical sensor for simultaneous determination of zinc, cadmium and lead using screen-printed carbon (Figure 1.8a).[182] The functionalized graphene-based nanocomposite modified electrode showed better detection performance for Zn^{2+}, Cd^{2+} and Pb^{2+} compared to bare electrode by SWASV (Figure 1.8b). The detection limits of such sensors for Zn^{2+}, Cd^{2+} and Pb^{2+} detection amounted to 0.09 ng mL^{-1}, 0.06 ng L^{-1} and 0.08 ng L^{-1}, respectively.

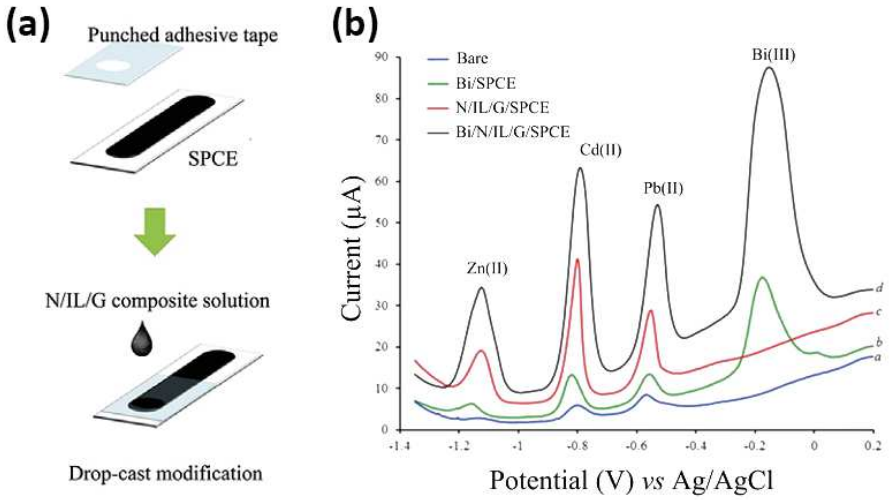

Figure 1.8. (a) Schematic drawing of the electrochemical sensor fabrication. (b) Square wave anodic stripping voltammetry (SWASV) curves of 50 ng mL^{-1} Zn(II), Cd(II) and Pb(II) in 0.1 M acetate buffer solution (pH 4.5). Reproduced with permission.[182]

Gong *et al.* reported ultrasensitive Hg^{2+} electrochemical sensor by using monodispersed Au nanoparticles onto the graphene nanosheet matrix as the enhanced sensing platform.[262] The detection limit was found to be as low as 6 ppt. The interference from other heavy metal ions such as Cu^{2+}, Cr^{3+}, Co^{2+}, Fe^{3+}, Zn^{2+} and I^{-} ions associated with Hg^{2+} analysis could be effectively inhibited. Another example relies on the use of cysteine-functionalized GO (sGO) and carbonyldiimidazole as a cross-linker *via* the formation of amide and carbamate bonds.The sGO/polypyrrole (PPy) nanocomposite film was grown on the working electrode surface of a screen-printed electrode (SPE) *via* controlled one-

step electrochemical deposition.[183] The sGO/PPy-SPE was used to detect lead ions in water by differential pulse voltammetry (DPV). The DPV signals were linear in the ranges of 1.4−14 000 ppb of Pb^{2+}. The measurable detection limit of the sensor is 0.07 ppb, being 2 orders of magnitude below the threshold value for drinking water set by the World Health Organization. The average removal efficiency of Pb^{2+} deposited on the electrode amounted to 99.2%, with relative standard deviation (RSD) of 3.8%. The selective detection of the GO/PPy composites was investigated by mixing GO/PPy with various metal ions such as Pb^{2+}, Na^{+}, Mg^{2+}, Cd^{2+}, Cu^{2+}, Hg^{2+} and Ag^{+}. The results clearly show that the GO/PPy composites film can selective detection of Pb^{2+} and impassive by the presence of other metal ions. In addition, the developed device can be used multiple times.

In this part of the introduction, we have provided an overview on the recent advances in the metal ion sensing. Different types of 2DMs employed for specific and selective recognition of heavy metals have been discussed in this chapter. By taking advantage of their unique properties 2DMs can be successfully explored to construct a wide range of optical and electrical sensing platforms for the detection of various heavy metal ions. Chemical modification of GO has proven to provide promising solution for improving the sensing performance with high specificity, enhanced sensitivity and low detection limit. Chemical metal sensors based on 2DMs have demonstrated high sensitivity detection of a wide variety of heavy metal ions at low concentrations, due to the maximum sensor surface area per unit volume. Their favourable structural and compositional synergy allows them to be excellent electrode materials for fabricating various fluorescent and electrochemical sensing platforms, such as FET-based sensors. Moreover, electrochemical measurements have shown numerous advantages for trace heavy-metal detection, including rapid analysis, good selectivity, and sensitivity. Optical detection systems are other alternatives to the electrochemical detection methods. These represent attractive analytical tools whenever continuous monitoring and real-time information is desired.

1.2. 2DMs based sensing of (bio)molecules

Ultrafast sensing of chemically and biologically active molecules at a low concentrations is critical in a wide range of research fields and in particular for applications, such as chemical analysis[263] and healthcare,[264, 265] monitoring the environment or diagnostic diseases.[266] Because of their particular physico-chemical properties, graphene-based materials have been used to fabricate various types of chemical sensors including electrochemical,[122, 265, 267-296] FET,[297-301] fluorescent[302-309] and surface enhanced Raman spectroscopy-based sensors.[263, 310-312] Graphene based materials have been used to develop various types of sensors to detect molecules such as glucose,[122, 267-275, 277, 279, 297, 313-317], DNA,[122, 280, 282, 299, 301, 303, 304, 307, 309, 318-321] hydrazine,[283, 322-325] dopamine,[122, 265, 276, 284-291, 293, 306, 326, 327] ascorbic acid,[122, 265, 286, 293, 328, 329] H_2O_2,[122, 295, 330-332] or other aromatic molecules.[263, 305, 308, 310, 311, 330] Graphene-based materials offer various advantages, when compared to other carbon-based nanomaterials like CNTs or fullerenes. Moreover, the particular strength of graphene, quality of its crystal structure, as well as its band structure and high conductivity allows the preparation of devices with extremely low noise levels and relatively low 1/f noise.[300]

1.2.1. (Bio)molecular fluorescence sensors

The use of fluorescence as readout in the detection of chemical species and biomolecules holds potential for low-cost, effective and highly sensitive device applications. Graphene/graphene oxide are known to be excellent quenching materials therefore graphene-based materials became suitable for sensing *via* influence on fluorescence properties.[321] One of the approaches bases on FRET and is useful for quantitative determination of target molecules. Typically, this kind of set up consists of a donor, an acceptor and a bridge. The acceptor such as GO can effectively quench fluorescence of the donor. The addition of specific molecules or surface modification may cause change in the fluorescence intensity and can be utilized as a sensor assuming the phenomenon is correlated with concentration (Figure 1.9a-b).[302, 304] Dong and co-workers reported on the FRET from quantum dots (QDs) to GO.[303] In particular, the authors demonstrated that QDs substituted with molecular beacon (MB) as a recognition unit towards targeted molecule can strongly interact with GO surface, to allow the design of novel sensitive and selective platforms for fluorescence-quenching detection of DNA. In general GO's quenching properties were used to decrease fluorescence intensity in the presence of QDs – an effective donor supplied with MB that provides efficient energy transfer to GO (Figure 1.9c).

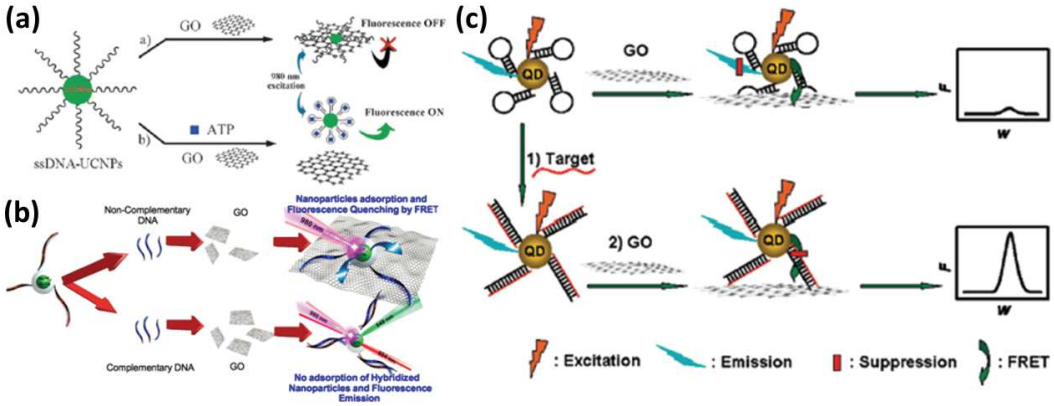

Figure 1.9. (a) Schematic representation of the upconversion fluorescence resonance energy transfer used for ATP sensing. Reproduced with permission. [304] (b) Depending on the presence of complementary DNA emission is observed or completely quenched, detection of specific DNA hybridization. Reproduced with permission.[302] (c) DNA sensing. Molecular beacon decorated QDs quenched by GO platform, in the presence of complementary DNA emission is significantly enhanced. Reproduced with permission [303]

Fluorescent graphene quantum dots (GQDs) were also applied for detection of aromatic nitro compounds (*e.g.* TNT) working as a quenchers in a wide range sustaining linear correlation.[305] Another DNA sensor using FRET between upconversion nanoparticles and GO was reported by Alonso-Cristobal *et al*.[302] Correlation between concentration of ssDNA (Figure 1.10a-b) and luminescence intensity was presented. Effective detection limit was experimentally shown to be in the picomolar range.

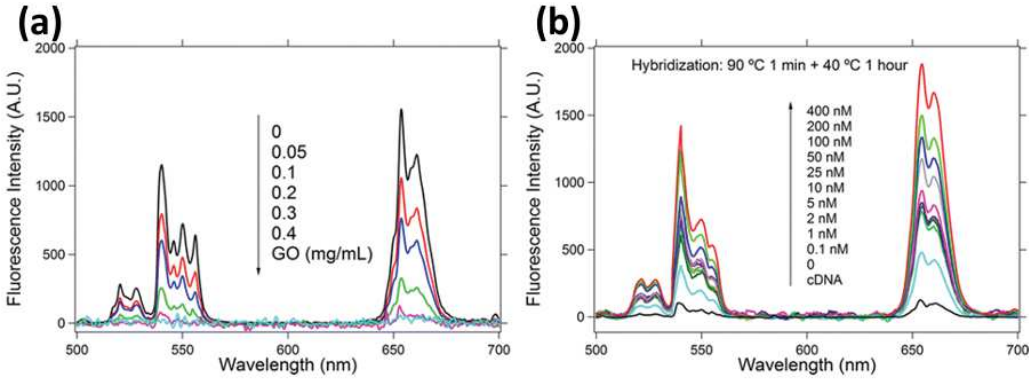

Figure 1.10. Up-conversion fluorescence spectra of the UCNPsSiO$_2$-ssDNA nanoparticles (0.4 mg mL^{-1}) a) in the presence of different concentrations of GO, and b) in the presence of different concentrations of complementary ssDNA and 0.3 mg mL^{-1} of GO. Reproduced with permission.[302]

GO-based platform for DNA and proteins sensing reported by Lu and co-workers includes ssDNA supplied with fluorescent organic dye that strongly adsorbs on GO's surface simultaneously entailing high quenching efficiency.[307] The addition of complementary ssDNA sequence causes efficient fluorescence increase and may be used to determine desired nucleotide sequences. Experiments also proved the dependence on different proteins concentrations. The results revealed that the presence of human thrombin might be determined without the interference of other proteins.

1.2.2. Field-effect transistors for (bio)molecular sensors

Due to their high selectivity, fast response and excellent limit of detection, graphene-based FET-based sensors became very popular for label-free ultrasensitive biomolecule sensing. By and large, graphene-based materials are used as conducting component in the channel between drain and source electrodes, and subsequently gate potential is applied.[298] Two different approaches are being pursued for construction of FET sensors, i.e., back gating (usually Si/SiO_2 thin layer)[297, 298] or top gating (electric double layer in electrolyte)[301, 317] also known as solution gated graphene transistors (SGGTs). Both methods have been schematically presented in Figure 1.11. In general, charged molecules can induce an effective gating field, which influences the conductance of the channel by balancing the charge transfer and gating effect. The change in current as measured allows the analyte determination.

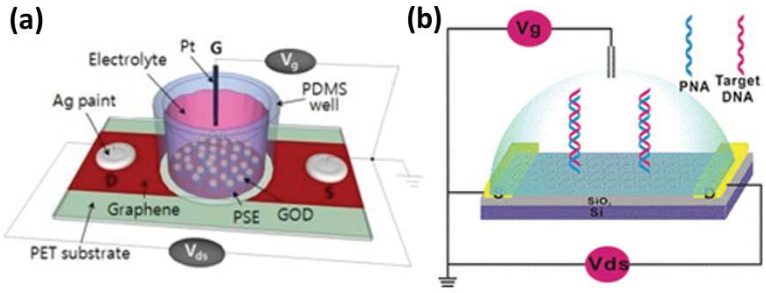

Figure 1.11. Schematic representation: (a) Graphene top gate FET sensor. Reproduced with permission.[298] (b) Graphene oxide back-gate FET sensor. Reproduced with permission.[301]

Huang and co-workers presented CVD-grown graphene FET sensor functionalized with specific redox mediators for glucose and glutamate detection.[297] Glucose sensing is usually based on an enzymatic reaction catalysed by glucose oxidase. Since the products of oxidation process are H_2O_2 and gluconic acid, direct measurement of H_2O_2 is useful for glucose detection. The detection limits were found being at 0.1 mM and 5 μM for glucose and glutamate, respectively. Another CVD-grown glucose sensor was assembled by Kwak *et al.*[298] Solution-gated field-effect transistor (SGFET) was constructed utilizing graphene channel modulated by the gate potential applied from the top gate electrode and transmitted through the solution. Such SGFET sensor was

exploited to detect glucose in the range of 3.3-10.9 mM. Moreover, it provided high resolution and continuous real-time monitoring. To reach the largest sensing response, graphene transistors are operated at the point of maximum transconductance, which leads to large noise that influences the device sensitivity. To avoid such phenomenon Fu and co-workers exploited the sensing properties of single layered graphene near its neutrality point.[299] This approach led to a significant decrease of signal-to-noise ratio, thereby making it possible to observe positive signals coming from single stranded DNA (ssDNA) at level of picomolar concentrations (pM). Moreover, to target specific hybridization corresponding with HIV-virus related ssDNA, functionalization of GFET surface with pyrene-linked peptide nucleic acid (pPNA) was performed. Noteworthy, the 1/f noise in graphene based FET sensors was found to vary with the number of graphene layers, therefore subsequent optimization of this class of sensors is anticipated.[300] Another approach in which hydrazine-reduced GO was used to fabricate FET sensor on SiO_2/Si substrate was proposed by Cai *et al.*[301] DNA sensor was prepared by drop-casting rGO suspension onto sensing channel as the conducting material. 1-Pyrenebutanoic acid succinimidyl ester (PASE) used as molecular linker was fixed on the graphene surface *via* π-π stacking interactions and peptide nucleic acid (PNA) molecules were covalently anchored. Subsequently, a complementary DNA was applied onto device and specific hybridization caused the shift of I_{ds}-V_g curves and allowed the measurement. The detection limit was estimated being as low as 100 fM.

1.2.3. Electrochemical (bio)molecular sensors

Electrochemical sensing is an effective and powerful technique used for qualitative and quantitative determination of bioactive and functional molecules.[279, 317, 327] Numerous advantages including low limit of detection, high selectivity and detection in the presence of interferences made graphene-based materials appealing for fabrication of electrochemical sensors. Because of these reasons, electrochemical sensors belong to the most widespread graphene-based sensors in recent years. The most common approach relies on the use of electrodes based on graphene[294, 329] or modified graphene-based nanostructures.[293, 326, 330] Fast electron transfer and effective electrocatalytic activity of graphene allows the effective detection of target molecules while oxidation.[333] Among its numerous physico-chemical properties, graphene has wide electrochemical potential window (ca. 2.5 V in phosphate buffer)[122] and is characterized by lower charge transfer resistance (comparing with glass electrode)[122] and well characterized redox potentials against most common redox couples.[334] Keeley *et al.* developed an electrochemical sensor based on graphene exfoliated in DMF for ascorbic acid (AA) detection.[329] The electrode was prepared by drop-casting centrifuged graphene supernatant solution onto pyrolysed photoresist film. Cyclic voltammetry investigation revealed wide range of linearity and limit detection up to 0.12 mM. Another effective electrode was prepared by mixing platinum nanoparticle and graphene nanosheet.[330] Such hybrid system displayed the capacity to detect traces of trinitrotoluene (TNT), a typical explosive compound, with detection limits as low as 0.3 ppm and satisfactory reproducibility. Luo *et al*. presented electrochemical glucose sensor based on Cu decorated graphene sheets.[273] As prepared electrode exhibited a low detection limit of 0.5 μM and very fast response (<2s) and its response linearity up to 4.5 mM. Additionally, a synergistic effect of copper and graphene toward glucose oxidation was observed.

As aforementioned, the majority of graphene-based sensors rely on the chemical modification of GO, which exhibits numerous oxygen-rich functional groups that can interact *via* dipole-dipole or strong electrostatic interactions with (charged) molecules, and can be covalently functionalized with functional molecules, enhancing the occurrence of adsorption events. In particular, covalent grafting of organic molecules on GO offers the flexibility for various functionalizations to enhance the sensor performance.

Moreover, the combination of its abundant structural defects and chemical groups facilitates the charge transfer and thus ensure high electrochemical activity. Noteworthy, the chemical and electrical properties of rGO are highly tuneable and can be engineered through control of the reduction process. Zhou *et al*. exploited a chemically reduced GO modified glassy carbon electrode (CR-GO/GC) for electrochemical sensing of free purine and pyrimidine acids and several other biologically active molecules.[122] It was demonstrated that CR-GO/GC electrode provides greater electrocatalytic activity to guanine (G), adenine (A), thymine (T) and cytosine (C) oxidation than commonly used glassy carbon (GC) and graphite/glassy carbon graphite/GC electrodes (Figure 1.12). Moreover, the analytical performance of glucose, ethanol, dopamine and other biological molecules detection was enhanced *e.g.* compared with graphite/GC and GC electrodes the CR-GO/GC electrode. In particular, while amperometric measurement of reduced nicotinamide adenine dinucleotide (NADH) exhibited faster response time, wider linear range (40-800 μM), lower detection limit (10.00 μM) and higher sensitivity (2.68 μA mM^{-1} cm^{-2}). Gao and co-workers carried out the chemical reduction of GO obtaining hydroxyapatite/rGO composite used as effective electrochemical sensor of hydrazine.[324] The composite dispersed in 1% acetic acid was applied on GCE and dried resulting in high-performance electrode with outstanding performance of electrocatalytic oxidation of N_2H_4. The as-prepared electrode exhibited synergic effect of components during detection of hydrazine, being greater than the electrodes fabricated with rGO and hydroxyapatite separately. Wang and co-workers devised a facile approach relying on the efficient preparation of nitrogen-doped graphene *via* nitrogen plasma treatment of chemically synthesized graphene, which exhibits excellent electrocatalytic activity toward hydrogen peroxide reduction.[267] Detection of H_2O_2 as one of the products of catalytic glucose oxidation can be applied for selective and sensitive glucose determination during enzymatic processes. Noteworthy, N-doped graphene electrode exhibited high concentration-dependent response and was able to detect up to 0.01 mM of glucose in the presence of interferences. N-doped electrodes can also find their use in detection of important biomolecules such as ascorbic acid (AA), dopamine (DA) and uric acid (UA).[265] Efficient oxidation and large peak separation provides simultaneous determination of those three biomolecules with detection limits up to $2.2 \cdot 10^{-6}$, $2.5 \cdot 10^{-7}$ and $4.5 \cdot 10^{-8}$ M for AA, DA and UA, respectively. Furthermore, differential pulse

voltammetry (DPV) experiment revealed that electrochemical response of target biomolecules increases linearly with increase of molecules concentrations.

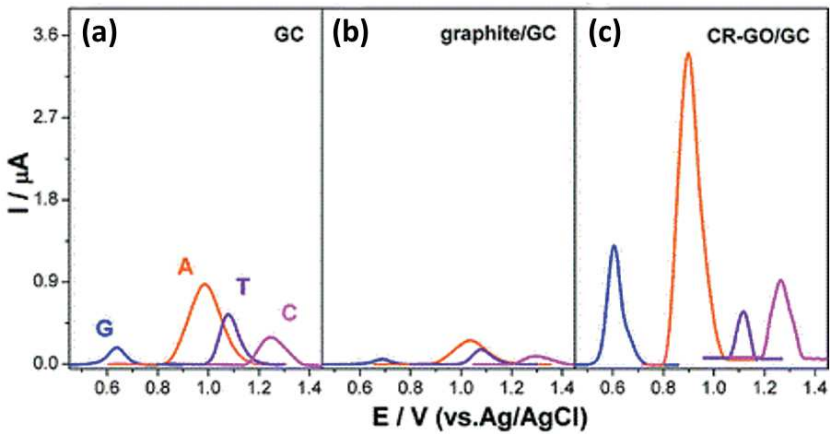

Figure 1.12. Differential pulse voltammograms (DPVs) of guanine (blue), adenine (orange), thymine (violet), and cytosine (magenta) at a) GC electrode, b) graphite/GC electrode, and c) CR-GO/GC electrode, Reproduced with permission. [122]

1.2.4. (Bio)molecular sensing *via* surface enhanced raman scattering

Surface enhanced Raman scattering (SERS) represents a most powerful analytical technique for sensitive chemical sensing, which became an attractive solution for detection of aromatic compounds. Typically, weak Raman signals are intensified through enhancement of the local electromagnetic field, occurring with the charge transfer between adsorbed molecules and metal surface. Consequently, to observe SERS signal, molecules must be adsorbed or be placed close to a metal surface. The most common approach bases on modification of graphene-based material surface with metallic nanoparticles (NPs).[263, 311] Optimum size, shape, charge and surface chemistry of NPs are being taken into account to project non-toxic and effective sensors.[154]

Lu *et al.* proposed the use of Ag and AuNP-decorated single-layer rGO film anchored on Si surface to detect popular organic dyes rhodamine 6G (R6G), methyl violet (MV), rhodamine B (RB) and methylene blue (MB) at nanomolar concentrations.[263] Such molecules easily adsorb on rGO surface while Ag and Au nanoparticles provide dramatic enhancement in the Raman intensities coming from the sample. Moreover, a correlation between NPs size and observed signals have been monitored, and it could be controlled through the reaction time. Another modification with AgNPs for ultrasensitive detection of aromatic molecules was demonstrated by Liu and co-workers.[310] Additional enhancement of the Raman signals was ensured by GO treated with 3-mercaptopropyltrimethoxysilane (MPTMS), further functionalized with Ag-NPs. An effective detection of differently charged molecules was successfully characterized and presented. In particular, experiments with PPh_3 used as target molecule exhibited limit of detection as low as 10^{-9} M. Graphene grown on copper foil and AgNPs anchored on Si substrate can also be used to prepare SERS active substrate for detection of TNT by alkaline hydrolysis.[311] High pH values provide efficient hydrolysis of TNT and enhance intensity in Raman spectra signals. Extremely high limit of detection (up to $6.6 \cdot 10^{-10}$ M) and excellent anti-interference ability confirms perspective potential of SERS sensors. Shanta and Cheng prepared hydrazine reduced GO combined with silver nanoprisms and utilized such hybrid system for trace detection of tetrachlorobiphenyls (PCBs).[312] As prepared chip successfully allowed for multiplex measurement of several environmentally important aromatic compounds. Proposed SERS sensor provided low

limit of detection (up to 100 nM) and simultaneous analysis of multiple isomers.Values such as limit of detection and linearity range for detection of vary biomolecules have been summarized in Table 1.4**.**

Table 1.4. Comparison of sensing properties of different graphene-based sensors.

Material	Type of sensor	Analyte	Limit of detection	Linearity Range	Ref.
DMF-exfoliated graphene	electrochemical	AA	0.12 mM	0.4-6.0 mM	329
Pt-NPs-graphene		H_2O_2 TNT	80 nM 0.3 ppm	1-500 µM 0.5-40 ppm	330
Cu-NPs-graphene		glucose	0.5 µM	0-4.5 mM	273
rGO		H_2O_2 NADH	0.05 µM 10 µM	0.05-1500 µM 40-800 µM	122
Hydroxyapatite-rGO		NH_2NH_2	0.43 µM	2.5 µM - 1.16 mM	324
N-doped graphene		glucose	0.01 mM	0.1-1.1 mM	267
N-doped graphene		AA DA UA	2.2 µM 0.25 µM 4.5×10^{-8} M	5.0-1300 µM 0.5-170 µM 0.1-20 µM	265
CVD-grown graphene	FET	glucose glutamate	0.1 mM 5 µM	- 5 - 1200 µM	297
CVD-grown graphene		glucose	-	3.3-10.9 mM	298
CVD-grown graphene		DNA	2 pm	-	299
rGO		DNA	100 fM	10 fM-1 nM	301
QDs-GO	fluorescent	DNA	12 nM	50-1500 nM	303
Graphene QDs		TNT	2.2 µM	$4.95\times10^{--4}$-$1.82\times10^{--1}$g/L	305
NPs-GO		DNA	5 pm	-	302
Au/Ag-NPs-rGO	SERS	R6G MV RB MB	nm	-	263
AgNPs-GO		PPh_3	1 nM	$5\times10^{--6}$-1×10^{-9} M	310
AgNPs-graphene		TNT	0.66 nM	1-100 nM	311
rGO-NP		R6G PCB	100 pM 100 nM	0-1000 nM 100 µM - 100 nM	312

List of abbreviations. DMF : dimethylformamide, AA : ascorbic acid, NPs : nanoparticles, TNT : 2,4,6-trinitrotoluene, NADH : β-nicotinamide adenine dinucleotide, NH_2NH_2 : hydrazine, DA : dopamine, UA : uric acid, QDs : quantum dots, SERS : Surface Enhanced Raman Scattering, R6G : rhodamine 6G, MV : methyl violet, RB : rhodamine B, MB : methylene blue, PPh_3 : triphenylphosphine.

In this section we have discussed 2DMs and 2DM-based composites for the sensing of (bio)molecular species. A range of unique physico-chemical properties offered by 2DMs allows fabrication of various types of chemical sensors including fluorescent, electrochemical, FET and SERS. Recent literature includes investigations of most important biological molecules with particular attention to molecules relevant in medical sciences. Among various advantages of 2DMs based sensors the extremely low limit of detections (reaching the picomolar level), ultrafast detection (<1s) and wide linearity of response signals should be emphasized. Moreover, most of 2DMs based sensors exhibit high selectivity and allow determination of multiple target molecules even in the presence of common interferences. Possibility of further modifications of 2DMs allows achieving multicomponent systems offering better performances in effective determination of target analytes. Noteworthy, the spectrum of molecules detectable with presented sensors is quite narrow. Also, there are a few issues that should be considered while development of new sensing materials such as stability, reusability and biocompatibility. Electrochemical sensing seems to be one of most widespread approach applied in chemical sensing, which affirms superior electrical properties of graphene and TMD's.

1.3. Aim and organization of the thesis

In the modern scientific world, many groups carry out intensive research in the field of potential applications of 2DMs. The dissemination of this topic led to the study of this area of material chemistry within the framework of presented doctoral dissertation, with particular emphasis on adsorption and electrical properties. The main goal of research in this doctoral dissertation concerns of achieving high-quality functionalized two-dimensional materials based on graphene and graphene oxide with particular emphasis on adsorption and energy storage properties. Novel high-performance adsorbent (BPEI-GO) prepared *via* covalent modification of graphene oxide have been developed, which was characterized by high stability, high specific surface area and high affinity towards various chemical substances. On the other hand, newly obtained compounds based on modified silica and GO (SiO_2NH_2-GO) was investigated with their adsorption properties of selected cationic dyes. By providing insight into the comprehensive physical and chemical characterizations of functionalized 2DMs, this dissertation aims to achieve in-depth understanding of the fundamental properties of prepared hybrid materials in perspective of their future potential applications in chemical sensors and electronics. Thanks to that, we developed different functionalized 2DMs using *top-down* approach in order to explore the adsorption properties and to reach profound comprehension of the relationship between their structure and properties. In particular, this thesis intends to explore the use of *top-down* methods to modify 2DMs in order to achieve a control over their properties that is necessary for the integration of these materials in multifunctional devices. This thesis has been divided in the following parts:

Chapter 2 will introduce the analytic techniques applied in this dissertation for the morphological (high-resolution transmission electron microscopy (HR-TEM)) and qualitative (RAMAN spectroscopy, X-ray photoelectron spectroscopy (XPS)) characterizations of the produced hybrid materials. Multiscale characterization of modified 2DMs was performed by analytical and spectroscopic methods to confirm *e.g.* purity and structure. Additionally, newly obtained compounds based on modified graphene oxide was investigated and their adsorption properties with respect to selected pollutant using flame atomic adsorption spectrometry (FAAS) in order to heavy metal ions adsorption and/or UV-vis spectroscopy in context of cationic dyes adsorption.

Together with the fundamental principles of the technique, each chapter highlight the main achievements in the characterization of graphene-based materials.

Both chapters (1 and 2) are followed by three main experimental sections which are similarly organized. They contain an introduction part to the project, then a part of materials and methods where the details focused on characterization and specimen preparation are presented. After that, we described a part that includes the results of the research and finally, we summarized of the project at the end of the chapter.

Chapter 3 is the first experimental chapter which deals with the *bottom-up* method to develop of novel high-performance adsorbents prepared *via* covalent modification of GO using organic polymer with anchoring amine moiety. Polymer, which were characterized by high stability, high specific surface area and high affinity towards various chemical substances. This chapter explores one of the possible applications functionalized 2DMs in the field of chemical adsorption and show that BPEI-GO offers great potential as selective adsorbent for heavy metal ions.

Chapter 4 focuses on similar synthetic methodology as previously presented and describes the possible application of functionalized GO using aminosilica molecules in the field of adsorption cationic dyes from aqueous solution. This work show that SiO_2NH_2-GO hybrid material can be successfully used as very fast and efficient adsorbent in real life application.

Chapter 5 exploits the electrical properties of modified electrochemical exfoliation graphene (EEG) with Mo_{132}-DTAB subunits by non-covalent interactions in the context of potential application as supercapacitors. The hybrid material was generated through relatively simple approach which relies on the use of surfactant (DTAB) to form the surfactant encapsulated cluster based on a functionalized Keplerate type-polyoxometalate Mo_{132}-DTAB, which can physisorb on the electrochemically exfoliated graphene. The produced composite has been characterized in detail, demonstrating that innovative porous three-dimensional systems of Mo_{132}-DTAB-EEG synergically combine with each other a large POM redox potential and high graphene electrical conductivity material allows to exhibit significantly higher specific, volumetric and surface capacitance parameters.

In the final chapter 6, conclusion will be drawn of the main experimental results of this thesis. The dissertation ends suggestion concerning future studies, discussing the

opportunities and challenges, which must be overcome for the introduction of 2DMs in water purification treatment process. It was proved that appropriate design and functionalization of 2DMs based on graphene and GO would allow one to obtain novel, high-performance architectures with pre-designed electrical properties in terms of energy storage applications and adsorption properties with particular emphasis on sorption of cationic dyes and heavy metal ions from aqueous solution

1.4. References

1. K. S. Kim, Y. Zhao, H. Jang, S. Y. Lee, J. M. Kim, K. S. Kim, J.-H. Ahn, P. Kim, J.-Y. Choi and B. H. Hong, *Nature*, 2009, **457**, 706.
2. Y. Zhu, S. Murali, M. D. Stoller, K. J. Ganesh, W. Cai, P. J. Ferreira, A. Pirkle, R. M. Wallace, K. A. Cychosz, M. Thommes, D. Su, E. A. Stach and R. S. Ruoff, *Science*, 2011, **332**, 1537-1541.
3. M. Liu, X. Yin, E. Ulin-Avila, B. Geng, T. Zentgraf, L. Ju, F. Wang and X. Zhang, *Nature*, 2011, **474**, 64.
4. A. K. Geim and K. S. Novoselov, *Nat. Mater.*, 2007, **6**, 183.
5. K. S. Novoselov, A. K. Geim, S. V. Morozov, D. Jiang, M. I. Katsnelson, I. V. Grigorieva, S. V. Dubonos and A. A. Firsov, *Nature*, 2005, **438**, 197.
6. Q. H. Wang, K. Kalantar-Zadeh, A. Kis, J. N. Coleman and M. S. Strano, *Nat. Nanotechnol.*, 2012, **7**, 699.
7. C. Schafhaeutl, *J. Prakt. Chem.*, 1840, **19** 159–174.
8. B. C. Brodie, *Phil. Trans. Roy. Soc. London.* , 1859, **149**, 249–259.
9. H. P. Boehm, A. Clauss, G. O. Fischer and U. Hofmann, *Zeitschrift für anorganische und allgemeine Chemie*, 1962, **316**, 119-127.
10. K. S. Novoselov, A. K. Geim, S. V. Morozov, D. Jiang, Y. Zhang, S. V. Dubonos, I. V. Grigorieva and A. A. Firsov, *Science*, 2004, **306**, 666-669.
11. M. d. P. L. Lopez, J. L. V. Palomino, M. L. S. Silva and A. R. Izquierdo, *Optimization of the Synthesis Procedures of Graphene and Graphite Oxide* IntechOpen, 2016.
12. M. C. Lemme, L.-J. Li, T. Palacios and F. Schwierz, *MRS Bulletin*, 2014, **39**, 711-718.
13. J.-C. Charlier, P. C. Eklund, J. Zhu and A. C. Ferrari, in *Carbon Nanotubes: Advanced Topics in the Synthesis, Structure, Properties and Applications*, eds. A. Jorio, G. Dresselhaus and M. S. Dresselhaus, Springer Berlin Heidelberg, Berlin, Heidelberg, 2008, pp. 673-709.
14. A. C. Ferrari, F. Bonaccorso, V. Fal'ko, K. S. Novoselov, S. Roche, P. Bøggild, S. Borini, F. H. L. Koppens, V. Palermo, N. Pugno, J. A. Garrido, R. Sordan, A. Bianco, L. Ballerini, M. Prato, E. Lidorikis, J. Kivioja, C. Marinelli, T. Ryhänen, A. Morpurgo, J. N. Coleman, V. Nicolosi, L. Colombo, A. Fert, M. Garcia-Hernandez, A. Bachtold, G. F. Schneider, F. Guinea, C. Dekker, M. Barbone, Z. Sun, C. Galiotis, A. N. Grigorenko, G. Konstantatos, A. Kis, M. Katsnelson, L. Vandersypen, A. Loiseau, V. Morandi, D. Neumaier, E. Treossi, V. Pellegrini, M. Polini, A. Tredicucci, G. M. Williams, B. Hee Hong, J.-H. Ahn, J. Min Kim, H. Zirath, B. J. van Wees, H. van der Zant, L. Occhipinti, A. Di Matteo, I. A. Kinloch, T. Seyller, E. Quesnel, X. Feng, K. Teo, N. Rupesinghe, P. Hakonen, S. R. T. Neil, Q. Tannock, T. Löfwander and J. Kinaret, *Nanoscale*, 2015, **7**, 4598-4810.
15. Q. H. Wang, K. Kalantar-Zadeh, A. Kis, J. N. Coleman and M. S. Strano, *Nat. Nanotechnol.*, 2012, **7**, 699.
16. M. W. Barsoum, *Prog. Solid State Chem.*, 2000, **28**, 201-281.
17. L. Li, Y. Yu, G. J. Ye, Q. Ge, X. Ou, H. Wu, D. Feng, X. H. Chen and Y. Zhang, *Nat. Nanotechnol.*, 2014, **9**, 372.

18. S. P. Koenig, R. A. Doganov, H. Schmidt, A. H. C. Neto and B. Özyilmaz, *Appl. Phys. Lett.*, 2014, **104**, 103106
19. H. Liu, A. T. Neal, Z. Zhu, Z. Luo, X. Xu, D. Tománek and P. D. Ye, *ACS Nano*, 2014, **8**, 4033-4041.
20. N. O. Weiss, H. Zhou, L. Liao, Y. Liu, S. Jiang, Y. Huang and X. Duan, *Adv. Mater.*, 2012, **24**, 5782-5825.
21. S. Stankovich, D. A. Dikin, G. H. B. Dommett, K. M. Kohlhaas, E. J. Zimney, E. A. Stach, R. D. Piner, S. T. Nguyen and R. S. Ruoff, *Nature*, 2006, **442**, 282.
22. T. Y. Kim, C.-H. Park and N. Marzari, *Nano Lett.*, 2016, **16**, 2439-2443.
23. S. V. Morozov, K. S. Novoselov, M. I. Katsnelson, F. Schedin, D. C. Elias, J. A. Jaszczak and A. K. Geim, *Phys. Rev. Lett.*, 2008, **100**, 016602.
24. C. Lee, X. Wei, J. W. Kysar and J. Hone, *Science*, 2008, **321**, 385-388.
25. V. Berry, *Carbon*, 2013, **62**, 1-10.
26. F. Guo, G. Silverberg, S. Bowers, S.-P. Kim, D. Datta, V. Shenoy and R. H. Hurt, *Environ. Sci. Technol.*, 2012, **46**, 7717-7724.
27. D. Pierleoni, Z. Y. Xia, M. Christian, S. Ligi, M. Minelli, V. Morandi, F. Doghieri and V. Palermo, *Carbon*, 2016, **96**, 503-512.
28. D. Prasai, J. C. Tuberquia, R. R. Harl, G. K. Jennings and K. I. Bolotin, *ACS Nano*, 2012, **6**, 1102-1108.
29. A. Gupta, T. Sakthivel and S. Seal, *Prog. Mater. Sci.*, 2015, **73**, 44-126.
30. A. S. Mayorov, R. V. Gorbachev, S. V. Morozov, L. Britnell, R. Jalil, L. A. Ponomarenko, P. Blake, K. S. Novoselov, K. Watanabe, T. Taniguchi and A. K. Geim, *Nano Lett.*, 2011, **11**, 2396-2399.
31. D. C. Elias, R. V. Gorbachev, A. S. Mayorov, S. V. Morozov, A. A. Zhukov, P. Blake, L. A. Ponomarenko, I. V. Grigorieva, K. S. Novoselov, F. Guinea and A. K. Geim, *Nat. Phys.*, 2011, **7**, 701.
32. A. Kuc, N. Zibouche and T. Heine, *Phys. Rev. B*, 2011, **83**, 245213.
33. M. D. Stoller, S. Park, Y. Zhu, J. An and R. S. Ruoff, *Nano Lett.*, 2008, **8**, 3498-3502.
34. E. Yoo, J. Kim, E. Hosono, H.-s. Zhou, T. Kudo and I. Honma, *Nano Lett.*, 2008, **8**, 2277-2282.
35. J.-S. Kim, H.-W. Yoo, H. O. Choi and H.-T. Jung, *Nano Lett.*, 2014, **14**, 5941-5947.
36. D. J. Late, Y.-K. Huang, B. Liu, J. Acharya, S. N. Shirodkar, J. Luo, A. Yan, D. Charles, U. V. Waghmare, V. P. Dravid and C. N. R. Rao, *ACS Nano*, 2013, **7**, 4879-4891.
37. K. Kalantar-zadeh and J. Z. Ou, *ACS Sens.*, 2016, **1**, 5-16.
38. Y. Song, Y. Luo, C. Zhu, H. Li, D. Du and Y. Lin, *Biosens. Bioelectron.*, 2016, **76**, 195-212.
39. A. K. Geim, *Science*, 2009, **324**, 1530-1534.
40. X. Li, W. Cai, J. An, S. Kim, J. Nah, D. Yang, R. Piner, A. Velamakanni, I. Jung, E. Tutuc, S. K. Banerjee, L. Colombo and R. S. Ruoff, *Science*, 2009, **324**, 1312-1314.
41. Y. Zhang, L. Zhang and C. Zhou, *Acc. Chem. Res.*, 2013, **46**, 2329-2339.
42. C. Berger, Z. M. Song, T. B. Li, X. B. Li, A. Y. Ogbazghi, R. Feng, Z. T. Dai, A. N. Marchenkov, E. H. Conrad, P. N. First and W. A. de Heer, *J. Phys. Chem. B*, 2004, **108**, 19912-19916.

43. Y. Zhu, S. Murali, W. Cai, X. Li, J. W. Suk, J. R. Potts and R. S. Ruoff, *Adv. Mater.*, 2010, **22**, 3906-3924.
44. S. Basu and P. Bhattacharyya, *Sens. Actuators, B*, 2012, **173**, 1-21.
45. Y. Hernandez, V. Nicolosi, M. Lotya, F. M. Blighe, Z. Sun, S. De, I. T. McGovern, B. Holland, M. Byrne, Y. K. Gun'Ko, J. J. Boland, P. Niraj, G. Duesberg, S. Krishnamurthy, R. Goodhue, J. Hutchison, V. Scardaci, A. C. Ferrari and J. N. Coleman, *Nat. Nanotechnol.*, 2008, **3**, 563.
46. A. Ciesielski and P. Samorì, *Adv. Mater.*, 2016, **28**, 6030-6051.
47. K. R. Paton, E. Varrla, C. Backes, R. J. Smith, U. Khan, A. O'Neill, C. Boland, M. Lotya, O. M. Istrate, P. King, T. Higgins, S. Barwich, P. May, P. Puczkarski, I. Ahmed, M. Moebius, H. Pettersson, E. Long, J. Coelho, S. E. O'Brien, E. K. McGuire, B. M. Sanchez, G. S. Duesberg, N. McEvoy, T. J. Pennycook, C. Downing, A. Crossley, V. Nicolosi and J. N. Coleman, *Nat. Mater.*, 2014, **13**, 624.
48. M. Eredia, S. Bertolazzi, T. Leydecker, M. El Garah, I. Janica, G. Melinte, O. Ersen, A. Ciesielski and P. Samorì, *J. Phys. Chem. Lett.*, 2017, **8**, 3347-3355.
49. M. López, J. L. Palomino, M. Silva and A. R. Izquierdo, *Recent Advances in Graphene Research - Optimization of the Synthesis Procedures of Graphene and Graphite Oxide*, IntechOpen Limited, 2016.
50. V. Singh, D. Joung, L. Zhai, S. Das, S. I. Khondaker and S. Seal, *Prog. Mater. Sci.*, 2011, **56**, 1178-1271.
51. S. Eigler and A. Hirsch, *Angew. Chem., Int. Ed.*, 2014, **53**, 7720-7738.
52. X. Zhang, A. Ciesielski, F. Richard, P. Chen, E. A. Prasetyanto, L. De Cola and P. Samorì, *Small*, 2016, **12**, 1044-1052.
53. S. Wang, P.-J. Chia, L.-L. Chua, L.-H. Zhao, R.-Q. Png, S. Sivaramakrishnan, M. Zhou, R. G.-S. Goh, R. H. Friend, A. T.-S. Wee and P. K.-H. Ho, 2008, **20**, 3440-3446.
54. B. Yuan, C. Bao, L. Song, N. Hong, K. M. Liew and Y. Hu, *Chem. Eng. J.*, 2014, **237**, 411-420.
55. V. Chandra and K. S. Kim, *Chem. Commun.*, 2011, **47**, 3942-3944.
56. L. Hu, Z. Yang, L. Cui, Y. Li, H. H. Ngo, Y. Wang, Q. Wei, H. Ma, L. Yan and B. Du, *Chem. Eng. J.*, 2016, **287**, 545-556.
57. H. T. Xing, J. H. Chen, X. Sun, Y. H. Huang, Z. B. Su, S. R. Hu, W. Weng, S. X. Li, H. X. Guo, W. B. Wu, Y. S. He, F. M. Li and Y. Huang, *Chem. Eng. J.*, 2015, **263**, 280-289.
58. F. Zhang, B. Wang, S. He and R. Man, *J. Chem. Eng. Data*, 2014, **59**, 1719-1726.
59. Y. Yang, Y. Xie, L. Pang, M. Li, X. Song, J. Wen and H. Zhao, *Langmuir*, 2013, **29**, 10727-10736.
60. Y. L. F. Musico, C. M. Santos, M. L. P. Dalida and D. F. Rodrigues, *J. Mater. Chem. A*, 2013, **1**, 3789-3796.
61. X. Zhang, A. Ciesielski, F. Richard, P. Chen, E. A. Prasetyanto, L. De Cola and P. Samorì, *Small*, 2016, **12**.
62. F. Najafi, O. Moradi, M. Rajabi, M. Asif, I. Tyagi, S. Agarwal and V. K. Gupta, *J. Mol. Liq.*, 2015, **208**, 106-113.
63. R. Sitko, B. Zawisza, E. Talik, P. Janik, G. Osoba, B. Feist and E. Malicka, *Anal. Chim. Acta*, 2014, **834**, 22-29.
64. S. Kumar, R. R. Nair, P. B. Pillai, S. N. Gupta, M. A. R. Iyengar and A. K. Sood, *ACS Appl. Mater. Interfaces*, 2014, **6**, 17426-17436.

65. X. Yang, C. Chen, J. Li, G. Zhao, X. Ren and X. Wang, *RSC Adv.*, 2012, **2**, 8821-8826.
66. X. Zou, Y. Yin, Y. Zhao, D. Chen and S. Dong, *Mater. Lett.*, 2015, **150**, 59-61.
67. L. Cui, Y. Wang, L. Gao, L. Hu, L. Yan, Q. Wei and B. Du, *Chem. Eng. J.*, 2015, **281**, 1-10.
68. C. J. Madadrang, H. Y. Kim, G. Gao, N. Wang, J. Zhu, H. Feng, M. Gorring, M. L. Kasner and S. Hou, *ACS Appl. Mater. Interfaces*, 2012, **4**, 1186-1193.
69. V. Georgakilas, M. Otyepka, A. B. Bourlinos, V. Chandra, N. Kim, K. C. Kemp, P. Hobza, R. Zboril and K. S. Kim, *Chem. Rev.*, 2012, **112**, 6156-6214.
70. B. Cai, S. Zhang, Z. Yan and H. Zeng, *ChemNanoMat*, 2015, **1**, 542-557.
71. E. A. Meyer, R. K. Castellano and F. Diederich, *Angew. Chem. Int. Ed.*, 2003, **42**, 1210-1250.
72. S. K. Burley and G. A. Petsko, *FEBS Lett.*, 1986, **203**, 139-143.
73. P. Tarakeshwar, K. S. Kim, E. Kraka and D. Cremer, *J. Chem. Phys.*, 2001, **115**, 6018-6029.
74. E. C. Lee, B. H. Hong, J. Y. Lee, J. C. Kim, D. Kim, Y. Kim, P. Tarakeshwar and K. S. Kim, *J. Am. Chem. Soc.*, 2005, **127**, 4530-4537.
75. S. J. Grabowski, *J. Phys. Chem. A*, 2001, **105**, 10739-10746.
76. P. Tarakeshwar, H. S. Choi and K. S. Kim, *J. Am. Chem. Soc.*, 2001, **123**, 3323-3331.
77. E.-i. Kim, S. Paliwal and C. S. Wilcox, *J. Am. Chem. Soc.*, 1998, **120**, 11192-11193.
78. K. E. Riley, M. Pitoňák, P. Jurečka and P. Hobza, *Chem. Rev.*, 2010, **110**, 5023-5063.
79. C. A. Hunter and J. K. M. Sanders, *J. Am. Chem. Soc.*, 1990, **112**, 5525-5534.
80. C. A. Hunter, *Chem. Soc. Rev.*, 1994, **23**, 101-109.
81. E. C. Lee, D. Kim, P. Jurečka, P. Tarakeshwar, P. Hobza and K. S. Kim, *J. Phys. Chem. A*, 2007, **111**, 3446-3457.
82. I. Geronimo, E. C. Lee, N. J. Singh and K. S. Kim, *J. Chem. Theory Comput.*, 2010, **6**, 1931-1934.
83. W. Wang and P. Hobza, *ChemPhysChem*, 2008, **9**, 1003-1009.
84. D. Dougherty and D. Stauffer, *Science*, 1990, **250**, 1558-1560.
85. D. Kim, S. Hu, P. Tarakeshwar, K. S. Kim and J. M. Lisy, *J. Phys. Chem. A*, 2003, **107**, 1228-1238.
86. S. Tsuzuki, M. Yoshida, T. Uchimaru and M. Mikami, *J. Phys. Chem. A*, 2001, **105**, 769-773.
87. S. E. Wheeler and K. N. Houk, *J. Am. Chem. Soc.*, 2009, **131**, 3126-3127.
88. M. A. Gebbie, W. Wei, A. M. Schrader, T. R. Cristiani, H. A. Dobbs, M. Idso, B. F. Chmelka, J. H. Waite and J. N. Israelachvili, *Nat. Chem.*, 2017, **9**, 473.
89. A. S. Mahadevi and G. N. Sastry, *Chem. Rev.*, 2013, **113**, 2100-2138.
90. P. B. Crowley and A. Golovin, *Proteins: Struct., Funct., Bioinf.*, 2005, **59**, 231-239.
91. J. P. Gallivan and D. A. Dougherty, *Proc. Natl. Acad. Sci. U.S.A.*, 1999, **96**, 9459-9464.
92. K. S. Kim, P. Tarakeshwar and J. Y. Lee, *Chem. Rev.*, 2000, **100**, 4145-4186.
93. D. Quiñonero, C. Garau, C. Rotger, A. Frontera, P. Ballester, A. Costa and P. M. Deyà, *Angew. Chem. Int. Ed.*, 2002, **41**, 3389-3392.

94. B. L. Schottel, H. T. Chifotides and K. R. Dunbar, *Chem. Soc. Rev.*, 2008, **37**, 68-83.
95. Y. S. Rosokha, S. V. Lindeman, S. V. Rosokha and J. K. Kochi, *Angew. Chem. Int. Ed.*, 2004, **43**, 4650-4652.
96. P. De Hoog, P. Gamez, I. Mutikainen, U. Turpeinen and J. Reedijk, *Angew. Chem.*, 2004, **116**, 5939-5941.
97. R. E. Dawson, A. Hennig, D. P. Weimann, D. Emery, V. Ravikumar, J. Montenegro, T. Takeuchi, S. Gabutti, M. Mayor, J. Mareda, C. A. Schalley and S. Matile, *Nat. Chem.*, 2010, **2**, 533.
98. A. Frontera, P. Gamez, M. Mascal, T. J. Mooibroek and J. Reedijk, *Angew. Chem. Int. Ed.*, 2011, **50**, 9564-9583.
99. B. L. Schottel, H. T. Chifotides, M. Shatruk, A. Chouai, L. M. Pérez, J. Bacsa and K. R. Dunbar, *J. Am. Chem. Soc.*, 2006, **128**, 5895-5912.
100. H. T. Chifotides and K. R. Dunbar, *Acc. Chem. Res.*, 2013, **46**, 894-906.
101. C. Garau, A. Frontera, D. Quiñonero, P. Ballester, A. Costa and P. M. Deyà, *J. Phys. Chem. A*, 2004, **108**, 9423-9427.
102. D. Kim, P. Tarakeshwar and K. S. Kim, *J. Phys. Chem. A*, 2004, **108**, 1250-1258.
103. A. Hashimoto, K. Suenaga, A. Gloter, K. Urita and S. Iijima, *Nature*, 2004, **430**, 870.
104. W. Zhou, X. Zou, S. Najmaei, Z. Liu, Y. Shi, J. Kong, J. Lou, P. M. Ajayan, B. I. Yakobson and J.-C. Idrobo, *Nano Lett.*, 2013, **13**, 2615-2622.
105. F. Banhart, J. Kotakoski and A. V. Krasheninnikov, *ACS Nano*, 2011, **5**, 26-41.
106. L. G. Cançado, A. Jorio, E. H. M. Ferreira, F. Stavale, C. A. Achete, R. B. Capaz, M. V. O. Moutinho, A. Lombardo, T. S. Kulmala and A. C. Ferrari, *Nano Lett.*, 2011, **11**, 3190-3196.
107. S. Feng, Z. Lin, X. Gan, R. Lv and M. Terrones, *Nanoscale Horiz.*, 2017, **2**, 72-80.
108. A. Ambrosi and M. Pumera, *Chem. - Eur. J.*, 2010, **16**, 10946-10949.
109. K. C. Santosh, C. L. Roberto, A. Rafik, M. W. Robert and C. Kyeongjae, *Nanotechnology*, 2014, **25**, 375703.
110. D. Liu, Y. Guo, L. Fang and J. Robertson, *Appl. Phys. Lett.*, 2013, **103**, 183113
111. S. Tongay, J. Suh, C. Ataca, W. Fan, A. Luce, J. S. Kang, J. Liu, C. Ko, R. Raghunathanan, J. Zhou, F. Ogletree, J. Li, J. C. Grossman and J. Wu, *Sci. Rep.*, 2013, **3**, 2657.
112. H. Nan, Z. Wang, W. Wang, Z. Liang, Y. Lu, Q. Chen, D. He, P. Tan, F. Miao, X. Wang, J. Wang and Z. Ni, *ACS Nano*, 2014, **8**, 5738-5745.
113. J. Xie, H. Zhang, S. Li, R. Wang, X. Sun, M. Zhou, J. Zhou, X. W. Lou and Y. Xie, *Adv. Mater.*, 2013, **25**, 5807-5813.
114. L. Rodriguez-Perez, M. a. A. Herranz and N. Martin, *Chem. Commun.*, 2013, **49**, 3721-3735.
115. G. L. C. Paulus, Q. H. Wang and M. S. Strano, *Acc. Chem. Res.*, 2013, **46**, 160-170.
116. S. Niyogi, E. Bekyarova, M. E. Itkis, H. Zhang, K. Shepperd, J. Hicks, M. Sprinkle, C. Berger, C. N. Lau, W. A. deHeer, E. H. Conrad and R. C. Haddon, *Nano Lett.*, 2010, **10**, 4061-4066.
117. J. M. Englert, C. Dotzer, G. Yang, M. Schmid, C. Papp, J. M. Gottfried, H.-P. Steinrück, E. Spiecker, F. Hauke and A. Hirsch, *Nat. Chem.*, 2011, **3**, 279.

118. H. Liu, S. Ryu, Z. Chen, M. L. Steigerwald, C. Nuckolls and L. E. Brus, *J. Am. Chem. Soc.*, 2009, **131**, 17099-17101.
119. M. Quintana, K. Spyrou, M. Grzelczak, W. R. Browne, P. Rudolf and M. Prato, *ACS Nano*, 2010, **4**, 3527-3533.
120. D. Chen, H. Feng and J. Li, *Chem. Rev.*, 2012, **112**, 6027-6053.
121. D. R. Dreyer, S. Park, C. W. Bielawski and R. S. Ruoff, *Chem. Soc. Rev.*, 2010, **39**, 228-240.
122. M. Zhou, Y. Zhai and S. Dong, *Anal. Chem.*, 2009, **81**, 5603-5613.
123. J. T. Robinson, F. K. Perkins, E. S. Snow, Z. Wei and P. E. Sheehan, *Nano Lett.*, 2008, **8**, 3137-3140.
124. S. Wu, Q. He, C. Tan, Y. Wang and H. Zhang, *Small*, 2013, **9**, 1160-1172.
125. W. Yuan and G. Shi, *J. Mater. Chem. A*, 2013, **1**, 10078-10091.
126. Q. He, S. Wu, Z. Yin and H. Zhang, *Chem. Sci.*, 2012, **3**, 1764-1772.
127. G. Zhao, J. Li, X. Ren, C. Chen and X. Wang, *Environ. Sci. Technol.*, 2011, **45**, 10454-10462.
128. R. Sitko, E. Turek, B. Zawisza, E. Malicka, E. Talik, J. Heimann, A. Gagor, B. Feist and R. Wrzalik, *Dalton Trans.*, 2013, **42**, 5682-5689.
129. G. Eda and M. Chhowalla, *Adv. Mater.*, 2010, **22**, 2392-2415.
130. G. Ko, H. Y. Kim, J. Ahn, Y. M. Park, K. Y. Lee and J. Kim, *Curr. Appl. Phys.*, 2010, **10**, 1002-1004.
131. D. R. Dreyer, A. D. Todd and C. W. Bielawski, *Chem. Soc. Rev.*, 2014, **43**, 5288-5301.
132. S. Eigler and A. Hirsch, *Angew. Chem. Int. Ed.*, 2014, **53**, 7720-7738.
133. C. K. Chua and M. Pumera, *Chem. Soc. Rev.*, 2014, **43**, 291-312.
134. L. Zhou, B. He, Y. Yang and Y. He, *RSC Adv.*, 2014, **4**, 32570-32578.
135. C. Tsai, H. Li, S. Park, J. Park, H. S. Han, J. K. Nørskov, X. Zheng and F. Abild-Pedersen, *Nat. Commun.*, 2017, **8**, 15113.
136. S. Bertolazzi, S. Bonacchi, G. Nan, A. Pershin, D. Beljonne and P. Samorì, *Adv. Mater.*, 2017, **29**, 1606760
137. K. Cho, M. Min, T.-Y. Kim, H. Jeong, J. Pak, J.-K. Kim, J. Jang, S. J. Yun, Y. H. Lee, W.-K. Hong and T. Lee, *ACS Nano*, 2015, **9**, 8044-8053.
138. E. P. Nguyen, B. J. Carey, J. Z. Ou, J. van Embden, E. D. Gaspera, A. F. Chrimes, M. J. S. Spencer, S. Zhuiykov, K. Kalantar-zadeh and T. Daeneke, *Adv. Mater.*, 2015, **27**, 6225-6229.
139. A. Aliprandi, D. Pakulski, A. Ciesielski and P. Samorì, *ACS Nano*, 2017, **11**, 10654-10658.
140. B. M. Venkatesan and R. Bashir, *Nat. Nanotechnol.*, 2011, **6**, 615.
141. S. Garaj, W. Hubbard, A. Reina, J. Kong, D. Branton and J. A. Golovchenko, *Nature*, 2010, **467**, 190.
142. S. Mao, J. Chang, H. Pu, G. Lu, Q. He, H. Zhang and J. Chen, *Chem. Soc. Rev.*, 2017, **46**, 6872-6904.
143. Y. Liu, X. Dong and P. Chen, *Chem. Soc. Rev.*, 2012, **41**, 2283-2307.
144. D. Chen, L. Tang and J. Li, *Chem. Soc. Rev.*, 2010, **39**, 3157-3180.
145. M. J. Allen, V. C. Tung and R. B. Kaner, *Chem. Rev.*, 2010, **110**, 132-145.
146. S. Cui, H. Pu, S. A. Wells, Z. Wen, S. Mao, J. Chang, M. C. Hersam and J. Chen, *Nat. Commun.*, 2015, **6**, 8632.
147. Y. Wang, Z. Li, J. Wang, J. Li and Y. Lin, *Trends Biotechnol.*, 2011, **29**, 205-212.

148. Z. Tang, H. Wu, J. R. Cort, G. W. Buchko, Y. Zhang, Y. Shao, I. A. Aksay, J. Liu and Y. Lin, *Small*, 2010, **6**, 1205-1209.
149. C. Zhu, Z. Zeng, H. Li, F. Li, C. Fan and H. Zhang, *J. Am. Chem. Soc.*, 2013, **135**, 5998-6001.
150. D. Dinda, A. Gupta, B. K. Shaw, S. Sadhu and S. K. Saha, *ACS Appl. Mater. Interfaces*, 2014, **6**, 10722-10728.
151. X. Ling, L. Xie, Y. Fang, H. Xu, H. Zhang, J. Kong, M. S. Dresselhaus, J. Zhang and Z. Liu, *Nano Lett.*, 2010, **10**, 553-561.
152. X. Ling, W. Fang, Y.-H. Lee, P. T. Araujo, X. Zhang, J. F. Rodriguez-Nieva, Y. Lin, J. Zhang, J. Kong and M. S. Dresselhaus, *Nano Lett.*, 2014, **14**, 3033-3040.
153. S. Schlücker, *Angew. Chem. Int. Ed.*, 2014, **53**, 4756-4795.
154. S. Laing, L. E. Jamieson, K. Faulds and D. Graham, *Nat. Rev. Chem.*, 2017, **1**, 0060.
155. A.-I. Henry, B. Sharma, M. F. Cardinal, D. Kurouski and R. P. Van Duyne, *Anal. Chem.*, 2016, **88**, 6638-6647.
156. M. F. Cardinal, E. Vander Ende, R. A. Hackler, M. O. McAnally, P. C. Stair, G. C. Schatz and R. P. Van Duyne, *Chem. Soc. Rev.*, 2017, **46**, 3886-3903.
157. S. Nie and S. R. Emory, *Science*, 1997, **275**, 1102-1106.
158. K. Kneipp, Y. Wang, H. Kneipp, L. T. Perelman, I. Itzkan, R. R. Dasari and M. S. Feld, *Phys. Rev. Lett.*, 1997, **78**, 1667-1670.
159. L. Sun, H. Hu, D. Zhan, J. Yan, L. Liu, J. S. Teguh, E. K. L. Yeow, P. S. Lee and Z. Shen, *Small*, 2014, **10**, 1090-1095.
160. X. Ling, S. Huang, S. Deng, N. Mao, J. Kong, M. S. Dresselhaus and J. Zhang, *Acc. Chem. Res.*, 2015, **48**, 1862-1870.
161. A. J. Bandodkar, I. Jeerapan and J. Wang, *ACS Sens.*, 2016, **1**, 464-482.
162. E. Singh, M. Meyyappan and H. S. Nalwa, *ACS Appl. Mater. Interfaces*, 2017, **9**, 34544-34586.
163. H. Lee, T. K. Choi, Y. B. Lee, H. R. Cho, R. Ghaffari, L. Wang, H. J. Choi, T. D. Chung, N. Lu, T. Hyeon, S. H. Choi and D.-H. Kim, *Nat. Nanotechnol.*, 2016, **11**, 566.
164. S. Chowdhury and R. Balasubramanian, *Adv. Colloid Interface Sci.*, 2014, **204**, 35-56.
165. L. Fan, C. Luo, M. Sun and H. Qiu, *J. Mater. Chem.*, 2012, **22**, 24577-24583.
166. H. Wang, X. Yuan, Y. Wu, H. Huang, X. Peng, G. Zeng, H. Zhong, J. Liang and M. Ren, *Adv. Colloid Interface Sci.*, 2013, **195-196**, 19-40.
167. D. S. Sholl and R. P. Lively, *Nature*, 2016, **532**, 435-437.
168. I. Ali, *Chem. Rev.*, 2012, **112**, 5073-5091.
169. T. Zhang, Z. Cheng, Y. Wang, Z. Li, C. Wang, Y. Li and Y. Fang, *Nano Lett.*, 2010, **10**, 4738-4741.
170. H. G. Sudibya, Q. He, H. Zhang and P. Chen, *ACS Nano*, 2011, **5**, 1990-1994.
171. G. Zhou, J. Chang, S. Cui, H. Pu, Z. Wen and J. Chen, *ACS Appl. Mater. Interfaces*, 2014, **6**, 19235-19241.
172. J. H. An, S. J. Park, O. S. Kwon, J. Bae and J. Jang, *ACS Nano*, 2013, **7**, 10563-10571.
173. W. Fu, C. Nef, A. Tarasov, M. Wipf, R. Stoop, O. Knopfmacher, M. Weiss, M. Calame and C. Schonenberger, *Nanoscale*, 2013, **5**, 12104-12110.
174. K. Maehashi, Y. Sofue, S. Okamoto, Y. Ohno, K. Inoue and K. Matsumoto, *Sens. Actuators, B*, 2013, **187**, 45-49.

175. S. Jiang, R. Cheng, R. Ng, Y. Huang and X. Duan, *Nano Res.*, 2015, **8**, 257-262.
176. G. Zhou, J. Chang, H. Pu, K. Shi, S. Mao, X. Sui, R. Ren, S. Cui and J. Chen, *ACS Sens.*, 2016, **1**, 295-302.
177. P. Li, D. Zhang, C. Jiang, X. Zong and Y. Cao, *Biosens. Bioelectron.*, 2017, **98**, 68-75.
178. Z.-Q. Zhao, X. Chen, Q. Yang, J.-H. Liu and X.-J. Huang, *Chem. Commun.*, 2012, **48**, 2180-2182.
179. P. K. Sahoo, B. Panigrahy, S. Sahoo, A. K. Satpati, D. Li and D. Bahadur, *Biosens. Bioelectron.*, 2013, **43**, 293-296.
180. Y. Wei, C. Gao, F.-L. Meng, H.-H. Li, L. Wang, J.-H. Liu and X.-J. Huang, *J. Phys. Chem. C*, 2012, **116**, 1034-1041.
181. J. Li, S. Guo, Y. Zhai and E. Wang, *Electrochem. Commun.*, 2009, **11**, 1085-1088.
182. S. Chaiyo, E. Mehmeti, K. Žagar, W. Siangproh, O. Chailapakul and K. Kalcher, *Anal. Chim. Acta*, 2016, **918**, 26-34.
183. R. Seenivasan, W.-J. Chang and S. Gunasekaran, *ACS Appl. Mater. Interfaces*, 2015, **7**, 15935-15943.
184. J. Cui, S. Xu and L. Wang, *Sci. China Mater.*, 2017, **60**, 352-360.
185. Z. S. Qian, X. Y. Shan, L. J. Chai, J. R. Chen and H. Feng, *Biosens. Bioelectron.*, 2015, **68**, 225-231.
186. M. Li, X. Zhou, W. Ding, S. Guo and N. Wu, *Biosens. Bioelectron.*, 2013, **41**, 889-893.
187. Y. Wen, F. Xing, S. He, S. Song, L. Wang, Y. Long, D. Li and C. Fan, *Chem. Commun.*, 2010, **46**, 2596-2598.
188. K. Mao, Z. Wu, Y. Chen, X. Zhou, A. Shen and J. Hu, *Talanta*, 2015, **132**, 658-663.
189. Y. Yang, T. Liu, L. Cheng, G. Song, Z. Liu and M. Chen, *ACS Appl. Mater. Interfaces*, 2015, **7**, 7526-7533.
190. X. Liu, L. Li, Y. Wei, Y. Zheng, Q. Xiao and B. Feng, *Analyst*, 2015, **140**, 4654-4661.
191. Y. Wang, J. Hu, Q. Zhuang and Y. Ni, *ACS Sustain. Chem. Eng.*, 2016, **4**, 2535-2541.
192. X. Zuo, H. Zhang, Q. Zhu, W. Wang, J. Feng and X. Chen, *Biosens. Bioelectron.*, 2016, **85**, 464-470.
193. B. L. Li, J. Wang, H. L. Zou, S. Garaj, C. T. Lim, J. Xie, N. B. Li and D. T. Leong, *Adv. Funct. Mater.*, 2016, **26**, 7034-7056.
194. C. Liu, Z. Sun, L. Zhang, J. Lv, X. F. Yu, L. Zhang and X. Chen, *Sens. Actuators, B*, 2018, **257**, 1093-1098.
195. P. Li, D. Zhang, J. Liu, H. Chang, Y. e. Sun and N. Yin, *ACS Appl. Mater. Interfaces*, 2015, **7**, 24396-24402.
196. W. Gu, X. Pei, Y. Cheng, C. Zhang, J. Zhang, Y. Yan, C. Ding and Y. Xian, *ACS Sens.*, 2017, **2**, 576-582.
197. G. Zhao, X. Ren, X. Gao, X. Tan, J. Li, C. Chen, Y. Huang and X. Wang, *Dalton Trans.*, 2011, **40**, 10945-10952.
198. W. Peng, H. Li, Y. Liu and S. Song, *J. Mol. Liq.*, 2017, **230**, 496-504.
199. İ. Duru, D. Ege and A. R. Kamali, *J. Mater. Sci.*, 2016, **51**, 6097-6116.
200. S. Wang, X. Li, Y. Liu, C. Zhang, X. Tan, G. Zeng, B. Song and L. Jiang, *J. Hazard. Mater.*, 2018, **342**, 177-191.

201. R. Sitko, P. Janik, B. Feist, E. Talik and A. Gagor, *ACS Appl. Mater. Interfaces*, 2014, **6**, 20144-20153.
202. Z. Xu, Y. Zhang, X. Qian, J. Shi, L. Chen, B. Li, J. Niu and L. Liu, *Appl. Surf. Sci.*, 2014, **316**, 308-314.
203. W. Jia and S. Lu, *Korean J. Chem. Eng.*, 2014, **31**, 1265-1270.
204. H. Hadi Najafabadi, M. Irani, L. Roshanfekr Rad, A. Heydari Haratameh and I. Haririan, *RSC Adv.*, 2015, **5**, 16532-16539.
205. X. Li, H. Zhou, W. Wu, S. Wei, Y. Xu and Y. Kuang, *J. Colloid Interface Sci.*, 2015, **448**, 389-397.
206. C. Cheng, S. Li, J. Zhao, X. Li, Z. Liu, L. Ma, X. Zhang, S. Sun and C. Zhao, *Chem. Eng. J.*, 2013, **228**, 468-481.
207. S. Luo, X. Xu, G. Zhou, C. Liu, Y. Tang and Y. Liu, *J. Hazard. Mater.*, 2014, **274**, 145-155.
208. Y. Wang, S. Liang, B. Chen, F. Guo, S. Yu and Y. Tang, *PLoS One*, 2013, **8**, e65634.
209. V. R. Dandu Kamakshi Gari and M. Kim, *Monatsh. Chem.*, 2015, **146**, 1445-1453.
210. L. Cui, Y. Wang, L. Hu, L. Gao, B. Du and Q. Wei, *RSC Adv.*, 2015, **5**, 9759-9770.
211. G. Zhou, C. Liu, Y. Tang, S. Luo, Z. Zeng, Y. Liu, R. Xu and L. Chu, *Chem. Eng. J.*, 2015, **280**, 275-282.
212. L. Yang, Z. Li, G. Nie, Z. Zhang, X. Lu and C. Wang, *Appl. Surf. Sci.*, 2014, **307**, 601-607.
213. M. Tan, X. Liu, W. Li and H. Li, *J. Chem. Eng. Data*, 2015, **60**, 1469-1475.
214. J. Yang, J.-X. Wu, Q.-F. Lü and T.-T. Lin, *ACS Sustain. Chem. Eng.*, 2014, **2**, 1203-1211.
215. Z. Dong, F. Zhang, D. Wang, X. Liu and J. Jin, *J. Solid State Chem.*, 2015, **224**, 88-93.
216. S. Sheshmani, M. Akhundi Nematzadeh, S. Shokrollahzadeh and A. Ashori, *Int. J. Biol. Macromol.*, 2015, **80**, 475-480.
217. R. Sitko, P. Janik, B. Zawisza, E. Talik, E. Margui and I. Queralt, *Anal. Chem.*, 2015, **87**, 3535-3542.
218. Y. Q. He, N. N. Zhang and X. D. Wang, *Chin. Chem. Lett.*, 2011, **22**, 859-862.
219. Y. Wang, T. Yan, L. Gao, L. Cui, L. Hu, L. Yan, B. Du and Q. Wei, *Desalin. Water Treat.*, 2016, **57**, 3975-3984.
220. L. Fan, C. Luo, M. Sun, X. Li and H. Qiu, *Colloids Surf., B*, 2013, **103**, 523-529.
221. X. Guo, B. Du, Q. Wei, J. Yang, L. Hu, L. Yan and W. Xu, *J. Hazard. Mater.*, 2014, **278**, 211-220.
222. R. Sitko, B. Zawisza, E. Talik, P. Janik, G. Osoba, B. Feist and E. Malicka, *Anal. Chim. Acta*, 2014, **834**, 22-29.
223. H. T. Xing, J. H. Chen, X. Sun, Y. H. Huang, Z. B. Su, S. R. Hu, W. Weng, S. X. Li, H. X. Guo, W. B. Wu, Y. S. He, F. M. Li and Y. Huang, *Chem. Eng. J.*, 2015, **263**, 280-289.
224. Y. Yang, W.-q. Wu, H.-h. Zhou, Z.-y. Huang, T.-t. Ye, R. Liu and Y.-f. Kuang, *J. Cent. South Univ.*, 2014, **21**, 2826-2831.
225. L. Li, Z. Wang, P. Ma, H. Bai, W. Dong and M. Chen, *J. Pol. Res.*, 2015, **22**, 150.
226. T. Jiang, W. Liu, Y. Mao, L. Zhang, J. Cheng, M. Gong, H. Zhao, L. Dai, S. Zhang and Q. Zhao, *Chem. Eng. J.*, 2015, **259**, 603-610.

227. W. Wu, Y. Yang, H. Zhou, T. Ye, Z. Huang, R. Liu and Y. Kuang, *Water, Air, Soil Pollut.*, 2012, **224**, 1372.
228. I. E. Mejias Carpio, J. D. Mangadlao, H. N. Nguyen, R. C. Advincula and D. F. Rodrigues, *Carbon*, 2014, **77**, 289-301.
229. D. Chen, H. Zhang, K. Yang and H. Wang, *J. Hazard. Mater.*, 2016, **310**, 179-187.
230. X.-j. Hu, Y.-g. Liu, H. Wang, A.-w. Chen, G.-m. Zeng, S.-m. Liu, Y.-m. Guo, X. Hu, T.-t. Li, Y.-q. Wang, L. Zhou and S.-h. Liu, *Sep. Purif. Technol.*, 2013, **108**, 189-195.
231. W. M. Algothmi, N. M. Bandaru, Y. Yu, J. G. Shapter and A. V. Ellis, *J. Colloid Interface Sci.*, 2013, **397**, 32-38.
232. Y. Wang, X. Liu, H. Wang, G. Xia, W. Huang and R. Song, *J. Colloid Interface Sci.*, 2014, **416**, 243-251.
233. V. P. Chauke, A. Maity and A. Chetty, *J. Mol. Liq.*, 2015, **211**, 71-77.
234. S. Li, X. Lu, Y. Xue, J. Lei, T. Zheng and C. Wang, *PLoS One*, 2012, **7**, e43328.
235. Y. Lei, F. Chen, Y. Luo and L. Zhang, *J. Mater. Sci.*, 2014, **49**, 4236-4245.
236. A. S. K. Kumar, S. S. Kakan and N. Rajesh, *Chem. Eng. J.*, 2013, **230**, 328-337.
237. H. Ge and Z. Ma, *Carbohydr. Polym.*, 2015, **131**, 280-287.
238. X. Yuan, Y. Wang, J. Wang, C. Zhou, Q. Tang and X. Rao, *Chem. Eng. J.*, 2013, **221**, 204-213.
239. H. Jabeen, V. Chandra, S. Jung, J. W. Lee, K. S. Kim and S. B. Kim, *Nanoscale*, 2011, **3**, 3583-3585.
240. L. Li, C. Luo, X. Li, H. Duan and X. Wang, *Int. J. Biol. Macromol.*, 2014, **66**, 172-178.
241. L. Li, H. Duan, X. Wang and C. Luo, *New J. Chem.*, 2014, **38**, 6008-6016.
242. L. Li, F. Liu, H. Duan, X. Wang, J. Li, Y. Wang and C. Luo, *Colloids Surf., B*, 2016, **141**, 253-259.
243. F.-y. Guo, Y.-g. Liu, H. Wang, G.-m. Zeng, X.-j. Hu, B.-h. Zheng, T.-t. Li, X.-f. Tan, S.-f. Wang and M.-m. Zhang, *RSC Adv.*, 2015, **5**, 45384-45392.
244. S. Tongay, J. Zhou, C. Ataca, J. Liu, J. S. Kang, T. S. Matthews, L. You, J. Li, J. C. Grossman and J. Wu, *Nano Lett.*, 2013, **13**, 2831-2836.
245. V. Chandra and K. S. Kim, *Chem. Commun.*, 2011, **47**, 3942-3944.
246. Y. Zhang, T. Yan, L. Yan, X. Guo, L. Cui, Q. Wei and B. Du, *J. Mol. Liq.*, 2014, **198**, 381-387.
247. F. Najafi, O. Moradi, M. Rajabi, M. Asif, I. Tyagi, S. Agarwal and V. K. Gupta, *J. Mol. Liq.*, 2015, **208**, 106-113.
248. F. Fang, L. Kong, J. Huang, S. Wu, K. Zhang, X. Wang, B. Sun, Z. Jin, J. Wang, X.-J. Huang and J. Liu, *J. Hazard. Mater.*, 2014, **270**, 1-10.
249. L. Liu, C. Li, C. Bao, Q. Jia, P. Xiao, X. Liu and Q. Zhang, *Talanta*, 2012, **93**, 350-357.
250. H. Qi, H. Liu and Y. Gao, *J. Mol. Liq.*, 2015, **208**, 394-401.
251. F. Peng, T. Luo, L. Qiu and Y. Yuan, *Mater. Res. Bull.*, 2013, **48**, 2180-2185.
252. S. Chen, J. Hong, H. Yang and J. Yang, *J. Environ. Radioact.*, 2013, **126**, 253-258.
253. H. Cheng, K. Zeng and J. Yu, *J. Radioanal. Nucl. Chem.*, 2013, **298**, 599-603.
254. L. Chen, D. Zhao, S. Chen, X. Wang and C. Chen, *J. Colloid Interface Sci.*, 2016, **472**, 99-107.

255. M. Zambianchi, M. Durso, A. Liscio, E. Treossi, C. Bettini, M. L. Capobianco, A. Aluigi, A. Kovtun, G. Ruani, F. Corticelli, M. Brucale, V. Palermo, M. L. Navacchia and M. Melucci, *Chem. Eng. J.*, 2017, **326**, 130-140.
256. K. P. Carter, A. M. Young and A. E. Palmer, *Chem. Rev.*, 2014, **114**, 4564-4601.
257. C. Zhu, D. Du and Y. Lin, *2D Mater.*, 2015, **2**, 32004.
258. E. Treossi, M. Melucci, A. Liscio, M. Gazzano, P. Samori and V. Palermo, *J. Am. Chem. Soc.*, 2009, **131**, 15576-+.
259. K. Chen, G. Lu, J. Chang, S. Mao, K. Yu, S. Cui and J. Chen, *Anal. Chem.*, 2012, **84**, 4057-4062.
260. T. H. Kim, J. Lee and S. Hong, *J. Phys. Chem. C*, 2009, **113**, 19393-19396.
261. C. M. Willemse, K. Tlhomelang, N. Jahed, P. G. Baker and E. I. Iwuoha, *Sensors*, 2011, **11**, 3970.
262. J. Gong, T. Zhou, D. Song and L. Zhang, *Sens. Actuators, B*, 2010, **150**, 491-497.
263. G. Lu, H. Li, C. Liusman, Z. Yin, S. Wu and H. Zhang, *Chem. Sci.*, 2011, **2**, 1817-1821.
264. M. Zhang, C. Liao, Y. Yao, Z. Liu, F. Gong and F. Yan, *Adv. Funct. Mater.*, 2014, **24**, 1036-1036.
265. Z.-H. Sheng, X.-Q. Zheng, J.-Y. Xu, W.-J. Bao, F.-B. Wang and X.-H. Xia, *Biosens. Bioelectron.*, 2012, **34**, 125-131.
266. F. Yan, M. Zhang and J. Li, *Adv. Healthc. Mater.*, 2014, **3**, 313-331.
267. Y. Wang, Y. Shao, D. W. Matson, J. Li and Y. Lin, *ACS Nano*, 2010, **4**, 1790-1798.
268. C. Shan, H. Yang, J. Song, D. Han, A. Ivaska and L. Niu, *Anal. Chem.*, 2009, **81**, 2378-2382.
269. X. Kang, J. Wang, H. Wu, I. A. Aksay, J. Liu and Y. Lin, *Biosens. Bioelectron.*, 2009, **25**, 901-905.
270. C. Shan, H. Yang, D. Han, Q. Zhang, A. Ivaska and L. Niu, *Biosens. Bioelectron.*, 2010, **25**, 1070-1074.
271. Z. Wang, X. Zhou, J. Zhang, F. Boey and H. Zhang, *J. Phys. Chem. C*, 2009, **113**, 14071-14075.
272. Y. Liu, D. Yu, C. Zeng, Z. Miao and L. Dai, *Langmuir*, 2010, **26**, 6158-6160.
273. J. Luo, S. Jiang, H. Zhang, J. Jiang and X. Liu, *Anal. Chim. Acta*, 2012, **709**, 47-53.
274. H. Wu, J. Wang, X. Kang, C. Wang, D. Wang, J. Liu, I. A. Aksay and Y. Lin, *Talanta*, 2009, **80**, 403-406.
275. T. T. Baby, S. S. J. Aravind, T. Arockiadoss, R. B. Rakhi and S. Ramaprabhu, *Sens. Actuators, B*, 2010, **145**, 71-77.
276. S. Alwarappan, A. Erdem, C. Liu and C.-Z. Li, *J. Phys. Chem. C*, 2009, **113**, 8853-8857.
277. G. Zeng, Y. Xing, J. Gao, Z. Wang and X. Zhang, *Langmuir*, 2010, **26**, 15022-15026.
278. K. Zhou, Y. Zhu, X. Yang and C. Li, *Electroanalysis*, 2010, **22**, 259-264.
279. N. Q. Dung, D. Patil, T. T. Duong, H. Jung, D. Kim and S.-G. Yoon, *Sens. Actuators, B*, 2012, **166**, 103-109.
280. X. Dong, Y. Shi, W. Huang, P. Chen and L.-J. Li, *Adv. Mater.*, 2010, **22**, 1649-1653.
281. M. Du, T. Yang and K. Jiao, *J. Mater. Chem.*, 2010, **20**, 9253-9260.

282. O. Niwa, J. Jia, Y. Sato, D. Kato, R. Kurita, K. Maruyama, K. Suzuki and S. Hirono, *J. Am. Chem. Soc.*, 2006, **128**, 7144-7145.
283. C. Wang, L. Zhang, Z. Guo, J. Xu, H. Wang, K. Zhai and X. Zhuo, *Microchim. Acta*, 2010, **169**, 1-6.
284. N. G. Shang, P. Papakonstantinou, M. McMullan, M. Chu, A. Stamboulis, A. Potenza, S. S. Dhesi and H. Marchetto, *Adv. Funct. Mater.*, 2008, **18**, 3506-3514.
285. Y.-R. Kim, S. Bong, Y.-J. Kang, Y. Yang, R. K. Mahajan, J. S. Kim and H. Kim, *Biosens. Bioelectron.*, 2010, **25**, 2366-2369.
286. C.-L. Sun, H.-H. Lee, J.-M. Yang and C.-C. Wu, *Biosens. Bioelectron.*, 2011, **26**, 3450-3455.
287. C. X. Lim, H. Y. Hoh, P. K. Ang and K. P. Loh, *Anal. Chem.*, 2010, **82**, 7387-7393.
288. S. Hou, M. L. Kasner, S. Su, K. Patel and R. Cuellari, *J. Phys. Chem. C*, 2010, **114**, 14915-14921.
289. L. Wu, L. Feng, J. Ren and X. Qu, *Biosens. Bioelectron.*, 2012, **34**, 57-62.
290. L. Tan, K.-G. Zhou, Y.-H. Zhang, H.-X. Wang, X.-D. Wang, Y.-F. Guo and H.-L. Zhang, *Electrochem. Commun.*, 2010, **12**, 557-560.
291. F. Li, J. Chai, H. Yang, D. Han and L. Niu, *Talanta*, 2010, **81**, 1063-1068.
292. Y. Fan, H.-T. Lu, J.-H. Liu, C.-P. Yang, Q.-S. Jing, Y.-X. Zhang, X.-K. Yang and K.-J. Huang, *Colloids Surf., B*, 2011, **83**, 78-82.
293. T. Peik-See, A. Pandikumar, H. Nay-Ming, L. Hong-Ngee and Y. Sulaiman, *Sensors* 2014, **14**, 15227-15243.
294. G. P. Keeley, A. O'Neill, M. Holzinger, S. Cosnier, J. N. Coleman and G. S. Duesberg, *Phys. Chem. Chem. Phys.*, 2011, **13**, 7747-7750.
295. Y. Fang, S. Guo, C. Zhu, Y. Zhai and E. Wang, *Langmuir*, 2010, **26**, 11277-11282.
296. S. Karapetis, S. Bratakou, G.-P. Nikoleli, C. Siontorou, D. Nikolelis and N. Tzamtzis, *Electroanalysis*, 2016, **28**, 2171.
297. Y. Huang, X. Dong, Y. Shi, C. M. Li, L.-J. Li and P. Chen, *Nanoscale*, 2010, **2**, 1485-1488.
298. Y. H. Kwak, D. S. Choi, Y. N. Kim, H. Kim, D. H. Yoon, S.-S. Ahn, J.-W. Yang, W. S. Yang and S. Seo, *Biosens. Bioelectron.*, 2012, **37**, 82-87.
299. W. Fu, L. Feng, G. Panaitov, D. Kireev, D. Mayer, A. Offenhäusser and H.-J. Krause, *Sci. Adv.*, 2017, **3**, 1701247.
300. G. Liu, S. Rumyantsev, M. S. Shur and A. A. Balandin, *Appl. Phys. Lett.*, 2013, **102**, 93111.
301. B. Cai, S. Wang, L. Huang, Y. Ning, Z. Zhang and G.-J. Zhang, *ACS Nano*, 2014, **8**, 2632-2638.
302. P. Alonso-Cristobal, P. Vilela, A. El-Sagheer, E. Lopez-Cabarcos, T. Brown, O. L. Muskens, J. Rubio-Retama and A. G. Kanaras, *ACS Appl. Mater. Interfaces*, 2015, **7**, 12422-12429.
303. H. Dong, W. Gao, F. Yan, H. Ji and H. Ju, *Anal. Chem.*, 2010, **82**, 5511-5517.
304. C. Liu, Z. Wang, H. Jia and Z. Li, *Chem. Commun.*, 2011, **47**, 4661-4663.
305. L. Fan, Y. Hu, X. Wang, L. Zhang, F. Li, D. Han, Z. Li, Q. Zhang, Z. Wang and L. Niu, *Talanta*, 2012, **101**, 192-197.
306. J.-L. Chen, X.-P. Yan, K. Meng and S.-F. Wang, *Anal. Chem.*, 2011, **83**, 8787-8793.
307. C.-H. Lu, H.-H. Yang, C.-L. Zhu, X. Chen and G.-N. Chen, *Angew. Chem. Int. Ed.*, 2009, **48**, 4785-4787.

308. Y. Lin, Y. Tao, F. Pu, J. Ren and X. Qu, *Adv. Funct. Mater.*, 2011, **21**, 4565-4572.
309. F. Li, Y. Huang, Q. Yang, Z. Zhong, D. Li, L. Wang, S. Song and C. Fan, *Nanoscale*, 2010, **2**, 1021-1026.
310. X. Liu, L. Cao, W. Song, K. Ai and L. Lu, *ACS Appl. Mater. Interfaces*, 2011, **3**, 2944-2952.
311. Z. Chen, L. Qiu, Y. Tian, Y.-I. Lee, X. Hou and L. Wu, *Anal. Methods*, 2017, **9**, 3105-3113.
312. P. V. Shanta and Q. Cheng, *ACS Sens.*, 2017, **2**, 817-827.
313. Y. Song, K. Qu, C. Zhao, J. Ren and X. Qu, *Adv. Mater.*, 2010, **22**, 2206-2210.
314. S. Alwarappan, C. Liu, A. Kumar and C.-Z. Li, *J. Phys. Chem. C*, 2010, **114**, 12920-12924.
315. P. Wu, Q. Shao, Y. Hu, J. Jin, Y. Yin, H. Zhang and C. Cai, *Electrochim. Acta*, 2010, **55**, 8606-8614.
316. Y. Zhang, Y. Wang, J. Jia and J. Wang, *Sens. Actuators, B*, 2012, **171**, 580-587.
317. M. Zhang, C. Liao, C. H. Mak, P. You, C. L. Mak and F. Yan, *Sci. Rep.*, 2015, **5**, 8311.
318. S. He, B. Song, D. Li, C. Zhu, W. Qi, Y. Wen, L. Wang, S. Song, H. Fang and C. Fan, *Adv. Funct. Mater.*, 2010, **20**, 453-459.
319. J. Balapanuru, J.-X. Yang, S. Xiao, Q. Bao, M. Jahan, L. Polavarapu, J. Wei, Q.-H. Xu and K. P. Loh, *Angew. Chem. Int. Ed.*, 2010, **49**, 6549-6553.
320. Z. Wang, J. Zhang, P. Chen, X. Zhou, Y. Yang, S. Wu, L. Niu, Y. Han, L. Wang, P. Chen, F. Boey, Q. Zhang, B. Liedberg and H. Zhang, *Biosens. Bioelectron.*, 2011, **26**, 3881-3886.
321. C.-H. Lu, J. Li, J.-J. Liu, H.-H. Yang, X. Chen and G.-N. Chen, *Chem. - Eur. J.*, 2010, **16**, 4889-4894.
322. R. Devasenathipathy, V. Mani and S.-M. Chen, *Talanta*, 2014, **124**, 43-51.
323. J. Ding, S. Zhu, T. Zhu, W. Sun, Q. Li, G. Wei and Z. Su, *RSC Adv.*, 2015, **5**, 22935-22942.
324. F. Gao, Q. Wang, N. Gao, Y. Yang, F. Cai, M. Yamane, F. Gao and H. Tanaka, *Biosens. Bioelectron.*, 2017, **97**, 238-245.
325. Z. Yang, Q. Sheng, S. Zhang, X. Zheng and J. Zheng, *Microchim. Acta*, 2017, **184**, 2219-2226.
326. Y. Wang, Y. Li, L. Tang, J. Lu and J. Li, *Electrochem. Commun.*, 2009, **11**, 889-892.
327. J. Du, R. Yue, F. Ren, Z. Yao, F. Jiang, P. Yang and Y. Du, *Gold Bull.*, 2013, **46**, 137-144.
328. J. Ping, J. Wu, Y. Wang and Y. Ying, *Biosens. Bioelectron.*, 2012, **34**, 70-76.
329. G. P. Keeley, A. O'Neill, N. McEvoy, N. Peltekis, J. N. Coleman and G. S. Duesberg, *J. Mater. Chem.*, 2010, **20**, 7864-7869.
330. S. Guo, D. Wen, Y. Zhai, S. Guo and E. Wang, *ACS Nano*, 2010, **4**, 3959-3968.
331. K. Zhou, Y. Zhu, X. Yang, J. Luo, C. Li and S. Luan, *Electrochim. Acta*, 2010, **55**, 3055-3060.
332. L. Li, Z. Du, S. Liu, Q. Hao, Y. Wang, Q. Li and T. Wang, *Talanta*, 2010, **82**, 1637-1641.
333. J. Wang, *Chem. Rev.*, 2008, **108**, 814-825.
334. L. Tang, Y. Wang, Y. Li, H. Feng, J. Lu and J. Li, *Adv. Funct. Mater.*, 2009, **19**, 2782-2789.

Chapter 2.

Characterization techniques

This chapter will cover the different characterization techniques used in this work to structurally characterize graphene- and graphene oxide- based hybrid materials. Samples were characterized using *e.g.* Raman spectroscopy, HR-TEM and XPS analytic methods. Each technique will be presented through some theoretical background and the relevant results from the investigation of the 2DMs and functionalized 2DMs.

2.1. Morphological characterization

This section will describe the fundamentals of High-resolution transmission electron microscopy (HR-TEM) imaging, in the framework of a collaboration with Dr. Vittorio Morandi at the Institute for Microelectronics and Microsystems in Bologna (IMM). Samples for HR-TEM analysis were performed using drop-casting method on a carbon-coated copper grid, followed by solvent evaporation. HR-TEM images were obtain on a FEI Tecnai F20 TEM equipped with a Schottky emitter and operated at 120-200 keV.

2.1.1. High-resolution transmission electron microscopy (HR-TEM)

The HR-TEM is a powerful technique used in the field of 2DMs materials for analyze the quality, shape, density, thickness and size (see chapter 5). In HR-TEM, a sample in the form of a thin foil is exposed to a high-energy (typically 60-300 keV) electron beam which are accelerated to nearly the speed of light, and the interactions between the electrons and atoms can be used to observe specific features. If the sample is ultra-thin in according to the average free path of the electron in the system, the electrons mostly pass through the sample without any change of energy. The other electrons lose their energy, which is transformed into different forms, like Auger electrons, X-rays, etc. In HR-TEM the beam of electrons from the electron gun is concentrated into a small, coherent beam using of the condenser lens. This beam is limited by the condenser instrument, excluding high angle electrons. The beam then impacts the sample and parts of it are transmitted depending upon the electron transparency and thickness of the sample. Sample holders are fitted so that the specimen can be tilted to obtain a particular diffraction condition. Thanks to that, there is possibility to analyze 3-dimensional crystals by combine several views, taken from different angles, into a 3D map. This technique is referred electron crystallography. In the other case, blocking the electrons reflected by putting the aperture allows the unscattered electrons to go through it, and using these to obtain a contrast image is referred to as light field. The reflected electrons can also be used to create an image, called a dark field image. Next, the image is zoomed and focused

onto an imaging device, like a layer of photographic film, a fluorescent screen, or a sensor such as a scintillator (Figure 2.1). Crystallographic information like dislocations and grain boundaries can also be obtained from diffraction patterns. Some of HR-TEM are equipped with an X-ray emitter (Energy Dispersive Spectroscopy – EDS), which can also collect elemental and chemical state maps.

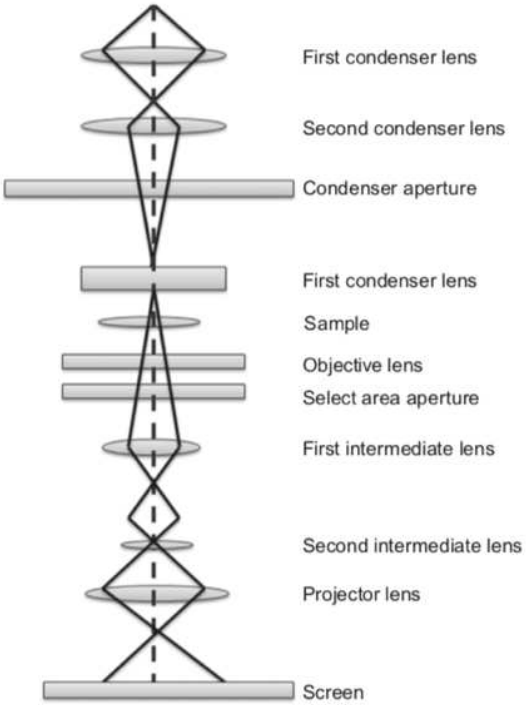

Figure 2.1. Basic components of HR-TEM. Reproduced with permission.[1]

HR-TEM allow imaging the samples at a significantly higher resolution than optical microscopes, due to the smaller de Broglie wavelength of electrons. For this reason, the HR-TEM can provide the images at atomic scale level. The wavelength of the electrons (λ) depends on the acceleration voltage (eV) according to the Equation 2:

$$\lambda = h/(2meV)^{1/2} \quad \text{(Equation 2)}$$

where: m - mass of the electron, *h* - Plank's constant.

The contrast of a HR-TEM image arises from the interference in the image plane of the electron wave with itself. There are two important mechanism which produce image contrast in the electron microscope:

- Diffraction contrast: diffracted electrons leaving at the lower surface of the crystalline specimen are intercepted by the objective aperture and prevented to contribute to the image. The image contrast is produced by changes in absorption coefficient from one to another region of the specimen. At medium and low resolution, the contrast in the image would arise from amplitude reduction in region of large scattering where the scattered rays are intercepted by the objective aperture.

- Phase contrast: some of the diffracted beams leaving the specimen are recombined to form the image so that the phase difference in the image. Phase contrast arises from the interference between waves included within the objective aperture and whose plane should be controlled by an accurate focusing to produce a contrast. Diffraction contrast is the dominant mechanism revealing object details larger than 1.5 nm in crystalline specimens. Phase contrast is the dominant mechanism for an object detail smaller than 1 nm and is important in high-resolution studies, in early stages of short-range order and amorphous materials. Phase contrast is the basic mechanism describing image formation in high resolution electron microscopy.

Recently, Kupta *et al.* used electron irradiation (HR-TEM) to prove a plausible interaction pathways between reduced graphene oxide (RGO) and cationic dyes (malachite green) which are deduced from nanostructural features (Figure 2.2).[2] The heterogenous and folded features are clearly observed in the GO nanosheets (Figure 2.2a) and are related to the presence of sp^3 hybridized carbon atoms functionalized with oxygen and structural defects. On the other hand, Figure 2.2b shows rGO nanosheets aggregated with each other owing to intermolecular interaction which provide multilayer appearance to the rGO. Additionally, HR-TEM images (Figure 2.2c) show lamellar structure of rGO with interlayer spacing of ~0.34 nm in the (002) plane.

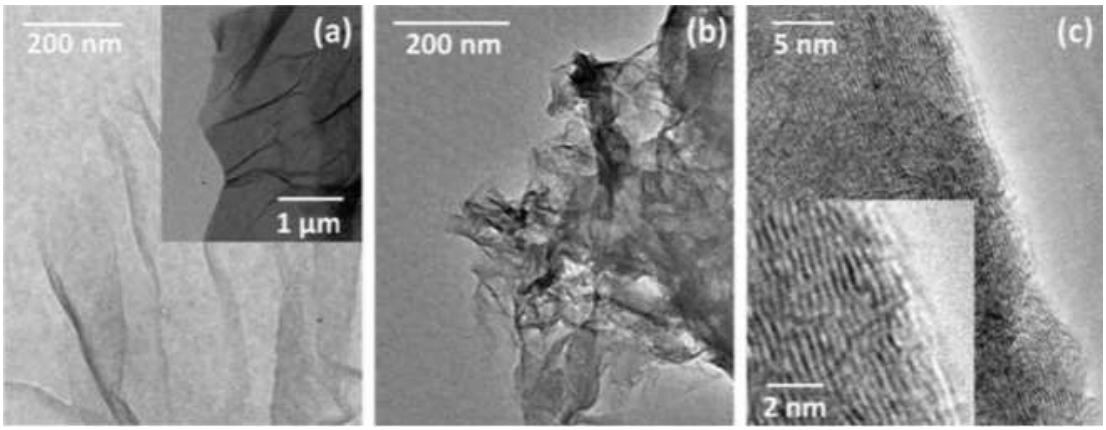

Figure 2.2. HR-TEM images of a) GO and b-c) rGO. The atomic thick lamellae in (002) plane are explicitly seen in the inset of image of rGO (c). Reproduced with permission.[2]

Similar to GO, rGO is structurally inhomogeneous material and exhibits holes, graphitic domain and structural defects. The disorder sites are likely from presence of residual oxygen functionalities which maintain even after the reduction. Figure 2.3 shows high-resolution TEM images of rGO consisting of holes with size of 4–6 nm encircled by brown color. There are several defect sites thoroughly distributed in the rGO skeleton and are indicated by white arrows (Figure 2.3a-b).

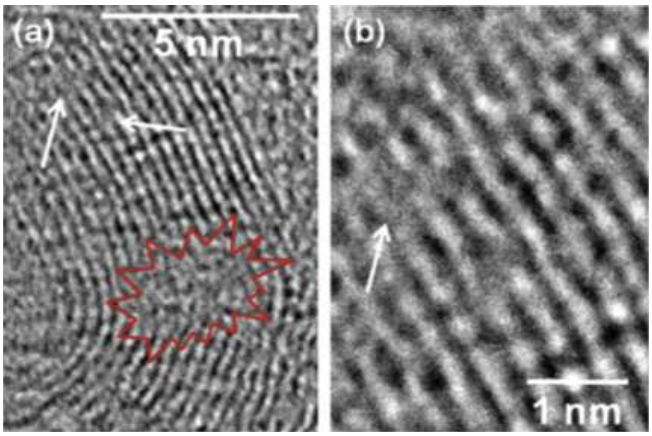

Figure 2.3. a-b) HRTEM images of RGO demonstrating the holes area (red encircled color) and defect sites (white arrows). Reproduced with permission.[2]

Another interesting application involving HR-TEM was presented by Zhan and co-workers.[3] They demonstrate an experimental analysis of highly efficient removal of pathogenic bacteria with magnetic graphene composite (G-Fe_3O_4). Based on the HR-TEM results, they observed single-sheet structure of graphene oxide and the

monodisperse of iron oxide (Fe_3O_4) nanoparticles on the surface of graphene (Figure 2.4a). As illustrated in the typical HRTEM image of G-Fe_3O_4 (Figure 2.4b), lattice fringes of Fe_3O_4 (d = 0.29 nm) can be found clearly, demonstrating that Fe_3O_4 sample is highly crystalline. Furthermore, the electron diffraction patterns of G-Fe_3O_4 (inset of Figure 2.4b) can be indexed to the highly crystalline reflections of cubic inverse spinel Fe_3O_4 structure, which is in accordance with the below result of XRD.

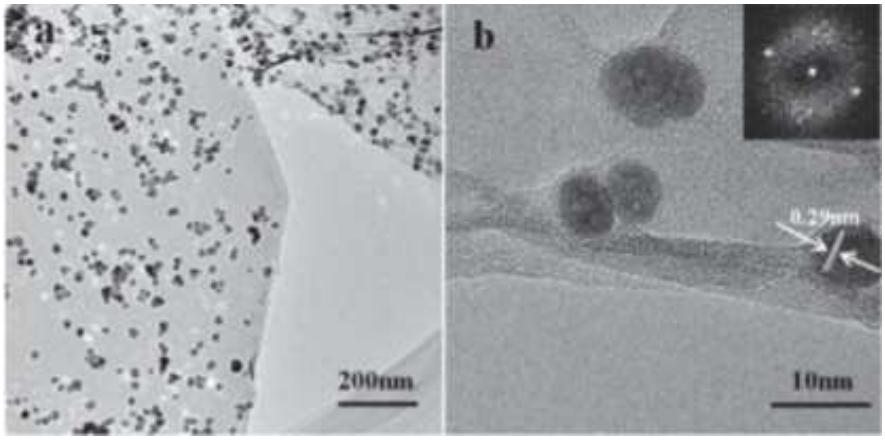

Figure 2.4. a) TEM and b) HR-TEM image of G-Fe_3O_4 nanocomposite. Reproduced with permission.[3]

One of the fundamental limits related to the resolution are wavelength (λ) of the electrons used to generate the image as well as the quality of the objective lens. This type of limit is also called the point resolution limit and it can be estimated using the formula $\sim C^{1/4}\lambda^{3/4}$, where C is the coefficient of spherical aberration and is the main factor that decides lens quality. To resolve abovementioned issue, the applying of higher acceleration voltages, which decreasing the electron wavelength is needed. Furthermore, this approach includes the exploit of high-tech and expensive tools with acceleration voltages in the range of 1200 kV and the resolution higher than 1 Å. Besides morphological characterization, HR-TEM can give elemental analysis of the sample. It is possible indirectly due to the additional energy dispersive X-ray (EDX) detector, which accumulate necessary information coming from inelastically scattered electrons.

In this dissertation HR-TEM was used for the characterization of graphene-based nanocomposite (Mo_{132}-DTAB-EEG) produced by relatively simple approach which relies on the use of surfactant (DTAB) to form the surfactant encapsulated cluster based on a functionalized Keplerate type-polyoxometalate Mo_{132}-DTAB, which can physisorb on

the EEG (chapter 5). HR-TEM analysis proved that the surface of the electrochemically exfoliated graphene sheets is covered with 3D features of Mo_{132}-DTAB substrate. EDX measurements were performed as an additional analysis to determine the structure of both GO-BPEI, SiO_2NH_2-GO as well as Mo_{132}-DTAB-EEG hybrid materials (chapters 3,4 and 5).

2.2. Qualitative characterization

2.2.1. Raman spectroscopy

Raman spectroscopy makes use of Raman scattering or inelastic scattering of monochromatic laser light, and it is used to study the rotational, vibrational, and other modes of a graphene and related materials. In addition, this technique can provide information about the effects of doping, temperature and strain.[4] Furthermore, the favorable advantage of Raman technique is fast and non-destructive analysis, although its interpretation is quite often not so simple. This technique is usually used to analyze of molecules but since 2006, when for the first time it was used the Raman characterization of graphene from Ferrari *et al*, it has been widely employed to assess the quality and structural integrity of the exfoliated 2DMs, as well as the number of layers of the nanosheets. Raman spectroscopy is a technique based on interaction between the phonons and the laser light affect on a shift in energy, which gives information about the modes of quasiparticles in the system. Each peak in a Raman spectrum corresponds to the vibrational frequency of a bond of the analyzed sample. Usually, a laser beam is used to lighting the sample. The electromagnetic radiation from the laser hit spot is collected with a lens and passed through a collimator. The molecule will become excited to an excited state from a ground state and is relaxed into a vibrational excited state. This creates the stokes Raman scattering. Suppose the molecule was already in the vibrational state, then it is called antistokes Raman scattering. A change in polarizability is required for the molecule to exhibit Raman scattering. The intensity of the Raman scattering depends on the change in polarizability, whereas the Raman shift is based on the vibrational level involved. Advanced version of Raman spectroscopy includes stimulated Raman spectroscopy; surface enhanced Raman spectroscopy, and resonance Raman spectroscopy.

Raman spectroscopy is a type of very responsive analysis method, even to slight differences in structure. Thanks to that, it is also possible to distinguish the different allotropes of carbon, *e.g.* graphite, diamond, and graphene, which vary only in the orientation of the carbon-carbon bonds. While the diamond is characterized by only one

peak amounts to 1332 cm^{-1}, graphene and graphite Raman spectra reveal two main peaks at 1580 cm^{-1} and 2680 cm^{-1} which are generally labeled as G and 2D peaks, respectively. G peak is correlated with the relative motions of sp^2 carbon atoms, thus is a characteristic peak of material with graphitic structure (for that reason it takes this name) like graphene and graphite. The G mode of graphite possess E_{2g} symmetry and consist in-plane bond-stretching vibration of pairs of sp^2 carbon atoms.[5] In turn, D peak (defect band) is associated to the presence of defects in the system. In reality, this peak responds to a mode of the sp^2 carbon rings which symmetry is forbidden for Raman selection rules in pristine graphite and graphene, whereas only becomes active in the presence of disorder (Figure 2.5).

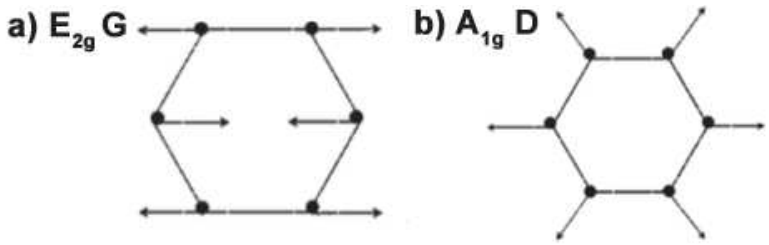

Figure 2.5. Graphene motion in the G and D modes. a) E2g G mode of sp^2 rings, b) A_{1g} D breathing mode in rings. Reproduced with permission.[5]

Defect band appear only when the sp^2 conjugation is interrupted by vacancies and interstitial defects. Finally, the 2D band is the second order of the D band. Nevertheless, it originates from a vibrational process which consists two phonons and it doesn't require to be activated as the D band. Hence, it is also present without the D band. In turn, the G peak can provide an information on the thickness of the material as its position changes from bulk to mono and bilayers.[6] Nevertheless, the other factors, such as doping or strain, can have impact on position of the peak. In pristine graphene and graphite Raman spectra present weak D band signal, as presented on Figure 2.6. Whereas the D band in graphite comprise of two peaks, called D_1 and D_2 (up chart), D peak in pristine graphene is a single sharp peak (bottom chart).

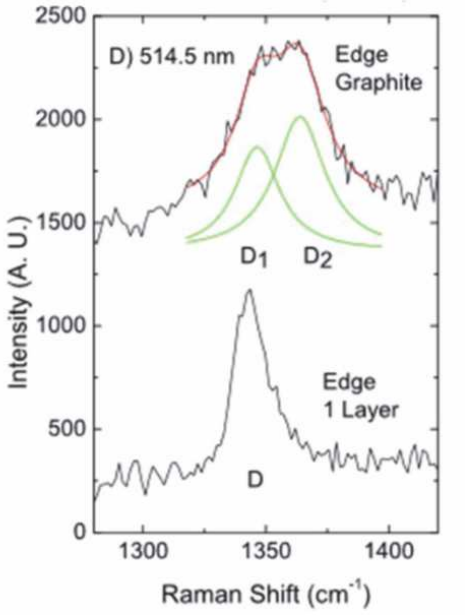

Figure 2.6. D peaks at the single layer graphene (bottom) and edge of graphite (up). Reproduced with permission.[5]

While D band is intense, it means that there are many defects in the structure of material. That's why, the ratio between the intensities of I_D and I_G can be exploited to estimate the level of disorder in graphene sheets. The I_D/I_G ratio presents two different relation in function of the amount of disorder. In the range of low defect density, I_D/I_G ratio increases with the defects because a higher density of defects produces a more elastic scattering. Nevertheless, when I_D/I_G ratio reaches appropriate value, that correspond to the beginning of the regime of high defect density, this ratio will begin to decrease as shown on Figure 2.7.

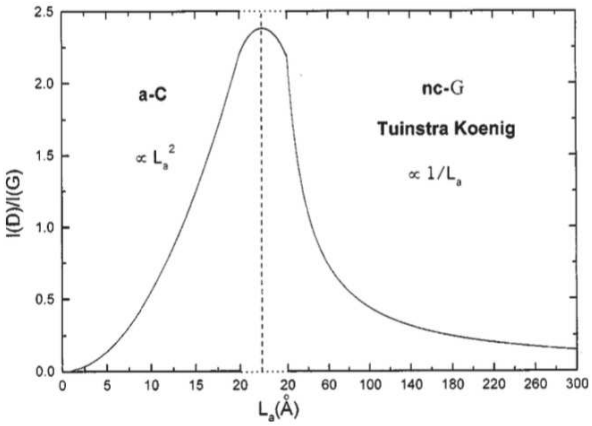

Figure 2.7. Transition between the two regimes of low and high defect density and relation between Id/Ig and defect distance. Reproduced with permission.[5]

Similarly, to the case of graphene, Raman spectroscopy can be used as fast an non-destructive method for graphene-based materials. In the work, Kumar *et al.* used Raman spectroscopy to characterized hybrids of single-layer graphene oxide with manganese ferrite magnetic nanoparticles as an adsorbent for efficient removal of Pb^{2+}, As^{3+}, and As^{5+} from contaminated water.[7] As shown on Figure 2.8 Raman spectrum of GO shows two clear peaks at 1590 and 1342 cm^{-1} related to first- order E_{2g} mode from sp^2 carbon domains (G - band) and disorder mode (D - defect band), respectively (Figure 2.8. spectrum a). In turn, Raman spectrum of the $MnFe_2O_4$ nanoparticles (Figure 2.8. spectrum b) shows a peak at ~600 cm−1, which can be attributed to Fe−O bond stretching. Finally, Raman spectrum of the GONH (Figure 2.8. spectrum c) shows the Raman lines of NPs as well as that of GO which confirms the formation of GONH hybrid materials.

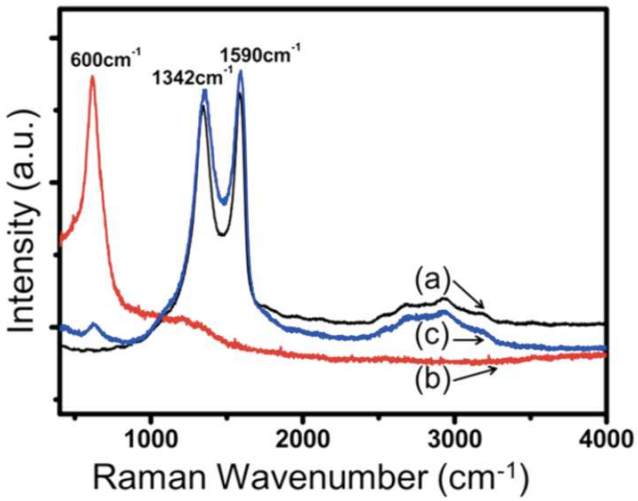

Figure 2.8. Raman spectra of a) GO b) $MnFe_2O_4$ nanoparticles and c) GONH. Reproduced with permission.[7]

Based on these and other studies, Raman spectroscopy can be used to determine the content of defects in graphene. Thus, in this dissertation Raman spectroscopy has been used to assess the quality of the graphene coated-materials (see chapters 3 and 4).

2.2.2. X-ray photoelectron spectroscopy (XPS)

In this paragraph, there will be discussed some useful information to reading the following chapters regarding the analysis of graphene-based materials of XPS. The X-ray photoelectron spectroscopy is a commonly used quantitative spectroscopic surface analysis technique useful for determine the elemental composition of a material, as well as to achieve knowledge on the chemical binding. The basic principle of this technique concerns the photoelectric effect. Under ultra-high vacuum, a material is irradiated with X-rays causing electron emission from the core orbital of the elements at the surface. The kinetic energy measurements and the number of electrons that have escaped from the material surface provide the XPS spectra. This energy transfer decides about the emission of photoelectrons from the core levels of the material. Binding energy can be calculated, as the energy of the X-ray used to excite the electron from a core orbital is a known quantity, by using the Equation 3:

$$E_{binding} = E_{photon} - E_{kinetic} - \Phi \quad \text{(Equation 3)}$$

where: $E_{binding}$ - energy of the emitted electron, E_{photon} - X-ray photon energy used, $E_{kinetic}$ - kinetic energy of the emitted electron, Φ - work function.

The binding energy of electron depends on the element from which the electron is emitted, more in particular from the orbital, and from the chemical environment of the atom as well. By measuring the kinetic energy ($E_{kinetic}$) of the collected electrons which reach the detector, it is possible to calculate the binding energy of the electrons and in this way to identify the different elements at the surface's sample and their chemical state. As a result, a survey of the surface composition of the probed area will be obtained. Except giving information about the type of atoms which produce a determined molecular system, the investigation of ionization energy of internal electrons enables to get information on the charge density of an atom. More in general, XPS can also be used for detecting contaminants in the sample. X-ray is able to penetrate material through several hundreds of nanometers, while the emitted photoelectron only comes from some nanometers of the material. That's why this technique is relevant with the analysis of nanometer thin 2DMs and functionalized 2DMs materials. XPS can be used not only an

elemental analysis but gives also details on the functional groups which occur in the studied material. Moreover, the binding energy for a valence electron in a given atom is dependent to chemical environment of the atom which determines a spatial redistribution of the electrons. For example, when two different atoms are bonded which possess another electronegativity, the valence electrons will be attracted by the more electronegative atom. This phenomenon of the electrons results in a change in binding energy. X-ray photoelectron spectroscopy is defined as a very sensitive surface technique because of the quick mean free path of the photoelectrons in the analyzed material. The obtained free electrons can pass through inelastic scattering events causing loss in their energy, whereas some of the electrons don't possess enough energy to escape the material because of the collision with other atoms in the solid structure. The mean free path of an electron against inelastic scattering changes with the kinetic energy of the valence electron is fitted using parabolic function as presented in Figure 2.9.

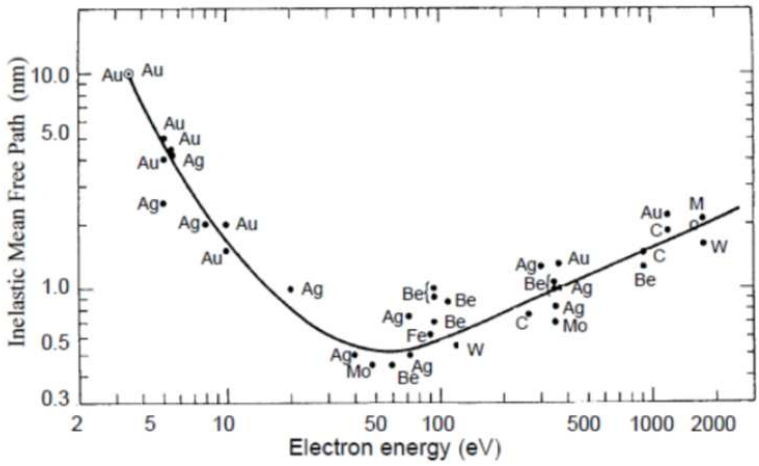

Figure 2.9. Universal curve of electron inelastic mean free path in function of electron energy (eV). Reproduced with permission.[8]

During XPS analysis a local shortage of electrons on the surface of the sample is observed. While not conductive samples are analyzed, they cannot to compensate this deficiency of electrons, resulting to the charge effect. That's why, the whole spectrum is shifted in higher binding energy. To overcome this drawback, the studies of insulating samples are carried out using suitable flood gun active to produce unfocused electron beam with low energy. It is required to offset the charging of the sample. Additionally, the spectra are calibrated, usually respect to the binding energy of the adventitious carbon.

The main noteworthy parts of an XPS spectrometer are the X-ray source and an electron energy analyzer. Mostly in XPS device the X-rays are received using magnesium (Mg) or aluminum (Al) anticathode which produce the correspondent energy Kα of 1284 eV and 1487 eV, respectively. Then, the X-ray beam is concentrated on the analyzed material from which photoelectrons are emitted. The photoelectrons are then gathered by a layout of lens and focused on the analyzer, where they are separated according to their kinetic energy. Lastly, they are calculated and recorded in the detector.

In the apparatus available in Nanochemistry laboratory in Strasbourg that was used for the XPS analysis presented in this dissertation, the very high vacuum is provided by turbomolecular pumps which let a step-wise reduce of the pressure between two independent chambers: the antechamber, where the sample is placed and waited until an optimal pressure of ~ 10^{-7} mBar is achieved, and the analysis divider, where the sample is transferred for the analysis that is carried out at a pressure of 10^{-9} mBar. Whereas this analysis technique is usually used for the analysis of metals, polymers and molecular systems, recently XPS has been extensively exploited for the analysis of 2DMs as well. In this dissertation XPS analysis were used for estimating the quality of the graphene-based materials.

2.3. Methods for quantification of adsorption of metal ions and organic molecules

2.3.1. Flame absorption atomic spectrometry (FAAS)

The FAAS consists in measuring the monochromatic radiation emitted by the free atoms of the compound. This method requires three main processes: evaporation of the sample, atomization and excitation of the sample. In order to absorb the specific radiation, a sufficiently large number of atoms must be in the basic state. Earlier excitation is not needed, which is a great advantage of the atomic absorption method. The basis of the AAS technique is the Kirchhoff law of the radiation, according to which the element absorbs the radiation of such wavelength as it emits in an excited state. The absorbance is described following the Equation 4 presented below:

$$A=\gamma \frac{N_p f l}{a} \quad \text{(Equation 4)}$$

where: γ - constant coefficient, N_p - number of atoms in the ground state, f - oscillator power, l - distance on which radiation absorption occurs, a- coefficient depending on line width and contour.

According to the Lambert-Beer law (Equation 5) the absorbance at a particular wavelength is directly proportional to the number of atoms in the volume unit, *i.e.* their concentration and the thickness of the absorbent layer.

$$A = \varepsilon c l \quad \text{(Equation 5)}$$

where: A - absorbance, ε - absorptivity, c - concentration, l - path length.

This dependence is the basis for quantitative AAS methods. The first works using AAS method was published between 1953-1955. Walsh presented not only the theoretical basis of the method, but also proposed apparatus and analytical application.[8] Atomic absorption was introduced on a wide scale in the 60's years and became one of the most widely used instrumental methods.

The flowchart of the FAAS is presented on Figure 2.10. Radiation from the source emitting the characteristic linear spectrum of the element being determined passes through the atomizer, falls into a gap of monochrome which separates the resonant lines from the others, and then in the detector is processed and the electrical signal, measured on the meter.

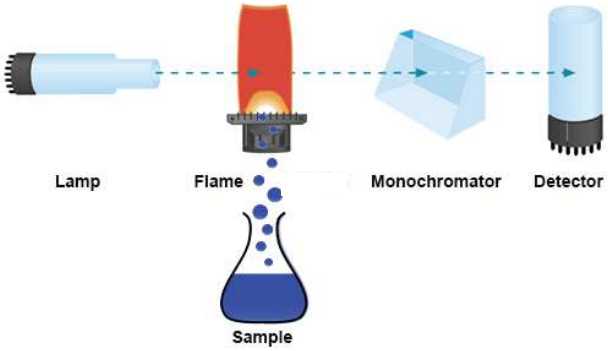

Figure 2.10. Flowchart of FAAS

The free atoms of the element generated during the atomization pass from the ground state to the excited state. The ratio of the number of excited atoms (N_k) to the number of atoms in the ground state (N_p) is small, which makes the absorption spectrum much simpler than the emissive spectrum. The ratio of N_k/N_p at a given temperature, is defined by the Boltzmann formula, decreases exponentially with an increase in the frequency of the resonant line. Noteworthy, the elements whose atoms possess resonant lines in the long-term range, *e.g.* Na^+, K^+, Li^+, can be marked with a greater sensitivity of the emission method, while Zn^{2+} or Mg^{2+}, whose emission lines in the shortwave range are very weak, is determined with high sensitivity of the absorption method. For high sensitivity and precise measurement, the radiation source used in atomic absorption spectrometers should emit stable radiation with the greatest possible intensity and a narrow outline from the width of the emitted lines. Therefore, the use of cavity cathode lamp in AAS analysis is appropriate. The main advantage of the lamp with a cavity cathode in comparison with other excitation sources is their high versatility. It is true, that we need suitable lamps for the analysis of the individual elements, while the fact that this method can be applied to each form of the sample to denote the elements both difficult and easily induced is undoubtedly its trump. The detection of metallic elements in a cavity cathodic lamp is, on average, one order of magnitude higher than that of the arc excitation sources. In

addition, cavity cathodic is primarily used for the determination of hard-to-generate elements, in the analysis of very small samples, in trace analysis and for the marking of isotopic composition. This type of lamp was used in this work to excitation the elements of heavy metal ions (Pb^{2+}, Cd^{2+}, Cu^{2+}) and the determination of the concentration of the salt solution of the element after the adsorption process. To mark a particular element, its necessary to separate it from the sample as free atoms. The most commonly used atomizer is the air-acetylene flame, the nitric oxide-acetylene (for the elements that make up the hard-dissociating oxides) and the air-methane (for readily ionizing metals). The FAAS methodology measures the ratio of the radiation intensity without dispensing the sample to the radiation intensity when dispensing the solution analyzed using the photomultiplier.

In the atomic absorption analysis, as in other instrumental methods, there are some disturbances related to the presence of accompanying substances in the analyzed solution. The disruption of the AAS method can be divided into three groups:

- Spectral disturbances: arise as a result of overlapping lines or absorbent and emissive bands. For example, two different elements in the solution can possess absorbent lines of similar wavelengths and can absorb emitted radiation *e.g.* vanadium absorbent lines with a wavelength of 308.21 nm can absorb aluminum lines 308.15 nm.

- Physical disturbances: result from changes in the physical properties of the solutions, they affect the spraying performance of the sample (nebulizer).

- Chemical disturbances: caused by chemical reactions in the flame. However, an adequate knowledge of the composition of the analyzing samples allows the elimination of these distortions. The use of a reducing flame makes it possible to reduce or prevent the formation of the oxides created.

Sitko *et al.* indicate the adsorptive properties of neat graphene oxide (GO) towards divalent metal ions (Cu^{2+}, Cd^{2+}, Pb^{2+}) using flame atomic absorption spectrometry (FAAS).[9] This work includes also adsorption of Zn^{2+} on GO, which has so far not been reported. On the other hand, Tan and co-workers enhanced sorption capacities for copper ions by L-tryptophan-functionalized graphene oxide composite (L-Trp/GO).[10] The L-Trp/GO was successfully produced *via* the nucleophilic substitution reaction. As an efficient approach, this one-step strategy could be used to synthesize high quality of graphene oxide/L-tryptophan (GO/L-Trp) without any toxicity. Moreover, it also showed that GO/L-Trp could be reused after desorption, suggesting potential application in

wastewater treatment. In order to avoid discrepancies in the experimental results, all FAAS investigations were carried out in triplicate and experimental data reported were the average of at least three repetitive measurements with a 5% relatively standard deviation. The sorption for Cu^{2+} and Pb^{2+} were typical monomolecular layered and sorption capacities were 588 $mg \cdot g^{-1}$ and 222 $mg \cdot g^{-1}$ at 293 K, respectively, indicated that it could be an effective adsorbent for toxic heavy metal removal.

2.3.2 UV-vis spectrophotometry

Electromagnetic radiation passing through a given centre can undergo different processes: absorption, reflection and dispersion. Spectrophotometric methods use the phenomenon of radiation absorption of the appropriate wavelength. The condition for this phenomenon is that the energy of the incident radiation corresponds to the difference of the electron levels of the molecule, *i.e.* that the electron absorbing molecules can be transferred from the ground state to an excited state (the reverse process is studied using fluorescent spectroscopies). The spectrophotometric methods are divided in terms of the length of radiation applied to the three essential groups:

- Ultraviolet (UV) spectrophotometry in the wavelength of electromagnetic radiation range of 200-380 nm.
- Spectrophotometry in the visible light wavelengths range from 280 to 780 nm.
- Spectrophotometry in infrared light wavelengths range from 1 to 16 μm.

There are no theoretical or apparatus differences between the visible light and the UV spectrophotometry, while infrared spectrometry is completely different. Ultraviolet (UV) and visible (vis) spectrophotometry have been in general use for the last 65 years (first commercial UV-Vis spectrophotometer was built in 1941) and over this period have become one of the most important instruments in the modern analytical laboratory. This method consists of a deuterium or tungsten lamp for the ultraviolet and visible region wavelengths, respectively, sample and reference beams, a detector, and a monochrome (Figure 2.11). Cuvettes are used for sample holding and are kept inside the instrument for introducing samples to the light path. Glass, plastic, silica, or quartz cells can be used as cuvettes. Plastic and glass cuvettes absorb wavelengths below 310 nm, so they cannot be used for absorbance studies below that wavelength. Therefore, quartz cuvettes are used for absorption measurements in the ultraviolet range as they are transparent to the wavelengths above 180 nm.

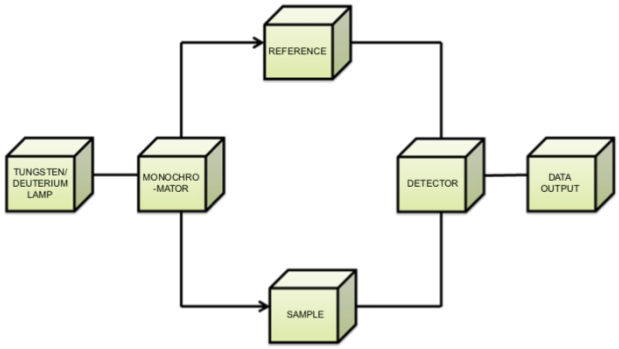

Figure 2.11. Flowchart of UV-vis spectrophotometer. Reproduced with permission.[9]

UV-vis spectroscopy refers to absorption spectroscopy, which concern the measurements of the absorption of radiation, as a function of frequency or wavelength, due to its interaction with a sample. The ratio between the sample and reference beam intensities is recorded by the detector. When a difference is found in the intensities, that means the reference beam's intensity is higher than the sample, and the particular wavelength is plotted as having the high ultraviolet absorbance. UV-vis spectrum refers to the reflectance or absorbance spectra in the UV-visible region. When the light beam is passed through the solution, a part of the light may be absorbed, and the rest will be transmitted through the solution. The ratio of light entering the sample to the light that exits the sample at a fixed wavelength is called transmittance. The negative logarithm of transmittance is called absorbance. To quantitative determine concentrations of an absorbing species in solution, the Lambert-Beer law has to be used (Equation 5). Due to the physical or chemical reasons, there may be deviations from the adsorption law which are shown in Figure 2.12 as the relationship between the absorbance and the concentration of the solution.

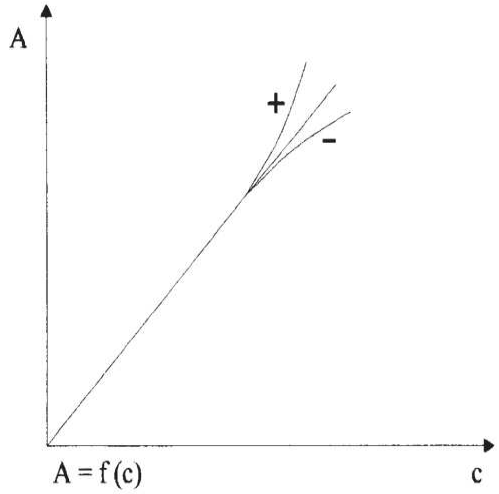

Figure 2.12. Relationship between the absorbance (A) and the concentration of the solution (c) as an example of deviaions from the adsorption law. Reproduced with permission.[10]

If the shape of the absorption spectrum of a substance modify with a change in the concentration of the substance in the solution, there are chemical deviations. In this situation, molecules can interact with each other (dissociation, association) or with solvent molecules. Only the use of a strongly acidic or alkaline environment will cause the adsorption process to not be affected by the change in concentration. Another possibility of avoiding a derogation from the Lambert-Beer law is to measure at a wavelength corresponding to the point of intersection of the absorption curves called the isosbestic point. Dissociation reactions resulting in a negative deviation from the Beer law occur *e.g.* in solutions of weak colored complex compounds. As the solution is diluted, dissociation and disintegration of the complex occurs. The most important reason for physical deviations from the Beer law is the non-monochrome radiation. As a rule, these are negative deviations, but the markings in the high-tech spectrophotometers are negligible.

In the literature we can find a plenty of example which concerns UV-vis measurements to calculate maximum adsorption capacity in adsorption process for different pollutants. Yang and co-workers prepare of reduced GO functionalized with poly(acrylamide) by *in situ* free-radical polymerization.[11] The benzenoid compound, methylene blue was adsorbed on RGO/PAM composited, and the adsorption capacity was measured on a UV−vis spectrophotometer (SHIMADZU UV-2450 spectrophotometer) at a wavelength of 664 nm. All spectrophotometric measurements in the presented work

were performed on the Metertek SP830 spectrophotometer with a tungsten lamp using a 1 cm thick cuvette. UV-vis was used for the study of adsorption process of cationic dyes (methylene blue, rhodamine b, methyl violet) by graphene-based adsorbent (see chapter 4).

2.3.3. Study of adsorption isotherms, kinetic and thermodynamic parameters

The maximum adsorption capacity values were determined using Langmuir and Freundlich models which are widely used for estimation of the adsorption of pollutants using carbonaceous materials.[12-16] The Langmuir isotherm model[17, 18] focuses on the adsorption process on monolayer homogenous surface excluding all interactions between adsorbed molecules. This model is expressed as:

$$q_e = \frac{q_{max} K_L C_e}{1+(K_L C_e)} \text{ (Equation 6)}$$

where: K_L - enthalpy of adsorption (L mg^{-1}), C_e - equilibrium concentration of pollutant (heavy metal ions), q_e - amount of pollutant adsorbed at equilibrium time (in our experiments it was determined by using flame atomic absorption spectrometry), q_{max} - maximum amount of metal ions adsorbed per unit weight of adsorbent (mg g^{-1}).

While the Freundlich isotherm model[19] can be used to describe adsorption of heterogenous and micro-porous surface, the model assumes that multilayer systems of pollutant can be observed on the adsorbent surface and it can be represented by the following equation:

$$q_e = K_F C_e^{1/n} \text{ (Equation 7)}$$

where: K_F (mg^{1-n} L^n g^{-1}) and $1/n$ are Freundlich adsorption constants corresponding to the adsorption intensity and the adsorption capacity.

The kinetics of an adsorption process are studied using the pseudo-first (Equation 8) and pseudo-second (Equation 9) order rate adsorption kinetic models. In particular, the

amount of metal ions adsorbed by BPEI-GO and AC (mg g^{-1}) as a function of time are calculated by applying Equation 10. These models are expressed as:

$$\ln(q_e - q_t) = lnq_e + k_1 t \text{ (Equation 8)}$$

$$\frac{t}{q_t} = \frac{1}{k_2 q_e^2} + \frac{t}{q_e} \text{ (Equation 9)}$$

$$q_t = \frac{(C_0 - C_t)V}{m_{adsorbent}} \text{ (Equation 10)}$$

where q_e - equilibrium adsorption capacity, q_t - adsorption capacity at a given time, k_1 - rate constant (1/min), k_2 - rate constant [g/min mg], t - time (min), C_t - concentration of free metal ions at given time [mg/l], C_e - equilibrium concentration of free metal ions [mg/l], V - volume [l], m - mass [g].

In order to fully understand the nature of adsorption the thermodynamic parameters such as standard Gibbs free energy change (ΔG^o), the enthalpy change (ΔH^o) and entropy change (ΔS^o) have been calculated using equilibrium constants changing as a function of temperature. The free energy changes of the sorption reaction are given by the following equation:

$$\Delta G^o = -RT \ln K_d \text{ (Equation 11)}$$

where: R - ideal gas constant (8.314 J $mol^{-1}K^{-1}$), T - absolute temperature (K), K_d - distribution coefficient. The distribution coefficient (K_d) was defined as the following equation:

$$K_d = \frac{q_e}{C_e} \text{ (Equation 12)}$$

In this equation, q_e (mg g^{-1}) is the amount of metal in adsorbent, C_e (mg L^{-1}) is the amount of metal in solution and the values of K_d was obtained by plotting $\ln(q_e/C_e)$ against C_e and extrapolating to zero C_e. The enthalpy ΔH^o and the entropy ΔS^o changes were calculated from the van't Hoff equation:

$$\ln K_d = -\frac{\Delta H^0}{RT} + \frac{\Delta S^0}{R} \text{ (Equation 13)}$$

2.4. References

1. D. Titus, E. James Jebaseelan Samuel and S. M. Roopan, in *Green Synthesis, Characterization and Applications of Nanoparticles*, eds. A. K. Shukla and S. Iravani, Elsevier, 2019, pp. 303-319.
2. K. Gupta, D. Gupta and O. P. Khatri, *Appl. Surf. Sci.*, 2019, **476**, 647-657.
3. S. Zhan, D. Zhu, S. Ma, W. Yu, Y. Jia, Y. Li, H. Yu and Z. Shen, *ACS Appl. Mater. Interfaces*, 2015, **7**, 4290-4298.
4. A. C. Ferrari and D. M. Basko, *Nat. Nanotechnol.*, 2013, **8**, 235.
5. A. C. Ferrari and J. Robertson, *Phys. Rev. B*, 2000, **61**, 14095.
6. A. Gupta, G. Chen, P. Joshi, S. Tadigadapa and Eklund, *Nano Lett.*, 2006, **6**, 2667-2673.
7. S. Kumar, R. R. Nair, P. B. Pillai, S. N. Gupta, M. A. R. Iyengar and A. K. Sood, *ACS Applied Materials & Interfaces*, 2014, **6**, 17426-17436.
8. A. Walsh, *Spectrochim. Acta*, 1955, **7**, 108-117.
9. R. Sitko, E. Turek, B. Zawisza, E. Malicka, E. Talik, J. Heimann, A. Gagor, B. Feist and R. Wrzalik, *Dalton Trans.*, 2013, **42**, 5682-5689.
10. M. Tan, X. Liu, W. Li and H. Li, *J. Chem. Eng. Data*, 2015, **60**, 1469-1475.
11. Y. Yang, Y. Xie, L. Pang, M. Li, X. Song, J. Wen and H. Zhao, *Langmuir*, 2013, **29**, 10727-10736.
12. İ. Duru, D. Ege and A. R. Kamali, *J. Mat. Sci.*, 2016, **51**, 6097-6116.
13. G. Zhao, X. Ren, X. Gao, X. Tan, J. Li, C. Chen, Y. Huang and X. Wang, *Dalton Trans.*, 2011, **40**, 10945-10952.
14. R. Sitko, P. Janik, B. Feist, E. Talik and A. Gagor, *ACS Appl. Mater. Interfaces*, 2014, **6**, 20144-20153.
15. F. Zhang, B. Wang, S. He and R. Man, *J. Chem. Eng. Data*, 2014, **59**, 1719-1726.
16. N. Sui, L. Wang, X. Wu, X. Li, J. Sui, H. Xiao, M. Liu, J. Wan and W. W. Yu, *RSC Adv.*, 2015, **5**, 746-752.
17. I. Langmuir, *J. Am. Chem. Soc.*, 1916, **38**, 2221-2295.
18. I. Langmuir, *J. Am. Chem. Soc.*, 1918, **40**, 1361-1403.
19. H. M. F. Freundlich, *J. Phy. Chem.*, 1906, 385-470.

Chapter 3.

Adsorption properties on graphene oxide-branched polyethyleneimine materials

The preparation of new hybrid graphene-based component with high surface area and high affinity towards appropriate pollutant paves the way towards the understanding of the mechanism of their adsorption at the surface. Systems based on graphene oxide can be obtained *via bottom-up* approach. In this chapter highly porous foams based on graphene oxide functionalized with polyethylenimine are generated and used with unprecedented efficiency for adsorbing heavy metal ions. A multiscale analysis of the BPEI-GO nanocomposite provided evidence for the covalent grafting of BPEI on GO and the formation of low crystalline porous foams. The uptake experiments revealed that the BPEI-GO's adsorption of toxic cations is strongly dependent on the pH in range from 2 to 10, as a result of the different interactions at the supramolecular level between the metal ions and the BPEI-GO foam. The maximum uptake capacities for Cu^{2+}, Cd^{2+} and Pb^{2+} are achieved at pH = 5 and exhibit values as high as 1096, 2051 and 3390 mg g^{-1}, respectively, being *ca.* over 20 times greater than standard sorbents like activated carbon. The BPEI-GO composite can be easily regenerated as proven by performing adsorption cycles. Also, the thermodynamic parameters including standard Gibbs free energy (ΔG^o), the enthalpy change (ΔH^o) and entropy change (ΔS^o) revealed the exothermic and spontaneous nature of the adsorption process.

3.1. Introduction

One of the greatest worldwide problems caused by industrial and agricultural activities associated with an ongoing population growth is a gigantic amount of the contaminants released to the environment, thereby lowering quality and increasing scarcity of clean water.[1, 2] These pollutants, which range from heavy metals and organic dyes to micropollutants such as nitrosamines[3] cause numerous environmental and public health problems even in low concentrations,[4, 5] and may cause cancerogenic and mutagenic effects, which can lead to health disorders such as dysfunction of the liver, brain and central nervous system.[6-8] Because of that, an improved or new low-cost technology for high-performance removal of pollutants from aqueous solution are necessary. Among various removal techniques, those relying on the capturing of the pollutant (*i.e.* analyte) by an adsorbent (*i.e.* receptor) are chemically programmable and attractive because of wide range of potential sorption materials with the high efficiency and affinity towards diverse pollutants.[9, 10] Typically, carbon materials such as activated carbon (AC) are commonly used in adsorption process because of their significant capacity towards wide range of contaminants.[11] However, carbon materials also possess certain limitations caused by their high production cost, difficult recycling process and restricted selectivity. Compared to AC and other alternative adsorbents, 2DMs offer many benefits. Two-dimensional materials are regarded as the most effective adsorbents for sequestering various type of pollutants such as heavy metal ions and cationic dyes because of their planar structure and extremely high surface to volume ratio. The adsorption abilities of 2DMs was estimated through the q_{max} defined as the mathematical relation between the adsorbed contaminant expressed in milligrams by one gram of adsorbent at constant temperature (see chapter 1, Equation 1). Conventional methods for the quantification of heavy metal ions include plasma mass spectrometry (ICP-AES) and polarography and atomic absorption/emission spectroscopy (*e.g.* FAAS, UV-vis) described in chapter 2.

In the field of sensing it is generally preferred to make use of non-covalent interactions between the sorbents*, i.e.* the active material, and the analyte to ensure a quick response and a fast recovery rate (*i.e.* real-time monitoring). One of the most interesting 2D material, thanks to its adsorption capability into highly porous structures is GO. As a

proof, Sitko and co-workers investigated neat GO, which exhibits ultrahigh adsorption capacity for copper, cadmium and lead ions.[12] The adsorption of the studied dyes was followed by Freundlich isotherm (higher value of correlation coefficient than in Langmuir isotherm model). Nevertheless, the use of pristine 2DM nanosheets has some drawbacks. A major limitation is represented by the poor porosity, which limits the number available recognition sites. In particular, 2DM nanosheets produced *via* liquid-phase exfoliation (LPE) exhibit a strong tendency to self-aggregate and form even micron-sized stacked structures. Moreover, nanosheets produced *via* LPE exhibit low charge carrier as well as low field-effect mobility. In addition, the water solubility of GO hampers its use in common systems, due to the fact that residual GO cannot be easily removed and regenerated after adsorption process. To overcome this drawback, bridging of GO sheets with organic and inorganic subunits to form three-dimensional porous structure have been explored. Noteworthy, the adsorption of pollutants on 2DMs depends on numerous factors such as temperature, initial concentration of the solution, pH and phase contact time which play crucial roles in the adsorption capacity.[11] In order to determine the parameters that guarantee the best process performance, individual factors have to be analyzed. Understanding the dynamic adsorption capabilities of metal ions on the surface of 2DMs is therefore extremely important and will be discussed in this chapter prior to the use of 2DMs in sensing devices for heavy metal ions.

3.2. Materials and methods

3.2.1. Generation of BPEI-GO *via bottom-up* approach

In the past few years, GO/branched polyethylenimine (BPEI-GO) hybrid structures generated through the condensation of the carbonyl moieties and ring-opening reactions of the epoxy groups, was applied as composite for numerous applications including humidity sensing,[13] adsorption of organic dyes and gasses,[14] energy storage [15] and biochemical,[16-18] to name a few. Branched polyethyleneimine (Figure 3.1) was chosen due to the fact that these commercially available biocompatible molecules have been previously extensively studied in adsorption and encapsulation processes in the presence of guest molecules.[25] BPEI in fact incorporates a high number of amine groups, which exist in primary, secondary and tertiary forms,[22, 23] with a branching site at every 3-3.5 nitrogen atom in any given BPEI chain segment, which can be potentially protonated. Thus, at low pH of the solutions BPEI has a high cationic charge density, therefore it can form coordination complexes with heavy metal ions solely in environment characterized by a pH close to neutral or in basic solutions.[24]

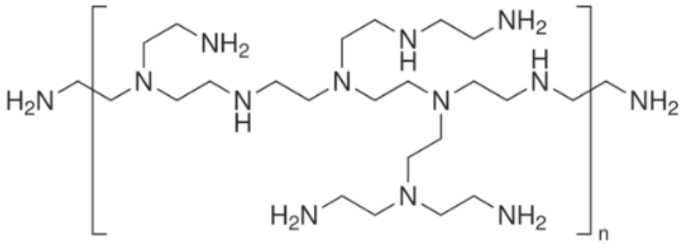

Figure 3.1. Structure of branched polyethylenimine (BPEI).

In this work, BPEI-GO composite was produced *via* the condensation reaction between the amine units exposed on branched polymer (BPEI-branched polyethyleneimine) and commercially available GO (Graphenea). A batch of BPEI-GO is prepared as follows: a mixture of ethanol (100 mL) and GO (100 mL, 4 mg mL^{-1}) is sonicated for 30 min and then 100 mL of BPEI in ethanol (4 mg mL^{-1}) is added. The mixture is rigorously stirred overnight under reflux. The resulting powder is then filtered and washed several times with water/ethanol mixture (1:1 *vol:vol*) in order to remove the unreacted BPEI. Finally,

the BPEI-GO is freeze-dried for 48 h under vacuum to obtain black solid foam-like material, which was used, without further treatments, for characterization and adsorption process.

3.2.2. Morphological characterization by BET and SEM

The porous structure of BPEI-GO was investigated using N_2 adsorption-desorption isotherms at 77K. The specific surface area was measured using a Micromeritics ASAP 2050 surface area and porosity analyzer. Prior to the BET measurements, the samples were outgassed for 10 hours at 100 °C. Adsorption isotherms were calculated for nitrogen adsorption at 77 K and pressures up to 1 bar. A specific surface area of BPEI-GO composite calculated by Branauer-Emmett-Teller (BET) model amounts to 220 $m^2 g^{-1}$ (Figure 3.2a). Obtained value is much higher in comparison to the starting GO material, which displays a specific surface area calculated as 10 $m^2 g^{-1}$, suggesting that branched polyethyleneimine act as a spacer between GO sheets. Noteworthy, that specific surface area of GO is strictly depending on the level of water content and the values are in the range from 10 to 100 $m^2 g^{-1}$. To get a morphological insight, scanning electron microscopy (SEM) images are recorded. SEM with energy dispersive X-ray detector (EDX) presents images which proved the porous and uniform structure of BPEI-GO material (Figure 3.2b-c).

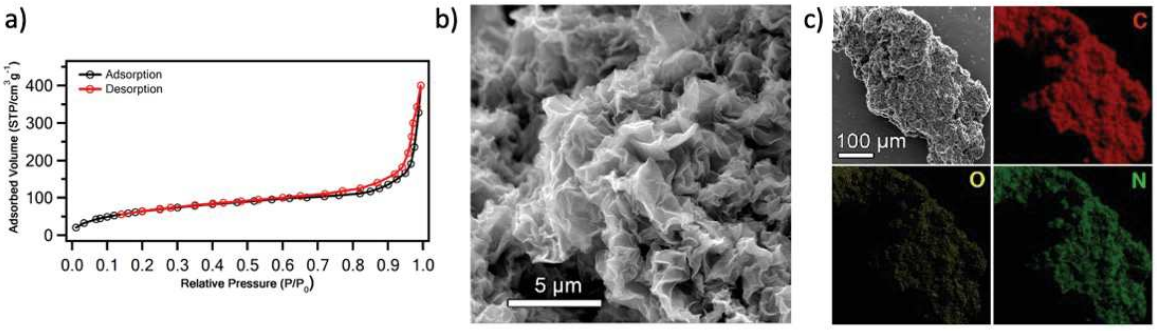

Figure 3.2. a) BET adsorption-desorption isotherms of the BPEI-GO composite b) SEM image of BPEI-GO.

The characterization was carried out using an FEI Quanta 250 FEG instrument with energy-dispersive X-ray (EDX) analyses. The accelerating voltage was 5 keV

incident beam energy. SEM samples were prepared by mounted on carbon conductive tabs followed by gold coating.

3.2.3. Chemical and structural composition

The sample for XPS characterization were prepared by collecting ~5 mg of GO and BPEI-GO and attached to copper film. The XPS analysis was carried out using the Thermo Scientific KAlpha XPS machine available at the Nanochemistry lab (ISIS). After background substraction, the C1s, O1s and N1s peaks were deconvoluted using constrains on the relative intensity ratio of the doublets and the full width half maximum. As aforementioned, this works focused on the adsorption of heavy metal ions (Pb^{2+}, Cu^{2+}, Cd^{2+}) *via* functionalized graphene oxide. The presence of these ions in water contributes to the contamination of the environment. The lack of biodegradability and the long half-life of heavy metals are particularly dangerous for the health of living organisms. This leads to their accumulation in tissues causing poisoning, damage to the nervous system or tumors.[26] The growth of 3D covalently functionalized architectures with a high degree of functionalization have been attained by exploring the functionalization of GO through the ring-opening reaction of epoxy groups. High resolution XPS was used to gain subsequent details about chemical composition of BPEI-GO hybrid material. This methodology was also exploited to investigate the nature of adsorption process of heavy metal ions on BPEI-GO. In the wide energy spectrum of pristine GO, only two peaks at 286.7 eV and 532.3 eV are found, and are attributed to C1s and O1s, respectively (see Figure 3.3a). In contrast, the appearance of the N1s peak is observed in the wide energy spectrum of BPEI-GO (see Figure 3.3b).

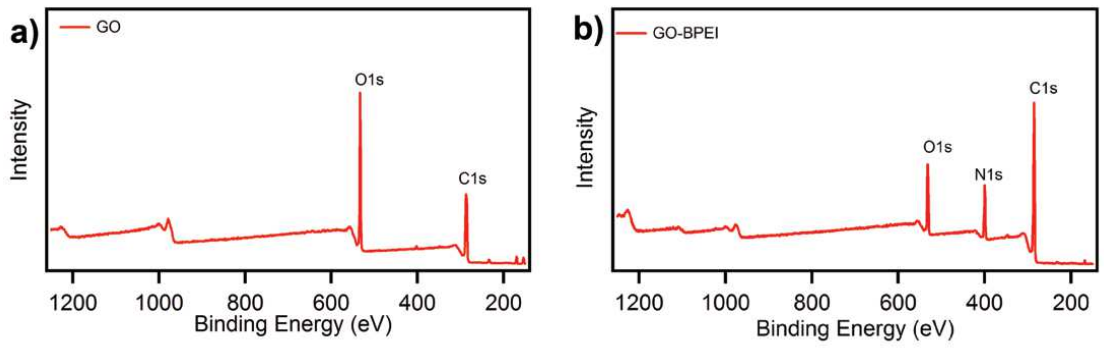

Figure 3.3. XPS wide energy spectra of (a) GO and (b) BPEI-GO.

The relevant difference between the carbon (C1s), nitrogen (N1s) and oxygen (O1s) peaks proved the presence of new covalent bond obtained between the primary form amine groups from BPEI and oxygen-containing functional groups on the surface of GO (Figure 3.4**)**. The C1s XPS spectrum of the neat GO (Figure 3.4a) shows two main peaks at 284.6 eV (C-C) and 286.8 eV (C-O) and one smaller peak at 288.3 eV, which is ascribed to C=O bonds.[4] Compared to GO, the C1s spectrum of the BPEI-GO hybrid material (Figure 3.4b) appears differently and has four peaks, including sharp peaks at 284.6 eV and 285.7 eV and broader peaks at 286.2 eV and 287.9 eV which can be assigned to C-C, C-N, C-O and C=O bonds, respectively. While similar O1s spectra are observed for GO and BPEI-GO (Figure 3.4c-d), successful functionalization of GO with BPEI is particularly evidenced in the N1s spectra. The high-resolution N1s spectrum of GO sample does not show any nitrogen signal (Figure 3.4e). Conversely, clear signal is observed in BPEI-GO samples (Figure 3.4f), and it can be deconvoluted into three peaks, *i.e.* at 398.8 eV, 399.5 eV and 401.0 eV, which can be ascribed to primary, secondary/tertiary and quaternary amines, respectively.[27, 28]

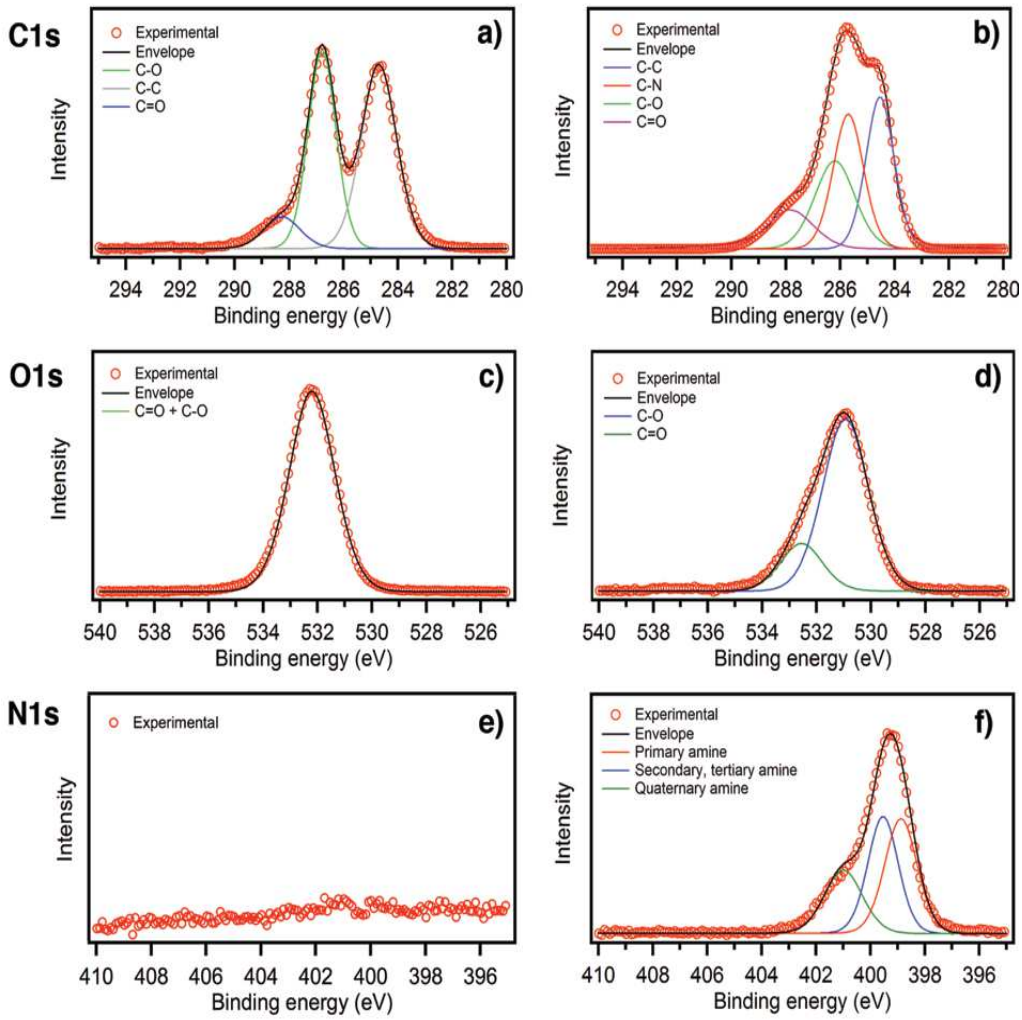

Figure 3.4. High-resolution C1s, O1s and N1s spectra of GO (a,c,e), and BPEI-GO (b,d,f).

BPEI-GO was further characterized by Raman spectroscopy a non-destructive technique used to study the structural changes of graphene oxide-based materials. As shown on Figure 3.5 the Raman spectrum of GO displays two prominent peaks around 1350 cm^{-1} (D band) and at 1600 cm^{-1} (G band), correspond to sp^3 hybrid orbital and sp^2 hybridized carbon atoms from the aromatic regions of GO. As we mentioned in chapter 2, chemical modification of graphene-derived materials is often characterized by the changes in the ratio of the D and G bands areas. In fact, I_D/I_G is commonly used to quantify the disorder level in graphene. After the functionalization of GO with BPEI the I_D/I_G intensity ratio increases from 1.00 to 1.30 and is attributed to the increase of the sp^3 carbon atoms after functionalization and is consistent with other reports. Moreover, the graphene band shifts to a lower wavenumber, reaching 1589 cm^{-1} for the GO-BPEI, which is

consistent with the observed effect of the functionalization of graphitic materials. The results indicate that BPEI was effectively grafted onto the surfaces of the graphene oxide through nucleophilic reaction between the amine groups of BPEI and the epoxy and carboxyl groups of GO.

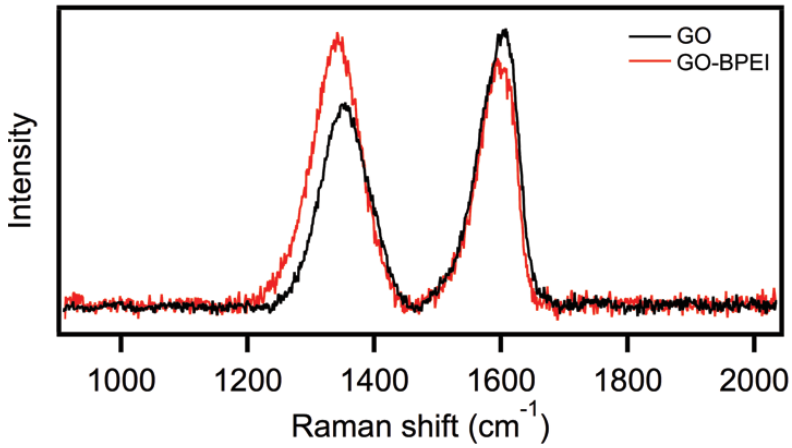

Figure 3.5. Raman spectra of GO and BPEI-GO composite.

3.3. Results

3.3.1. Adsorption of heavy metal ions on BPEI-GO using FAAS measurements

The adsorption experiments are carried out by mixing 5 mg of adsorbate, *i.e.* GO, BPEI, or GO-BPEI, and 100 mL of Pb^{2+}, Cd^{2+} or Cu^{2+} aqueous solutions at the desired concentration and pH. After addition of GO-BPEI foam into the salt solution with $NaNO_3$ the pH is adjusted with HNO_3 (0.1 M) and KOH (0.1 M). The suspensions are then rigorously stirred for 12 h to achieve the adsorption equilibrium and subsequently filtered through polytetrafluoroethylene (PTFE) membranes (0.22 μm). The concentration of metal ions is determined using flame atomic absorption spectrometry (F-AAS) with deuterium arc background correction, equipped with a hollow cathode lamp (Varian 280FS). An air–acetylene burner is used. The wavelengths (spectral band pass) are 217.0 nm (0.5 nm), 324.8 nm (0.5 nm), 228.8 nm (0.5 nm) and for Pb^{2+}, Cu^{2+}, and Cd^{2+}, respectively. The nebulizer flow rate is set to 5.0 mL min^{-1}. The adsorption capacity variation upon GO-BPEI foam regeneration is defined as: (q_e/q_{max}) x100 where: q_e- adsorption capacity in equilibrium state, q_{max}- maximum adsorption capacity. To study the maximum adsorption capacity of BPEI-GO composite, uptake of heavy metal ions by mixing adsorbent with Pb^{2+}, Cd^{2+}, Cu^{2+} solutions at desired pH and concentration were conducted. The pH of the salt solutions was controlled by HNO_3 (0.1 M) and KOH (0.1 M) solutions. The uptake capability of heavy metal ions by BPEI-GO was established at pH = 5 due to the fact, that in the pH higher than $pH_{pzc} \sim 4.3$ (pH point of zero charge-value of pH which refers to neutral charge of adsorbent) the surface of BPEI-GO foam is negatively charged and results in an increased capacity to adsorb positive charges pollutants. Nevertheless, at too high pH, heavy metal ions used in experiment exist as *e.g.* $[PbOH]^+$ and $[CuOH]^+$ species. As a result, the interactions between BPEI-GO composite and pollutants are evidently weakened, which has a direct impact on the adsorption capacity values. The maximum adsorption capacity values were determined using Langmuir and Freundlich models (see chapter 2, Equations 6 and 7).Isotherm parameters

are acquired by fitting GO-BPEI adsorption equilibrium data to the isotherm models and are listed in Table 3.1.

Table 3.1. Parameters for Freundlich and Langmuir adsorption isotherm models. The parameters for adsorption models of Cu^{2+}, Cd^{2+} and Pb^{2+} metal ions sorption on GO-BPEI foam.

Metal ion	**Freundlich**			**Langmuir**		
	n	K_F	R^2	q_{max}	K_L [x10^{-2}]	R^2
Cu^{2+}	2.7 ± 0.3	151 ± 15	0.897	1096 ± 25	3.8 ± 0.3	0.994
Cd^{2+}	2.6 ± 0.3	258 ± 26	0.919	2051 ± 46	3.4 ± 0.2	0.996
Pb^{2+}	2.9 ± 0.2	525 ± 34	0.963	3390 ± 67	4.1 ± 0.4	0.997

It should be noted the *n* values calculated from the Freundlich model are found to fall in the range between 2 and 3, indicating good adsorption of metal ions onto BPEI-GO foam.[37] The adsorption isotherms for the control samples (GO, BPEI) as well as for the BPEI-GO composite (Figure 3.6) were better correlated using Langmuir model than by the Freundlich model, suggesting that adsorption process of heavy metal ions (Pb^{2+}, Cd^{2+}, Cu^{2+}) onto GO, BPEI and BPEI-GO is not exactly monolayer coverage related. Moreover, accurate analyses of adsorption properties confirmed that the enrichment of GO with additional coordinating pockets in the BPEI-GO system resulted in an adsorption of unprecedently high values (with respect to carbonaceous materials) of q_{max} for heavy metal ions (Cu^{2+} - 1096 mg g^{-1}, Cd^{2+} - 2051 mg g^{-1}, Pb^{2+} - 3390 mg g^{-1}).

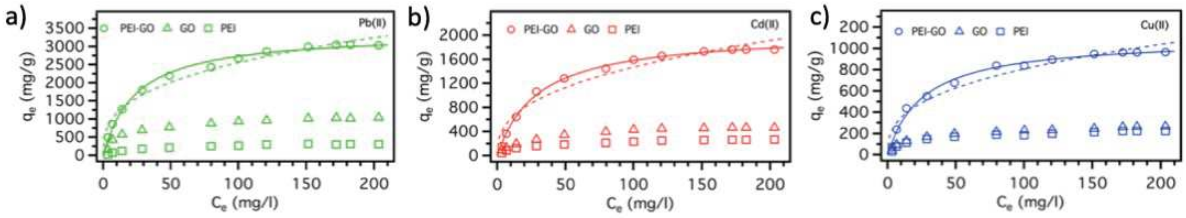

Figure 3.6. Adsorption isotherms on BPEI-GO for a) Pb^{2+}, b) Cd^{2+} and c) Cu^{2+} ions at pH = 5 ($C_{GO,BPEI,BPEI-GO}$ = 0.05 g L^{-1}, T = 25 °C, stirring speed = 200 rpm, t = 12 h). The experimental adsorption data are fitted with Langmuir (solid lines) and Freundlich (dashed lines) models.

The obtained q_{max} values presented in mmol g^{-1} are 16.4, 17.3, and 18.3, for Pb^{2+}, Cu^{2+}, and Cd^{2+} respectively, suggesting that 1 g of BPEI-GO composite is able to adsorb ca. 17 mmol of heavy metal ions from 1L solution of polluted water. In comparison with commonly used adsorbents *i.e.* AC, and their modified derivative with polyethyleneimine (AC-PEI), the maximum adsorption capacities values reveals that BPEI-GO outperforms AC being ca. over 40, 60 and 160 times efficient adsorbent for Pb^{2+}, Cu^{2+} and Cd^{2+}, respectively (Table 3.2). [38, 39]

Table 3.2. Maximum adsorption capacity q_{max} values of Pb^{2+}, Cu^{2+} and Cd^{2+} on AC, AC-PEI and BPEI-GO calculated by Langmuir adsorption isotherm model.

Metal ions	Q_{max} [mmol g^{-1}]		
	AC	AC-PEI	BPEI-**GO**
Pb^{2+}	0.27± 0.02	0.68 ± 0.02	16.4 ± 0.4
Cu^{2+}	0.40± 0.03	0.77 ± 0.02	17.3 ± 0.4
Cd^{2+}	0.11± 0.01	0.88 ± 0.03	18.3 ± 0.5

To gain further insight into the adsorption process, the kinetics of Pb^{2+}, Cd^{2+} and Cu^{2+} heavy metal ions adsorption on BPEI-GO material were studied by applying the principles discussed in chapter 2 (see Equations 8-10). The calculated kinetic parameters for adsorption of Cu^{2+}, Cd^{2+} and Pb^{2+} ions on BPEI-GO foam at pH 5 are listed in Table 3.3. This knowledge is necessary for comprehension of the adsorption process and for choosing the best desorption strategy. The q_e values calculated from the pseudo-first and pseudo-second-order kinetic models are close to experimental q_e values, yet, the latter model seems to give better results. In particular, the calculated q_e values of the Cu^{2+}, Cd^{2+} and Pb^{2+} adsorption acquired using the pseudo-second-order kinetic model amount to

763, 1186 and 1612 mg/g, which are closer to the experimental q_e values of 757, 1171 and 1592 mg/g, respectively.

Table 3.3. Coordination kinetic rate constants and unit adsorption capacity of BPEI-GO towards Cu^{2+}, Cd^{2+}, Pb^{2+}.

Metal ion	**Pseudo-first order kinetics**			**Pseudo-second order kinetics**			q_e *(exp)*
	q_e	k_1 [x10^{-3}]	R^2	q_e	k_2 [x 10^{-5}]	R^2	
Cu^{2+}	727±18	8.3±0.3	0.982	763±21	3.4 ± 0.2	0.995	757 ± 20
Cd^{2+}	1085 ± 30	9.1 ± 0.6	0.952	1186 ± 34	2.9 ± 0.2	0.984	1171 ± 32
Pb^{2+}	1465 ± 37	13 ± 1	0.979	1612 ± 40	1.4 ± 0.1	0.988	1592 ± 39

Moreover, the analysis of the fitting parameters reveals that the experimental data is fitted better with the pseudo-second-order kinetic model as evidenced by the correlation coefficients (Figure 3.7). Obtained results showed that the adsorption of heavy metal ions on the composite surface at the beginning increase very fast and then it reaches a plateau. The same characteristic shape of curve was noticed in adsorption by raw GO, but the kinetic rate was higher.[12]

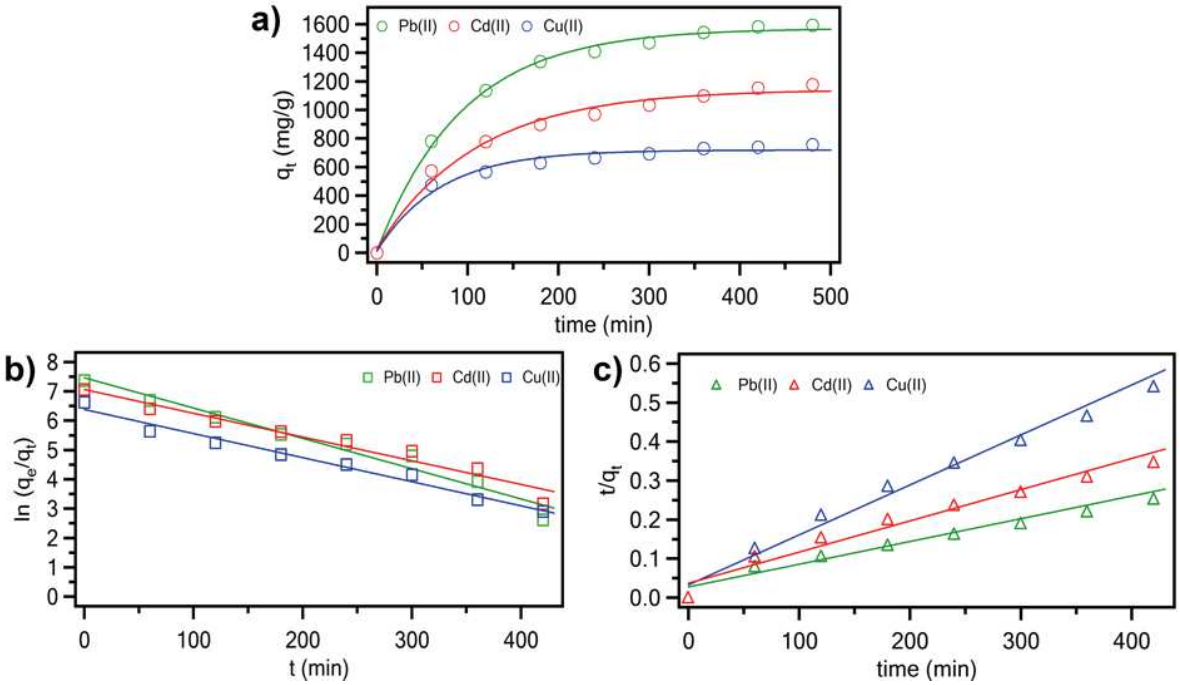

Figure 3.7. Time dependent heavy metal ions sorption on BPEI-GO foam (a) (C_0 = 0.1 g L^{-1}, $C_{BPEI-GO}$ = 0.05 g L^{-1} T = 25 °C, stirring speed = 200 rpm, t = 8h, pH = 5). The kinetic plots obtained pseudo-first (b) and pseudo-second (c) order model reactions.

The values of ΔH° and ΔS° can be calculated by the Van't Hoff Equation (see chapter 2, Equation 13) and can be determined from intercept and slope by plotting the values of ln K_d *vs.* 1/T (Figure 3.8).

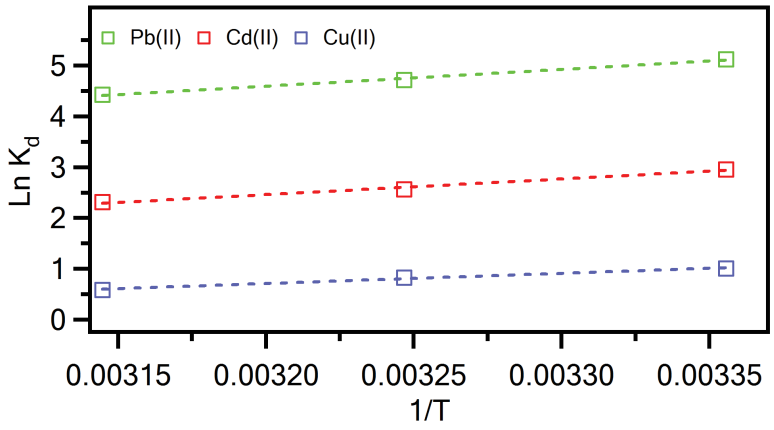

Figure 3.8. The linear curve of ln K_d *vs* 1/T for Pb^{2+}, Cd^{2+}, Cu^{2+} adsorption calculate to determine thermodynamic parameters.

The thermodynamic parameters from the fitting line such as Gibbs free energy change (G°), the enthalpy change (ΔHº), the entropy change (ΔSº) and correlation coefficient (R^2) are listed in Table 3.4.

Table 3.4. Thermodynamic parameters for adsorption of Pb^{2+}, Cd^{2+}, Cu^{2+}onto BPEI-GO composite.

Metal ions	T (K)	ln K_d	ΔG° (KJ mol^{-1})	ΔH° (KJ mol^{-1})	ΔS° (KJ mol^{-1}K^{-1})	R^2
Pb^{2+}	298	5.12	-12.69	-27.26	49.01	0.994
	308	4.72	-12.09			
	318	4.43	-11.72			
Cd^{2+}	298	2.95	-7.32	-25.34	60.59	0.990
	308	2.57	-6.58			
	318	2.31	-6.12			
Cu^{2+}	298	1.01	-2.50	-16.51	46.92	0.989
	308	0.83	-2.12			
	318	0.59	-1.56			

The distribution ratio (K_d) of Pb^{2+}, Cd^{2+}, Cu^{2+} onto BPEI-GO composite are decreased with the increase in temperature, implying that the adsorption process is exothermic. The negative values of ΔGº at various temperatures indicated the spontaneous nature of the adsorption process. The decreasing in ΔGº values with increasing temperature shows a decrease in feasibility of sorption at higher temperature. However, the low negative values ΔGº measured in temperature 318K (-11,72, -6,12 and -1,56 kJ.mol^{-1}, respectively for Pb^{2+}, Cd^{2+}, Cu^{2+}) ascertains the favourability of the adsorption process. Furthermore, the more negative value of ΔGº for Pb^{2+} than that of Cd^{2+} and Cu^{2+} implies the BPEI-GO composite favours the adsorption of Pb^{2+} more than Cd^{2+} and Cu^{2+}. The negative value of ΔH° confirms the exothermic nature of the adsorption process as confirmed by the fact that as the temperature rises from 298 to 318K. This result also supports the suggestion that the adsorption capacity of adsorbent decreases with increasing temperature. The positive values of ΔSº (49.01, 60.59 and 46.92 for Pb^{2+}, Cd^{2+} and Cu^{2+}, respectively) confirm the increment randomness in the system solid/solution interface during the adsorption process which can be reflected by the affinity of the BPEI-GO for heavy metal cations and suggested some conformational changes in BPEI-GO. This might be also

attributed to the substitution of water hydration molecules for metal ions by chelating group. Both kinetic and thermodynamic parameters determined during studies confirmed the spontaneous and exothermic nature of the adsorption process. In search of the best adsorbent, its regeneration is as important as its high affinity to the contaminants, which is necessary from the practical point of view of sorption material on industrial scale. Thus, the adsorbent material needs to combine a high adsorption capacity with good desorption characteristics. Such combinations would considerably enhance the efficiency of the adsorbent and possibly allow its use in real life applications. To study the reversible adsorption of heavy metal ions onto the BPEI-GO foam, the composite is repeatedly immersed in the aqueous solutions of heavy metal ions and treated with 0.1 M solution of either ethylenediaminetetraacetic acid (EDTA) or nitric acid. The adsorbent is washed several times with MiliQ water, freeze-dried overnight and used as adsorbent in subsequent adsorption cycles. The adsorption experiments are then carried out by mixing BPEI-GO and Pb^{2+}, Cd^{2+} and Cu^{2+} aqueous solutions at pH = 5. Noteworthy, the use of EDTA for regeneration of GO-based adsorbents has some drawbacks. While EDTA has a high affinity for metal ions, as reflected in its high complexation constants for Cu^{2+} (18.8), Pb^{2+} (18.1) and Cd^{2+} (16.5), it can also interact with GO through strong electrostatic forces and block its binding sites.[40, 41] Such characteristics of EDTA may affect the reusability of BPEI-GO foam in the long term. As illustrated in Figure 3.9 high decrease in the adsorption capacity is monitored for GO-BPEI treated with EDTA. In particular, the adsorption capacity decreases over ten cycles by 28% for Cu, 55% for Pb and 72% for Cd ions. On the other hand, HNO_3 treatment allows reaching high regeneration efficiency. The overall decrease in adsorption capacity is found smaller than in the EDTA treated foam, and it amounts to 45% for Cu, 20% for Pb and 33% for Cd ions. Noteworthy, the decrease in the adsorption capacity after tenth cycle is most likely related to the decrease in the number of BPEI-GO coordination pockets and therefore in the decrease of the binding sites after each regeneration step. As a consequence of the strong acidic environment the decomposition of BPEI-GO can take place, and in particular hydrolysis of amide bonds may occur. It was shown that there is a possibility of effective regeneration of BPEI-GO adsorbent using commonly used solutions of 0.1 M EDTA[42] or 0.1 M HNO_3[43] (Figure 3.9b). It was shown that HNO_3 allows for reaching higher regeneration efficiency than EDTA. It was presented that after 10 cycles the

general decrease in adsorption affinity was smaller using HNO_3 than EDTA solution and it amounts to 45% for Cu^{2+}, 20% for Pb^{2+} and 33% for Cd^{2+} ions, which is consistent with the raw GO regeneration results presented in literature.[44]

In most cases, contaminated water contains a combination of different types of ions, which is a major limitation to highlight the most efficient adsorbent. That is why a series of experiments was performed by replacing distilled water with tap water, which contains mono- and divalent alkali metal ions including Na^+, K^+, Mg^{2+} Ca^{2+} at the concentration of 16 mg/L, 7 mg/L 10 mg/L and 75 mg/L, respectively. Adsorption capacity values obtained in a single adsorption tests in tap water environment are almost the same with those received for distilled water experiments (Figure 3.9b).

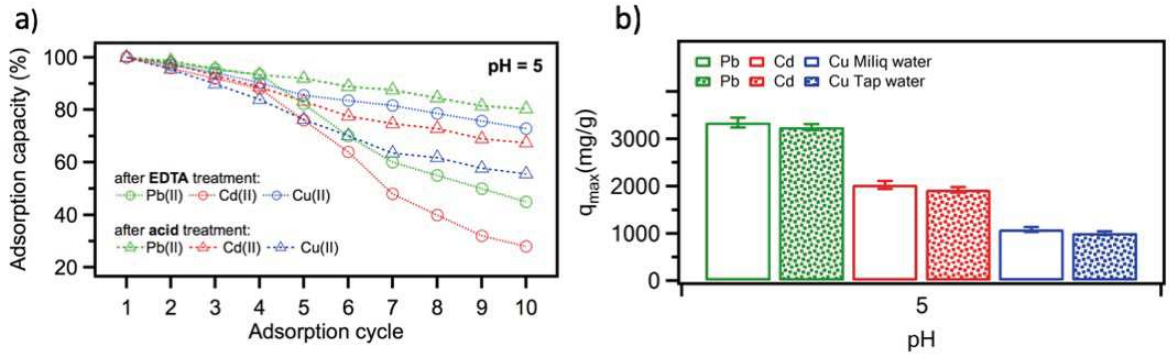

Figure 3.9. a) Adsorption capacity as a function of BPEI-GO foam regeneration cycle using EDTA and HNO_3 solutions. b) The effect of environmental conditions on the adsorption Pb^{2+}, Cd^{2+} and Cu^{2+} ions by BPEI-GO composite.

In order to confirm the chemical nature of adsorption of metal ions on GO-BPEI, additional XPS wide range energy spectra were performed before and after metal ions sorption (Figure 3.10) and confirms the presence of metal ions after the adsorption cycle.

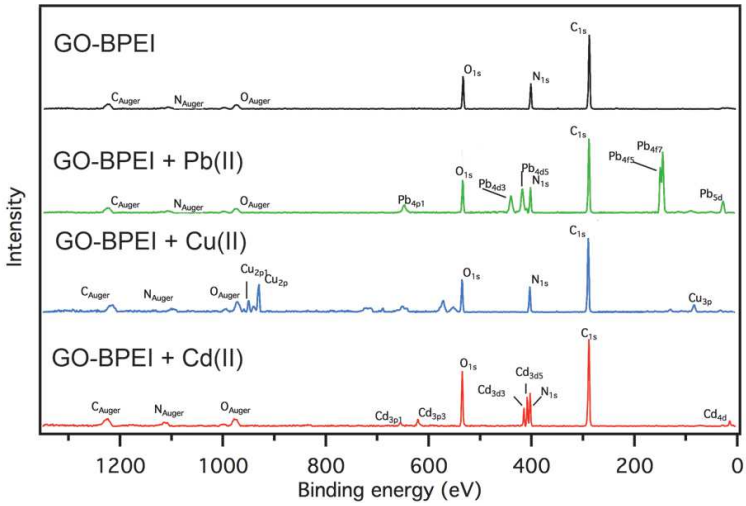

Figure 3.10. The XPS spectra recorded before and after metal ions adsorption on BPEI-GO.

3.4. Conclusions

In summary, in this section we have shown that the BPEI-GO composite synthesized by easy and high-performance approach displayed very interesting adsorption affinity, stability and reusability toward sequestering of heavy metal ions. GO-based 3D foams are particularly appealing for the efficient removal of heavy metal ions from water since they expose numerous oxygen- and nitrogen-containing functional groups, which can interact at the supramolecular level with the metal ions. The GO-BPEI foam generates supramolecular pockets that are particularly suitable for sequestering specific metal ions. This is evidenced by remarkably high maximum adsorption capacities towards heavy metal ions at pH 5: 1096, 2051, and 3390 mg g^{-1} for Cu^{2+}, Cd^{2+} and Pb^{2+}, respectively. These values are much larger than those of any known sorbents including GO and GO-based adsorbents. The non-covalent, thus reversible nature of interactions between the GO based foam and the metal ions is key in order to re-generate the foam. We have showed that the adsorbed metal ions can be removed with treatments of either EDTA or nitric acid. Thermodynamic calculations showed that the adsorption process of heavy metal ions had exothermic and spontaneous nature. The results obtained in this work exceed the state of the art of functionalized GO-based metal ions adsorbent. The BPEI-GO based material represents the promising way to involve high-efficiency and low-cost water purification technologies and offer a new avenue towards the effective removal of heavy metal pollutants at large scale.

3.5. References

1. C. J. Vörösmarty, P. B. McIntyre, M. O. Gessner, D. Dudgeon, A. Prusevich, P. Green, S. Glidden, S. E. Bunn, C. A. Sullivan, C. R. Liermann and P. M. Davies, *Nature*, 2010, **467**, 555.
2. K. Bakker, *Science*, 2012, **337**, 914-915.
3. J. O. Lundberg, E. Weitzberg, J. A. Cole and N. Benjamin, *Nat. Rev. Microbio.*, 2004, **2**, 593-602.
4. R. P. Schwarzenbach, B. I. Escher, K. Fenner, T. B. Hofstetter, C. A. Johnson, U. von Gunten and B. Wehrli, *Science*, 2006, **313**, 1072-1077.
5. J. Lubchenco, *Science*, 1998, **279**, 491-497.
6. C.-H. Weng and Y.-F. Pan, *J. Hazard. Mater.*, 2007, **144**, 355-362.
7. M. A. M. Salleh, D. K. Mahmoud, W. A. W. A. Karim and A. Idris, *Desalination*, 2011, **280**, 1-13.
8. Z. Aksu, *Process Biochem.*, 2005, **40**, 997-1026.
9. F. Perreault, A. Fonseca de Faria and M. Elimelech, *Chem. Soc. Rev.*, 2015, **44**, 5861-5896.
10. D. L. Gin and R. D. Noble, *Science*, 2011, **332**, 674-676.
11. A. Dąbrowski, *Adv. Colloid Interface Sci.*, 2001, **93**, 135-224.
12. R. Sitko, E. Turek, B. Zawisza, E. Malicka, E. Talik, J. Heimann, A. Gagor, B. Feist and R. Wrzalik, *Dalton Trans.*, 2013, **42**, 5682-5689.
13. Z. Yuan, H. Tai, Z. Ye, C. Liu, G. Xie, X. Du and Y. Jiang, *Sens. Actuator B-Chem.*, 2016, **234**, 145-154.
14. Z. Y. Sui, Y. Cui, J. H. Zhu and B. H. Han, *ACS Appl. Mater. Interfaces*, 2013, **5**, 9172-9179.
15. Y. Huang, D. Wu, A. Dianat, M. Bobeth, T. Huang, Y. Mai, F. Zhang, G. Cuniberti and X. Feng, *J. Mater. Chem. A*, 2017, **5**, 1588-1594.
16. B. Chen, M. Liu, L. Zhang, J. Huang, J. Yao and Z. Zhang, *J. Mater. Chem.*, 2011, **21**, 7736-7741.
17. S. Kumar, S. Raj, K. Sarkar and K. Chatterjee, *Nanoscale*, 2016, **8**, 6820-6836.
18. L. Zhang, Z. Lu, Q. Zhao, J. Huang, H. Shen and Z. Zhang, *Small*, 2011, **7**, 460-464.
19. Y. Liu, Y. Fan, Y. Yuan, Y. Chen, F. Cheng and S.-C. Jiang, *J. Mater. Chem.*, 2012, **22**, 21173-21182.
20. Y. Yan, Q. An, Z. Xiao, W. Zheng and S. Zhai, *Chem. Eng. J.*, 2017, **313**, 475-486.
21. J. Meng, J. Cao, R. Xu, Z. Wang and R. Sun, *J. Mater. Chem. A*, 2016, **4**, 11656-11665.
22. J. Jia, A. H. Wu and S. J. Luan, *Colloids Surf., A*, 2014, **449**, 1-7.
23. X. Zhang, A. Ciesielski, F. Richard, P. Chen, E. A. Prasetyanto, L. De Cola and P. Samorì, *Small*, 2016, **12**, 1044-1052.
24. A. H. Wu, J. Jia and S. J. Luan, *Colloids Surf. A*, 2011, **384**, 180-185.
25. Y. Liu, Y. Fan, Y. Yuan, Y. Chen, F. Cheng and S.-C. Jiang, *J. Mat. Chem.*, 2012, **22**, 21173-21182.
26. M. Jaishankar, T. Tseten, N. Anbalagan, B. B. Mathew and K. N. Beeregowda, *Interdiscip. Toxicol.* , 2014, **7**, 60-72.

27. O. C. Compton, D. A. Dikin, K. W. Putz, L. C. Brinson and S. T. Nguyen, *Adv. Mater.*, 2010, **22**, 892-896.
28. N. D. K. Tu, J. A. Lim and H. Kim, *Carbon*, 2017, **117**, 447-453.
29. İ. Duru, D. Ege and A. R. Kamali, *J. Mat. Sci.*, 2016, **51**, 6097-6116.
30. G. Zhao, X. Ren, X. Gao, X. Tan, J. Li, C. Chen, Y. Huang and X. Wang, *Dalton Trans.*, 2011, **40**, 10945-10952.
31. R. Sitko, P. Janik, B. Feist, E. Talik and A. Gagor, *ACS Appl. Mater. Interfaces*, 2014, **6**, 20144-20153.
32. F. Zhang, B. Wang, S. He and R. Man, *J. Chem. Eng. Data*, 2014, **59**, 1719-1726.
33. N. Sui, L. Wang, X. Wu, X. Li, J. Sui, H. Xiao, M. Liu, J. Wan and W. W. Yu, *RSC Adv.*, 2015, **5**, 746-752.
34. I. Langmuir, *J. Am. Chem. Soc.*, 1916, **38**, 2221-2295.
35. I. Langmuir, *J. Am. Chem. Soc.*, 1918, **40**, 1361-1403.
36. H. M. F. Freundlich, *J. Phy. Chem.*, 1906, 385-470.
37. B. H. Hameed, *J. Hazard. Mater.*, 2008, **154**, 204-212.
38. C. Y. Yin, M. K. Aroua and W. M. A. W. Daud, *Water Sci. Technol.*, 2007, **56**, 95-101.
39. C. Y. Yin, M. K. Aroua and W. M. A. W. Daud, *Water Air Soil Pollut.*, 2008, **192**, 337-348.
40. L. M. Cui, Y. G. Wang, L. Gao, L. H. Hu, L. G. Yan, Q. Wei and B. Du, *Chem. Eng. Sci.*, 2015, **281**, 1-10.
41. C. J. Madadrang, H. Y. Kim, G. Gao, N. Wang, J. Zhu, H. Feng, M. Gorring, M. L. Kasner and S. Hou, *ACS Appl. Mater. Interfaces*, 2012, **4**, 1186-1193.
42. W. Peng, H. Li, Y. Liu and S. Song, *J. Mol. Liq.*, 2017, **230**, 496-504.
43. S. Wang, X. Li, Y. Liu, C. Zhang, X. Tan, G. Zeng, B. Song and L. Jiang, *J. Hazard. Mater.*, 2018, **342**, 177-191.
44. X. Li, S. Wang, Y. Liu, L. Jiang, B. Song, M. Li, G. Zeng, X. Tan, X. Cai and Y. Ding, *J. Chem. Eng. Data*, 2016, **62**.

Chapter 4.

Graphene oxide based mesoporous SiO_2NH_2 hybrid for fast and efficient removal of organic cationic contaminants

In this chapter, we have developed a novel mesoporous silica - graphene oxide hybrid material (SiO_2NH_2-GO) operating as highly efficient and rapid adsorbent for removal of cationic organic dyes from water. The fabrication of such a three dimensional (3D) SiO_2NH_2-GO composite has been achieved *via* the condensation reaction between the amine units exposed on 3-aminopropyl-functionalized silica nanoparticles and the epoxy groups on GO's surface resulting in homogeneous powder with large specific surface area (405.5 $m^2\ g^{-1}$) and high pore volume (0.714 $cm^3\ g^{-1}$). As proof-of-concept, SiO_2NH_2-GO was used for the removal from water of archetypical dyes such as methylene blue (MB), rhodamine B (RhB) and methyl violet (MV) revealing outstanding maximum adsorption capacity towards these organic pollutants reaching 300, 358 and 178 mg g^{-1} for MB, RhB and MV, respectively at pH 10. Moreover, the adsorption process exhibit that ~ 99.7 % of MB, RhB and MV have been removed and the equilibrium state has been reached in 3 min. The accurate studies of the adsorption isotherms as well as the kinetics of MB, RhB and MV from aqueous solution proved that the cationic dyes adsorb immediately, in accordance with Langmuir adsorption isotherm and pseudo-second order kinetics model. Finally, the composite was used in solid phase extraction (SPE) as column packing material, for continuous water purification from aforementioned organic dyes, thereby highlighting the great potential of SiO_2NH_2-GO for the large-scale removal of cationic dyes from aqueous solutions.

4.1. Introduction

The increasing contamination of aquatic systems with organic and inorganic pollutants remains an emerging issue in the field of environmental science.[1] Since the dye manufacturing was introduced, more than 100k water-soluble organic different dyes are being used in a wide range of industries such as textile, paper, printing, leather, polymer, cosmetics and others.[2, 3] Noteworthy, organic dyes are considerably toxic for health and environment even in low concentrations,[4-6] and may cause cancerogenic and mutagenic effects, which can lead to health disorders such as dysfunction of the liver, brain and central nervous system.[5, 7, 8] It is well known that about 10-15 % of all dyes used in the industry are lost in the wastewater during processing. Therefore, the development of highly-efficient and low-cost purification methods is highly desirable.[9-11] Biodegradation of organic dyes is time-consuming and ineffective, therefore adsorbents with high (photo)chemical stability gained considerable attention in purification systems causing development of high performance and eco-friendly materials for adsorption.[12, 13] Among various dye removal techniques, adsorption process based on capturing the adsorbate (pollutants) by an adsorbent is attractive due to wide range of potential sorption materials with high efficiency and affinity toward miscellaneous contaminants.[14-16] Recently, atomically thin two-dimensional materials (2DMs) gathered a great interest in the scientific community due to their outstanding mechanical, electrical, optical and thermal properties, combined with a high chemical stability.[17] In particular, their highest surface-to-volume ratio endorses these materials as suitable candidates for the efficient adsorption of a wide range of contaminants.[18-21] On the other hand, 2DMs are insoluble and difficult to be dispersed in aqueous solutions due to their hydrophobic nature and tendency to aggregated in aqueous solution via strong van der Waals interactions. Moreover, their hydrophobic character also hampers the adsorption process of cationic dyes or heavy metal ions from aqueous solution on their surfaces. In this context, the adsorption capacity of 2DMs can be significantly increased by decorating them with functional groups. Notably, graphene oxide (GO), an oxidized version of graphene with oxygen-containing functional groups such as epoxy, carbonyl and carboxylic moieties provides a multitude of facile functionalization possibilities as well as a good water dispersibility.[22-24] Therefore, GO-based nanomaterials have been recently considered as attractive

candidates for sequestering pollutants from aquatic systems,[24, 25] possessing superior features over the other adsorbents such as activated carbon, which interacts with pollutants *e.g.* water-soluble organic dyes *via* weak hydrophilic interactions resulting in weak purification performance.[26] Moreover, oxygen containing groups may undergo ionization or can act as electron acceptors, which allows the occurrence of electrostatic interactions, π-π stacking and hydrogen bonding and eventually also ion exchange between dye molecules and GO's surface.[27, 28] It was found that GO exhibits ultrahigh adsorption capacity towards cationic dyes and outperforms other adsorbents. In particular, the adsorption capacity of GO and other different forms like reduced GO (rGO), magnetic graphene oxide (MGO) and reduced magnetic graphene oxide (MrGO) was studied by Akrami *et. al.* for adsorb methylene blue (MB), which is one of the most widely used cationic dye. Presented work exhibit the values to be as high as 116 mg/g (GO), 168 mg/g (MGO), 82 mg/g (rGO) and 114 mg/g (MrGO).[29] Yet, the high dispersibility of GO in water hampers its use in industrial systems since the residual GO cannot be easily removed from post-adsorption dispersions and may cause secondary pollution. To overcome this drawback, the functionalization of GO with organic and inorganic moieties have been explored which resulted in a large library of GO-based materials exhibiting strong adsorption affinity towards various pollutants.[30-39] In this case, the fabrication of functionalized materials through covalent reactions between pristine GO nanosheets are particularly attractive. Another major limitation of neat GO arises from its poor porosity, which limits the number of available coordination sites. The problem can be potentially overcome by covalently bridging GO layers with molecular pillars to form three-dimensional macroscopic porous structures. Mesoporous silica, introduced in the 1990s by Kresge,[40] is attracting a growing interest for water treatment chemistry due to its various remarkable properties such as high specific surface area, large pore size, chemical inertness. However, mesoporous silica itself does not exhibit high adsorption capacity towards organic dyes. Yet, because of an abundant repertory of surface functional groups it can be chemically tailored for excellent selectivity towards specific contaminants, good stability and low-cost of production.[41-43] In this section, we report a facile and low-cost method to produce novel GO-based adsorbent obtained via the condensation between 3-aminopropylsilica particles (SiO_2NH_2) and GO for the effective removal of cationic dyes including methylene blue (MB), rhodamine B (RhB) and methyl violet (MV) from water

(Figure 4.1). Different adsorption parameters were systematically studied including pH, temperature, time and adsorption mechanism to gain in-depth insight into the adsorption process. The adsorption kinetics and isotherms of MB, RhB and MV cationic dyes on SiO_2NH_2-GO material were estimated with the pseudo-first and -second order as well as Freundlich and Langmuir isotherm model. Moreover, the SiO_2NH_2-GO hybrid was used as solid phase extraction (SPE) column packing material which allows achieving high flow-rate with excellent recovery, precision and adsorption at the level of 99% of initial dye content.

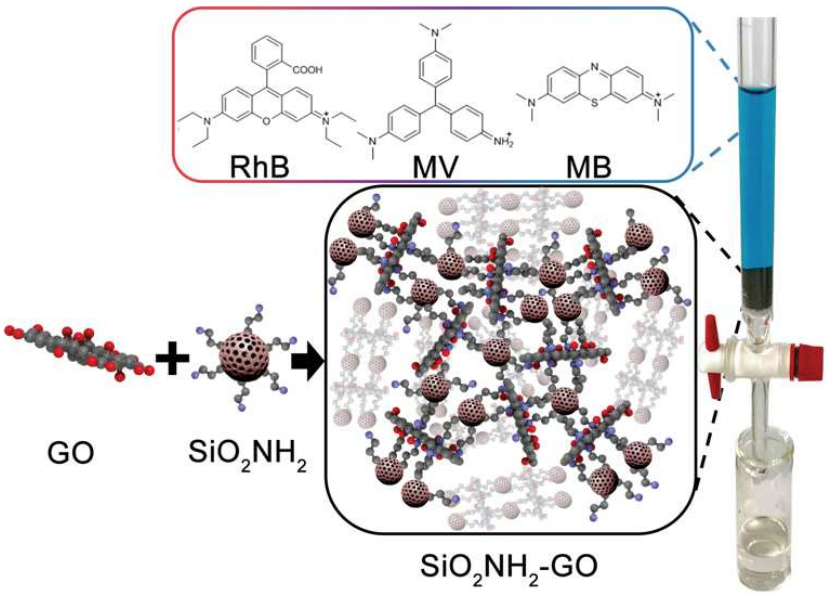

Figure 4.1. Chemical structures of the adsorbent (SiO_2NH_2-GO) and cationic dyes: methylene blue (MB) rhodamine B (RhB) and methyl violet (MV).

4.2. Materials and methods

4.2.1. Synthesis of SiO_2NH_2-GO

The fabrication of such a three-dimensional SiO_2NH_2-GO composite has been achieved *via* the condensation reaction between the amine units exposed on 3-aminopropyl-functionalized silica nanoparticles and the epoxy groups on GO surface. The preparation method is similar to that presented above (chapter 3, section 3.2). A batch of SiO_2NH_2-GO is prepared as follows: a mixture of ethanol (50 ml) and GO (50 ml, 4 mg mL^{-1}) was sonicated for 15 min and then suspension of 3-(aminopropyl)-functionalized silica (1 g) dispersed in 200 ml of ethanol was added. The mixture was rigorously stirred overnight under reflux. The precipitate was then filtrated and rinsed with a large amount of water and ethanol. The resulting black powder was then freeze-dried for 24h under vacuum.

4.2.2. Morphological characterization of SiO_2NH_2-GO

In order to understand the nature of the interaction between the SiO_2NH_2 and GO, a multiscale analysis has been carried out. Scanning electron microscopy (SEM) was employed to study the morphology of the multicomponent systems. The images in Figure 4.2a show that SiO_2NH_2-GO possess a homogenous porous structure. Energy-dispersive X-ray spectroscopy (EDX) investigation (Figure 4.2b**)** provided evidence for the uniform distribution of the SiO_2NH_2 particles within the hybrid SiO_2NH_2-GO material.

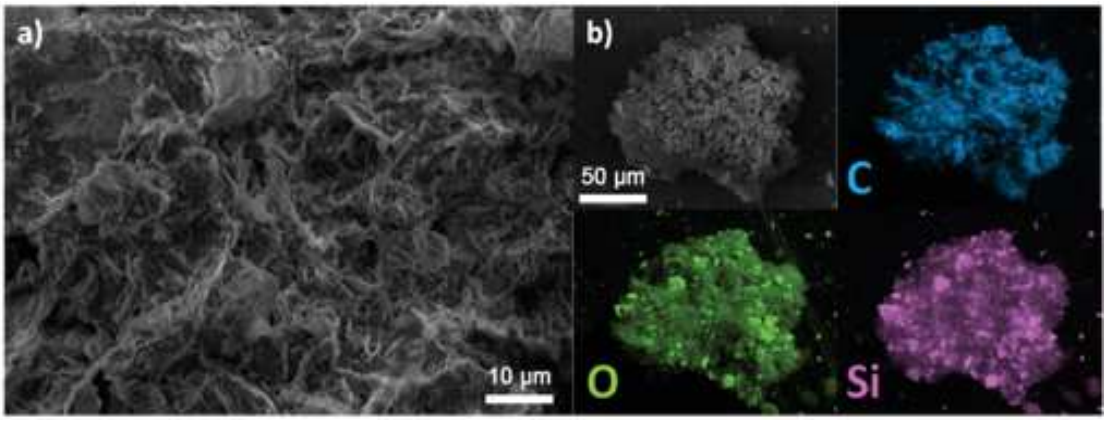

Figure 4.2. (a) Scanning electron microscopy (SEM) image displaying the morphology of SiO_2NH_2-GO, (b) SEM image of SiO_2NH_2-GO fragmented foam and EDX elemental mapping of carbon (C, blue), oxygen (O, green) and silicon (Si, purple).

The porosity of SiO_2NH_2-GO was investigated by adsorption-desorption isotherms of N_2 at 77K. It revealed a specific surface area, as calculated by Brunauer-Emmett-Teller (BET) model, of 405.5 m^2g^{-1}. Such value is much greater than the one quantified in the starting GO material which displays a specific surface area of ca. 108 m^2 g^{-1}. The nearly four-fold enhancement in the specific surface area provides clear evidence for the significant increase in the inter sheets spacing (Figure 4.3a). The average pore size diameter, as calculated with the Barrett-Joyner-Halenda (BJH) model, amounts to 70.4 Å.

Fourier transform infrared spectroscopy was used to prove the covalent cross-linkage of the SiO_2NH_2 particles to GO (Figure 4.3b). The pristine GO displays typical peaks corresponding to a variety of oxygen-containing functional groups. The peak at 1724 cm^{-1} is attributed to the C=O stretching of carboxylic acid groups, 1624 cm^{-1} to the sp^2 C=C bonds, 1216 cm^{-1} and 1054 cm^{-1} to C–O stretching of epoxy and alkoxy groups, respectively and a broad band due to O–H stretching vibrations in carboxyl and alcohol functionalities around 3390 cm^{-1}.[44] The spectra of SiO_2NH_2 exhibit very strong and broad band at 1075 cm^{-1} which is usually assigned to the Si-O-Si asymmetric stretching vibrations, whereas the band at 801 cm^{-1} corresponds to Si-O-Si symmetric stretching vibrations. Once the aminosilica interacts with GO, a reaction between amine groups of SiO_2NH_2 with epoxy units located on the plane of GO flakes takes place. As a result, the reaction is accompanied by a strong decrease in the intensity of the C-O band with appearance of strong and broad absorption at 1075 and 801 cm^{-1}, which was not

monitored in the neat GO and corresponds to Si-O-Si bond from SiO_2NH_2 material. Moreover, additional adsorption slight peak appeared in SiO_2NH_2-GO at 1623 cm^{-1} which were assigned to the sp^2 C=C bonds. Such a result confirmed the structural integrity of SiO_2NH_2 whose architecture is well retained in the hybrid structures SiO_2NH_2-GO.

The crystallinity, and in particular the interlayer distance within GO and SiO_2NH_2-GO were investigated by wide-angle X-ray scattering (WAXS). A typical sharp peak 2θ at ~10.01° for pristine GO corresponds to an interlayer spacing of 0.87 nm due to the (002) reflection of stacked GO sheets, in accordance with the previously reported value.[45, 46] Additionally, an amorphous peak at 2θ = 22.15° was recorded and corresponds to silica particles characterized by variable Si-O-Si bond angles (Figure 4.3c). Upon functionalization of GO with SiO_2NH_2, the 2θ peak shifts toward lower angles 2θ = 8.35°, indicating higher interlayer distance 1.06 nm when compared to GO. Such shift clearly confirms intercalation of silica particles in between graphene oxide interlayer space. Moreover, the high intensity of broad peak coming from amorphous content confirms significant amount of silica in SiO_2NH_2-GO hybrid material.

High-resolution X-ray photoelectron spectroscopy (XPS) measurements of pristine GO and SiO_2NH_2-GO made it possible to gain further information onto the chemical composition of materials (Figure 4.3d-f). The significant difference between the carbon (C1s), oxygen (O1s) and nitrogen (N1s) peaks provided evidence for the chemical bond formation between the oxygen-containing functional groups on the surface of GO and amine groups from SiO_2NH_2. In particular, wide energy spectrum exhibited the appearance of new peaks in SiO_2NH_2-GO hybrid material at 400.4 eV, 144.6 eV and 102.0 eV corresponding to N1s, Si2s and Si2p signals, respectively. The C1s XPS spectrum of the neat GO (Figure 4.3d) shows three main peaks at 285 eV (C-C/C=C), 287.5 eV (C-O) and 289.4 eV corresponding to carboxylic species present on edges of GO. In turn, the C1s spectra of SiO_2NH_2-GO clearly show changes in the chemical structure of GO by introduction of SiO_2NH_2 (Figure 4.3e). Compared to GO, the C1s spectra of SiO_2NH_2-GO feature a new prominent peak at 286.2 eV, which can be assigned to C-N bonds present in amino silica and also generated *via* the reaction of amine groups with opening epoxy rings (Figure 4.3f).The high resolution O1s spectrum of SiO_2NH_2-GO indicates the presence of both Si-O and C-O peaks at 532.2 eV and 533.5 eV, respectively also existing in O1s spectra of GO and SiO_2NH_2 solely. Moreover, changes

due to the introduction of nitrogen species within the GO structure are observed in the high-resolution N1s spectra indicating the successful functionalization of SiO_2NH_2 with the GO nanosheets. The N1s spectrum of SiO_2NH_2 can be deconvoluted into two main peaks at 399.0 eV and 401.8 eV which can be ascribed to N-C and N-H bonds. Notably, the amount of N-C bonds increases due to reaction between amine groups of silica with epoxy-carbon atoms on GO's surface.

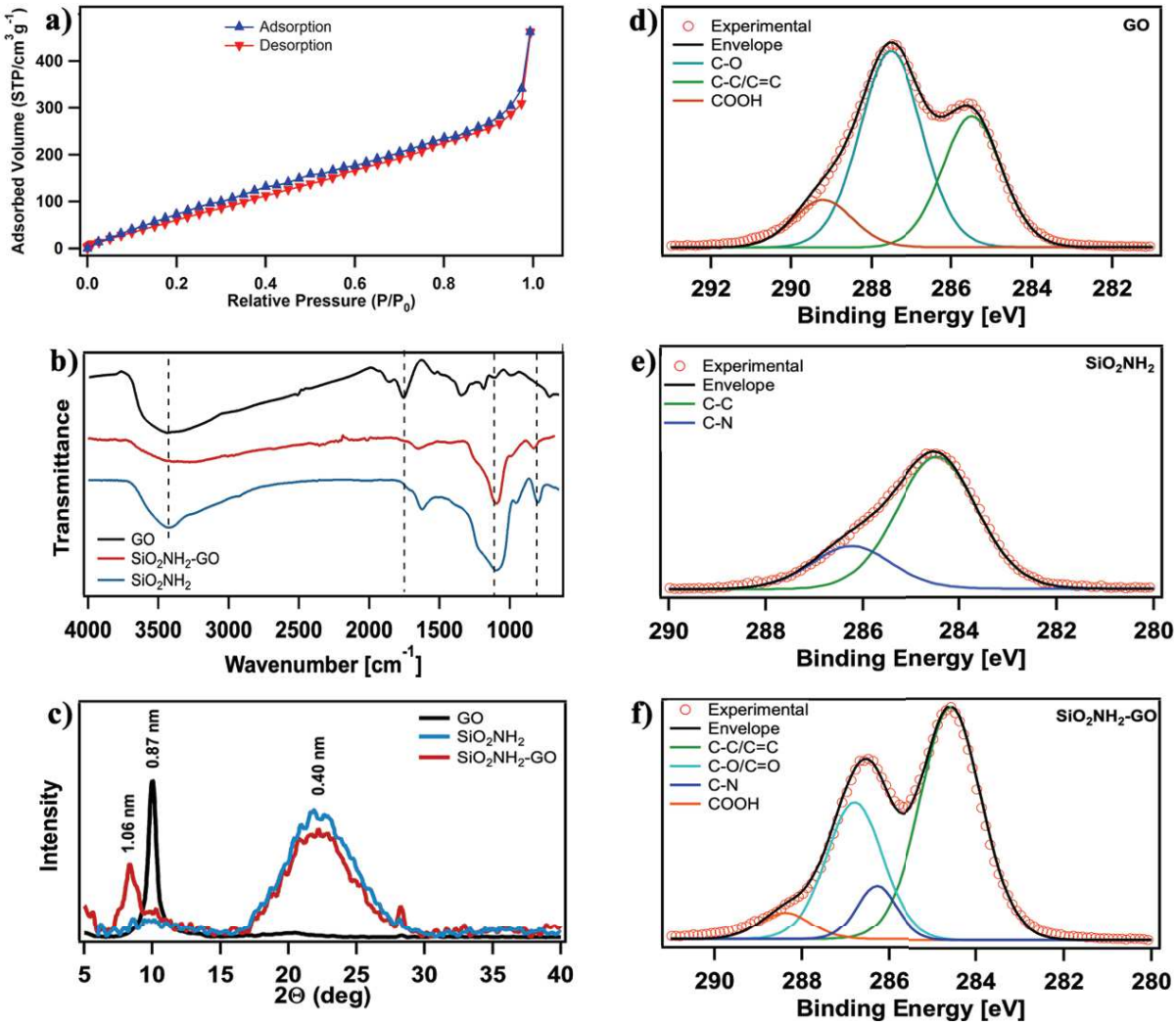

Figure 4.3. (a) BET adsorption/desorption isotherm of N_2 for SiO_2NH_2-GO composite. (b) FTIR spectra of GO, SiO_2NH_2 and SiO_2NH_2-GO composite. (c) XRD patterns of GO, SiO_2NH_2 and SiO_2NH_2-GO composite. C1s high-resolution XPS spectra of: (d) GO, (e) SiO_2NH_2 and (f) SiO_2NH_2-GO.

The SiO_2NH_2-GO hybrid was further characterized by Raman spectroscopy which is widely used for characteristics of carbonaceous materials. Raman spectra (Figure 4.4) exhibit two prominent peaks of GO, *i.e.* the D band (1358 cm^{-1}) corresponding to sp^3 hybridized carbon atoms and the G band (1592 cm^{-1}) originated from the scattering of the E_{2G} photon of the sp^2 hybridized carbon bond from the aromatic regions of GO.[47, 48] Comparably, in spectrum of SiO_2NH_2-GO the value of G band shifts to a lower wavenumber, reaching 1586 cm^{-1}, thereby confirming the covalent functionalization of the graphitic materials.[49] Typically, chemical modification of graphene materials is often characterized by the changes in the ratio of the D and G bands areas. As we can previously describe the intensity ratio I_D/I_G is commonly used to determine the degree of functionalization of graphene-based nanostructures.[50] As the result of the functionalization, the I_D/I_G intensity ratio increases from 0.93 to 1.12, offering an indirect evidence of the increased content in sp^3 carbon atoms upon functionalization.

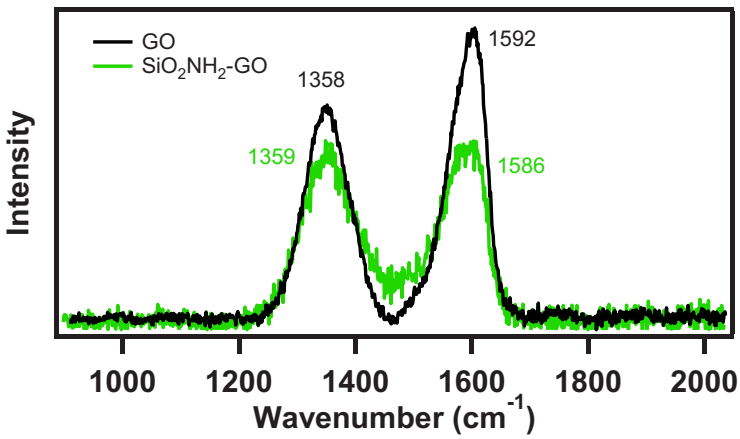

Figure 4.4. Raman spectra recorded for graphene oxide and SiO_2NH_2-GO composite.

4.3. Results

4.3.1. Adsorption of cationic dyes on SiO_2NH_2-GO using UV-vis measurements

The adsorption of organic dyes on SiO_2NH_2-GO was carried out by mixing 5 mg of adsorbent and 15 ml of dye solution at the desired concentration, then solution pH was adjusted with HCl (0.1 M) or NaOH (0.1 M) to study the effect of initial pH. The mixtures then were intensively stirred for 24 hours at room temperature to achieve the adsorption equilibrium. The adsorbent was separated from the dye solution by centrifugation and the equilibrium concentration of the dye in solution was determined by means of UV-Vis spectroscopy. To investigate the superior adsorption capacity of the SiO_2NH_2-GO, batch tests of the adsorption performance of SiO_2NH_2, GO and SiO_2NH_2-GO were conducted. Three prototypical water-soluble cationic dyes were chosen, *i.e.* methylene blue (MB), rhodamine B (RhB) and methyl violet (MV). The maximum adsorption capacity (q_{max}) was investigated using previously presented mathematical relation of the organic pollutant (dyes in this case) adsorbed by one gram of adsorbent to the equilibrium solution concentration at constant temperature (Equation 1 in chapter 2). Both Freundlich and Langmuir adsorption isotherm models were used for the analysis of organic dyes adsorption (Equations 6 and 7 in chapter 2). Q_{max} and additional parameters obtained from Langmuir and Freundlich isotherm models are summarized in Table 4.1.

Table 4.1. Parameters for Freundlich and Langmuir isotherm models for adsorption of MB, RhB and MV on SiO_2NH_2-GO composite.

Dye	Freundlich			Langmuir		
	n	K_F	R^2	q_{max}	$K_L(x10^{-2})$	R^2
MB	2.6±0.2	25.2±4	0.875	300±7	1.4±0.1	0.996
RhB	3.5±0.3	66.38±9	0.889	358±7	3.6±0.3	0.998
MV	2.5±1	16.65±1	0.984	178±8	1.7±0.2	0.989

Noteworthy, that the adsorption isotherms of organic dyes on SiO_2NH_2-GO composite are fitted better by Langmuir model than by the Freundlich, suggesting not exiting monolayer coverage (Figure 4.5a-c).

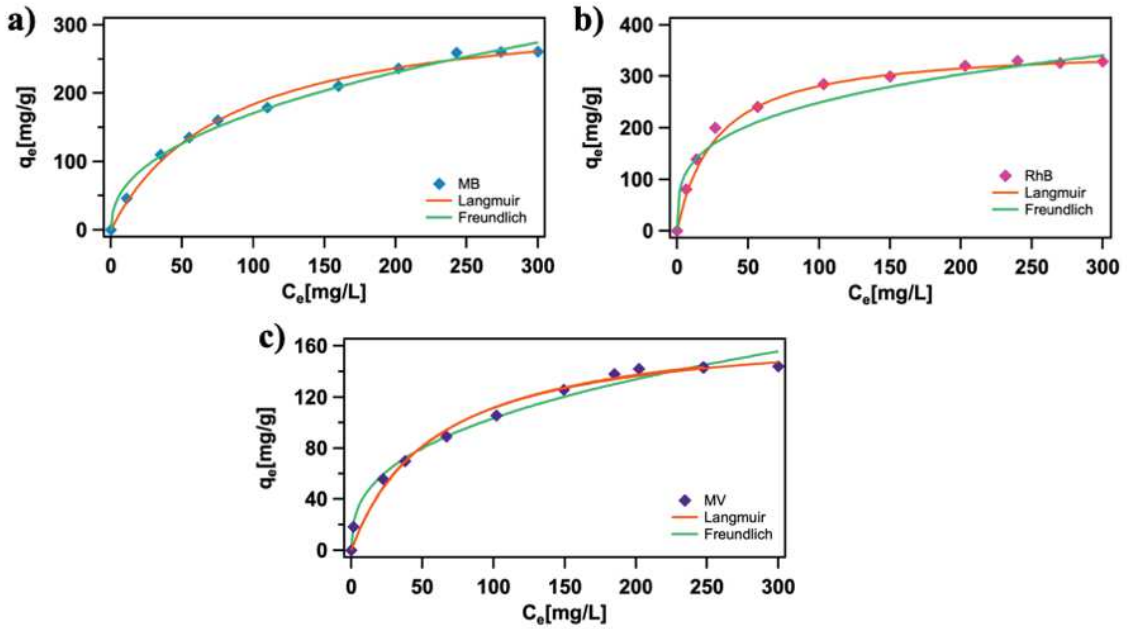

Figure 4.5. Uptake of organic dyes as the function of initial concentration of (a) methylene blue (b) rhodamine B and (c) methyl violet. The uptake experiments were carried out at pH=10 (stirring speed 400 rpm, t=24h).

For the sake of comparison, control experiments, in which starting materials of GO and SiO_2NH_2 are used as adsorbents, are also carried out and presented below in Table 4.2 and Figures 4.6-4.7.

Table 4.2. Parameters for Freundlich and Langmuir isotherm models for adsorption of MB, RhB and MV on SiO_2NH_2 and GO compounds at pH = 10.

Adsorbent	Dye	Freundlich			Langmuir		
		n	K_F	R^2	q_{max}	K_L(x10^{-2})	R^2
SiO_2NH_2	MB	2.9±0.4	8.9±2.1	0.867	68±3	1.9±0.3	0.989
	RhB	2.5±0.3	7.6±1.7	0.963	83±5	1.5±0.2	0.995
	MV	2.4±0.4	3.7±0.7	0.931	44±2	1.4±0.2	0.997
GO	MB	2.7±0.4	15.2±2.1	0.892	141±7	1.6±0.2	0.991
	RhB	3.1±0.5	23.3±6.2	0.899	157±8	2.2±0.3	0.994
	MV	3.0±0.3	11.8±2.5	0.911	88±3	1.9±0.3	0.997

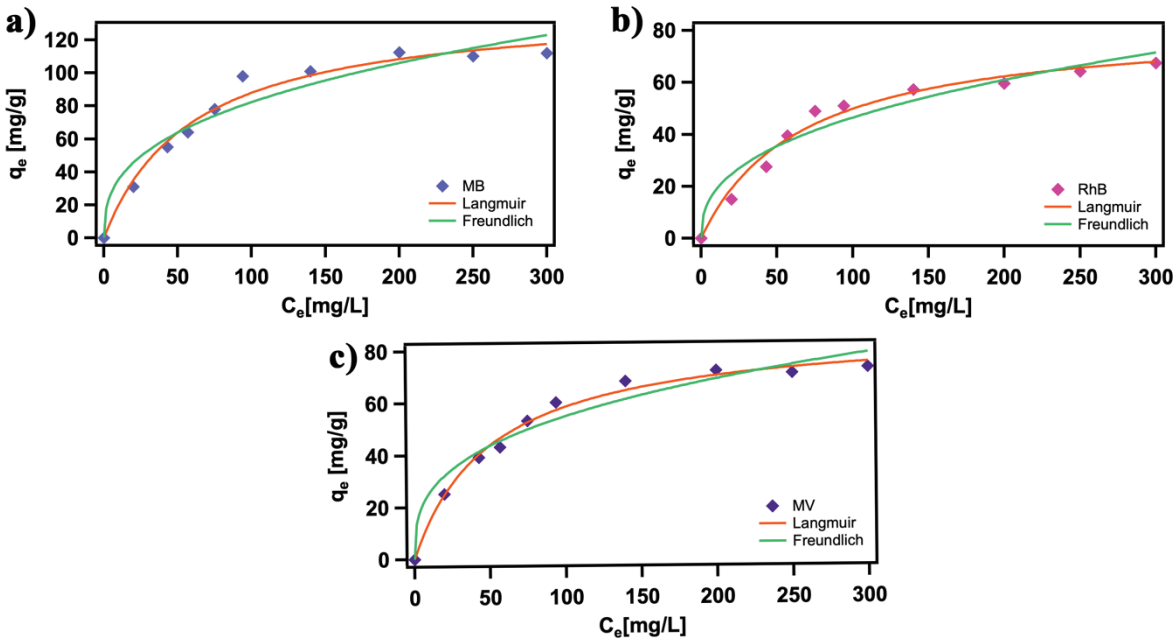

Figure 4.6. The Langmuir and Freundlich adsorption models of MB, RhB and MV on GO.

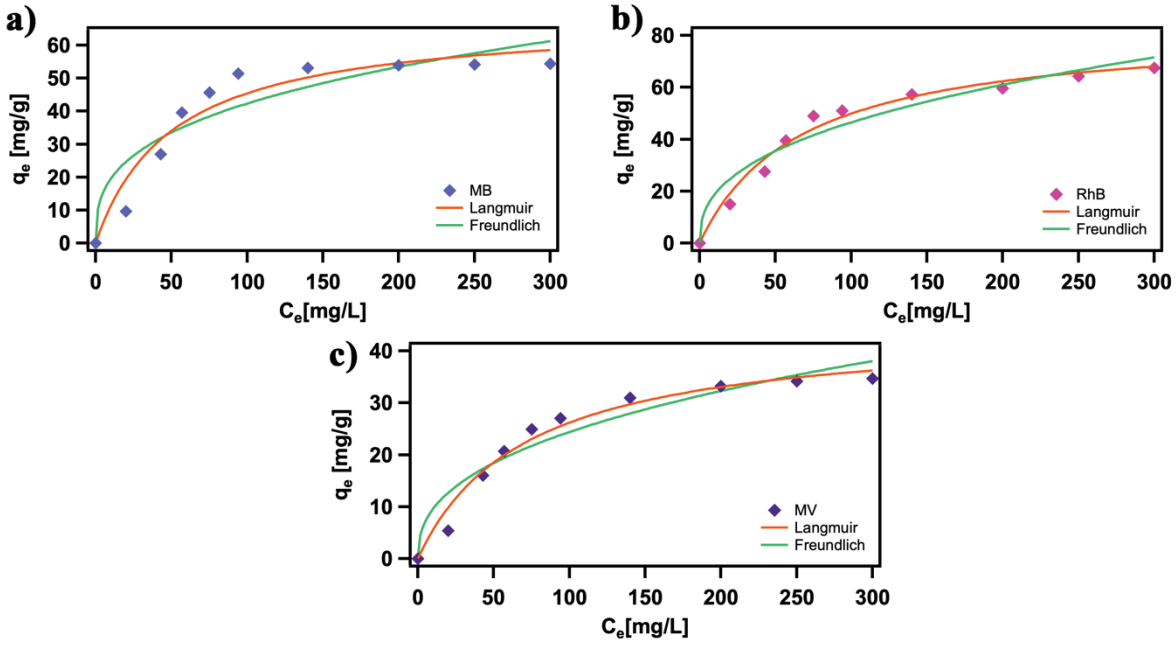

Figure 4.7. The Langmuir and Freundlich adsorption models of MB, RhB and MV on SiO_2NH_2.

The maximum adsorption capacities using SiO_2NH_2-GO at pH 10 are 300 mg g^{-1} for MB, 358 mg g^{-1} for RhB and 178 mg g^{-1} in case of MV. The q_{max} values expressed in mmol g^{-1} amount to 0.97, 0.79 and 0.42 for MB, RhB and MV, respectively, implying that 1 g of SiO_2NH_2-GO can adsorb from approx. 0.5 to 1 mmol of cationic dyes from aqueous solutions. These values can be considered as very promising for the sorbents of

cationic dyes compare to the previously reported chemically modified graphene materials.[28, 51, 52] Noteworthy, while the overall charge of investigated dyes is nearly identical, the maximum adsorption capacity expressed in mmol g^{-1} revealed the significant difference between MB, RhB and MV. In general, carbonaceous materials such as CNTs or activated carbons show the highest adsorption for MB, medium values for MV and the lowest adsorption for RhB.[53, 54] This variation is commonly attributed to the dye molecular size. For the larger dye molecules, adsorption can only occur at surface and it is difficult for the dyes to enter into the inner smaller pores of carbons. Such dye adsorption behavior is notably different for SiO_2NH_2-GO, where the maximum adsorption capacity of three dyes follows the trend MB > RhB > MV. Noteworthy, although in general the functionalization of GO results in formation of highly porous structures, the pore sizes of such systems are rather low. This trend is also reflected in the present case where the large surface area (405.5 m^2 g^{-1}) is accompanied by pore size of diameter of around 70 Å, which limits the accessible area for large dyes (RhB) penetration. On the other hand, the adsorption capacity of RhB on the SiO_2NH_2-GO surface is supplemented by the strong electrostatic interaction resulting from the presence of both positive and negative charges in RhB structure. Furthermore, the pKa values for MB, RhB and MV are 3.8, 3.7 and 9.4, respectively.[55, 56] As the maximum adsorption was investigated at pH 10, MB and RhB are completely deprotonated at this condition while MV might occur residual protonated groups which results in its lower adsorption capability.

4.3.2. Solid phase extraction (SPE) with SiO_2NH_2-GO

Currently exploited purification methods rely on time-consuming techniques usually generating problems including secondary pollutions or separation difficulties. Therefore, solid phase extraction process constitutes an attractive alternative for removal of contaminants such as cationic organic dyes. Due to the high value of kinetic rate of adsorption process, the high saturation uptake capacity, the optimal pore size and high specific surface area as well as loose and powdery structure of obtained adsorbent we opted to apply the SiO_2NH_2-GO as solid phase extraction column filling for rapid, effective and continuous adsorption of presented organic dyes. As the column was loaded with adsorbent, the filling was firstly activated with NaOH, to provide negative charge on the surface and enhance effectiveness of adsorption process. The uptake of the cationic dyes (MB, RhB and MV) from aqueous solutions were studied using as-prepared SiO_2NH_2-GO material at the desired concentration and pH. The initial pH of solution can strongly affect the surface charge of adsorbent by dissociation of functional groups on active sites of GO as well as the ionization of organic dyes. The point of zero charge (pH_{pzc}) indicates the value of pH which refers to neutral charge of adsorbent and constitutes one of the key factors for understanding the adsorption on carbon-based materials.[33, 57] The point of zero charge of SiO_2NH_2-GO corresponds to 7.0 (Figure 4.8).

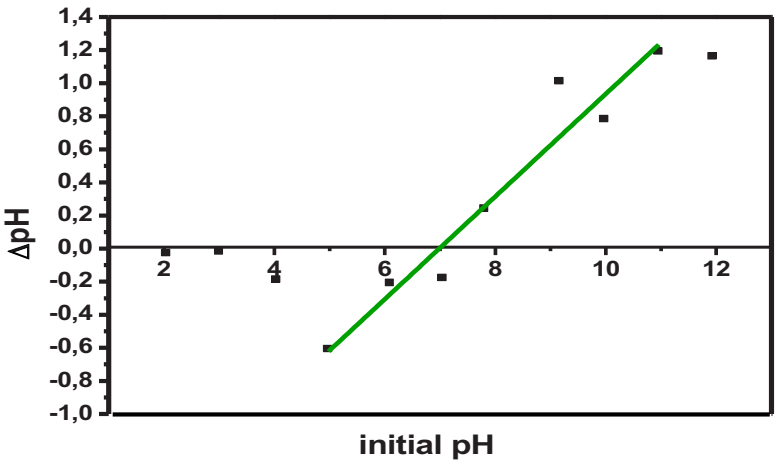

Figure 4.8. The chart presenting estimation of the point of zero charge pH_{pzc}.

Thus, at pH>7 (pH>pH_{pzc}), the surface charge of composite is negative. As a consequence, the significant adsorption process is observed at pH>7 because the electrostatic interactions between the cationic dyes and SiO_2NH_2-GO become stronger. Comparably the adsorption capacity of MB is almost ~5.2 times greater at pH=10 than value obtained in acidic conditions. Notably, dramatic difference is observed for MV, where basic conditions allow to increase the adsorption capacity even 33 times.

Reusability of the column filling was conducted following the procedure described in previous section. As presented on Figure 4.9, the removal efficiency decreases about 7% after first 2 cycles. Further experiments showed that each cycle causes a slight decrease of adsorption capacity, which might be explained by the collapsing of pores due to high volumetric flow of analyte over the experiments (~4L per cycle) resulting in lower pore volume after adsorption. After 10 cycles the system is still able to adsorb from approx. 0.3 to 0.5 mmol of cationic dyes from aqueous solutions, which is more than 60% of initial adsorption capacity.

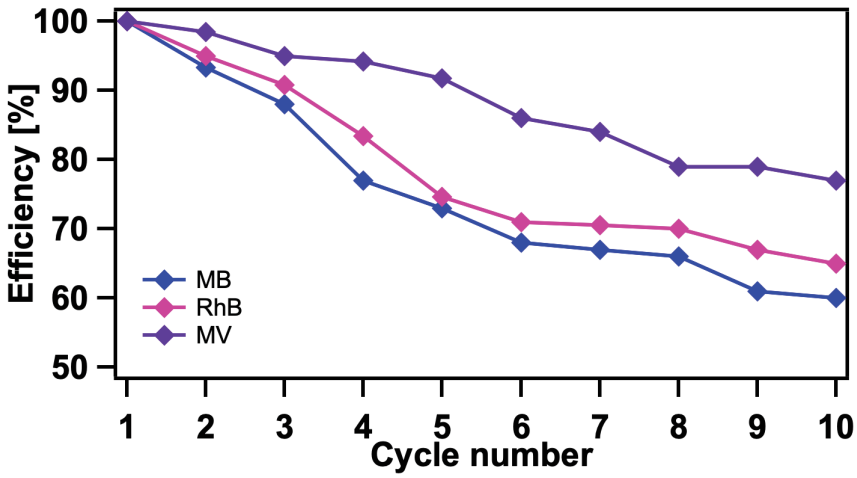

Figure 4.9. Reusability studies of SiO_2NH-GO after 10 cycles.

To gain further insight into the adsorption process, the effect of pH was analyzed and FTIR spectra after adsorption were recorded. The effect of pH on the adsorption rate of MB, RhB and MV on the SiO_2NH_2-GO was examined at pH ranging from 2 to 12. The adsorption capacities with different pH are presented in Figure 4.10. At low pH conditions (pH=4) only approx. 20% for MB and RhB and less than 35% for MV of the initial dyes

were removed, with further increase in pH value the adsorption efficiency increases. MB, RhB and MV are cationic dyes, which were favorably adsorbed through electrostatic interactions with negatively charged functional groups on the surface of SiO_2NH_2-GO composite. Alongside, the planar structure of GO favours the presence of π-π interactions. In our case organic dyes can act as π-electron acceptors of residual π-electron rich regions of graphene oxide providing co-participation of π-π stacking in adsorption mechanism previously reported for graphene based nanostructures.[58, 59]

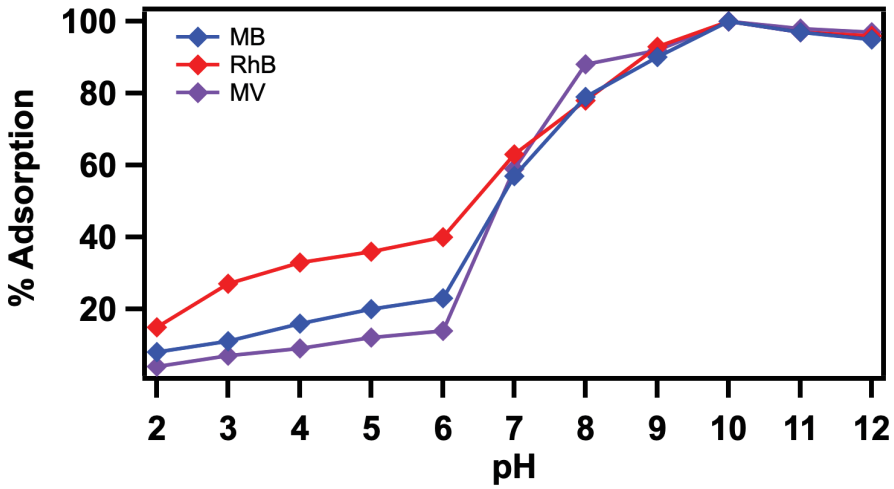

Figure 4.10. Uptake of organic dyes as the function of initial concentration conducted at different pH values. Blue columns represent methylene blue, pink - rhodamine B and violet – methylene violet.

On the other hand, we have used FTIR to monitor the interaction between dyes and SiO_2NH_2-GO in the solution (Figure 4.11). The spectra recorded after adsorption of dye displayed a significant increase of the peak at 3418 cm^{-1} which can be attributed to presence of hydrogen bonds and indicates that such interactions might be also important in organic dyes adsorption. Moreover, after adsorption of MB there is a slight shift from 1607 to 1601 cm^{-1} corresponding to C=C bonds and confirming π-π interactions.

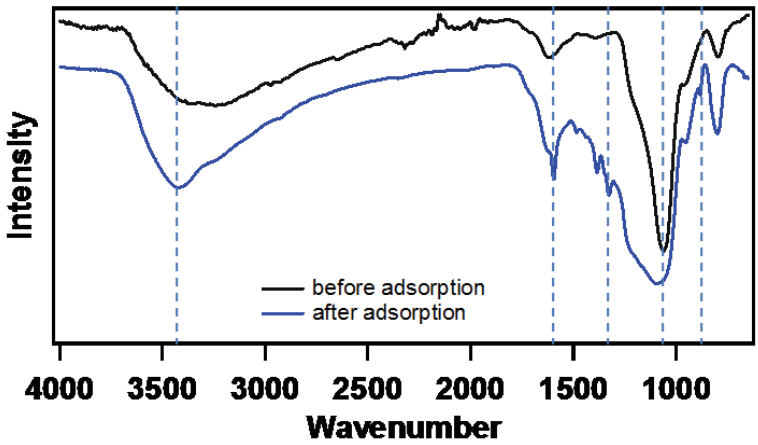

Figure 4.11. FT-IR spectra before and after adsorption of methylene blue (MB) on SiO_2NH_2-GO composite.

Unfortunately, understanding the exact adsorption mechanism is a more complex task, which is beyond the scope of this work. However, it is fair to conclude that the aforementioned results suggest that tested cationic dyes can be easily adsorbed *via* electrostatic interactions and this type of interactions play a significant role in the adsorption of MB, RhB and MV on the SiO_2NH_2-GO. In according to kinetic studies, the experimental values of adsorption capacity and linear regression coefficient showed that the adsorption of cationic dyes is better fitted by pseudo-second order kinetics, which indicate that the adsorption process is driven by the strong surface complexation of cationic dyes with the oxygen and nitrogen containing groups of SiO_2NH_2-GO.

The thermodynamic analysis such as standard Gibbs free energy change (ΔG^o), the enthalpy change (ΔH^o) and entropy change (ΔS^o) were calculated for better understanding of the nature of adsorption behavior (see chapter 2, Equations 11-13). The values of ΔH^o and ΔS^o can be calculated from the slope and intercept, respectively by plotting the values of lnK_d vs. 1/T (Figure 4.12).

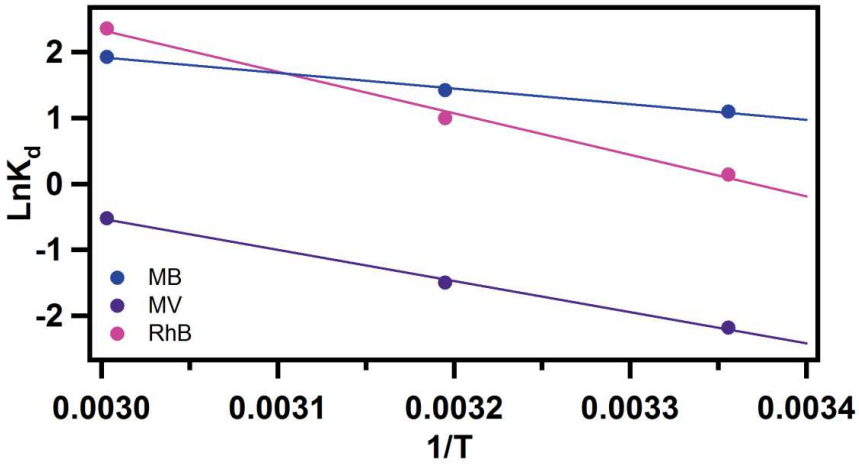

Figure 4.12. The linear curve of lnK_d vs 1/T for MB, RhB and MV adsorption to determine thermodynamic parameters.

The thermodynamic parameters from the fitting line such as Gibbs free energy change ($G°$), the enthalpy change (ΔH^o), the entropy change (ΔS^o) and correlation coefficient (R^2) are listed in Table 4.3.

Table 4.3. Thermodynamic parameters for adsorption of cationic dyes (MB, RhB, MV) onto SiO_2NH_2-GO composite.

Dye	T(K)	ΔG° (KJ mol^{-1})	ΔH° (KJ mol^{-1})	ΔS° (KJ mol^{-1} K^{-1})	R^2
MB	298	-2.7	-19.6	74.9	0.994
	313	-3.7			
	333	-5.3			
RhB	298	-0.3	-52.6	177.1	0.992
	313	-2.4			
	333	-6.5			
MV	298	5.4	-38.8	112.9	0.997
	313	3.0			
	333	1.4			

The negative values of ΔG^o confirmed the spontaneous nature of the adsorption process. The distribution ratio (K_d) of cationic dyes onto SiO_2NH_2-GO composite are decreased

with the increase in temperature, implying that the adsorption process is exothermic, which was further confirmed by the negative values of ΔHº. On the other hand, the positive values of ΔS^o shows the increment randomness at the surface of adsorbent during the adsorption process which can be reflected by the affinity of the SiO_2NH_2-GO for the cationic dyes.

A kinetic investigation of the adsorption process can be accomplished by evaluating the rate and mechanism of mass transfer of adsorbate from liquid phase to solid adsorbent surface. The time required to reach equilibrium is an important parameter for dye removal. The pseudo-second-order kinetics model has been extensively used to predict dye adsorption kinetics.[28, 60] It reveals that the adsorption displays a remarkable increase at the beginning of the experiments and then it reaches a plateau. To establish the time dependence of adsorption process, the adsorption capacitance of SiO_2NH_2-GO for MB, RhB and MV solutions of initial concentrations of 50 mg g^{-1} at diverse contact time were measured. Figure 4.13 presents that the initial rate of cationic dyes adsorb increased sharply with time and reached a maximum ~99.7% within 3 min, and then it reaches a plateau. This result indicates that a monolayer of dye molecules at the surface on the SiO_2NH_2-GO composite is formed. When the initially fast adsorption process is over, the dyes adsorption kinetic rate was adjusted by mass transport in the composite material.[61, 62]

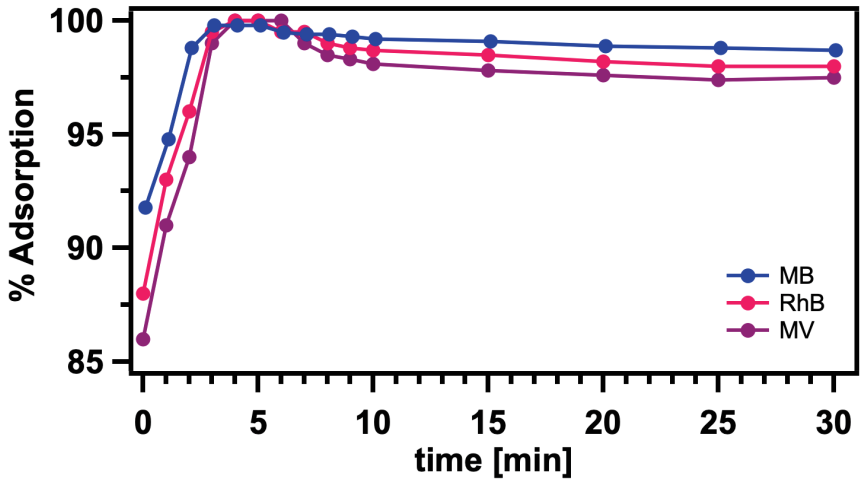

Figure 4.13. Time dependent organic dyes sorption on SiO_2NH_2-GO material (C_0= 50 mg g^{-1} T= 25 °C, stirring speed = 300 rpm, pH = 7).

The experimental values of adsorption capacity and linear regression coefficient showed that the adsorption of cationic dyes is better fitted by pseudo-second order kinetics (Figure 4.14b) than pseudo first order kinetics (Figure 4.14a), which indicate that the adsorption process is driven by the strong surface complexation of cationic dyes with the oxygen and nitrogen containing groups of SiO_2NH_2-GO.

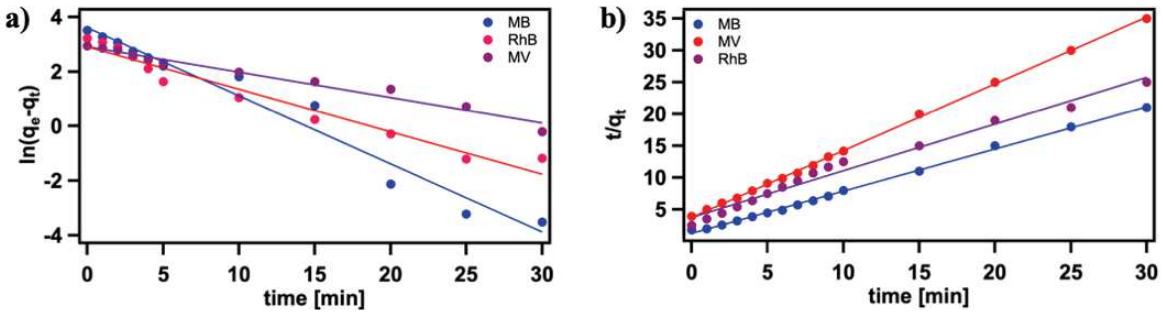

Figure 4.14. The kinetic plots obtained by a) pseudo-first and b) pseudo-second order model reactions.

Additionally, the calculated kinetic parameters for adsorption of MB, RhB and MV dyes at pH 10 are listed below in Table 4.4.

Table 4.4. Coordination kinetic rate constants and unit adsorption capacity of functionalized graphene oxide material (SiO_2NH_2-GO) towards cationic dyes (MB, RhB, MV).

Dye	**Pseudo-first order model**			**Pseudo-second order model**			q_e(exp)
	R^2	k_1 x [10^{-2}]	q_e	R^2	k_2 x [10^{-2}]	q_e	
MB	0.921	4.1 ± 0.3	58.4 ± 4.4	0.998	0.95 ± 0.13	45.6 ± 2.2	42.5 ± 2.1
RhB	0.989	2.5 ± 0.2	25.4 ± 1.9	0.992	0.73 ± 0.11	28.1 ± 1.5	28.3 ± 1.4
MV	0.988	1.5 ± 0.1	22.1 ± 1.3	0.993	0.21 ± 0.04	21.1 ± 1.1	20.2 ± 1

4.4. Conclusions

In summary, we have presented an easy and effective approach towards synthesis of SiO_2NH_2-GO composite, and its high efficiency for removal of cationic dyes from water. Various complementary characterization methods were employed to confirm the covalent attachment of 3-aminosilica-functionalized silica to GO. The novel porous material, with its high specific surface area (405.5 m^2 g^{-1}), exhibited high affinity toward cationic organic pollutants. The adsorption experiments show that cationic dyes (MB, RhB and MV) can be quantitatively adsorbed at pH 10 with maximum adsorption capacity as high as 300, 358 and 178 mg g^{-1}, respectively. Moreover, the obtained composite exhibited the high value of kinetic rate and was additionally efficiently investigated toward continuous adsorption from aforementioned organic dyes as column filling in solid phase extraction process. Noteworthy, the presented system displayed excellent adsorption efficiency of ~99.7% for MB, RhB and MV in 3 min, stability and reusability toward removal of cationic organic dyes paving the way to development silica-GO based materials of high-efficiency and low-cost water purification technologies.

4.5. References

1. P. J. J. Alvarez, C. K. Chan, M. Elimelech, N. J. Halas and D. Villagrán, *Nat. Nanotech.*, 2018, **13**, 634-641.
2. S. M. Ghoreishi and R. Haghighi, *Chem. Eng. J.*, 2003, **95**, 163-169.
3. H. Zollinger, *VCH Publishers, New York*, 1987, 92-100.
4. N. Buvaneswari and C. Kannan, *J. Hazard. Mater.*, 2011, **189**, 294-300.
5. Z. Aksu, *Process Biochem.*, 2005, **40**, 997-1026.
6. U. Shanker, M. Rani and V. J. E. C. L. Jassal, *Environ. Chem. Lett.*, 2017, **15**, 623-642.
7. C.-H. Weng and Y.-F. Pan, *J. Hazard. Mater.*, 2007, **144**, 355-362.
8. M. A. M. Salleh, D. K. Mahmoud, W. A. W. A. Karim and A. Idris, *Desalination*, 2011, **280**, 1-13.
9. Y. Liu, F. Li, Q. Xia, J. Wu, J. Liu, M. Huang and J. Xie, *Nanoscale*, 2018, **10**, 4771-4778.
10. Y. Han, Z. Xu and C. Gao, *Adv. Funct. Mater.*, 2013, **23**, 3693-3700.
11. Q. Ma, Y. Yu, M. Sindoro, A. G. Fane, R. Wang and H. Zhang, *Adv. Mater.*, 2017, **29**, 1605361.
12. I. Ali, *Chem. Rev.*, 2012, **112**, 5073-5091.
13. W. Ma, J. Li, X. Tao, J. He, Y. Xu, J. C. Yu and J. Zhao, *Angew. Chem. Int. Ed.*, 2003, **42**, 1029-1032.
14. A. V. Desai, B. Manna, A. Karmakar, A. Sahu and S. K. Ghosh, *Angew. Chem. Int. Ed.*, 2016, **55**, 7811-7815.
15. P. Tan, J. Sun, Y. Hu, Z. Fang, Q. Bi, Y. Chen and J. Cheng, *J. Hazard. Mater.*, 2015, **297**, 251-260.
16. J. Ma, F. Yu, L. Zhou, L. Jin, M. Yang, J. Luan, Y. Tang, H. Fan, Z. Yuan and J. Chen, *ACS Appl. Mater. Interfaces*, 2012, **4**, 5749-5760.
17. C. N. R. Rao, H. S. S. Ramakrishna Matte and U. Maitra, *Angew. Chem. Int. Ed.*, 2013, **52**, 13162-13185.
18. K. Yang, J. Wang and B. Chen, *J. Mater. Chem. A*, 2014, **2**, 18219-18224.
19. J. Wang, J. Hao, D. Liu, S. Qin, C. Chen, C. Yang, Y. Liu, T. Yang, Y. Fan, Y. Chen and W. Lei, *Nanoscale*, 2017, **9**, 9787-9791.
20. S. Luo, X. Xu, G. Zhou, C. Liu, Y. Tang and Y. Liu, *J. Hazard. Mater.*, 2014, **274**, 145-155.
21. K. Ai, C. Ruan, M. Shen and L. Lu, *Adv. Funct. Mater.*, 2016, **26**, 5542-5549.
22. D. R. Dreyer, A. D. Todd and C. W. Bielawski, *Chem. Soc. Rev.*, 2014, **43**, 5288-5301.
23. V. Georgakilas, J. N. Tiwari, K. C. Kemp, J. A. Perman, A. B. Bourlinos, K. S. Kim and R. Zboril, *Chem. Rev.*, 2016, **116**, 5464-5519.
24. S. Eigler and A. Hirsch, *Angew. Chem. Int. Ed.*, 2014, **53**, 7720-7738.
25. V. Georgakilas, M. Otyepka, A. B. Bourlinos, V. Chandra, N. Kim, K. C. Kemp, P. Hobza, R. Zboril and K. S. Kim, *Chem. Rev.*, 2012, **112**, 6156-6214.
26. A. J. Fletcher, Y. Yüzak and K. M. Thomas, *Carbon*, 2006, **44**, 989-1004.
27. Z. Dong, D. Wang, X. Liu, X. Pei, L. Chen and J. Jin, *J. Mater. Chem. A*, 2014, **2**, 5034-5040.
28. Z. Cheng, J. Liao, B. He, F. Zhang, F. Zhang, X. Huang and L. Zhou, *ACS Sustain. Chem. Eng.*, ACS Sustainable Chemistry & Engineering, 2015.

29. M. Akrami, S. Danesh and M. Eftekhari, *J. Inorg. Org. Pol. Mater.*, 2019, DOI: 10.1007/s10904-019-01140-0.
30. X. Zhang, D. Liu, L. Yang, L. Zhou and T. You, *J. Mater. Chem. A*, 2015, **3**, 10031-10037.
31. K. C. Kemp, H. Seema, M. Saleh, N. H. Le, K. Mahesh, V. Chandra and K. S. Kim, *Nanoscale*, 2013, **5**, 3149-3171.
32. Z. Cheng, J. Liao, B. He, F. Zhang, F. Zhang, X. Huang and L. Zhou, *ACS Sustain. Chem. Eng.*, 2015, **3**, 1677-1685.
33. D. Pakulski, W. Czepa, S. Witomska, A. Aliprandi, P. Pawluć, V. Patroniak, A. Ciesielski and P. Samorì, *J. Mater. Chem. A*, 2018, **6**, 9384-9390.
34. C. Anichini, W. Czepa, D. Pakulski, A. Aliprandi, A. Ciesielski and P. Samorì, *Chem. Soc. Rev.*, 2018, **47**, 4860-4908.
35. R. Sitko, E. Turek, B. Zawisza, E. Malicka, E. Talik, J. Heimann, A. Gagor, B. Feist and R. Wrzalik, *Dalton Trans.*, 2013, **42**, 5682-5689.
36. F. Liu, S. Chung, G. Oh and T. S. Seo, *ACS Appl. Mater. Interfaces*, 2012, **4**, 922-927.
37. G. Z. Kyzas, E. A. Deliyanni and K. A. Matis, *J. Chem. Technol. Biotechnol.* , 2014, **89**, 196-205.
38. M. Yusuf, F. M. Elfghi, S. A. Zaidi, E. C. Abdullah and M. A. Khan, *RSC Adv.*, 2015, **5**, 50392-50420.
39. G. K. Ramesha, A. Vijaya Kumara, H. B. Muralidhara and S. Sampath, *J. Colloid Interface Sci.*, 2011, **361**, 270-277.
40. C. T. Kresge, M. E. Leonowicz, W. J. Roth, J. C. Vartuli and J. S. Beck, *Nature*, 1992, **359**, 710-712.
41. Z. Wu and D. Zhao, *Chem. Commun.*, 2011, **47**, 3332-3338.
42. C. T. Kresge, M. E. Leonowicz, W. J. Roth, J. C. Vartuli and J. S. Beck, *Nature*, 1992, **359**, 710.
43. P. N. E. Diagboya and E. D. Dikio, *Microporous Mesoporous Mater.*, 2018, **266**, 252-267.
44. S. Chakraborty, S. Saha, V. R. Dhanak, K. Biswas, M. Barbezat, G. P. Terrasi and A. K. Chakraborty, *RSC Adv.*, 2016, **6**, 67916-67924.
45. K. Krishnamoorthy, M. Veerapandian, K. Yun and S. J. Kim, *Carbon*, 2013, **53**, 38-49.
46. Y. Xu, H. Bai, G. Lu, C. Li and G. Shi, *J. Am. Chem. Soc.*, 2008, **130**, 5856-5857.
47. A. C. Ferrari, J. C. Meyer, V. Scardaci, C. Casiraghi, M. Lazzeri, F. Mauri, S. Piscanec, D. Jiang, K. S. Novoselov, S. Roth and A. K. Geim, *Phys. Rev. Lett.*, 2006, **97**, 187401.
48. D. Zhou and B.-H. Han, *Adv. Funct. Mater.*, 2010, **20**, 2717-2722.
49. W. Li, X.-Z. Tang, H.-B. Zhang, Z.-G. Jiang, Z.-Z. Yu, X.-S. Du and Y.-W. Mai, *Carbon*, 2011, **49**, 4724-4730.
50. M. M. Lucchese, F. Stavale, E. H. M. Ferreira, C. Vilani, M. V. O. Moutinho, R. B. Capaz, C. A. Achete and A. Jorio, *Carbon*, 2010, **48**, 1592-1597.
51. H. Gao, Y. Sun, J. Zhou, R. Xu and H. Duan, *ACS Appl. Mater. Interfaces*, 2013, **5**, 425-432.
52. F. He, J. Fan, D. Ma, L. Zhang, C. Leung and H. L. Chan, *Carbon*, 2010, **48**, 3139-3144.
53. H. WANG, X. ZHOU and Q. CHEN, *Nano*, 2013, **08**, 1350006.
54. S. Wang and Z. H. Zhu, *Dyes Pigm.*, 2007, **75**, 306-314.

55. J. R. Kim, B. Santiano, H. Kim and E. Kan, *Am. J. Anal. Chem.*, 2013, **Vol.04No.07**, 8.
56. P. Wang, M. Cheng and Z. Zhang, *J. Saudi Chem. Soc.*, 2014, **18**, 308-316.
57. A. S. K. Kumar and S.-J. Jiang, *J. Environ. Chem. Eng.*, 2016, **4**, 1698-1713.
58. Z. Pei, L. Li, L. Sun, S. Zhang, X.-q. Shan, S. Yang and B. Wen, *Carbon*, 2013, **51**, 156-163.
59. J. Xu, L. Wang and Y. Zhu, *Langmuir*, 2012, **28**, 8418-8425.
60. S. Nayab, A. Farrukh, Z. Oluz, E. Tuncel, S. R. Tariq, H. u. Rahman, K. Kirchhoff, H. Duran and B. Yameen, *ACS Appl. Mater. Interfaces*, 2014, **6**, 4408-4417.
61. S. Ghorai, A. K. Sarkar, A. B. Panda and S. Pal, *Biores. Technol.*, 2013, **144**, 485-491.
62. J. Rahchamani, H. Z. Mousavi and M. Behzad, *Desalination*, 2011, **267**, 256-260.

Chapter 5.

Electrical properties of novel polyoxometalate-surfactant-graphene hybrid materials

The development of novel materials for enhanced electrochemical energy storage applications, in particular for the fabrication of supercapacitors (SCs) displaying increased properties, is a milestone of both fundamental and technological relevance. Among nanostructured materials, polyoxometalates (POMs) combined with various carbon-based nanostructures represent a very promising class of hybrid systems for energy storage, yet, guidelines for their rational design and synthesis leading to high-performance SCs is still lacking. In this chapter we will discuss the production of a novel hybrid architecture based on Keplerate type POM (Mo_{132}) functionalized with dodecyltrimethylammonium bromide (DTAB), which upon mixing with electrochemically exfoliated graphene (EEG) nanosheets results in the formation of porous 3D superstructures. Mo_{132}-DTAB-EEG combines the redox activity of POMs and high electrical conductivity of graphene, all synergically mediated by the surfactant-assisted porosity enhancement, to form new electrode materials for SCs. Cyclic voltammetry and galvanostatic charge/discharge electrochemical studies revealed that the unique combination of these three components yields highly efficient energy storage materials. In particular, our highly porous hybrids system exhibits high specific capacitance of 65 F g^{-1} (93 F cm^{-3}, 93 mF cm^{-2}) combined with excellent stability (99% of specific capacitance retained) after 5000 charge/discharge cycles at different current densities, overall displaying significantly improved performance compared to pristine electrochemically exfoliated graphene material. High-resolution transmission electron microscopy analysis presented in this chapter was carried out in the collaboration with Dr. Luca Ortolani and Prof. Vittorio Morandi from CNR-IMM Bologna (Italy). SCs discussed in this chapter have been produced and analyzed under the supervision of Dr. Zhaoyang Liu from the Nanochemistry Lab (ISIS, Strasbourg).

5.1. Introduction

Although great effort has been devoted towards the development of high efficient fuel cells and lithium-ion batteries in the past years,[1-3] the low energy capacity and slow power capability are still significant limitations for wide-use applications of existing technological systems. Therefore, real exploitation of sustainable energy requires to develop novel high-performance and robust energy storage devices. Recently, supercapacitors defined as a new class of energy storage devices have drawn great attention due to the rapid charge/discharge, outstanding lifetime and unique stability. In principal, supercapacitors also known as the electrochemical capacitors are constructed from two highly porous electrode immersed into electrolyte solution and separated by insulator to prevent the transfer of energy between them. While external electric field will be applied to the electrodes, negative and positive charges start collecting on their surfaces. Supercapacitors can be classified into three groups, due to their energy storing principles as shown on Figure 5.1.

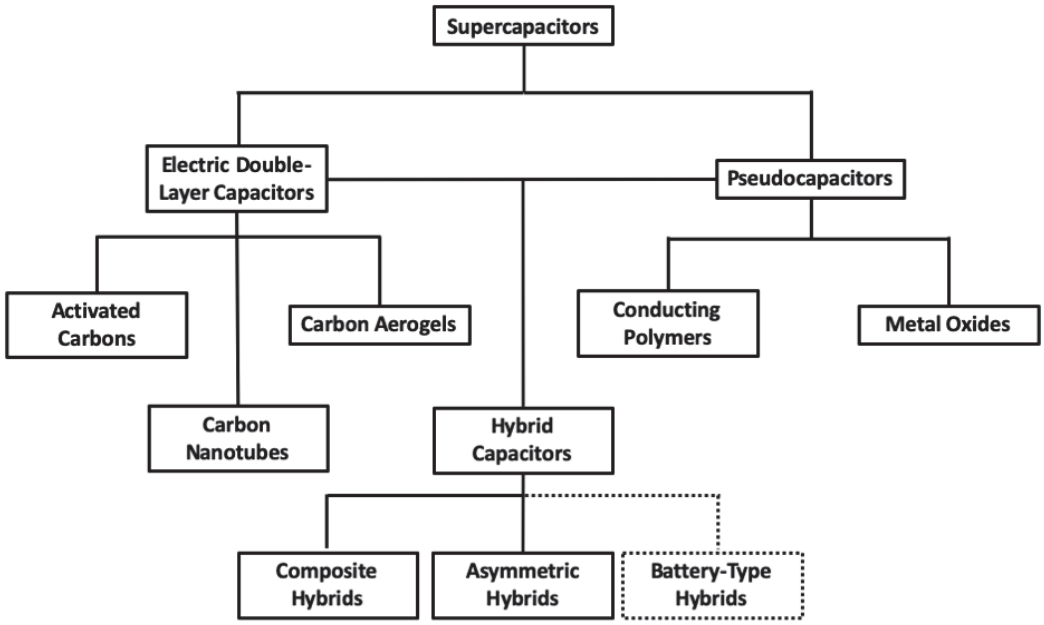

Figure 5.1. Taxonomy of supercapacitors. Reprinted with permission.[4]

The former called electrical double layer (EDL) relies on the mechanism which involves the accumulation of electric energy without any electron transfer between the electrodes.

The collection of charge is the consequence of the electrostatic interactions into Helmholtz double layer at the interface between electrodes and electrolyte. The standard electrode introduced in EDL supercapacitors are mainly based on carbonaceous materials such as activated carbon, carbon nanotubes and graphene which is one of the promising candidates for EDL supercapacitors.[5] This gapless semiconductor 2DM possess abovementioned exceptional electrical, mechanical and thermal properties, which give it enormous potential to improve the performance of the storage devices. To date, it has been shown that supercapacitors based on graphene are characterized by high capacity, rapid release of energy and a short time of re-loading.[6] The next group, called pseudocapacitors store energy through a redox faradaic reaction between electrolyte and electrode, which occurs on its surface. The typical pseudocapacitive electrode materials are metal oxides (*e.g.* MoO_3, MnO_2, RuO_2, NiO)[7-10] and conductive polymers (*e.g.* polyaniline, polythiophene).[11,12] Due to the higher energy density of metal oxides pseudocapacitors compared to the carbon materials EDL capacitors, the former is extensively studied as electrodes in supercapacitors. One of the very interesting family of compounds based on metal oxides are POMs, which consists of two main subunits: transition metal ions on the highest oxidation state (Mo^{6+}, V^{5+}, W^{6+}, Nb^{5+}) and terminal oxygen atoms that act as a bridge for other ions and ligands. This is due to their high molecular weight, high negative charge, very good solubility in polar solutions and high redox potential. Noteworthy, POMs reveal Faradaic charge-storage applications without disruption of their durable structure. Unfortunately, this type of materials is characterized by low electrical conductivity and the low diffusion of lithium ions. To overcome this drawback, the introduction of conductive materials such as graphene is needed. This not deeply explored type of pseudocapacitors mixed with carbon-based materials called hybrid supercapacitors possesses synergically linked both EDL and pseudocapacitive mechanisms, which is characterized by improved energy density and the specific capacitance of the electrode.

In order to enhance the device performance, including energy capacity, power density and recharge time, the ability to effectively control the electrodes nanostructure is essential.[13] Such a control can be achieved in POM based surfactant encapsulated clusters.[14] Noteworthy, although over 10 different topological types of POM architectures can be designed,[15] to date research on their application as SC materials was limited to the

prototypical Wells-Dawson and Keggin building blocks.[16, 17] While polyoxometalates may act as electron acceptors/donors to accelerate electron transfer and improve the overall conductivity of hybrid structures, their interaction with carbon-based materials is relatively weak, ultimately affecting the stability of the POM-based hybrid structures. To overcome this issue, herein we introduce for the first time the use of the Keplerate type polyoxometalate Mo_{132}, *i.e.* POM bearing 42 negative charges on its outer-sphere surface, that can be easily functionalized with a surfactant exposing long alkyl chains. Such molecules are known to possess a high adsorption energy on carbon-based surfaces which can be key towards the generation of stable, graphene-supported electroactive material for supercapacitors. The use of a facile, two-step synthetic methodology relying on surfactant-encapsulation made it possible to synthesize Mo_{132}-DTAB cluster (with Mo_{132} being $(NH_4)_{42}[Mo^{VI}_{72}Mo^{V}_{60}O_{372}(CH_3COO)_{30}(H_2O)_{72}]$ and DTAB consisting of dodecyltrimethylammonium bromide).[18, 19] Such hybrid system upon combination with the electrochemically exfoliated graphene (EEG) forms novel porous hybrid Mo_{132}-DTAB-EEG. Enhanced supercapacitive performances of the Mo_{132}-DTAB-EEG compared to EEG were recorded, which can be ascribed to higher porous nature of the novel POM based composite in combination with its excellent electrochemical stability when subjected to cycling in acidic aqueous environment (1M H_2SO_4). Thus, a simple and efficient methodology is provided that relies on two energy storage mechanisms, EDL originated from EEG and pseudocapacitance resulting from Mo_{132}, synergically mediated by the DTAB surfactant.

5.2. Materials and methods

5.2.1. Electrochemical exfoliation of graphene (EEG)

In this subchapter, we presented the methodology of production of EEG under anodic conditions by employing a typical electrolytic cell. The electrolytic cell was obtained by using some basic components such as a graphite foil as anode and a platinum wire as cathode immersed in an electrolyte. In the presented experiments we exploited ammonium sulfate $(NH_4)_2SO_4$ as electrolyte water solution at a concentration of 0.1 M. The exfoliation of graphite cathode in the form of foil appears as direct effect of the used electric voltage between the two electrodes arranged at a distance of ca. 2 cm. Using of ISO-TECH IPS-603 DC power supply, we employed electric voltage of +15 V which produce a starting current of around 0.4 A. After several minutes the produced powder was collected *via* vacuum filtration process on PTFE membranes with 5 μm pore's diameter and few rinsing steps was needed to remove salt residuals. Obtained EEG was dried in vacuum oven for 24h.

5.2.2. Preparation of Mo_{132}, Mo_{132}-DTAB, Mo_{132}-DTAB-EEG composite

Keplerate type polyoxometalate Mo_{132} was synthesized according to the procedure previously reported by Müller and co-workers.[20] Hydrazine sulfate salt (N_2H_4 x H_2SO_4) (0.8 g, 6.1 mmol) was added to a solution of ammonium heptamolybdate tetrahydrate ($(NH_4)_6Mo_7O_{24}$ x $4H_2O$) (5.6 g, 4.5 mmol) and ammonium acetate (CH_3COONH_4) (12.5 g, 162.2 mmol) in H_2O (250 mL). The solution was vigorously stirred for 10 min and 50% CH_3COOH (83 mL) was then added. The green reaction solution was stored in an open Erlenmeyer flask at room temperature without further stirring. After few days the color was changed and the precipitated red-brown crystals were filtered off over a glass frit membrane washed with 90% ethanol and diethyl ether, and finally dried in air. The preparation of the POM-surfactant (Mo_{132}-DTAB), hybrid material was carried out by exploiting the methodology previously described.[21] The amount of 4 g of the precursor Mo_{132} (0.14 mmol) were dissolved in H_2O (400 mL) to give a dark brown solution. To

this solution was subsequently added a large excess of DTAB - dodecyltrimethylammonium bromide surfactant (6.5 g, 21 mmol) solubilized in chloroform (400 mL) under vigorous stirring during 3 hours at room temperature. After almost complete extraction of POM into the organic phase, the latter is separated by decantation and absolute ethanol (about 400 mL) is added, provoking the precipitation of the target compound as a black powder which was isolated by filtration, washed with ethanol and dried in air. The obtained complex (Mo_{132}-DTAB) has a chemical formula of $(CH_3(CH_2)_{11}N(CH_3)_3)_{40}(NH_4)_2[Mo_{132}O_{372}(CH_3COO)_{30}(H_2O)_{72}]$ x $40H_2O$ as determined by elemental analysis.[22] To graft the Mo_{132}-DTAB molecules onto the surface of graphene (EEG), an acetone (100 ml) solution on Mo_{132}-DTAB (100 mg) was added to DMF (100ml) suspension of EEG (100 mg) under vigorous stirring at the room temperature for 12 hours. After allowing the mixture to stand for 3 hours, the solution became colorless and a black precipitate was formed which almost indicates that all the Mo_{132}-DTAB molecules were grafted onto surfaces of graphene. Finally, the precipitate was isolated by filtration, a membrane with a pore diameter of 5 μm, and subsequently was washed with ethanol and acetone several times and dried in air.

5.2.3. Preparation of Mo_{132}-DTAB-EEG electrode and electrochemical measurements

The supercapacitor working electrode was fabricated by mixing 80 wt% Mo_{132}-DTAB-EEG, 10 wt% carbon black and 10 wt% poly(tetrafluoroethylene) binder dispersed in water. After sufficient grinding the mixture in ethanol, the obtained paste was pressed onto a platinum mesh which served as current collector, followed by drying in a vacuum oven for 6 hours. Electrochemical measurements, including cyclic voltammetry, were performed with a PGSTAT204 instrument (Autolab). The electrochemical capacitive of Mo_{132}-DTAB-EEG was evaluated in a three-electrode system, applying 1 M H_2SO_4 as electrolyte, platinum plate and Ag/AgCl (saturated KCl) as the counter and reference electrodes, respectively. The scan rates varied from 1 mV/s to 100 mV/s. The specific capacitance is normalized by the weight of Mo_{132}-DTAB-EEG. The stability tests were performed at 100 mV/s for 5000 cycles. All electrochemical experiments were carried out at room temperature.

5.3. Results

5.3.1. Chemical and structural composition

Mo_{132} is a POM nanocapsule displaying an icosahedral symmetry and comprising over 500 atoms, being arguably one of the largest spherical POM ever produced.[23] Since its first successful synthesis by Müller,[20] this building block attracted a great interest because of its structural and catalytic properties.[24, 25] Hitherto, only one article reported on the use of Mo_{132} as composite component in metal oxide semiconductor photoelectrodes.[26] This is surprising, especially given that the redox electronic properties of Mo_{132} and its inherent porous structure are key characteristics which makes it ideal component for the generation of efficient SC devices. This prompted us to focus on this species to construct novel, electronically active hybrid materials and ultimately prove that the Keplerate clusters are promising class of POMs that are worth further studies towards energy applications. Size of Mo_{132} POM allows one to utilize its inorganic core for the effective formation of large surfactant-encapsulated clusters (SECs), effectively leading to decoration of POM with notable number of surfactant molecules. We have thus demonstrated herein a facile protocol for the fabrication of Mo_{132}-DTAB-EEG hybrid system, with dodecyltrimethylammonium bromide (DTAB) as the surfactant of choice. The role of the DTAB surfactant is crucial in the process of Mo_{132}-DTAB-G formation, since DTAB molecules not only increase the strength of van der Waals interactions between the Mo_{132} and electrochemically exfoliated graphene, but also results in synergically increased porosity of the Mo_{132}-DTAB-EEG and thus enhanced supercapacitive performance of the hybrid material. In theory it should be possible to screen a variety of different surfactants (surfs) to form a relevant family of Mo_{132}-surf-EEG hybrids, though it would be difficult to pre-determine which surfactant would be the most suitable for the electrochemical applications. Noteworthy, the influence of the surfactant on the morphology of obtained surfactant encapsulated clusters (SECs) is known phenomenon and could result in the synthesis of assemblies of different porosity, or even preclude the formation of SECs *per se*.[14] We have performed such preliminary studies by using four different surfactants, *i.e.* DTAB- dodecyltrimethylammonium bromide,

DDAB - didodecyldimethylammonium bromide, DODA- dioctadecyldimethyl ammonium bromide, TODA - octadecyltrimethylammonium bromide, accounting for different number and length of employed organic chains. Certain synthetic problems were encountered that concern the phase purity and homogeneity of synthesized species with DDAB and DODA as the surfactant, which resulted in successful formation of two hybrids materials with one alkyl chain (Mo_{132}-DTAB-EEG, Mo_{132}-TODA-EEG). Initial electrochemical tests showed that Mo_{132}-DTAB-EEG is far superior material than Mo_{132}-TODA-EEG, therefore the former one was used for further research. Mo_{132}-DTAB-EEG hybrid material can be efficiently generated by exploiting a self-assembly protocol which relies on two different types of non-covalent interaction: (a) Mo_{132}-DTAB system can be formed by using electrostatic interactions holding together the Keplerate POM Mo_{132} and the DTAB surfactant, and (b) the grafting of Mo_{132}-DTAB onto the electrochemically exfoliated graphene nanosheets (EEG) via van der Waals type interactions. Noteworthy, the use of one-pot reaction, with all three components mixed together simultaneously, led to disordered structures; therefore, a two-step synthesis has been employed to guarantee homogenous dispersion of the component in the hybrid structure.

The morphology and the chemical structure of the prepared hybrid material was confirmed using comprehensive analytical methods (*e.g.* FTIR, TGA, SEM, HR-TEM, BET). Both high-resolution transmission electron microscopy (HR-TEM) and SEM techniques indicates further proofs of the successful dispersion of the Mo_{132}-DTAB into the EEG matrix. HR-TEM analysis proved that the surface of the electrochemically exfoliated graphene sheets is covered with 3D features of Mo_{132}-DTAB substrate (Figure 5.2a) Moreover, HR-TEM characteristic showed that plenty of Mo_{132}-DTAB moieties are partially arranged onto the surface of EEG sheets. The POM-surfactant clusters observed as a darker regions were spaced by a distance consistent with two surfactants unit (2.9 nm), as already presented in other POM functionalized materials.[27] Moreover, SEM image presents that Mo_{132}-DTAB-EEG possess a highly porous and homogenous structure (Figure 5.2b), which is very appealing for increasing the electron transport while preserving good ionic conductivity.

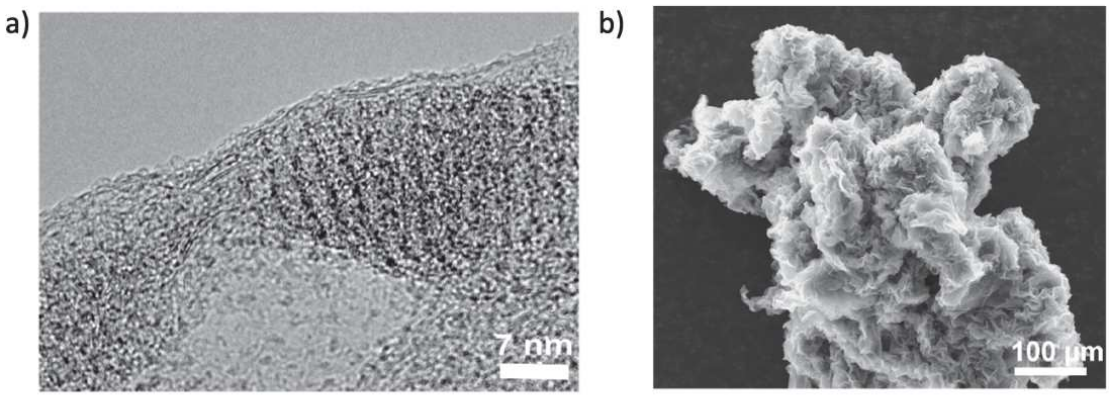

Figure 5.2. a) HR-TEM and b) SEM images of the Mo_{132}-DTAB-EEG.

On the other hand, a high specific surface area combined with a porous structure provides one of the important features necessary for the improvement of high-efficient composite materials used as electrode in energy storage applications.[28, 29] The obtained hybrid material is characterized by extremely high (in comparison to individual components) specific surface area and amounts to 321.9 m^2/g calculated by Brunauer-Emmett-Teller (BET) isotherm method (Figure 5.3a). The significant growth in the active surface of the composite is related to the incorporation of the POM-surfactant moieties between the successive graphene sheets. In comparison to many recently reported carbon/polyoxometalate hybrid materials, the specific surface area of Mo_{132}-DTAB-EEG is significantly higher.[30, 31] The porous nature of obtained hybrid material was studied using the pore-size distribution analysis presented in Figure 5.3b which confirm mesoporous structure, with average pore size diameters being 4.18 and 5.42 nm. Moreover, the pore volume of Mo_{132}-DTAB-EEG does significantly increase after functionalization with electrochemically exfoliated graphene, which is required during interaction the porous electrodes with ions in the electrochemical process.

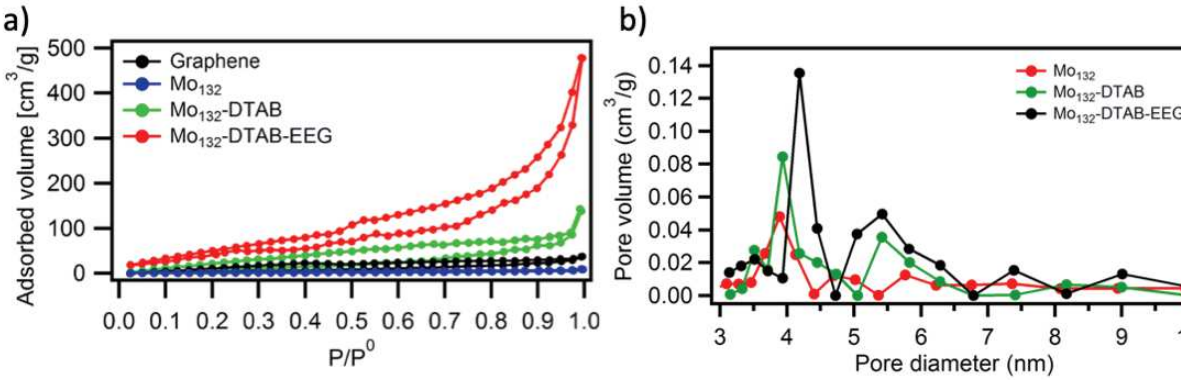

DTAB-EEG samples. b) Pore volume dV/dD plots for Mo_{132}, Mo_{132}-DTAB and Mo_{132}-DTAB-EEG composite.

characteristic bands of Mo_{132} are found in spectra of Mo_{132}-DTAB and Mo_{132}-DTAB-EEG at 721, 798, 864 (Mo-O-Mo) and 979 cm^{-1} (Mo=O).[22] Such result confirmed the structural integrity of polyoxometalate (Mo_{132}) whose architecture is well retained in the hybrid structures (Mo_{132}-DTAB and Mo_{132}-DTAB-EEG).

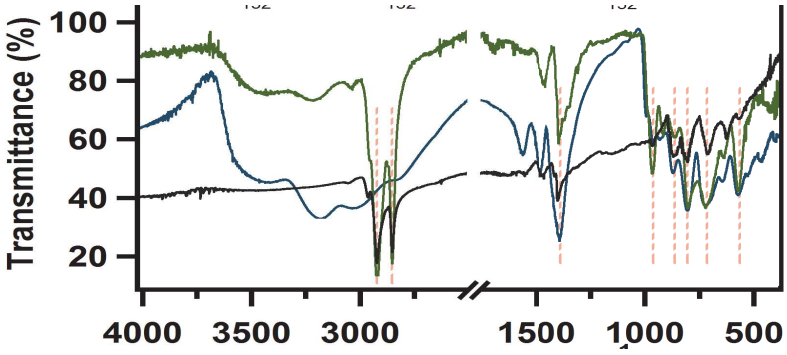

Figure 5.4. FT-IR spectra of Mo_{132}, Mo_{132}-DTAB and Mo_{132}-DTAB-EEG

The chemical composition and thermal stability of the as synthesized Mo_{132}-DTAB-EEG was firstly characterized by TGA and XRD, as shown in Figure 5.5. The Mo_{132}-DTAB-EEG curve (Figure 5.5a) displays a weight loss of. ca. 9% between room temperature and 170°C, in agreement with the loss of the solvation water molecules and those located within the cavity of the cluster. Sharper mass percentage drop is monitored around 350°C which can be associated to the decomposition of the DTAB. XRD powder

analysis of Mo_{132}, Mo_{132}-DTAB, DTAB and Mo_{132}-DTAB-EEG systems was performed to confirm the identity of the microcrystalline samples, including their phase purity (Figure 5.5b). In general, flattening of XRD signals that come from POM and DTAB surfactant prove that the material is homogenously dispersed in the EEG matrix. Two distinct broad peaks centered at a 2θ angle of 23.9° and 41.3° appeared, which are characteristic of carbon materials and specifically correspond to the (002) and (001) planes of graphene, respectively.[32] No peak related to the crystal structure of Mo_{132}-DTAB or the sole DTAB is observed, which highlights the absence of Mo_{132}-DTAB superstructures, *i.e.* agglomerates formed *via* self-assembly of neat Mo_{132}-DTAB clusters. Such evidences demonstrated that Mo_{132}-DTAB clusters are uniformly distributed over graphene nanosheets, thus yielding the desired product.[33]

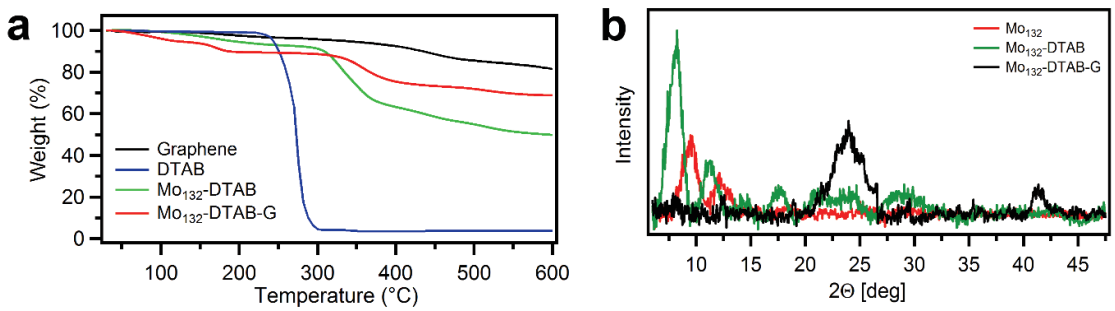

Figure 5.5. (a) TGA analysis and (b) XRD powder graph of Mo_{132}, Mo_{132}-DTAB and Mo_{132}-DTAB-EEG. Graph (b) was normalized according to the Mo_{132}-DTAB-EEG sample.

High resolution X-ray photoelectron spectroscopy (XPS) was performed to gain further information onto the chemical composition in the hybridmaterialcomprising Mo_{132}-DTAB and electrochemically exfoliated graphene (Figure 5.6). For the Mo_{132}-DTAB-EEG modified samples C, O and Mo still appeared as the major surface components (Figure 5.6a). As shown in Figure 5.6b, the presence of our peaks at 231.09, 232.36, 234.28 and 235.42 eV corresponding to $3d_{5/2}$ and $3d_{3/2}$, indicated that the valence state of Mo in the Mo_{132}-DTAB-EEG are +V and +VI,[34, 35] and unambiguously confirm the presence of Mo_{132} in the Mo_{132}–DTAB-EEG hybrid material. Moreover, by deconvoluting the high-resolution C 1s spectrum (Figure 5.6c), the presence of three carbon-containing functional groups was observed which can be assigned to single bonded carbon-carbon (C-C284.7 eV), epoxy groups (C-O 285.6 eV)and carboxylic

moieties (O=CO 288.1 eV).[36] According to N1s spectrum (Figure 5.6d), two peaks with binding energies of 398.4, and 401.8 eV were identified, which are associated to amine bond (C-N) and quaternary ammonium group (-NR_3^+),[37] indicating the successful coating of Mo_{132}-DTAB on the surfaces of EEG sheet. These type of functional groups can efficiently improve the electrical conductivity and induce a pseudocapacitance that should remarkably improve the capacity of supercapcitors. The presence of N species on the graphene surface could generate high pseudocapacitance by mechanisms of acting as electron donor to attract protons or enhancing charge density ofthe space charge layer strengthening the redox reactions of N-containing functional groups.[38, 39]

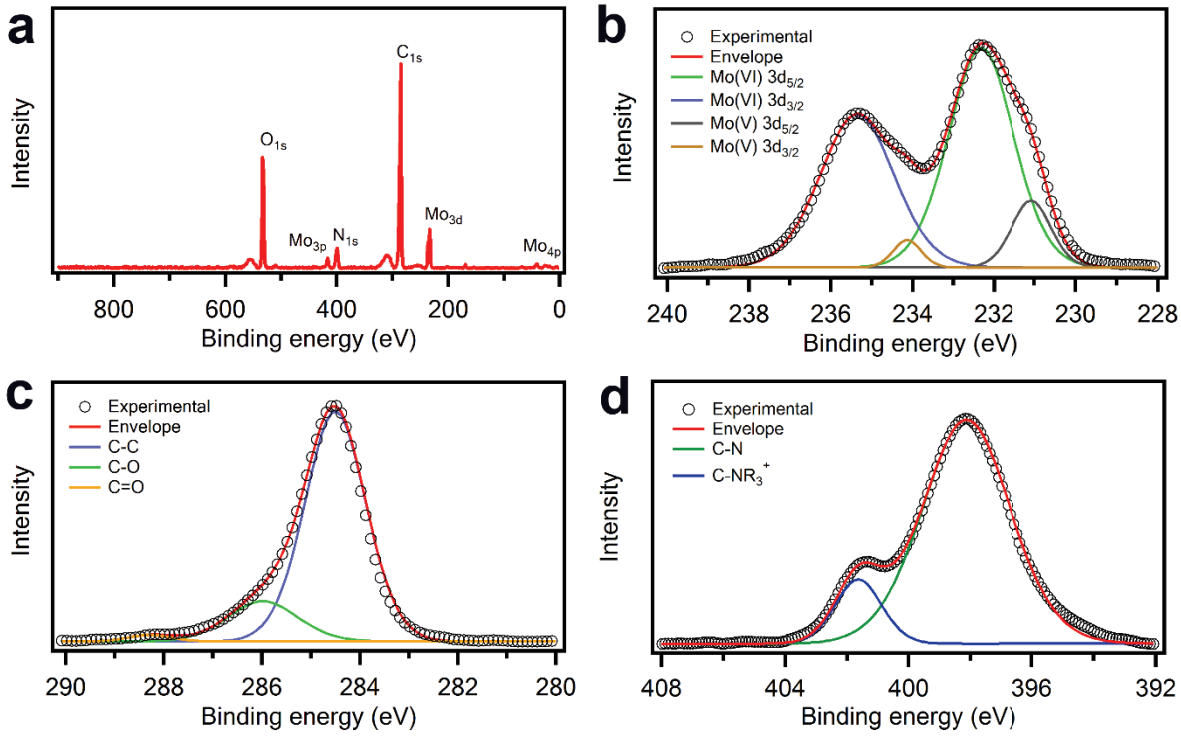

Figure 5.6. XPS spectra of Mo_{132}-DTAB-EEG: (a) wide range survey, and high-resolution (b)Mo 3d, (c) C1s and (d) N1s.

5.3.2. Adsorption of alkali metal ions on Mo_{132}-DTAB-EEG using FAAS measurements.

As we know, the POMs possess ability to adsorb alkali metal ions (including Na^+, Li^+), which makes them promising platforms for building advanced electrical materials. Therefore, initially the project was targeted on the investigation of our material towards alkali metal sorption. Preliminary results based on XPS analysis (Figure 5.7) showed that the Mo_{132}-DTAB-EEG composite can adsorb some amount of alkali metal ions (sodium).

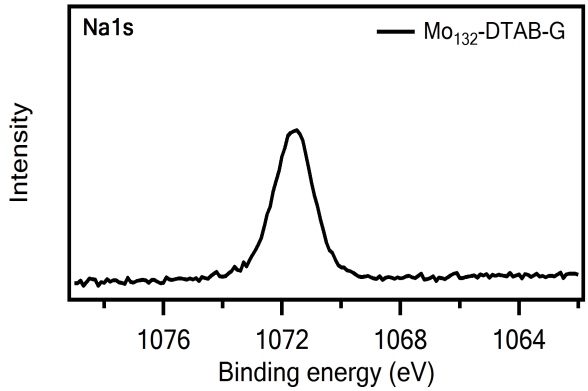

Figure 5.7. XPS wide energy spectra of Mo_{132}-DTAB-EEG after adsorption process of sodium ions.

Maximum adsorption capacity q_{max} value of calculated using previously presented methodology (see chapter 3 and 4) amount to 56 mg/g. After careful further analyses, the project has been altered because of weak adsorption capacity in comparison to the starting materials.

5.3.3. Electrochemical study

Presented synthetic method makes it possible to exploit the unique redox characteristics of the POM counterpart by simultaneously maximizing its effective surface area upon grafting onto graphene sheets via the DTAB surfactant. Such advantageous combination of different properties can be expected to favor the specific capacitance and thus enhance the electrochemical performance of the supercapacitor when Mo_{132}-DTAB-EEG is employed as electrode material. The electrochemical properties of the Mo_{132}-DTAB-EEG was studied using a three-electrode system assembled in electrolyte (1M H_2SO_4), whereas Ag/AgCl employed as the reference electrode and a platinum wire was serving as a counter electrode. The cyclic voltammetry analysis presents the high value of gravimetric specific capacitance amount to 65 F/g reached at scan rate of 1mV/s (Figure 5.8a), which is comparable with previously reported in the literature graphene-POM composites.[40] Noteworthy, the high molecular weight of huge spherical Keplerate clusters is able to restrict the gravimetric capacity, that is why surface and volumetric capacities are also presented as a more practical comparison parameters (93 F cm^{-3}, 93 mF cm^{-2}). Additionally, significant growth in those values was observed in comparison to the pristine graphene prepared *via* different methodologies (values in the range from 0.51 to 2.3 $mFcm^{-2}$ and from 3.1 to 17.9 Fcm^{-2}).[41] Presented increase can be caused by high redox potential of polyoxometalate cluster and the improved specific surface area of the Mo_{132}-DTAB-EEG hybrid material.

The specific shape of the CV curves and the improved performance of novel hybrid electrode in comparison with the sole EEG shows that combination of both electrochemical mechanisms (EDL and pseudocapacitance) is present herein. The former mechanism occurs between the monovalent metal ions and the negatively charged surface of electrode is mainly rendered by EEG, which is characterized by high electrical conductivity. The latter pseudocapacitance mechanism is a result of the reversible surface redox reactions between the electrolyte and the electrode, which contain the Mo_{132} POM cluster. Important to note, the presence of surfactants (DTAB) in the structure of organic-inorganic hybrid material helped to incorporate electroactive moieties, thus giving a graphene-based hybrid material with unique stability and without electrochemical drawbacks of the individual components (POM – low electronic conductivity; EEG –

limited charge storage capability). The detailed electrochemical cycling stability test of Mo_{132}-DTAB-EEG at a scan rate of 100 mV s^{-1} confirm that cycling does not cause significant degradation. After up to 5000 cycles the hysteresis loop doesn't change its shape (Figure 5.8b) and there is no obvious capacitance drop (*ca.* 99 % capacitance retention) as presented in Figure 5.8c, which indicates excellent electrochemical stability of the obtained Mo_{132}-DTAB-EEG system.

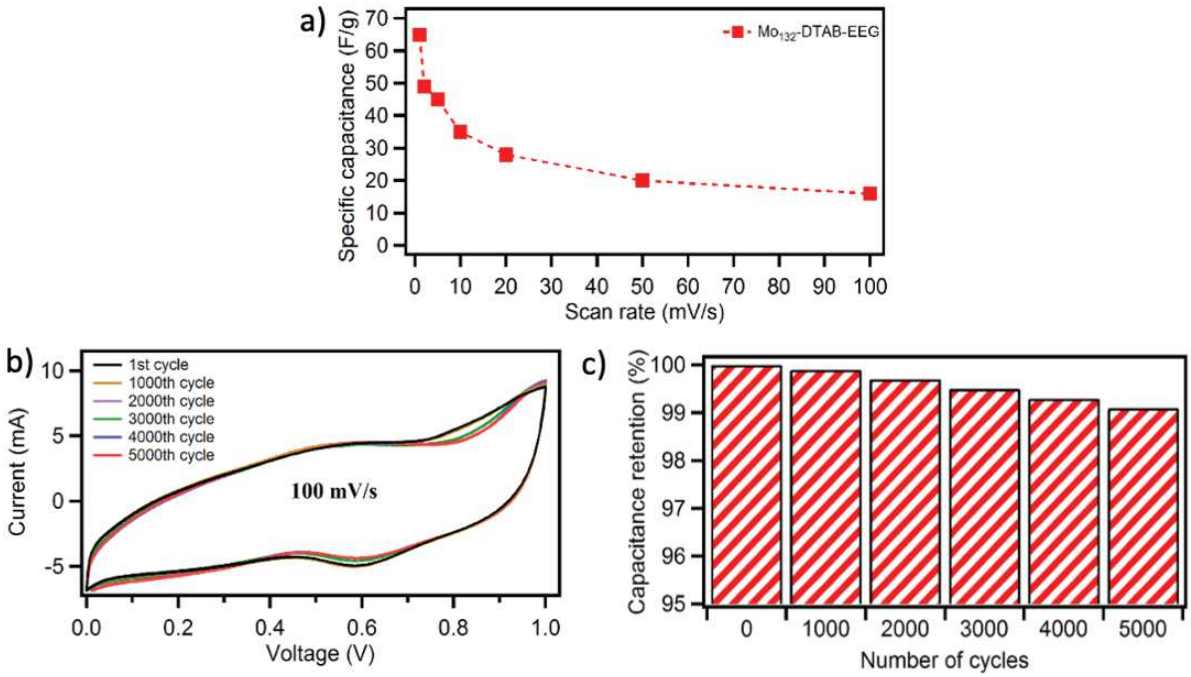

Figure 5.8. a) Comparison of specific capacitance vs scan rate for Mo_{132}-DTAB-EEG. Electrochemical cycling stability of Mo_{132}-DTAB-EEG electrode material, b) CV curves and c) capacitance retention measured at a scan rate of 100 mV s^{-1}.

The abovementioned results show that the Keplerate type POM Mo_{132} can be used to tailor novel Mo_{132}-DTAB-EEG composite material with effective energy storage performance. The Mo_{132}-DTAB-EEG was obtained using a facile and fast two-step synthetic route which focuses on the exploitation of DTAB to form the surfactant encapsulated cluster (SEC) Mo_{132}-DTAB. The next step concern formation a Mo_{132}-DTAB-EEG composite using van der Waals interaction between the EEG and SEC cluster, which present synergically enhanced porosity and thus increased supercapacitive efficiency. The presented hybrid material exhibits rich redox properties, with simultaneous high electrochemical stability of the system which may find very interesting application as electrode materials in the production of supercapacitors.

5.4. Conclusions

In summary, we have demonstrated for the first time that the Keplerate type polyoxometalate Mo_{132} can be used to tailor novel Mo_{132}-DTAB-EEG hybrids as electrode materials for supercapacitors. The hybrid material was generated by exploiting of a simple two-step synthetic methodology which relies on the use of DTAB to form the surfactant encapsulated cluster Mo_{132}-DTAB, which, *via* van der Waals interaction with the electrochemically exfoliated graphene, forms a Mo_{132}-DTAB-EEG composite displaying synergically increased porosity and thus enhanced supercapacitive performance. The novel porous material exhibits significantly higher specific, volumetric and surface capacitance parameters compared to the non-functionalized graphene in the acidic aqueous solution (1M H_2SO_4), 0-1 V potential window followed by excellent electrochemical cycling stability (99% of specific capacitance retained) after 5000 charge/discharge cycles. This work enriches the current family of POM-based carbon composites and provides a solid evidence that polyoxometalates of other chemical composition than Keggin or Wells-Dawson. The greater degree of functionalization that can be achieved when using Keplerate type polyoxometalate enables better tuning of a variety of physico-chemical properties of the hybrid system towards the emergence of a new generation of high performing multifunctional supercapacitors possessing enhanced stability.

5.5. References

1. C.-M. Park, J.-H. Kim, H. Kim and H.-J. Sohn, *Chem. Soc. Rev.*, 2010, **39**, 3115-3141.
2. H. Wu, G. Yu, L. Pan, N. Liu, M. T. McDowell, Z. Bao and Y. Cui, *Nat. Commun.*, 2013, **4**, 1943.
3. M. Armand and J. M. Tarascon, *Nature*, 2008, **451**, 652.
4. M. Gidwani, A. Bhagwani and N. Rohra, *Int. J. Eng. Invent.*, 2014, **4**, 22-27.
5. Z. Lin, E. Goikolea, A. Balducci, K. Naoi, P. L. Taberna, M. Salanne, G. Yushin and P. Simon, *Mater. Today*, 2018, **21**, 419-436.
6. Y. Zhu, S. Murali, M. D. Stoller, K. J. Ganesh, W. Cai, P. J. Ferreira, A. Pirkle, R. M. Wallace, K. A. Cychosz, M. Thommes, D. Su, E. A. Stach and R. S. Ruoff, *Science*, 2011, **332**, 1537-1541.
7. J. Yan, E. Khoo, A. Sumboja and P. S. Lee, *ACS Nano*, 2010, **4**, 4247-4255.
8. C.-L. Liu, K.-H. Chang, C.-C. Hu and W.-C. Wen, *J. Power Sources*, 2012, **217**, 184-192.
9. J.-W. Lang, L.-B. Kong, W.-J. Wu, Y.-C. Luo and L. Kang, *Chem. Commun.*, 2008, DOI: 10.1039/B800264A, 4213-4215.
10. T. Brezesinski, J. Wang, S. H. Tolbert and B. Dunn, *Nat. Mater.*, 2010, **9**, 146.
11. W. Chen, R. B. Rakhi and H. N. Alshareef, *J. Mater. Chem. A*, 2013, **1**, 3315-3324.
12. S. Nejati, T. E. Minford, Y. Y. Smolin and K. K. S. Lau, *ACS Nano*, 2014, **8**, 5413-5422.
13. P. Simon and Y. Gogotsi, *Nat. Mater.*, 2008, **7**, 845.
14. A. Nisar and X. Wang, *Dalton Trans.*, 2012, **41**, 9832-9845.
15. Jiangwei Zhang, Yichao Huang and Y. Wei, in *Trends in Polyoxometalates Research*, eds. Laurent Ruhlmann and D. Schaming, Nova Science Publishers, New York, 2015, ch. 3, pp. 37-71.
16. J. Suárez-Guevara, V. Ruiz and P. Gomez-Romero, *J. Mater. Chem. A*, 2014, **2**, 1014-1021.
17. U. Tadaharu, *ChemElectroChem*, 2018, **5**, 823-838.
18. P. Yin, D. Li and T. Liu, *Chem. Soc. Rev.*, 2012, **41**, 7368-7383.
19. L. Zhang, H. Li and L. Wu, *Soft Matter*, 2014, **10**, 6791-6797.
20. M. Achim, K. Erich, B. Hartmut, S. Marc and P. Frank, *Angew. Chem. Int. Ed.*, 1998, **37**, 3359-3363.
21. S. Floquet, E. Terazzi, A. Hijazi, L. Guenee, C. Piguet and E. Cadot, *New J. Chem.*, 2012, **36**, 865-868.
22. H. Li, Y. Yang, Y. Wang, C. Wang, W. Li and L. Wu, *Soft Matter*, 2011, **7**, 2668-2673.
23. A. Müller and P. Gouzerh, *Chem. Soc. Rev.*, 2012, **41**, 7431-7463.
24. A. Rezaeifard, R. Haddad, M. Jafarpour and M. Hakimi, *ACS Sustainable Chem. Eng.*, 2014, **2**, 942-950.
25. I. Baroudi, C. Simonnet-Jégat, C. Roch-Marchal, N. Leclerc-Laronze, C. Livage, C. Martineau, C. Gervais, E. Cadot, F. Carn, B. Fayolle and N. Steunou, *Chem. Mater.*, 2015, **27**, 1452-1464.

26. S. Xu, Y. Wang, Y. Zhao, W. Chen, J. Wang, L. He, Z. Su, E. Wang and Z. Kang, *J. Mater. Chem. A*, 2016, **4**, 14025-14032.
27. S. Floquet, E. Terazzi, A. Hijazi, L. Guénée, C. Piguet and E. Cadot, *New J. Chem.*, 2012, **36**, 865-868.
28. M. Winter and R. J. Brodd, *Chem. Rev.*, 2004, **104**, 4245-4270.
29. F. Wang, X. Wu, X. Yuan, Z. Liu, Y. Zhang, L. Fu, Y. Zhu, Q. Zhou, Y. Wu and W. Huang, *Chem. Soc. Rev.*, 2017, **46**, 6816-6854.
30. Y. Ji, L. Huang, J. Hu, C. Streb and Y.-F. Song, *Energy Environ. Sci.*, 2015, **8**, 776-789.
31. M. Zhang, T. Wei, A. M. Zhang, S.-L. Li, F.-C. Shen, L.-Z. Dong, D.-S. Li and Y.-Q. Lan, *ACS Omega*, 2017, **2**, 5684-5690.
32. H. Kim, K.-Y. Park, J. Hong and K. Kang, *Sci. Rep.*, 2014, **4**, 5278.
33. Y.-H. Ding, J. Peng, H.-Y. Lu, Y. Yuan and S.-U. Khan, *RSC Adv.*, 2016, **6**, 81085-81091.
34. Y. Zhu, Z. Yuan, W. Cui, Z. Wu, Q. Sun, S. Wang, Z. Kang and B. Sun, *J. Mater. Chem. A*, 2014, **2**, 1436-1442.
35. D. Anne, C. Jean-Daniel, M. Pierre, M. Jérôme, S. Francis, K. Bineta, H. L. R. Brudna, M. Frédéric and N. Louis, *Chem – Eur. J.*, 2009, **15**, 733-741.
36. T. Zhu, J. Zhou, Z. Li, S. Li, W. Si and S. Zhuo, *J. Mater. Chem. A*, 2014, **2**, 12545-12551.
37. Q. Hao, X. Xia, W. Lei, W. Wang and J. Qiu, *Carbon*, 2015, **81**, 552-563.
38. F. Su, C. K. Poh, J. S. Chen, G. Xu, D. Wang, Q. Li, J. Lin and X. W. Lou, *Energy Environ. Sci.*, 2011, **4**, 717-724.
39. X. Yang, D. Wu, X. Chen and R. Fu, *J. Phys. Chem. C*, 2010, **114**, 8581-8586.
40. D. P. Dubal, J. Suarez-Guevara, D. Tonti, E. Enciso and P. Gomez-Romero, *J. Mater. Chem. A*, 2015, **3**, 23483-23492.
41. Z. Liu, Z.-S. Wu, S. Yang, R. Dong, X. Feng and K. Müllen, *Adv. Mater.*, 2016, **28**, 2217-2222.

Chapter 6.

General conclusion and outlook

In summary, this doctoral dissertation mostly focuses on the issues related to the adsorption of pollutants by functionalized GO and explores the knowledge on molecular hybrids based on EEG. The examples discussed in this thesis highlight the importance of novel high-performance graphene-based materials in the wide spectrum of upcoming possibilities and applications from the sorption materials to the potential electrical applications. In each experimental part, the morphology and structure of obtained materials have been thoroughly characterized. Apart from the novelty aspects regarding the production of modified two-dimensional materials, this thesis provides the insights on the following structure/property relationship:

- Covalent modification of GO with an organic polymer (BPEI) very favourably affects the efficiency of the adsorption process. Multiscale analysis of received sorption materials confirmed high stability, high specific surface area and high affinity towards various chemical substances. The maximum adsorption capacity (q_{max}) values for heavy metal ions (Cu^{2+} - 1096 mg g^{-1}, Cd^{2+} - 2051 mg g^{-1}, Pb^{2+} - 3390 mg g^{-1}) significantly highlight this material in comparison to the majority of known carbon adsorbents.

- Functionalization of GO with mesoporous aminosilica (SiO_2NH_2) leads to obtaining an efficient and rapid adsorbent of organic cationic dyes (MB, RhB, MV). The material has been successfully used as a column filler in the SPE process, thus enabling very fast purification of water in continuous flow.

- The family of Keplerate-type polyoxometalates are a very interesting group of inorganic compounds that can form stable molecular hybrids with cationic surfactants resulting from weak electrostatic and π-π stacking interactions. Functionalization of electrochemically exfoliated graphene (EEG) using the POM-surfactant subunits (Mo_{132}-DTAB) proved that this type of organic-inorganic hybrids material is very stable and have interesting electrical properties with potential application in the production of supercapacitors. The innovative porous three-dimensional systems of Mo_{132}-DTAB-EEG

synergically combine with each other a large POM redox potential and high graphene electrical conductivity material allows to exhibit significantly higher specific, volumetric and surface capacitance parameters.

Overall, the type of hybrid materials presented in this thesis hold the potential of being used as a selective adsorbents in the water purification processes as well as in electrical applications. By providing insight into the comprehensive physical and chemical characterizations of functionalized 2DMs, this dissertation aims to achieve in-depth understanding of the fundamental properties of prepared hybrid materials in perspective of their future potential applications in chemical sorbents/sensors and electronics. Thanks to that, we developed different functionalized 2DMs using *top-down* approach in order to explore the adsorption properties and to reach profound comprehension of the relationship between their structure and properties. In particular, this thesis intends to explore the use of *top-down* methods to modify 2DMs in order to achieve a control over their properties that is necessary for the integration of these materials in multifunctional devices.

As a future work it is suggested that other detailed tests of adsorbent based on 2DMs involving the effect of the experimental conditions including the presence of multicomponent organic and inorganic contaminants and the effect of different background electrolytes should be investigated for better understanding adsorption process. Furthermore, in-depth knowledge on the mechanism of purification of contaminated wastewaters using 2DMs based adsorbents is still required. Moreover, scaling-up the synthesis methodology and production of adsorbents with higher stability and better reproducibility in adsorption process is desirable due to the further exploitation in the commercial facilities. Following the study on energy reduction through better designs and synthetic methodology is also encouraged. Cost-effective feasibility research should also be provided to compare with another low-cost sorbents, to verify the profitable commercial application. Next important problem with the use of 2DMs based adsorbents is its prospective toxicity to living beings and environment. This type of research would be helpful for us to understand the toxicity and tackle the problem of treated solutions. and worn sorbents. Significant progress in nanotechnology results in new knowledge in the field of graphene-based materials for various applications. These interesting composites are known to ensure specific functionalities in different

difficulties. It is important to note that although some limitations need to be overcome to improve the performance and selectivity of materials based 2DMs, the proper selection of the linker, modifying agent and reaction conditions are crucial in receiving functionalized hybrids based on 2DMs with appropriate properties as was presented in this work. This aspect combined with improved methods of processing 2DMs in high quality makes possible to use this material in many of the foreseen application.

List of abbreviations

^{1}HNMR - proton nuclear magnetic resonance

2DMs - two-dimensional materials

3D - three dimensional

A - adenine

AC - activated carbon

AC-PEI - activated carbon-polyethyleneimine

BPEI - branched polyethyleneimine

C - cytosine

CVD - chemical vapour deposition

DDAB - didodecyldimethylammonium bromide

D_h - hydrodynamic diameter

DLS - dynamic light scattering

DTAB - dodecyltrimethylammonium bromide

DODA - dioctadecyldimethyl ammonium bromide

EDC HCl - 1-ethyl-3-(3-dimethylaminopropyl) carbodiimide hydrochloride

EDTA - ethylenediaminetetraacetic acid

EEG - electrochemically exfoliated graphene

fGO - functionalized graphene oxide

FAAS - flame atomic absorption spectroscopy

FTIR - Fourier transform infrared spectroscopy

G - graphene

GFET - graphene field effect transistor

GO - graphene oxide

HCl - hydrochloric acic

H_2SO_4 - sulphuric acid

HNO_3 - nitric acid

HR-TEM - high resolution transmission electron microscopy

MoS_2 - molybdenum disulfide

MGO - magnetic graphene oxide

MrGO - magnetic reduced graphene oxide

NHS - N-hydroxy-succinimide

POM - polyoxometalate

SCs - supercapacitors

SEC - surfactant encapsulated cluster

SEM - scanning electron microscopy

SGFET - solution gated field effect transistor

SiC - silicon carbide

SPE - solid phase extraction

T - thymine

TMDs - transition metal dichalcogenides

TODA - octadecyltrimethylammonium bromide

UV-vis - ultraviolet-visible light spectroscopy

WAXS - wide-angle X-ray scattering

WS_2 - tungsten disulfide

XPS - X-ray photoelectron spectroscopy

Statement of work

The experiments and analysis data presented in this dissertation have been conducted and described by myself besides those presented below:

In chapter 4 UV-Vis spectrum and adsorption tests on SiO_2NH_2-GO were carried out by M.Sc. Włodzimierz Czepa (Adam Mickiewicz University in Poznań). Raman analysis were conducted by M.Sc. Samanta Witomska (Adam Mickiewicz University in Poznań).

In chapter 5 high-resolution transmission electron microscopy analysis were performed by Dr. Luca Ortolani and Prof. Vittorio Morandi from CNR-IMM Bologna (Italy). Fabrication of electrode and electrical characterization measurements on Mo132-DTAB-EEG materials and data analysis were carried out by Dr. Zhaoyang Liu, post-doc in Nanochemistry lab (ISIS, Strasbourg). Synthesis of Mo_{132}-DTAB-EEG hybrid material was performed in collaboration with dr Adam Gorczyński (Adam Mickiewicz University in Poznań)

The projects reported in this thesis were designed with Dr. Artur Ciesielski, Prof. Violetta Patroniak and Prof. Paolo Samorì.

Publications

1. **D. Pakulski**, W. Czepa, S. Del Buffa, A. Ciesielski, P. Samorì, *„Atom-thick membranes for water purification and blue energy harvesting”*, **Adv. Funct. Mater.** 2019, 1902394, IF= 13,325.

2. S. Witomska, W. Czepa, Z. Liu, A. Aliprandi, **D. Pakulski**, P. Pawluć, A. Ciesielski, P. Samorì, *„Graphene oxide hybrid sulphur-nitrogen polymer for high-performance pseudocapacitors”*, **J. Am. Chem. Soc.** 2019, 141, 482-487, IF= 14,357.

3. I. Janica, S. Del Buffa, A. Mikołajczak, M. Eredia, **D. Pakulski**, A. Ciesielski, P. Samorì, *„Thermal insulation with 2D materials: liquid phase exfoliated vermiculite functional nanosheets”,* **Nanoscale**, 2018, 10, 23182-23190, IF= 7,233.

4. **D. Pakulski**,* A. Gorczyński,* W, Czepa, Z. Liu, L. Ortolani, V. Morandi, V. Patroniak, A. Ciesielski, P. Samorì, *„Novel Keplerate type polyoxometalate-surfactant-graphene hybrids as advanced electrode materials for supercapacitors”* **Energy Storage Materials,** 2019, 17, 186-193 (equal contribution)*, IF = pending.

5. M. Krystek, **D. Pakulski,** V. Patroniak, M. Górski, L. Szojda, A. Ciesielski, P. Samorì, *„High performance graphene-based cementitious composites”,* **Adv. Sci.** 2019, 1801195, IF= 12,441.

6. C. Anichini,* W. Czepa,* **D. Pakulski,*** A. Aliprandi, A. Ciesielski, P. Samorì, *„Chemical sensing with 2D materials”* **Chem. Soc. Rev.** 2018, 47, 4860-4908, IF= 40,182 (equal contribution)*.

7. **D. Pakulski,** W. Czepa, S. Witomska, A. Aliprandi, P. Pawluć, V. Patroniak, A. Ciesielski, P. Samorì, *„Graphene oxide-branched polyethylenimine foams for efficient removal of toxic cations from water”,* **J. Mat. Chem. A,** 2018, 6, 9384-9390, IF=9,931.

8. A. Aliprandi,* **D. Pakulski**,* A. Ciesielski, P. Samorì, *"Punctured Two-Dimensional Sheets for Harvesting Blue Energy",* **ACS NANO**, 2017, 11, 10654-10658 **IF=13,709 (equal contribution)***.

9. G. Markiewicz*, **D. Pakulski***, A. Galanti, V. Patroniak, A. Ciesielski, A. R. Stefankiewicz, P. Samorì, *„Photoisomerisation and light-induced morphological switching of a polyoxometalate-azobenzene hybrid",* **Chem. Commun.** 2017, 53, 7278-7281, IF=6,290 (equal contribution)*.

10. A. Gorczyński, **D. Pakulski**, M. Szymańska, M. Kubicki, K. Bułat, T. Łuczak, V. Patroniak, „*Electrochemical deposition of the new manganese(II) Schiff-base complex on a gold template and its application for dopamine sensing in the presence of interfering biogenic compounds*", **Talanta**, 2016, 149, 347-355; IF = 3,973.

11. A. Gorczyński, D. Marcinkowski, **D. Pakulski**, Z. Hnatejko, M. Kubicki, J. M. Harrowfield, A. R. Stefankiewicz, V. Patroniak, „*Luminescent Activity of Metallosupramolecular Cd(II) Complexes Containing Dimethylterpyridine Ligand",* **Arab. J. Chem.** 2016 DOI: 10.1016/j.arabjc.2016.04.006. IF – 2,969.

Conferences and scientific achievements

A. Participation in scientific conferences:

PhD student is the author and co-author of more than twenty oral and poster presentations at domestic and international conferences throughout his academic career. All conferences held during PhD studies are presented below.

1) International conferences:

- **Date and place of the conference:** 13-19.4.2019, Dubai, United Arab Emirates
  Conference name: World Nanotechnology Conference
  Title: Functionalized graphene oxide as a new, high performance adsorbent of heavy metal ions and organic dyes
  Type of presentation: Poster presentation

- **Date and place of the conference:** 10-14.9.2018, San Sebastian, Spain
  Conference name: Graphene Week
  Title: Graphene based adsorbents for efficient and selective grasp of metal ions
  Type of presentation: Poster presentation

- **Date and place of the conference:** 30.8-4.9.2018, Sendai, Japan
  Conference name: 43th International Conference on Coordination Chemistry
  Title: Modified POM based on graphene - hybrid materials with alkali metal ions trapping properties
  Type of presentation: Poster presentation

- **Date and place of the conference:** 6-9.6.2018, Poznań, Poland
  Conference name: NanoTech Poland 2018
  Title: Chemically modified graphene oxide as a new, high performance adsorbent of heavy metal ions

Type of presentation: Poster presentation

- **Date and place of the conference:** 14-15.3.2018, Paris, France
  Conference name: II Assisess Franco-Polonaises de chimie
  Title: Functional graphene oxide as a new high-performance adsorbent of heavy metal ions
  Type of presentation: Poster presentation

- **Date and place of the conference:** 22-26.8.2017, Strasbourg, France
  Conference name: chem2dmat
  Title: Functionalized polyoxometalates based on graphene - hybrid materials for energy storage applications
  Type of presentation: Poster presentation

- **Date and place of the conference:** 12-16.2.2017, Queenstown, New Zealand
  Conference name: AMN8 International Conference on Advanced Materials and Nanotechnology
  Title: POM-graphene hybrid materials for water purification, gas adsorption and energy applications
  Type of presentation: Oral presentation

- **Date and place of the conference:** 8-10.2.2017, Dunedin, New Zealand
  Conference name: SANZ-O-MAG2
  Title: Complexes based on Schiff base ligand – synthesis, structure and magnetic properties
  Type of presentation: Poster presentation

- **Date and place of the conference:** 23-27.07.2016, Manchester, United Kingdom
  Conference name: Euro Science Open Forum
  Title: Graphene based membranes for water purification, gas adsorption and energy applications

Type of presentation: Poster presentation

2) Domestic conferences:

- **Date and place of the conference:** 15.3.2019, Poznań
  Conference name: I Poznan Microsymposium of Graphene
  Title: Modification of graphene oxide as a method to obtain efficient metal ions adsorbent
  Type of presentation: Poster presentation

- **Date and place of the conference:** 24-26.9.2018, Szczecin
  Conference name: 4th Polish conference "Graphene and 2D materials"
  Title: Chemically modified graphene oxide as a high-performance and selective adsorbent of heavy metal ions
  Type of presentation: Oral presentation

- **Date and place of the conference:** 18-19.11.2016, Kraków
  Conference name: Oxygenalia
  Title: Hybrid materials based on graphene for water purification, gas adsorption and energy applications
  Type of presentation: Poster presentation

- **Date and place of the conference:** 5.11.2016, Poznań
  Conference name: III Symposium of Young Scientists
  Title: Molecular hybrid based on graphene for capturing heavy metals and gas adsorption
  Type of presentation: Oral presentation

- **Date and place of the conference:** 19-23.09.2016, Poznań
  Conference name: 59 Congress of the Polish Chemical Society (PTChem)
  Title: Complexes with Schiff base ligands, synthesis, structure and investigation of their properties

Type of presentation: Poster presentation

- **Date and place of the conference:** 21-24.06.2016, Toruń
  Conference name: X Copernicus Doctoral Seminar
  Title: Searching for correlations between the supramolecular architecture of complexes and their specific properties
  Type of presentation: Oral and poster presentations

- **Date and place of the conference:** 14.11.2015, Poznań
  Conference name: II Symposium of Young Scientists
  Title: Complexes with transition metal ions as a precursor of new metal and supramolecular architectures with potential of single molecule magnets (SMMs)
  Type of presentation: Poster presentation

B. Patent application

The name of the invention: *"Preparation method of cementitious composite with the addition of graphene"*
Description of the invention: The subject of the invention is a method of producing a cementous composite with the addition of graphene, which is used in construction for the manufacture of structural and non-structural elements, where the increased strength or electrical conductivity of the material is of importance.
Number of patent application: P.424610
Registration date and place: 2018-02-16; Patent Office of the Republic of Poland.
The range of patent application: National
Authors of the invention: M. Krystek, D. Pakulski, L. Szojda, M. Górski, V. Patroniak, A. Ciesielski, P. Samorì

C. Participation in research projects:

- **Project name:** Grant nr *2017/27/N/ST5/00173* (PRELUDIUM)
  Period of participation in the research project: 7.2018 – in progress (7.2020)
  Function in the research project: Principal Investigator
  The purpose and effects of participation in the project:
  The aim of the project entitled "*Functionalized graphene oxide as a new, high-performance adsorbent of heavy metal ions*" is the synthesis and multifaceted characterization of a new generation of adsorbents for metal ions. The proposed project targets at the increase in the efficiency of the adsorption process of graphene oxide through its chemical functionalization with multidentate organic ligands. Such an approach will make it possible to control the affinity of GO towards specific metal ions and fabricate robust and highly functionalized 2D architectures, which can be then used as adsorbents for removal of heavy metal ions.

- **Project name:** Grant nr *2016/21/B/ST5/00175* (OPUS)
  Period of participation in the research project: 2.2017 – in progress (2.2020)
  Function in the research project: Investigator
  The purpose and effects of participation in the project:
  Scientific purpose of the project titled: "*Supramolecular interactions in systems based on polyoxometalates*" is synthesis and comprehensive physicochemical characterization of systems that comprise polyoxometalates (POMs) and quaterpyridine/Schiff-base ligands, altogether tethered by 3d(TM)/4f(RE) ions, in particular with regard to their magnetic and luminescent properties.

- **Project name:** Grant nr *2015/18/E/ST5/00188* (SONATA BIS)
  Period of participation in the research project: 5.2017 – in progress (5.2020)
  Function in the research project: Investigator
  The purpose and effects of participation in the project:
  The research project entitled "*New (supramolecular) approach to two-dimensional layered materials*" exploit principles of supramolecular chemistry to

develop new chemical methods towards the production of high-quality graphene and other two-dimensional materials with controlled composition, structure and function. The programmed interfacing with functional molecular assemblies via non-covalent, covalent and DCC approaches will enable tuning of the 2DMs fundamental physico-chemical properties such as capacity to recognize and host gas molecules, porosity and optical properties. The innovative supramolecular approach proposed in this project, may be a breakthrough method for finding the use of graphene and other two-dimensional materials in optoelectronics and devices aimed at the energy storage.

D. International internships:

- **Country**: France
  Institution: Université de Strasbourg, Institut de Science et d'Ingenerie Supramoleculaire (I.S.I.S.)
  Type of stay: Internship in the frame of ERASMUS program.
  Duration time: 1.2.2015–30.6.2015
  Description of activities:
  Research in the field of synthesis functional building blocks decorated with amine anchoring groups for further covalent functionalization of GO. During internship I was trained among others in Scanning Electron Microscopy (SEM) and X-ray photoelectron spectroscopy (XPS) technique to morphology characterization and structural composition of nanomaterials.
  Supervisor: Prof. Paolo Samori
  Auxiliary supervisor: Dr. Artur Ciesielski (HDR)

- **Country**: France

  Institution: Université de Strasbourg, Institut de Science et d'Ingenerie Supramoleculaire (I.S.I.S.)

  Type of stay: *Cotutelle* program (double doctorate) funded by French Embassy in Poland.

  Duration time: 15 months, from February to June in years 2017-2019.

  Description of activities:

  Research activities carried out during this program became the subject of presented thesis and concerned synthesis of functionalized two-dimensional materials (graphene and GO) and their comprehensive physico-chemical characterization with particular emphasis on adsorption and energy storage properties.

  Supervisor: Dr. Artur Ciesielski (HDR)

E. Awards:

1) French government scholarship in the frame of *cotutelle* program between Adam Mickiewicz University in Poznań and Université de Strasbourg in years 2017-2019.

2) Laureate of START program scholarship founded by Foundation for Polish Science, 2019.

3) Laureate of scientific scholarship of the city of Poznań, 2019.

4) Laureate of grant PRELUDIUM 14 founded by Polish National Science Center, 2018.

5) Prizes of Rector of Adam Mickiewicz University for the scientific achievements in years 2017-2018.

6) Laureate of grants to attend Euro Science Open Forum (ESOF) conference in Manchester, United Kingdom (July 2016), and Graphene Week conference in San Sebastian, Spain (July 2018).

7) Pro-quality scholarships for the best PhD students of Adam Mickiewicz University in Poznań in years 2016-2019.

8) Scholarship for the best students form Adam Mickiewicz University in Poznań funded by European Union from the European Social Funds, The Human Capital Operational Programme, Sub-measure 4.1.2. 2011/2012, 2012/2013.

9) Rector's Scholarship for the best students of Adam Mickiewicz University in Poznań 2011/2012.

Pakulski Dawid

„Graphene based materials and their potential applications”

Résumé en Français

Cette thèse de doctorat a pour objectif scientifique la synthèse de matériaux bidimensionnels fonctionnalisés (graphène et oxyde de graphène) et leur caractérisation physicochimique complète, avec un accent particulier apporté sur les propriétés d'adsorption et de stockage d'énergie. Nous avons démontré que la modification covalente de l'oxyde de graphène (GO) avec un polymère organique (BPEI) affecte très favorablement l'efficacité du processus d'adsorption. Les valeurs de la capacité maximale d'adsorption (q_{max}) des ions de métaux lourds favorisent de manière significative ce matériau par rapport à la majorité des adsorbants connus à base de carbone. En outre la fonctionnalisation de GO avec l'aminosilicate mésoporeuse (SiO_2NH_2) conduit à l'obtention d'un adsorbant efficace et rapide des colorants organiques cationiques (MB, RhB, MV). En plus nous avons prouvé que la fonctionnalisation du graphène (EEG), en utilisant les sous-unités de surfactant POM, a montré que ce type de matériau hybride organique-inorganique est très stable et présente des propriétés électriques intéressantes pouvant être utilisées dans la production de supercondensateurs

Mots clés: 2D matériaux, graphène, oxyde de graphène, adsorbant, supercondensateurs

Summary in English

Scientific purpose of this doctoral dissertation is synthesis of functionalized two-dimensional materials (graphene and graphene oxide) and their comprehensive physicochemical characterization, with particular emphasis on adsorption and energy storage properties. We could demonstrate that covalent modification of graphene oxide (GO) with an organic polymer (BPEI) very favorably affects the efficiency of the adsorption process. The maximum adsorption capacity (q_{max}) values for heavy metal ions significantly favour this material in comparison to the majority of known carbon adsorbents. Moreover, functionalization of GO with mesoporous aminosilica (SiO_2NH_2) leads to obtaining an efficient and rapid adsorbent of organic cationic dyes (MB, RhB, MV). In addition we proved that the functionalization of graphene (EEG) using the POM-surfactant subunits proved that this type of organic-inorganic hybrids material is very stable and have interesting electrical properties with potential application in the production of supercapacitors.

Keywords : 2D materials, graphene, graphene oxide, adsorbent, supercapacitors